Biophysical and biochemical characterisation of the SMR Proteins Hsmr and EmrE

Dissertation zur Erlangung des Doktorgrades der Naturwissenschaften

vorgelegt dem Fachbereich Biochemie, Chemie, Pharmazie
Institut für Biophysikalische Chemie
Johann Wolfgang Goethe Universität Frankfurt am Main
Zentrum für Biomolekulare Magnetische Resonanz Spektroskopie

von Ines Lehner
Frankfurt am Main 2008

D30

Vom Fachbereich Biochemie, Chemie und Pharmazie
Johann Wolfgang Goethe Universität als Dissertation
angenommen

Dekan:	Prof. Dr. Schwalbe
Gutachter:	Prof. Dr. Glaubitz
	Prof. Dr. Tampé

Datum der Disputation:

Acknowledgments

I would like to thank my supervisor Prof. C. Glaubitz for the opportunity to conduct my Ph.D. thesis research in his laboratory. In particular, I am grateful for the provision of excellent laboratory conditions, support and enthusiasm for the project.

I am thankful to the members of the Glaubitz group past and present. In particular I am indebted to Dr. Jakob Lopez and Daniel Basting for fruitful discussions, help with NMR experiments and python scripts.

I would like to thank Dr. Frank Bernhard, Professor Dötsch and the members of the Dötsch group for providing me with several plasmids and cell free extract.

I am indebted to my cooperation partners Björn Meyer, Dr. Karla Werner, Nina Morgner, Dr. Winfried Haase and Dr. Vitali Vogel. Additionally I would like to thank Dr. Chris Lu for advice regarding AUC experiments and Max Stadler for help with solution state NMR experiments.

Prof. S. Schuldiner is acknowledged for providing several SMR protein plasmids to the laboratory of Professor C. Glaubitz and Theofanis Manolikas is acknowledged for providing the EmrE E25A mutant.

Finally I would like to acknowledge the financial support of this thesis provided by the Sonderforschungsbereich 628 “Functional Membrane Proteomics” der Deutschen Forschungsgemeinschaft.

Abbreviations

ABC	adenosine triphosphate binding cassette
ac	acriflavine
ADP	adenosine diphosphate
APS	ammonium persulfate
ATP	adenosine triphosphate
AUC	analytical ultracentrifugation
OG	n-ß-octyl-D-glucopyranoside
bla	beta lactamase
BMRB	Biological Magnetic Resonance Bank
BNPAGE	Blue native PAGE
BSA	bovine serum albumin
bR	bacteriorhodopsin
bz	benzalkonium
CCCP	carbonyl cyanide 3-chlorophenylhydrazone
CHAPS	3-[(3-Cholamidopropyl)dimethylammonio]propanesulfonic acid
chl	chloramphenicol
CL	cardiolipin
cmc	critical micellar concentration
COSY	correlation spectroscopy
CP	cross polarisation
CSA	chemical shift anisotropy
CV	column volume
DDM	n-Dodecyl-ß-D-maltoside
DHBs	Matrix (2,5-dihydroxy benzoic acid:2-hydroxy-5-methoxy benzoic acid = 10:1
DHPC	1,2-diheptanoyl-*sn*-glycero-3-phosphocholine
DMPC	1,2-Dimyristoyl-*sn*-phosphatidylcholine
DMT	drug/metabolite transporter
DOPC	1,2-Dioleoyl-*sn*-phosphatidylcholine
DPC	Fos-*ß*-choline® 12
DQ	double quantum
DQSQ	double quantum single quantum
DTT	dithiothreitol
EDTA	ethylenediaminetetraacetic acid
EM	electron microscopy
EPR	electron paramagnetic resonance
ery	erythromycin
etbr	ethidium bromide
FM	feeding mix
FPLC	fast protein liquid chromatography
FTIR	Fourier transform infrared
GPCRs	G-protein coupled receptors
HEPES	4-(2-hydroxyethyl)-1-piperazineethanesulfonic acid
HR	high resolution
HRP	horseradish peroxidase
HSQC	heteronuclear single quantum coherence
IC_{50}	concentration at which 50 % inhibition is observed
IEX	ion exchange chromatography
IMAC	immobilised metal affinity chromatography
INEPT	insensitive nuclei enhanced by polarisation transfer

IPTG	isopropyl β-D-1-thiogalactopyranoside
K_d	dissociation constant
K_D	partition coefficient
K_i	dissociation constant of an inhibitor
K_m	Micheaelis-Menten constant
LB	Luria Bertani
LE	lysophosphatidylethanolamine
LILBID	laser induced liquid bead ion desorption
LMPG	1-myristoyl-2-hydroxy-sn-glycero-3-[phospho-RAC-(1-glycerol)]
LPPG	1-palmitoyl-2-hydroxy-sn-glycero-3-[phospho-RAC-(1-glycerol)]
MALDI	matrix assisted laser desorption
MAS	magic angle spinning
MATE	multidrug and toxic compound extrusion
Mcs	multiple cloning site
MET	multidrug endosomal transporter
MFS	major facilitator superfamily
M_{ox}	methionine oxidation
MS	mass spectrometry
MV^{2+}	methylviologen
MW	molecular weight
NG	*N*-nonyl-*β*-D-glucoside
Ni-NTA	nickel-nitrilotriacetic acid
NMR	nuclear magnetic resonance
NOESY	nuclear overhauser enhancement spectroscopy
OG	n-ß-octyl-D-glucopyranoside
ori	origin
PA	phosphatidic acid
PAGE	polyacrylamide gel electrophoresis
PDC	protein detergent complex
PDSD	proton driven spin diffusion
PE	phosphatidylethanolamine
PG	phosphatidylglycerol
PGP-me	phosphatidylglycerolmethylphosphate
PGS	phosphatidylglycerosulfate
pI	isoelectric point
PMF	proton motif force
PML	purple membrane lipids
POPC	1-palmitoyl-2-Oleoyl-s*n*-phosphatidylethanolamine
POPE	1-palmitoyl-2-Oleoyl-s*n*-phosphatidylethanolamine
POPG	1-palmitoyl-2-Oleoyl-s*n*-phosphatidylglycerol
ppm	parts per million
PS	phosphatidylserine
PSMR	paired small multidrug resistance
rbs	ribosomal binding site
RND	resistance nodulation cell division
RM	reaction mix
R_s	Stokes radius
RT	room temperature
R6G	rhodamine 6G
SDS	sodium dodecyl sulphate
SEC	size exclusion chromatography

SMF	sodium motif force
SMP	small multidrug pumps
SMR	small multidrug resistance
S/N	signal to noise
S-TGD-1	3-HSO-galactose1,6-mannose1,2-glucose1,1-sn-2,3-diphytanylglycerol.
SUG	suppressor of groEL mutations protein
TCA	trichloroacetic acid
TEMED	tetramethylethylendiamin
tet	tetracycline
TFA	trifluoroacetic acid
TFE	tetrafluoroethylene
TGD-1	galactose1,6-mannose1,2-glucose1,1-sn-2,3-diphytanylglycerol
TMSP	3-(trimethylsilyl)propionic acid
TOF	time of flight
TPB^+	tetraphenyl boron
TPP^+	tetraphenyl phosphonium
tri	trimethoprim
TROSY	transverse relaxation optimized spectroscopy
TV	total volume
UV	ultraviolet
van	vancomycin
VV	void volume
YT	yeast tryptophan

List of Figures

List of Tables

Contents

Summary

The increasing resistance of almost all pathogenic bacteria to antibiotics (multidrug resistance) causes a severe threat to public health. The mechanisms underlying multidrug resistance include the induced over expression of multidrug transporters which extrude a variety of lipophilic and toxic substrates in an energy dependent fashion through the membrane out of the cell. These proteins are found in all transporter families.
The work described in this thesis is dedicated to drug-proton antiporters from the small multidrug resistance (SMR) family. These efflux pumps with just four transmembrane helices per monomer are so far the smallest transporters discovered. Their oligomeric state, topology, three dimensional structure, catalytic cycle and transport mechanism are still rather controversial. Therefore, the aim of this thesis was to directly address these questions for the small multidrug resistance proteins *Halobacterium salinarium* Hsmr and *Escherichia coli* (*E. coli*) EmrE using a number of biophysical methods such as NMR, transport assays, mass spectrometry and analytical ultracentrifugation. Especially the work on Hsmr has been challenging due to the halophilic nature of this protein.

In **Chapter 1**, key questions and the most important biophysical techniques are introduced followed by Material and Methods in **Chapter 2**.

Depending on experimental requirements, cell free or 'classical' *in vivo* expression has been used for this thesis.

Cell free expression as an option for the production of small multidrug transporters has been explored in **Chapter 3**. It has been possible to produce the SMR family members Hsmr, EmrE, TBsmr and YdgF *in vitro*. The expression of Hsmr was investigated in more detail under different experimental conditions. Hsmr was either refolded from precipitate or maintained in a soluble form during expression in the presence of detergents and liposomes. Furthermore, amino acids for which no auxotrophic strains were available could be labelled successfully. This expression system has been also used for preparing labelled samples of EmrE as described in **Chapter 9**.

In vivo in *E. coli* expression of Hsmr, as described in **Chapter 4**, provided large amounts of proteins if fermenter production was used. Uniform labelling and selective unlabelling with stable isotopes (^{13}C, ^{15}N) for NMR spectroscopy was achieved *in vivo* in a more efficient and cost effective manner than using the cell free approach for this protein. Hsmr could be purified successfully from both *in vitro* and *in vivo* expression media. Hsmr is expressed *in vivo* and *in vitro* with N-terminal formylation. The N-terminal formylation is unstable and Hsmr in the presence of low salt concentrations was amenable to N-terminal degradation. It was found that Hsmr shows longest stability in Fos-*ß*-choline® 12 and sodium dodecyl sulphate, but best reconstitution conditions were found, when dodecyl maltoside is used and exchanged with *Escherichia coli* lipids. A molar protein lipid ratio of 1 to 100, amenable to solid state nuclear magnetic resonance, has been achieved. Sample homogeneity was shown by freeze fracture electron microscopy.

The oligomeric state of Hsmr in detergent has been assessed by SDS PAGE, blue native PAGE, size exclusion chromatography, analytical ultracentrifugation and laser induced liquid bead ion desorption mass spectrometry (LILBID) as described in **Chapter 5.** A

concentration and detergent dependent monomer-oligomer equilibrium has been found by all methods.

The activity of Hsmr under the sample preparation conditions used here was shown using radioactive and fluorescence binding as well as fluorescence and electrochemical transport assays **(Chapter 6)**. For transport studies, a stable pH gradient was generated by co-reconstitution of Hsmr with bacteriorhodopsin and subsequent sample illumination.

Based on the observed long term stability of Hsmr in Fos-ß-choline® 12 and sodium dodecyl sulphate, liquid state NMR experiments were attempted in order to assess the correct folding of Hsmr in detergent micelles **(Chapter 7)**. 1D proton and 2D HSQC spectra of U-^{15}N Hsmr revealed a poor spectral dispersion, low resolution and only a small number of peaks. These are at least partly due to long rotational correlation times of the large protein detergent complex.

This problem has been overcome by applying solid-state NMR to Hsmr reconstituted into *E. coli* lipids (**Chapter 8**). Uniform ^{13}C labelled samples were prepared and two dimensional proton-driven spin diffusion and double quantum-single quantum correlation spectra were acquired successfully. Unfortunately, the spectral resolution was not yet sufficient for further structural studies. Reasons for the observed linebroadening could be structural heterogeneity or molecular motions which interfere with the NMR timescale. Therefore, the protein mobility has been probed using static ^{2}H solid state NMR on Ala-d_3-Hsmr. It could be shown, that parts of Hsmr are remarkably mobile in the membrane and that this mobility can be limited by the addition of the substrate ethidium bromide. Ethidium bromide as well as tetraphenylphosphonium (TPP^+) is typical multidrug transporter substrates. The membrane interaction of TPP^+ in DMPC membranes has been resolved by ^{1}H MAS NMR. It was found that it penetrates into the interface region of the lipid bilayers and therefore behaves like many other transporter substrates adding to the hypothesis that the membrane could act as a pre-sorting filter.

Finally, **Chapter 9** is dedicated to the characterisation of the essential and highly conserved residue Glu-14 in EmrE by solid-state NMR. In order to avoid spectral overlap, the single Glu EmrE E25A mutant was chosen instead of the wildtype. The protein has been produced *in vitro* to take advantage of reduced isotope scrambling in the cell free expression system as verified by analytical NMR spectroscopy. Correct labelling of EmrE was tested by MALDI-TOF and solid-state NMR. The dimeric state of DDM solubilised EmrE has been probed by LILBID. The labelled protein was reconstituted into *E. coli* lipids to ensure a native membrane environment. Activity was determined by measuring ethidium bromide transport. Freeze fracture EM revealed very homogeneous protein incorporation even after many days of MAS NMR experiments.
2D ^{13}C double quantum filtered experiments were used to obtain chemical shift and lineshape information of Glu-14 in EmrE. Two distinct populations were found with backbone chemical shift differences of 4 - 6 ppm which change upon substrate binding. These findings indicate a structural asymmetry at the assumed dimerisation interface and are discussed in the context of a model for shared substrate/proton binding. These studies represent the first successful use of cell free expression to prepare labelled membrane proteins for solid-state NMR and allow for the first time an NMR insight into the binding pocket of a multidrug efflux pump.

Zusammenfassung

Die zu beobachtende Antibiotikaresistenz nahezu aller pathogener Bakterien (Multidrugresistenz) stellt ein ernstes medizinisches Problem dar. Einer der molekularen Mechanismen basiert auf der induzierten Überexpression von Multidrugtransportern, welche eine Vielfalt lipophiler und toxischer Substanzen unter Energieverbrauch durch die Membran aus der Zelle pumpen. Derartige Proteine lassen sich in fast allen Transporterfamilien finden.
Diese Dissertation widmet sich Substrat-Protonen-Antiportern der Small Multidrug Resistance (SMR) Familie, welche mit nur 4 transmembranen Helices zu den kleinsten bisher bekannten Transportern gehören. Ihr Oligomerisierungsgrad, 3D Struktur und die molekularen Details des Transportzyklus sind trotz intensiver Studien stark umstritten. Das Ziel dieser Dissertation war es daher zu versuchen, diese Fragen für die Proteine Hsmr, aus *Haslobacterium salinarium*, und EmrE, aus *Escherichia coli* (*E. coli*), mittels biophysikalischer Techniken wie Fluoreszenzspektroskopie, Massenspektrometrie, NMR und analytischer Ultrazentrifugation zu beantworten. Neben den allgemeinen zu erwartenden Problemen bei der Präparation von Membranproteinen stellte der halophile Charakter von Hsmr eine besondere Herausforderung dar.

In **Kapitel 1** werden die behandelten Proteine, die zu lösenden Fragstellungen und die wichtigsten Methoden eingeführt. Die benutzten Materialien und Methoden sind im Detail in **Kapitel 2** beschreiben. Je nach experimentellen Erfordernissen wurde zellfreie Synthese oder „klassische“ *in vivo* Expression in *E. coli* für die in dieser Dissertation beschriebenen Arbeiten benutzt. Die Möglichkeiten der zellfreien Synthese als Option für die Herstellung von SMR Proteinen werden in **Kapitel 3** untersucht. Es war möglich Hsmr, EmrE, TBsmr und YdgF *in vitro* in nachweisbaren Mengen zu produzieren. Die Expression von Hsmr wurde im Detail unter verschiedenen experimentellen Bedingungen studiert. Hsmr wurde entweder aus prezipitierter Form rückgefaltet oder direkt in der Gegenwart von Detergenzmizellen oder Liposomen exprimiert. Ein besonderer Vorteil zellfreien Synthese besteht gerade in der Möglichkeit bestimmte Aminosäuren mit stabilen Isotopen zu markieren für die keine auxotrophen Stämme für die *in vivo* Expression zur Verfügung stehen. Dieser Ansatz wurde für die Herstellung selektiv markierter EmrE Proben verfolgt, wie in **Kapitel 9** beschreiben.

Durch *in vivo* Expression von Hsmr in *E. coli* **(Kapitel 4)** konnten unter Verwendung eines Fermenters größere Proteinmengen bereitgestellt werden. Verschiedene U-^{13}C und ^{15}N Markierungsschemata konnten *in vivo* auf eine effizientere und kostengünstigere Art als mit der zellfreien Synthese verwirklicht werden. Hsmr konnte sowohl nach *in vitro* und *in vivo* Expression erfolgreich aufgereinigt werden. Hsmr wurde in beiden Fällen mit einer N-terminalen Formylierung exprimiert. Diese N-terminale Formylierung ist instabil. Bei niedriger Salzkonzentration war eine N-terminale Degradation des Proteins zu beobachten. Die Detergenzien die die größte Langzeitstabilität von Hsmr ermöglichen sind Fos-*ß*-choline® 12 und SDS. Die für die Rekonstituierung besten Bedingungen wurden aber für Dodecylmaltosid und *E. coli* Lipide gefunden. Es war so ein molares Lipid-Proteinverhältnis von 100:1 möglich, was weitergehende Festkörper-NMR Experimente erlaubt. Eine hohe Probenhomogenität wurde mittels Gefrierbruchelekronenmikroskopie nachgewiesen.
Der Oligomerisierungsgrad von Hsmr in Detergenzmizellen wurde mittels SDS PAGE, blau-nativer PAGE, Gelfiltration, analytischer Ultrazentrifugation und Laser induzierter Tröpfchen-Desorptions-Massenspektrometrie (LILBID), wie in **Kapitel 5** beschrieben,

untersucht. Es konnte gezeigt werden, dass das Gleichgewicht zwischen Monomeren und Oligomeren von der Proteinkonzentration, Salz und Detergenz abhängt.

Die Aktivität von Hsmr für die hier etablierten Präparationsbedingungen wurde über Substratbindung (Fluoreszenz, radioaktiv) und mittels Substrattransportmessungen (elektrochemisch, Fluoreszenz) nachgewiesen **(Kapitel 6)**. Das für den transmembranen Transport notwendige, zeitlich stabile elektrochemische Potential konnte dabei durch Ko-Rekonstituierung von Hsmr mit Bakteriorhodopsin über Probenbeleuchtung erzeugt werden. Da Hsmr in Fos-*ß*-choline® 12 und SDS längere Zeit stabil war, wurden Lösungs-NMR Experiment an ^{15}N markierten Proben durchgeführt, um die korrekte Faltung des Proteins in Mizellen zu verifizieren **(Kapitel 7)**. Leider konnten aber in ^{1}H-^{15}N HSQC Spektren nur wenige Resonanzen aufgelöst werden, was vermutlich zum Teil auf die lange Rotationskorrelationszeit dieses Proteindetergenzkomplexes zurückzuführen ist.

Dieses Problem konnte jedoch teilweise durch die Anwendung von Festkörper-NMR auf Hsmr in *E. coli* Lipiden gelöst werden **(Chapter 8)**. Es wurden eine Reihe von zweidimensionalen protonengetriebenen Spindiffusionsexperimenten sowie Doppel-Einzelquanten-Korrelationspektren an vollständig ^{13}C markierten Proben aufgenommen. Leider war die spektrale Auflösung für weiterführende Studien nicht gut genug. Gründe für die zu beobachtende Linienverbreiterung könnten strukturelle Heterogenität oder mit der NMR Zeitskala interferierende molekulare Bewegungen sein. Daher wurde die Proteinbeweglichkeit qualitativ mit statischer ^{2}H NMR an Ala-d3-Hsmr studiert. Es wurde dabei tatsächlich eine hohe molekular Beweglichkeit in Teilen des Proteins beobachtet, die jedoch nach Zugabe des Substrats Ethidiumbromid stark eingeschränkt wurde. Die Lokalisierung des Substrats TPP^{+} in einer DMPC Membran wurde mittels ^{1}H MAS NMR untersucht. Wie viele andere Substrate auch, lagert sich TPP^{+} in der Membran oberhalb der hydrophoben Kettenregion ein, was die Hypothese einer membranunterstützten Bindung an das Protein unterstützt.

Kapitel 9 widmet sich der Festkörper-NMR Charakterisierung des in der gesamten SMR Familie hochkonservierten Restes Glu14 in Helix 1 am Beispiel von EmrE. Zur Vereinfachung der Spektren wurde die Glu-Mutante EmrE E25A statt des Wildtyps ausgewählt. Um den metabolischen Abbau von U-^{13}C-Glu zu verhindern, wurde das Protein *in vitro* hergestellt. Markierungseffizienz und korrekter Einbau wurde mittels MALDI-TOF und NMR verifiziert. Um eine möglichst native Situation zu emulieren, wurde das markierte Protein in *E.coli* Lipide rekonstituiert. Proteinaktivität wurde über Ethidiumbromidtransport nachgewiesen. Mittels Gefrierbruchelektronenmikroskopie konnte ein sehr homogener Einbau des Proteins sogar nach mehreren Tagen MAS NMR Experimenten gesehen werden. ^{13}C chemische Verschiebungen für Glu14 wurden mittels Doppel-Einzelquanten-Korrelationspektren bestimmt. Es konnten zwei Populationen unterschieden werden, die für den Bereich des Proteinrückgrats chemische Verschiebungsdifferenzen von 4–6ppm aufweisen. Nahezu alle Resonanzen ändern sich nach Zugabe von Ethidiumbromid. Diese Beobachtungen weisen auf eine strukturelle Asymmetrie im Bereich des vermuteten Dimerisierungsinterfaces hin und werden im Kontext eines Modells für eine gemeinsame Substrat/Protonenbindungsstelle diskutiert. Diese Studie repräsentiert die erfolgreiche Anwendung der zellfreien Expression zur Herstellung markierter Membranproteine für die Festkörper-NMR. Diese Messungen ermöglichen erstmals einen Einblick in die Bindungstasche einen Multidrugtransporters.

Chapter 1 - Introduction

1.1 Biological Introduction

1. 1 Protein class introduction

1. 1. 1. 1 Membrane Proteins

Living cells are surrounded and compartmentalised by membranes. These lipid bilayers are a generally composed of nearly 50 % proteinaceous material which can be either integral, membrane spanning proteins, or peripheral, membrane associated, proteins. The role of these proteins is diverse including: energy conversion, transport of ions and molecules, sensing and transmitting stimuli. The abundance of different membrane proteins is highlighted by recently sequenced bacterial genomes which revealed that 3-10 % (3 % in *Mycobacterium tuberculosis* and 10 % in *Salmonella typhimurium*) of open reading frames are predicted to encode membrane transport proteins. Despite their abundance the difficulties associated with working on membrane proteins is for example reflected in the number of x-ray crystallographic structures that have been solved. Currently only 144 unique membrane protein structures are known [1]. For the important class of transport proteins the situation is even worse and at the end of 2003 only eight different 3D structures were known [1].

1. 1. 1. 2 Transport proteins

Transport of substances across a membrane may be passive or active and depends on the Gibbs free energy ΔG:

$$\Delta G = RT \log_e \frac{c_2}{c_1} + ZF\Delta V \qquad (1)$$

ΔG = Gibbs free energy, R = gas constant, T = temperature, c_2 = concentration, c_1 = concentration, Z = electrical charge, F = Faraday constant, ΔV = potential across the membrane

Channel proteins facilitate the downhill flux of a selection of specific molecules when opened. ΔG is negative for passive transport. In contrast active transport is defined as the uphill transport of a substance against the concentration gradient by coupling to an energy generating step. ΔG is positive for active transport. The net flux of molecules is thus determined by the thermodynamic gradient. In particular for charged molecules it is important to keep in mind that not only the concentration gradient but also the electrochemical gradient need to be overcome.

Often only proteins involved in active energy requiring transport of molecules are called transporter [2]. This nomenclature is also adopted in this thesis.
A further subclassification of transporter into primary and secondary transporter is based on their energy generating mechanism. Primary transporter, also called adenosine triphosphate binding cassette (ABC) transporter, utilise the energy provided by the hydrolysis of adenosine triphosphate (ATP) to adenosine diphosphate (ADP) for active transport while secondary transporter utilise an ion gradient, usually H^+ or Na^+, as driving force for active substrate transport. The secondary transport proteins can be further subdivided by the direction of substrate and driving ion transport. A transporter using unidirectional transport of ions and substrate is termed symporter while a transport in opposite directions leads to the classification as an antiporter. For secondary transporter a multitude of different translocation mechanisms and so far four different folds have been described [3]. This suggests the possibility of the occurrence of further subclasses. However in order to fulfil their function, all transport proteins must

negotiate a cycle which includes steps associated with substrate recognition, binding, translocation and release. It is expected that transporter show a high specificity for binding and transport of one or very few highly related substances and this is true for the majority of transporters. However, a subclass of proteins has been shown to exhibit a surprisingly broad substrate specificity which allows them to play important roles in multidrug resistance, cell volume regulation and peptide selection for translocation across membranes.

1. 1. 1. 3 Multidrug transporter

Multidrug drug resistance, particularly bacterial resistance to clinical antibiotics and neoplastic resistance to chemotherapeutic agents, are a widely known phenomenon. The World Health Organization recognised this as severe threat to global health and launched in 2001 a global strategy to combat this problem [4]. Basic defence mechanisms of bacteria include permeability barriers, inactivation of antimicrobials, modification of antibiotic targets and active drug efflux and these have been found to act synergistically [5, 6], see figure 1. The active efflux of toxic substances is mediated by so called multidrug transporter. These proteins can be primary and secondary active transport proteins and the latter are found in almost all transporter families [7]. To date six transport families which include multidrug transporter have been recognised [8], namely the ABC superfamily, and the secondary transporter families resistance nodulation cell division (RND) superfamily, major facilitator superfamily (MFS), drug/metabolite transporter (DMT) superfamily, multidrug and toxic compound extrusion (MATE) superfamily and multidrug endosomal transporter (MET) family. All secondary multidrug transporters so far discovered are antiporter. The unifying characteristic of all multidrug transport proteins however is the ability of a single protein to recognise a diverse array of substrates.

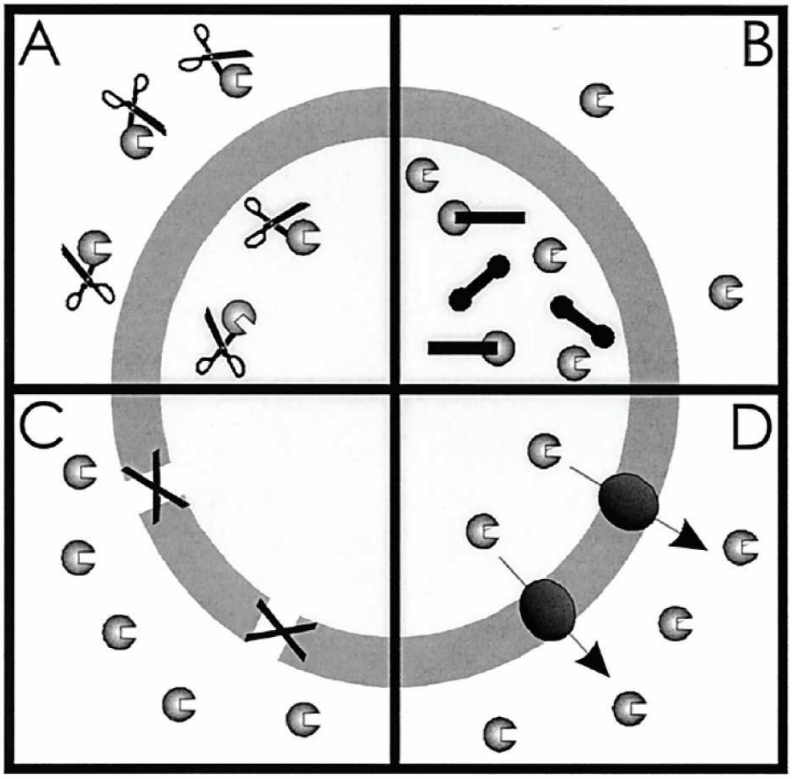

Figure 1. Bacterial defence mechanisms. A) Inactivation of the drug, B) alteration of drug target, C) prevention of drug uptake, D) active extrusion of drugs. Reproduced from [5].

The molecular mechanism of the broad substrate specificity of multidrug efflux pumps is not yet fully understood. For biophysical studies much sample is needed which is difficult to obtain due to the inherent difficulties in membrane protein sample preparations. Therefore alternative approaches have been pursued. Soluble proteins involved in transcriptional regulation of multidrug transporter such as BmrR and QacR have been investigated regarding their structure and mode of substrate binding [9-13]. It emerges that different ligands bind in the hydrophobic pocket at different but overlapping positions. The specificity is achieved exclusively by electrostatic and hydrophobic interactions. A charged amino acid in an otherwise hydrophobic environment, flexibility of the binding site and the lack of hydrogen bonds are further reoccurring molecular patterns [14].

Now, several 3D structures of multidrug transporter are known, including: the ABC-type transporter Sav1866 [15] and MsbA [16] and the secondary transporter AcrB from the RND superfamily [17, 18] and EmrE from the DMT superfamily and small multidrug resistance (SMR) protein family [19]. None of these answer the question of the route of drug entry into the transporter unequivocally. For ABC transporter three substrate uptake and efflux mechanisms have been discussed namely: a classical pump, an hydrophobic vacuum cleaner [20] and a flippase [21], see figure 2.

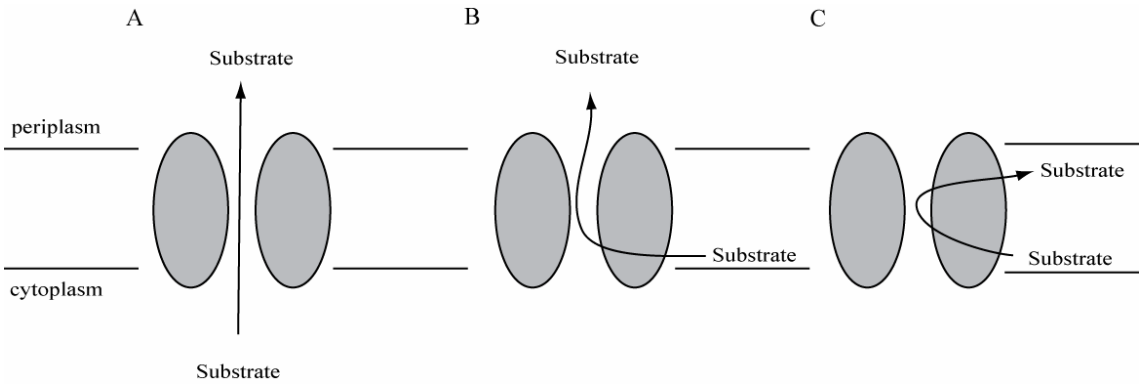

Figure 2. Schematic representation of the efflux mechanisms described for ABC multidrug transporter. A) classical pump, B) hydrophobic vacuum cleaner and C) flippase mechanism.

A classical pump takes up substrates from the aqueous phase and translocates them into the extracellular space. A flippase requires the substrates to enter the membranes inner leaflet, where they bind to the protein and are subsequently flipped to the outer leaflet. From the outer leaflet the substrates can diffuse into the extracellular space. The vacuum cleaner model suggests that drugs diffuse into the lipid phase from which they enter the protein which expels them into the extracellular aqueous phase.
Each 3D structure corresponds only to a snapshot of the protein during its transport cycle. Therefore, additional approaches are needed to elucidate the transport kinetics, substrate-protein interactions, oligomeric state or conformational changes during substrate translocation.

1. 1. 1. 4 SMR proteins

The topic of this thesis are investigations of multidrug transporters from the SMR family, a subclass of the DMT superfamily. The SMR family (TC#2.A.7.1 [22]) [23, 24] encompasses now more than 250 members from the bacterial and archeae kingdoms [25]. In general SMR proteins are small with only 100 to 140 amino acids, a molecular weight of roughly 12 kDa and have a four transmembrane helix topology, several highly conserved residues and transport a diverse array of aromatic, positively charged

substrates in antiport exchange for protons [26]. SMR proteins have overlapping but significantly different substrate specificities with measured affinities in the nM to mM range [27, 28]. Recently, SMR proteins have been subdivided into the multidrug transport protein subclasses small multidrug pumps (SMP), paired small multidrug resistance (PSMR) and suppressor of groEL mutations protein (SUG). The subclassification is based on phylogenetic analysis, different loci on the bacterial genome, homo- or heterooligomerisation and range of substrate specificity [25]. Table 1 gives a short overview of the characteristics of each subclass.

name of subclass	oligomerisation type	substrate specificity	typical member (organism)
SMP	homo	broad	EmrE (*E. coli*)
SUG	homo	narrow	SugE (*E. coli*)
PSMR	hetero	broad	YdgE/F (*E. coli*)

Table 1. Overview of SMR protein subclasses.

A sequence alignment of proteins from each SMR protein subclass is shown in figure 3 and the conserved residues as well as residues for which only conservative substitutions have been found are highlighted here.

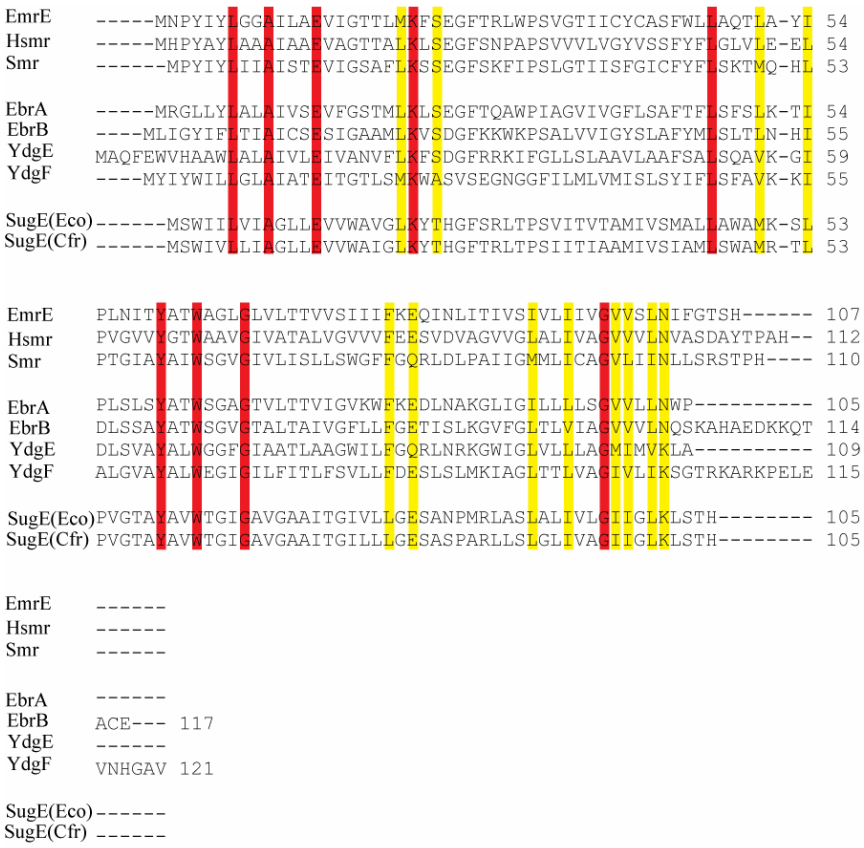

Figure 3. Sequence alignment of selected SMR proteins using ClustalW [29]. Three SMP proteins including the here investigated Hsmr and EmrE are aligned with 2 PSMR protein pairs and 2 SUG proteins. In red conserved residues are highlighted, while yellow indicates that only conservative substitutions are found.

1. 1. 1. 5 EmrE - the SMP subclass model protein

Most investigations have been conducted on EmrE, the model protein of the SMR protein family. EmrE has attracted significant interest for the class of SMR proteins due

to the controversies surrounding its: topological organization [30-34], oligomerisation state [35-38], transport cycle steps [27, 31, 39-41] and initial 3D structures [42, 43] which were later retracted. More precisely, the oligomeric organisation of EmrE has been investigated in detergent a solubilised state and incorporated into a lipid membrane. Different techniques have yielded different results, see table 2, but the accumulated evidence now strongly suggests that EmrE in a detergent or lipid environment is a functional and structural dimer.

oligomeric state	experimental methodology	reference
monomer	isothermal calorimetry	[37]
dimer	EPR (electron paramagnetic resonance) spectroscopy	[44]
	EM (electron microscopy) structure	[45] and [46]
	~~x-ray crystallography structure with substrate~~	[43] retracted
	x-ray crystallographic structure with substrate	[19]
	cysteine crosslinking	[47]
	whole cell growth assay	[48]
	analytical ultracentrifugation and size exclusion chromatography	[35]
	functional complementation of antiparallel proteins	[33]
	in vitro functional complementation	[36]
trimer	*in vivo* and *in vitro* negative dominance	[38]
	radioactive ligand binding	[27]
Tetramer	functional complementation of *in vitro* produced protein	[36]
	~~x-ray crystallography structure~~	[49] retracted

Table 2. Summary of experimental evidence for the EmrE oligomeric state.

Furthermore, the topological organisation of EmrE, with regards to the localisation of the N-terminus and C-terminus, has been investigated using several different techniques; see table 3. Controversial result have been obtained. Data obtained mainly in Professor Schuldiner's laboratory suggests a cytosolic location for the N-terminus and C-terminus and thus parallel dimers are formed. This organisation is expected as membrane proteins are inserted in a unique defined orientation into the membrane using an insertion machinery, which is for *E. coli* cytoplasmic membrane proteins usually the Sec translocase [50]. This machinery is guided by signal sequences and the charge distribution in the loops of membrane proteins [51].
Data obtained in many other laboratories suggest however that EmrE, which has low charge bias in its loops, is inserted in both orientations. The thus obtained EmrE molecules with N_{in}-C_{in} or N_{out}-C_{out} topology have been found to form dimers consisting of two oppositely oriented EmrE protomers. The observation of functional antiparallel EmrE dimers has led to the postulation that EmrE is a so called dual topology protein. The idea of dual topology proteins is highly attractive as it would provide a missing link in protein evolution [52]. Most membrane transport proteins have more than 4 transmembrane helices and show an internal symmetry which could be explained by gene duplication, gene fusion and charge drift. The discovery that the heterooligomeric PSMR proteins are only functional if the protomers are located in the membrane with

opposite topology [53], that PSMR proteins show a strong charge bias imposing a defined orientation in the membrane [54] and the observation that the essential E14 residues in both protomers are not functionally equivalent [55] further support the hypothesis that SMR proteins are indeed dual topology proteins.

topology	Method	reference
parallel dimer	genetically fused dimer	[56]
parallel dimer	antibodies + sulfhydryl reagents	[30]
parallel dimer	EPR	[57]
antiparallel dimer	computer modelling + EM	[58]
antiparallel dimer	charge bias	[33]
antiparallel dimer	x-ray crystallography	[19]
antiparallel dimer	reporter proteins	[59]
antiparallel dimer	mutations shift charge bias	[32]
antiparallel Dimer	cross linking	[60]

Table 3. Experimental evidence for EmrE functional oligomerisation as parallel or antiparallel dimer.

Similarly disputed is the 3D structure of EmrE, table 4, summarises the published attempts. So far only backbone computer model based on EM data of EmrE with TPP^+ (tetraphenyl phosphonium) bound in DMPC (dimyristoylglycero-rac-3-phosphocholin) 2D crystals and a backbone x-ray crystallographic structure of EmrE with TPP^+ bound in the detergent NG (*N*-nonyl-*β*-D-glucoside) are known.

technique	comment	reference / PDB code
solution NMR (nuclear magnetic resonance)	resonance assignment and secondary structure in solvents	[61]
solution NMR	partial resonance assignment and secondary structure of fragments	[62]
EM	7 Å	[45]
EM	with substrate TPP^+, 7 Å	[46]
computer modelling + EM	helix assignment and backbone only	[58]
~~x-ray crystallography~~	~~3.8 Å~~	[42] retracted /1s7b
~~x-ray crystallography~~	~~with substrate TPP^+, 3.7 Å~~	[43] retracted / 2f2m
x-ray crystallography	3.8 Å, backbone only	[19] 3b61
x-ray crystallography	with substrate TPP^+, 3.8 Å, backbone only	[19] 3b5d

Table 4. Structural investigations of EmrE.

The latest and thus far uncontested transport mechanism for EmrE is based partly on the 3D structure model of EmrE in DMPC and measured by electron microscopy. This model suggests that EmrE uses an alternate access mechanism [58]. See figure 4 for a schematic representation.

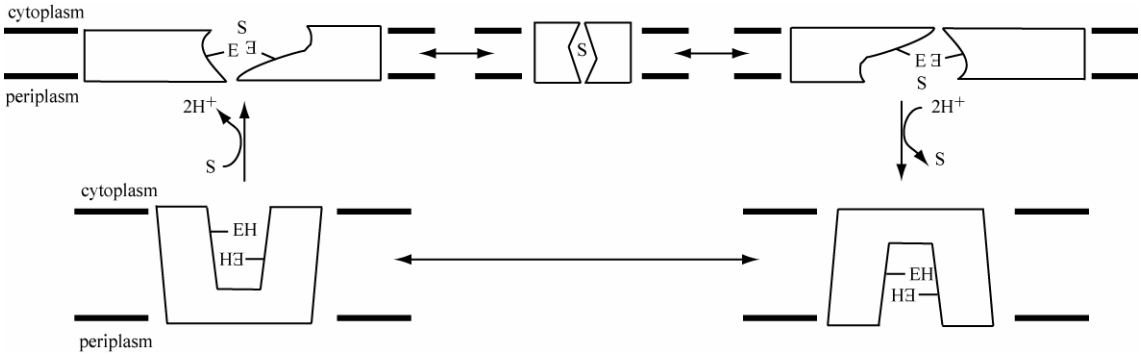

Figure 4. Schematic drawing of proposed alternate access mechanism for substrate transport as proposed by Fleishman *et al.* and modified according to recent findings by Basting *et al.* [58, 63].

The alternate access mechanism is characterised by a high affinity for substrates, a low affinity for protons on the cytoplasmic side and a low affinity for substrates and high affinity for protons on the periplasmic side. Binding of substrate on the cytoplasmic side to the two E14 residues in the dimer induces structural changes which lead to protein reorientation. The transport includes at least one occluded state as first detected in this laboratory [63]. The protein then faces the periplasm and the low substrate but high proton affinity leads to an exchange of substrate for 2 protons at the glutamates. The protonated E14s again cause structural rearrangements which lead to EmrE reorienting toward the cytoplasmic side. This last step couples the uphill substrate transport to the downhill proton transport. In the absence of $\Delta\psi$ and ΔpH gradients the protein is in the equilibrium exchange mode. Substrate can be exchanged non-productively and at a slow rate in both directions [64].

Several aspects regarding SMR proteins are generally undisputed including: E14 in TM helix 1 is an essential residue and directly involved in drug and proton binding [65-67], EmrE has a very broad substrate specificity, see table 5, substrate transport occurs via at least one occluded transport cycle intermediate [63] and the transport of monovalent and divalent substrates has the same stoichiometry, see table 6. This means that the transport of singly charged substrates is electrogenic while the transport of doubly charged substrates to is electro neutral [39].

substrate class	substrate
Dye	ethidium bromide
Dye	acriflavine
Dye	crystal violet
Dye	rhodamine 6G
quaternary ammonium compound	benzalkonium
quaternary ammonium compound	TPP^+
quaternary ammonium compound	methylviologen
antibiotic or bacteriostatic	trimethoprim
antibiotic or bacteriostatic	erythromycin
antibiotic or bacteriostatic	tetracycline
antibiotic or bacteriostatic	chloramphenicol
antibiotic or bacteriostatic	Vancomycin

Table 5. Known substrates of the SMP model protein EmrE [25].

substrate	stoichio-metry with monovalent substrate H^+:substrate	electro-genic transport with mono-valent substrate	substrate	stoichio-metry with divalent substrate H^+:substrate	electro-genic transport with divalent substrate	reference
TPP^+	1:2	Yes	MV^{2+}	1:2	no	[39]
TPP^+, ethidium bromide	1:2	Yes	-	-	-	[65]

Table 6. Stoichiometry of EmrE substrate transport.

1. 1. 1. 6 Hsmr and EmrE

Here work is focussed mainly on the *E. coli* SMR protein EmrE and the archeal SMR protein Hsmr from the halopilic organism *Halobacterium salinarium*. Both proteins are members of the SMP subclass. See figure 5 for a schematic SMR protein topology diagrams.

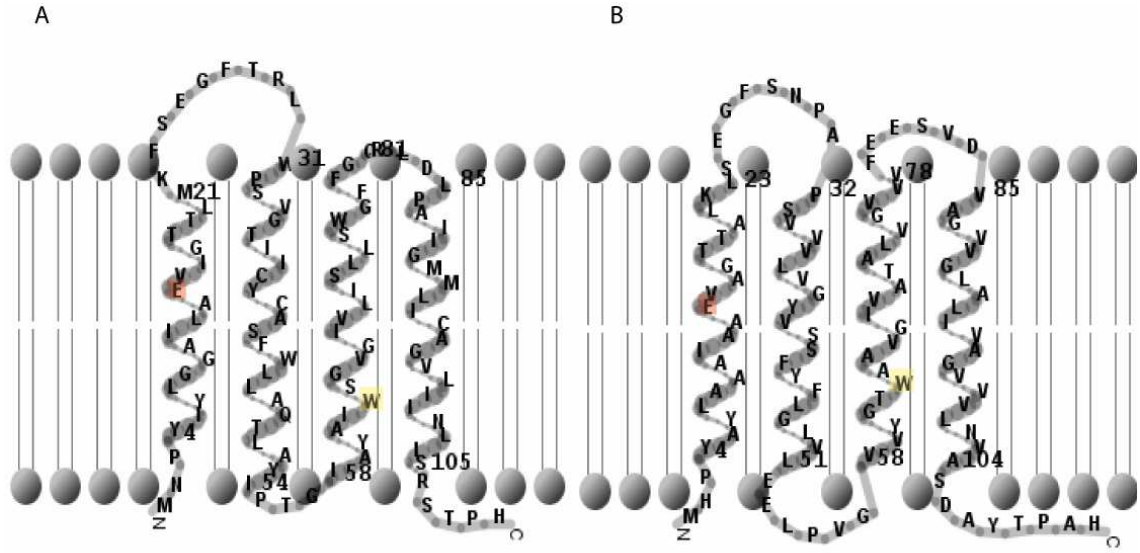

Figure 5. Schematic EmrE and Hsmr topology diagrams. Key residues E14 and W63 are highlighted in red and yellow respectively. A) EmrE and B) Hsmr. The program TMRPres2D was used to generate these diagrams. The TM region as displayed here were predicted previously [25, 28] and were visualised using TMPres2D [68].

In the topology diagram the essential amino acids E14 and W63 are highlighted. It can be seen that EmrE and Hsmr at non-conserved sites differ vastly in their amino acid sequences. Hsmr has a preponderance of alanine and valine residues as well as an increased number of negatively charged amino acids when compared to EmrE. Further key features of EmrE and Hsmr are tabulated in table 7.

protein	residue number	molecular weight (Da)	pI	% A + V amino acids	% + charged amino acids	% - charged amino acids	substrate specificity
Hsmr	112	11293.1	4.2	39.3	0.9	7.2	TPP^+, etbr, bz, ac
EmrE	110	11958.3	7.72	12.7	3.6	2.7	TPP^+, etbr, Bz, MV^{2+}, ac, crystal violet, R6G, SDS, tri, ery, tet, chl, van

Table 7. Main properties of the here investigated SMP proteins. Calculations of properties used the program ProtParam [69]. Etbr (ethidium bromide), bz (benzalkonium), ac (acriflavine), MV^{2+} methyl viologen, R6G (rhodamine 6G), SDS, (sodium dodecyl sulphate), chl (chloramphenicol), tri (trimethoprim), ery (erythromycin), tet (tetracycline) and van (vancomycin).

Noteworthy are the low isoelectric point (pI), large content of alanine and valine residues as well as the large number of negatively charged residues of Hsmr. These features are typical of halophilic proteins. Besides these differences it can be seen that EmrE and Hsmr have overlapping substrate specificity and a selection of these lipophilic substrates, typical for SMR proteins, is shown in figure 6.

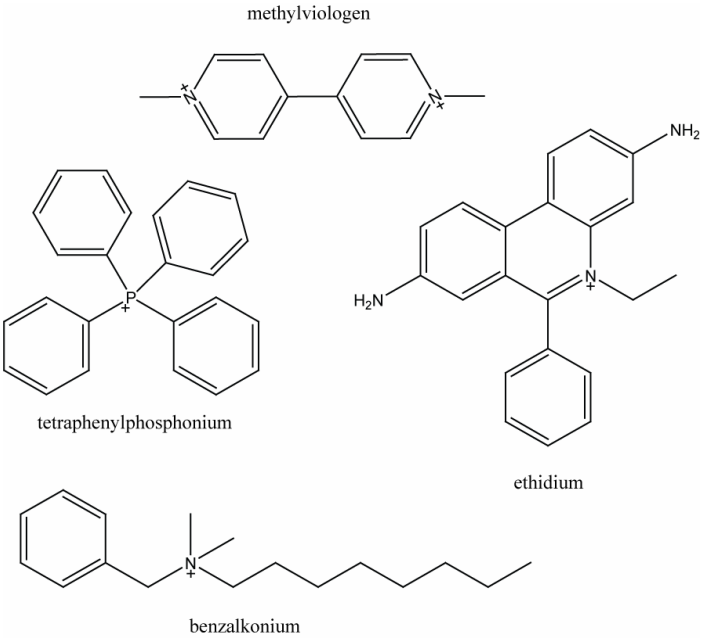

Figure 6. Selection of substrates of SMR proteins. Methylviologen, TPP^+, ethidium and benzalkonium. These substrates are commonly used in SMR protein activity assays. TPP^+, ethidium and benzalkonium are substrates of Hsmr and all four substances are substrates of EmrE.

In contrast to EmrE, Hsmr is poorly investigated. As a halophilic protein Hsmr is inherently difficult to study due to its requirement for high salt concentrations. The first publication describing Hsmr thus merely investigated the activity of unpurified protein and established a salt dependency of activity [28]. A later study circumvented this problem by using synthetic Hsmr transmembrane helix peptides in different detergent solutions and postulated a mechanism for dimeric and tetrameric oligomerisation using two helical faces of TM helix 4 [70]. The special features and challenges of the halophilic proteins are described later. The reduction of amino acid diversity in the transmembrane regions strongly suggests which side of each helix is facing the lipid membrane. This was utilised during the computer modelling of EmrE into the EM electron density to verify the final model [58]. A thorough investigation of Hsmr or any SMP protein other than EmrE has thus far not been conducted.

1. 1. 2 Introduction to halophilicity

1. 1. 2. 1 Introduction to halophiles

Organisms living under inhospitable conditions with respect to, for example, pH, temperature, pressure or salt are called extremophiles and often belong to the archaea domain. Organisms growing at salt concentrations approaching saturation are called halophiles and may be found among eukarya, bacteria and archaea [71]. *Halobacterium salinarium*, an archaea isolated from the Dead Sea, is an aerobic, mesophilic organism, but requires NaCl concentrations of 3.5 to 5 M salt for survival [72], which is the highest known salt tolerance today. *H. salinarium* does not require any further extreme conditions for growth, making it the ideal organism for studying the requirements for adaptation of organisms to high salt conditions.

Extremophiles are of great interest to the biotechnology industry. Thermophilic organisms have been studied in detail, and their proteins have been used in industrial processes in the food, chemical, pharmaceutical and paper sectors [73]. However, the industrial interest for halophiles has lagged behind, due to the lack of business opportunities, and academic interests have been blunted by the many difficulties associated with biochemical investigations in the presence of high salt concentrations. However, understanding halophilicity is becoming an increasingly attractive subject of study, as the biochemical nature of other extremophiles is elucidated and the general salinisation of the soil increases.

1. 1. 2. 2 Characteristics of halophilic proteins and membranes

Survival under high salt concentration requires the halophile to balance the osmotic pressure. This is generally achieved using a combination of compatible solutes such as sugars and amino acid derivatives, as well as high internal salt concentrations [74]. *H. salinarium* matches the outside osmotic pressure generated by 3.5 to 5 M NaCl by accumulating isotonic concentrations of NaCl and KCl in the cytoplasm [75]. Accordingly, both membrane and soluble proteins of halophiles need to be adapted to high salt concentrations. It has been observed that most halophilic proteins have an acidic pI, low lysine and aliphatic residue content but an increased occurrence of alanine, glycine and valine [76] [77].

In general, the presence of salts increases the solubility of a folded protein, but decrease its stability. Halophilic proteins overcome this problem by binding salt and thus screening the extensive network of negatively charged residues which then drives the folding process. The protein then has a salt and a solvation shell [78]. This is known as the solvation-stabilization hypothesis of halophilicity. Furthermore, salting out effects of salts such as NaCl strengthen the hydrophobic interactions which are thought to be

the major determinant of halophilic protein stability [75]. Indeed, salt concentrations larger than 1 M are required for the stability and activity of a protein, with in some cases instantaneous deactivation upon salt removal [75]. Whilst in some cases the salt requirements are salt type specific [78] usually the high salt concentrations are only required for the proteins activity and stability, whereas its structure is also conserved at low salt concentrations [79, 80]. This feature paved the way for the structure determination of several halophilic proteins by x-ray crystallography and NMR. Most notable are the solution NMR structures of HsFdx at 0.45 M NaCl [81] and of hvDHFR1 in the presence of 3.5 M NaCl [80].

Only few halophilic membrane proteins have been investigated directly, with most efforts focussed on genome sequencing or proteomics approaches. Notable exceptions include successful structural investigations of the rhodopsin family (bacteriorhodopsin [82], holorhodopsin [83] and sensory rhodopsin [84]) and non-structural work on an aspartate transport system that could be studied *in vivo* [85], and a CorA homologue involved in Mg^{2+} uptake [86]. Interestingly, ABC transporters seem to be the most prevalent type of transporter in halophiles, and all secondary transporters studied use Na^+ instead of H^+ as the coupling ion [87]. The use of sodium motif force (SMF) instead of the proton motif force (PMF) arises from the higher H^+ than Na^+ permeability of membranes at high salt concentrations [87]. In fact, typical bacterial membranes composed of phospholipids are neither able to support a PMF nor SMF at high salt concentrations and the lipids aggregate. Archaeal membranes are therefore composed of different lipids. The basic types of lipids in archaea are: C20 glycolipids or phospholipids composed of a glycerol or nonitol backbone with ether linked phytanyl chains which form a bilayer and C40 membrane-spanning tetraetherlipids [72, 88]. Figure 7 shows a typical C20 and C40 lipid of *H. salinarium*. The ether linkage between the phytanyl chain and the glycerol backbone make these lipids less prone to aggregation at high salt concentrations and the bulky core is responsible for low proton and Na^+ permeability [89].

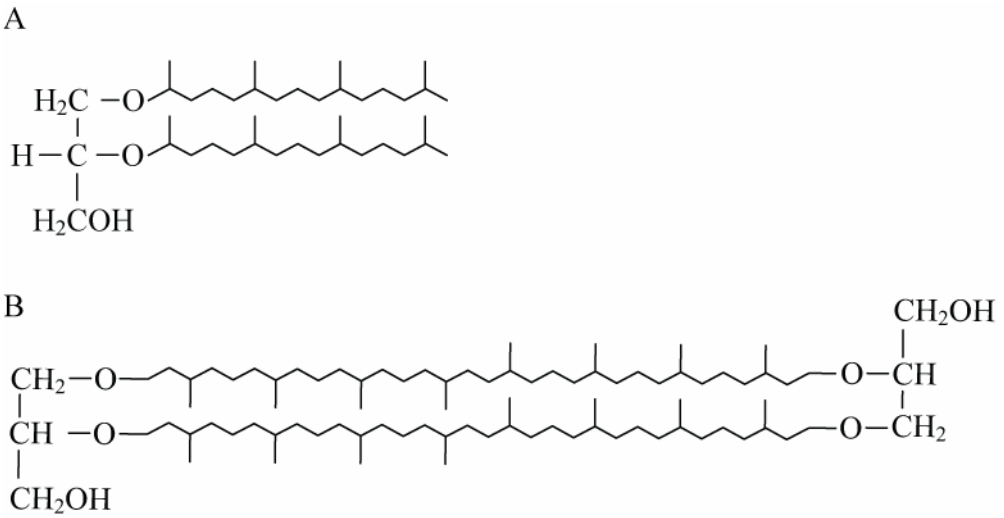

Figure 7 Archaeal lipids. A) C20 lipids sn-2,3-diphytanylglycerol also called archaeol and B) C40 lipids dibiphytanyldiglycerol tetraether also called caldarchaeol. [88]

1. 1. 3 Introduction to cell free expression

1. 1. 3. 1 History of cell free expression

To effectively study membrane proteins using biophysical techniques such as NMR new protein expression techniques such as cell free expression need to be used. Cell free

expression was first described in the 1960s [90]. Since then, many prokaryotic and eukaryotic expression systems have been developed, including: *E. coli*, *Thermus thermophilus*, rabbit reticulocyte, wheat germ, cancer cell and human placental extracts. Crude cell extracts supply the necessary enzymes, ribosomes and cofactors for expression [91] [92]. First attempts to use a cell free protein synthesis system composed solely of purified components were reported in the 1970s [93], and only recently have Shimizu *et al.* succeeded in making an *E. coli* cell free expression system entirely from purified proteins, cofactors and substrates. [94]

Cell free expression can be constituted of either translation or coupled transcription/translation systems, for eukaryotic and prokaryotic systems respectively. Currently, *E. coli* based coupled transcription/translation expression systems are most common. Early cell free expression systems utilized batch mode but the yields were very low due to extract deactivation and exhaustion of substrates [95]. Development of continuous-flow reactors allowed dramatically prolonged production times of up to 40 hours, but the yield only increased marginally due to loss of translation components [96]. Approaches using semi-continuous cell free expression were more successful, and yields up to 6mg/mL have been reported for soluble proteins. [95] [97]

1. 1. 3. 2 *E. coli* based cell free protein synthesis

Using *E. coli* based coupled transcription/translation systems, integral membrane proteins have been expressed and yields of 1 mg/mL for G-protein coupled receptors (GPCRs), [98] 1.3 mg/mL for MscL [99] and 3 mg/mL for EmrE have been achieved [36]. These proteins can be expressed either as precipitate or in the presence of detergents and lipids in a soluble form. However, yields in the presence of detergents are reduced in a detergent dependent fashion, correlating with the detergent cmc. Bacteriorhodopsin for example has been expressed as aggregate in quantities sufficient for biophysical studies such as Fourier transform infrared (FTIR) spectroscopy and could be shown to refold correctly into its native and active conformation using SDS and halobacterial lipids. [100] Furthermore, small multidrug resistance SMR proteins, GPCRs and ion channels have been expressed successfully in the presence of detergents and lipids. These proteins, were shown to be active, and were reconstituted successfully into artificial membranes [36] [99] [98]. However, to obtain typical eukaryotic post-translational modifications, a eukaryotic cell free expression system is necessary.

In conclusion, *in vitro* expression is a viable alternative to *in vivo* expression under many circumstances. A high yield of protein per mass of labeled amino acid used and low detergent and lipid requirements make cell free expression of membrane proteins economically viable despite its inherent high reagent costs [101].

1. 1. 3. 3. Advantages of cell free protein synthesis

A cell free expression system gives the experimenter a high degree of control over experimental parameters such as pH, redox potential or buffer system [102]. Furthermore, the direct manipulation of reaction conditions enables the use of cofactors and unnatural amino acids as well as their addition at any point of time.

For protein NMR studies, cell free synthesis offers the choice of virtually any selective amino acid labeling scheme, due to the absence of a cellular metabolism and greatly minimized amino acid scrambling [103, 104]. This is particularly attractive for amino acid labeling schemes for which no auxotrophic strains are available. Substantial time-savings compared to *in vivo* protein synthesis are achieved. Examples of time-savings are: PCR products can be used as DNA templates, shorter expression times, automation, shorter purification protocol and solution state NMR experiments on unpurified cell free

expression mixture [101, 103, 104]. Finally, even the production of toxic proteins and viruses is possible *in vitro* [102] [105].

1. 1. 3. 4 Advantages for cell free expression of membrane proteins

Especially for membrane proteins, cell free protein synthesis at a preparative scale is appealing, as comparatively high yields, e. g. 3 mg/mL for EmrE, are achievable. Additionally, production of proteins with the *E. coli* based cell free expression system has been reported for proteins that could not be synthesized *in vivo* in *E. coli* [49] [98]. This means that cell free expression systems can be used to obviate the use of elaborate eukaryotic cell culture in some cases. Particularly successful were cell free expression systems for the notoriously difficult to handle class of GPCRs [98, 106, 107].

1. 2 Introduction to NMR

1. 2. 1 Why NMR spectroscopy?

NMR spectroscopy has provided next to x-ray crystallography the largest amount of protein 3D structures. A total of 6924 out of 47407 protein structures in the protein databank are NMR derived (access date 29.11.2007). The vast majority of these were determined by solution state NMR. The quality of NMR structures was evaluated to correspond to a 2.0 Å resolution by x-ray crystallography [108]. As for x-ray crystallography the ease with which a structure can be determined depends mainly on protein stability and homogeneity. Additionally, both structural techniques are challenged by membrane proteins and their requirement for a membrane mimicking environment.

Unlike x-ray crystallography NMR offers not only the possibility to investigate protein structure but also protein dynamics. Particular to solution state NMR however is the limitation to small proteins. Initially, structures were obtained only of proteins with a maximum molecular weight of 12 kDa, isolated from natural sources using ^{1}H NMR of proteins. The use of coherent magnetization transfer by correlation spectroscopy (COSY) spectra was used for spin group assignment and incoherent magnetization transfer by nuclear overhauser enhancement spectroscopy (NOESY) spectra was used to obtain sequential residue assignment, secondary structure information and long-range constraints for structure calculations [109].

The size limitation has currently been stretched to above 100 kDa [110]. This is possible using ^{13}C and ^{15}N isotope labelled proteins in multidimensional NMR spectra, higher magnetic fields and the TROSY technique [111] to solve the problems of resonance overlap. Protein size is critical as it largely determines the rotational correlation time and therefore spectral resolution. A particular challenge for membrane proteins lies in the fact that the membrane mimetics used to provide integral membrane proteins with a native-like environment add to the molecular weight of the protein [112]. The protein detergent complex (PDC) thus determines the rotational correlation time. The largest membrane protein structure solved thus far by solution state NMR is OmpG in Fos-*ß*-choline® 12 (DPC) micelles with a protein only molecular weight of 33 kDa [113].

In contrast, solid state NMR is not inherently limited by the size of the molecule under investigation and thus is ideally suited for the investigation of membrane proteins in lipid environments. Apart from the greater sample preparation flexibility solid state NMR offers the possibility to measure internuclear distances, anisotropy, torsion angles, molecular dynamics and many more parameter with great accuracy. Solid state NMR is an established method in membrane biophysics but only recently is used as a tool for structural biology [114].

1. 2. 2 Brief introduction to NMR

The observed chemical shifts of nuclei are magnetic field strength dependent and for comparison between experiments reported as parts per million (ppm). More precisely the NMR interactions can be described by quantum mechanics using Hamiltonian operator. The general Hamiltonian takes the form:

$$H = H_{Ext} + H_{Int} \tag{2}$$

where $H_{Ext} = H_{RF} + H_0$ (3)

and $H_{Int} = H_{CS} + H_J + H_D + H_Q$ (4)

H = Hamiltoninan, H_{Ext} = external Hamiltonian, H_{Int} = internal Hamiltonian, H_{RF} = radiofrequency Hamiltonian, H_0 = static magnetic field Hamiltonian, H_{CS} = chemical shift Hamiltonian, H_J = scalar/J coupling Hamiltonian, H_D = dipolar coupling Hamiltonian, H_Q = quadrupolar coupling Hamiltonian

which includes all possible NMR interactions. In general solid state NMR is dominated by strong dipolar couplings and quadrupolar couplings and the term H_J can often be neglected.

For spin ½ nuclei such as ^{1}H, ^{13}C and ^{15}N the Hamiltonian simplifies to:

$$H = H_{CS} + H_D \tag{5}$$

For integers spins such as ^{2}H the Hamiltonian simplifies to:

$$H = H_{CS} + H_D + H_Q \tag{6}$$

In a typical solid state NMR experiment a multitude of NMR interactions are simultaneously present and except for the J-coupling these interactions are anisotropic. The higher information content including orientational information however comes at the expense of a more complex spectrum. The design of solid state NMR experiments therefore selectively removes all but the wanted nuclear interactions, leading to easily interpretable spectra with the desired information content. See figure 8 for the effect of the commonly used technique magic angle spinning (MAS) on the lineshape of a ^{13}C glycine spectrum. The fast rotation at the magic angle of 54.7 ° mimics the fast Brownian motion of small molecules in solution and thus removes the anisotropy.

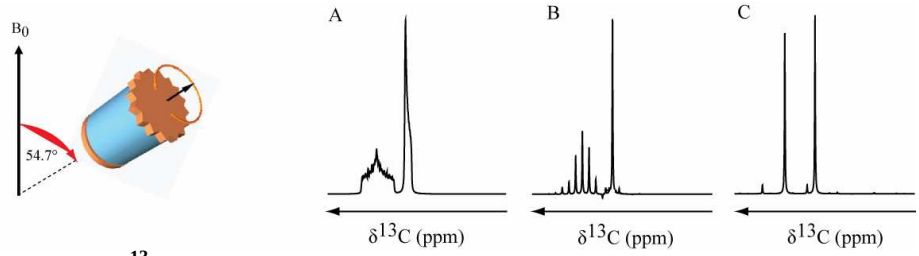

Figure 8. Glycine ^{13}C spectra simulated at different MAS speeds. A) Static spectrum of glycine, B) spectrum of glycine with 3000 Hz MAS and C) spectrum of glycine at 10000 Hz MAS. MAS is a rotation of the sample containing rotor at an angle of 54.7 ° with respect to the external magnetic field B_0. The fast rotation at the magic angle removes anisotropic interactions such as chemical shift anisotropy.

In solid state NMR experiments generally low gyromagnetic ratio nuclei are detected, leading to an intrinsically low signal to noise (S/N) ratio. This ratio can be improved by transferring magnetization from protons to low gyromagnetic ratio nuclei via cross polarisation (CP). During CP dipolar couplings are used to share magnetization between heteronuclei for signal enhancement. CP is the solid state NMR equivalent of a solution state NMR INEPT transfer which uses J-couplings for magnetization transfer between heteronuclei. Both techniques offer an identical theoretical signal enhancement for the low abundant, low gyromagnetic ratio nucleus X. The theoretical limitation of signal enhancement is given by:

$$\frac{\gamma_H}{\gamma_X} \tag{7}$$

γ_H = gyromagnetic ratio of nucleus type H (usually protons) and γ_X = gyromagnetic ratio of nucleus type X

For cross polarisation the so called Hartmann-Hahn match needs to be achieved:

$$\omega_H = \omega_X \tag{8}$$

ω_H = Larmor frequency of nucleus type H and ω_X = Larmor frequency of nucleus type X

which means that the applied radiofrequency B_1 and B_2 need to be adjusted since the gyromagnetic ratios γ are nuclei type dependent.

$$\gamma_H B_1(H) = \gamma_x B_2(X) \tag{9}$$

γ = gyromagnetic ratio, B_1 = magnetic field of radiofrequency pulse, B_2 = magnetic field of radiofrequency pulse, H = arbitrary nucleus (usually protons), X = different arbitrary nucleus (usually ^{13}C or ^{15}N)

To study specific interactions decoupling and recoupling experiments have to be carried out. Details of the experiments used in this thesis are given were relevant in Chapters 2, 8 and 9.

1. 2. 3 Solid State NMR for the Study of Membrane Proteins

Solid state NMR has been widely used in membrane biophysics, to study membrane bound peptides and increasingly for investigations of larger integral membrane proteins. Areas of application cover protein structure and dynamics, lipid-protein, substrate-protein, and substrate-membrane interactions. Static solid state NMR applied to macroscopically ordered membrane samples has been used to elucidate secondary structure and topological organisation of membrane bound peptides [115]. However, for polytopic membrane proteins such as SMR proteins static solid state NMR techniques are of limited use. Instead MAS seems more promising as it imposes fewer restrictions with respect to sample preparations. The number of membrane proteins available for biophysical studies has been dramatically increased by the advent of microbial expression systems (e.g. *E. coli*, yeast and baculovirus) optimized for membrane proteins, the availability of detergent screens and advanced purification technologies in addition to the sequencing of a number of prokaryotic and eukaryotic genomes. Solid state NMR is increasingly applied to isotope labelled membrane proteins in order to derive data about protein structure and dynamics. The possibility of a complete *de novo*

structure determination purely based on MAS NMR recoupling techniques was first demonstrated for small insoluble peptides [116, 117] and has been extended to soluble proteins studied in the solid state [118, 119]. Similar studies with membrane proteins have started to become possible. A number of studies have reported promising MAS NMR spectra of membrane proteins prepared as 2D crystals [120], 3D crystals [121] and also in proteoliposomes [122]. The first successful report of membrane protein assignment by solid state NMR was a 81 % sequence specific assignment of the residues of the α and β subunits of the photosynthetic light-harvesting 2 complex from *Rhodopseudomonas acidophila [123]*. Since then signal assignment and secondary structure determination of H^+ ATP synthase subunit c [124] and 144 kDa complex cytochrome bo_3 oxidase [125] have been reported. Clearly, the preparation of choice are liposomes as they are closest to the proteins native environment. Lipid reconstituted samples also offer the option of investigating the dynamics of the protein as it binds ligands [126], goes through its reaction cycle [127] or responds to changes in the lipid environment [128]. However, the currently very limited knowledge base does not yet allows us to derive general rules about how to prepare membrane proteins for solid state NMR and so screens have to be performed for each individual protein.
The potential role of solid state NMR in the process of drug discovery has been highlighted in a recent review [129]. The structures of ligands and drugs can be determined at their site of action by solid state NMR. This aids in defining the ligand binding site. In addition drug partitioning, drug-lipid interactions and drug polymorphism can be assessed by solid state NMR. It has also recently been shown to be a method capable of determining the backbone structure of a peptide ligand bound to its native GPCR [130]. Indeed these investigations are starting to become routine with structures of bradykinin, neurotensin and histamine being reported recently [130-132]. In this thesis *in vitro* expressed transport proteins are studied with respect to dynamics and ligand binding interactions using solid state NMR.

1. 2. 4 Solid State NMR Studies on Transporters

So far, only a limited number of solid state NMR studies on transporters have been reported [126, 133-142]. Applications cover in principle three areas: interactions of substrates with the membrane, detection of substrates bound to transporters, investigations of individual amino acids and methodological studies describing how to prepare isotope labelled transporters.
The first solid state NMR applications to transporters were presented by the labs of Watts and Henderson who demonstrated the detection of substrate bound to the sugar transporter GalP [137, 140]. This has triggered a number of further studies aimed at obtaining structural information concerning the position of the binding site [139], as well as the ligand/protein association constant [126]. Later it could be shown that isotope labelled transporters can be prepared at a quantity and purity suitable for ssNMR [143]. Recently, uniformLy $^{13}C^{15}N$ labelled EmrE in 2D DMPC crystals has been investigated. The chemical shift of E14 could be assigned using a mutant [136].
During this thesis structural studies on Hsmr, single amino acid investigations on EmrE, protein dynamic studies on Hsmr and drug-membrane interactions were made.

1. 3 Outline of thesis

The aim of this thesis is the investigation of SMR proteins of the SMP subfamily regarding structure, dynamics, oligomerisation state and functionality.
Reported structural investigations of the model protein EmrE have not yet led to a high resolution structure and controversies particularly regarding the topology require further investigations. In fact, most investigations were conducted under non-native conditions

and it is not certain that EmrE is indeed a typical representative of the SMP subfamily These aspects were addressed during this thesis.
Substrate binding to the essential glutamic acid in the proposed EmrE binding pocket was investigated by solid state NMR. And an additional SMP protein, the scarcely studied halopilic protein Hsmr from *H. salinarium* was investigated thoroughly using a variety of biochemical and biophysical techniques, mainly under native high salt conditions. Structural investigations of Hsmr and EmrE utilised among other techniques cell free expression for the production of selectively isotope labelled proteins and non-invasive solid state NMR in native-like lipid membranes. See figure 9 for an overview of all conducted experiments.

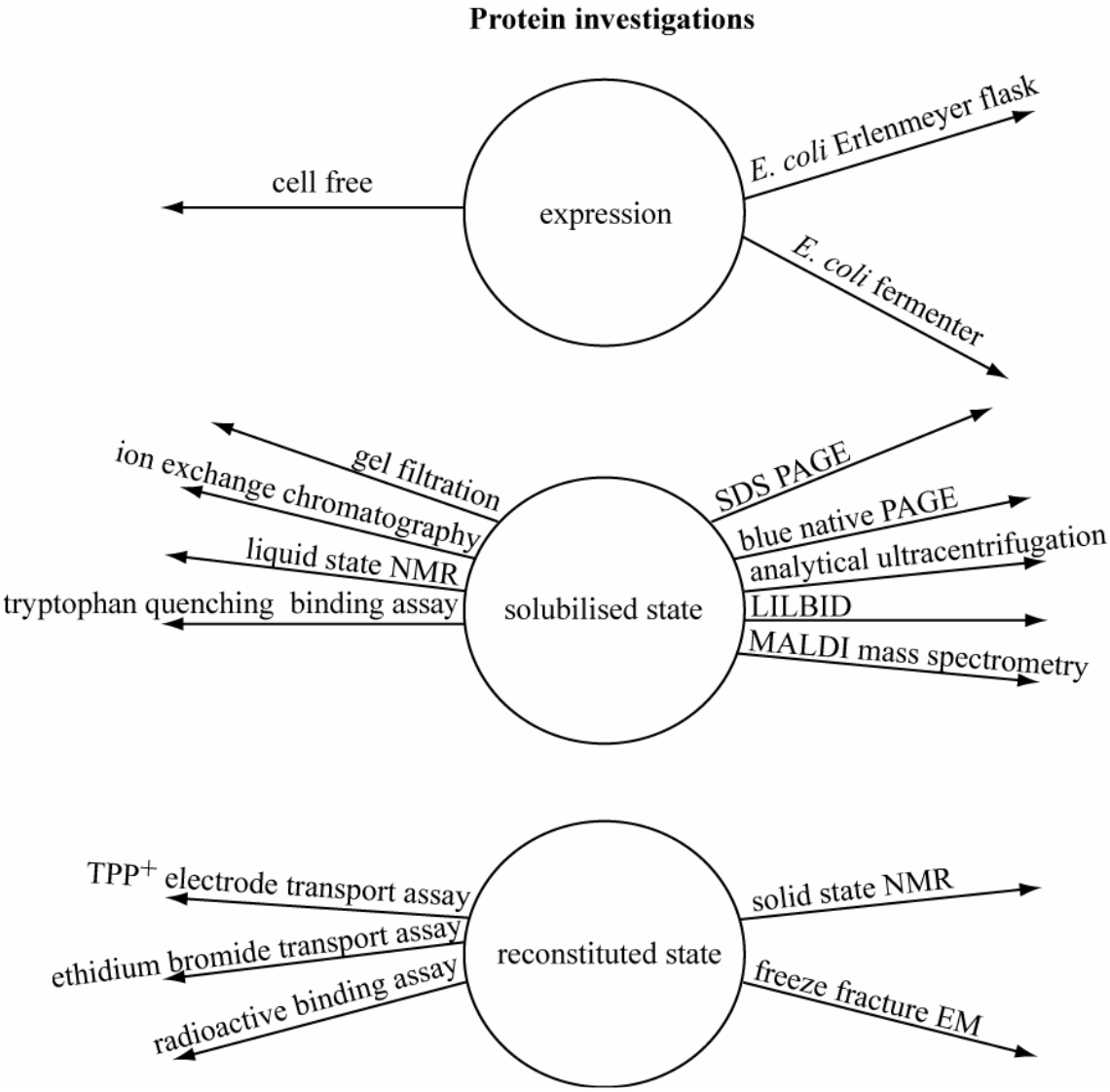

Figure 9. Overview of protein states investigated and methods used.

Chapter 2 - Materials and Methods

2. 1 Materials

2. 1. 1 General materials

Chemicals were purchased from Sigma (München) unless otherwise indicated. The following plasmids were purchased: pT7-7 from USB (Ohio, USA), pET21a+ from Merck KgA (Darmstadt, Germany), pIVEX2.1 from Roche Diagnostics (Mannheim, Germany) and the following *E. coli* cells: *E. coli* strain A19 from CGSC (New Haven, USA), T7 Express, BL21(DE3), XL-1 Blue, CT19 and TA15 from NewEngland Biolabs (Frankfurt am Main, Germany). Molecular biology enzymes were obtained from NewEngland Biolabs (Frankfurt, Germany). Complete protease inhibitors, tRNA 500 were purchased from Roche Diagnostics (Mannheim, Germany). The protein calibration mixture for mass spectrometry (MS) was from Applied Biosystems (Foster City, USA). Radioactive [^{3}H] TPP^+ (30 Ci/mmol) was purchased from GE Healthcare (München, Germany). 1-myristoyl-2-hydroxy-sn-glycero-3-[phospho-RAC-(1-glycerol)] (LMPG), 1-palmitoyl-2-hydroxy-sn-glycero-3-[phospho-RAC-(1-glycerol)] (LPPG), 1,2-diheptanoyl-*sn*-glycero-3-phosphocholine (DHPC) and lipids were obtained from Avanti Polar Lipids (Alabaster, USA). Nondetergent sulfobetaine (NSDB) substances were purchased from Merck KgA (Darmstadt, Germany). Fos-ß-choline® 12 (DPC) was obtained from Anatrace (Maumeen, USA). n-Dodecyl- ß-D-maltoside (DDM) was purchased from Applichem GmbH (Darmstadt, Germany). n-ß-octyl-D-glucopyranoside (OG) was obtained from Glycon Biochemicals (Luckenwalde, Germany). SM-2 Biobeads were obtained from BioRAD (München, Germany). The *E. coli* cell free extract was kindly provided by Birgit Schneider, Sina Reckel and Daniel Schwarz from the group of Prof. Dötsch (Frankfurt, Germany). Vectors coding for SMR proteins were provided by Prof. S. Schuldiner (Jerusalem, Israel) with the exception of pET21a+ EmrE E25A which was supplied by Theofanis Manolikas.

2. 1. 2 Gel and western blot materials

Protein standard for gels were obtained from Applichem (Darmstadt, Germany). 4 - 12 % NativePAGE™ Novex® System gels were ordered from Invitrogen (Carlsbad, USA). The primary antibody mouse anti-c-myc IgG clone 9E10 was purchased from Acris (Hiddenhausen, Germany) and the secondary antibody goat anti-mouse IgG horseradish peroxidase (HRP) conjugate order number sc-2005 was ordered from Santa Cruz Biotechnology (Santa Cruz, USA).

2. 1. 3 Chromatography and dialysis materials

The nickel-nitrilotriacetic acid (Ni-NTA) resin was obtained from Qiagen (Hilden, Germany). Chromatography columns: HiTrap desalting column, DEAE Sepharose fast flow IEX column, Superose 12 medium were from GE Healthcare (München, Germany). The Äkta Economy basic fast protein liquid chromatography (FPLC) system and gel filtration calibration kit were also obtained from GE Healthcare (München, Germany). Dialysis products: 12-14 kDa tubing, microdialyser and dispodialyser were obtained from Spectrum Laboratories Inc. (Breda, Netherlands).

2. 1. 4 Equipment

Western blots were imaged using the Lumi-Imager F1™ from Roche Diagnostics (Mannheim, Germany). The 10 L fermenter used was a Biostat C from Sartorius Stedem (Melsungen, Germany). For ultraviolet (UV) and visible spectrophotometry a Jasco V-550 spectrophotometer (Jasco, Gross-Umstadt, Germany) was used. Fluorescence

measurements were made on a Jasco FP-6500 Fluorescence spectrometer (Jasco, Gross-Umstadt, Germany).
Freeze fracturing was performed using a BAF 060 freeze-fracturing unit from Bal-Tec Inc. (Principality of Lichtenstein). A XL-A analytical ultracentrifuge from Beckman Coulter (Fullerton, USA) with an AN-50 TI rotor from Beckman Coulter (Fullerton, USA) was used for analytical ultracentrifugation. For preparative ultracentrifugation an Optima™ LE-80K ultracentrifuge from Beckman Coulter (Fullerton, USA) was used with rotors TI70, SW28 and SW50.1 all from Beckman Coulter (Fullerton, USA). TPP+ measurements used the calcium specific electrode (MI-600) and a reference electrode (MI-402) from Microelectrodes Inc. (Bedford, USA). Bruker style 4 mm zirconium rotor, KEL-F caps and bottom inserts were obtained from RototecSpintec (Biebesheim, Germany). The Ultraflex time of flight (TOF)/TOF mass spectrometer was from Bruker Daltonics (Bremen, Germany). The Voyager DE-Pro mass spectrometer was from Applied Biosystems (Foster City, USA). Avance and Avance II NMR spectrometer as well as the probeheads were obtained from Bruker Biospin (Rheinstetten, Germany).

2. 1. 5 Software

Numerical data analysis was carried out using algorithms supplied and programmed into OriginPro 7.5 by OriginLAB (Northampton, USA). A python script for visualising typical amino acid double quantum single quantum (DQSQ) spectra was written by Dr. J. Lopez. For the full matrix analysis of NOESY peak volumes python scripts written by Dr. J. Lopez were used. Potential measurements of the TPP^+ assay were recorded and analyzed with MetraHit and MetraWin10 were from Gossen Metrawatt (Nürnberg, Germany). Acquisition and analysis software used for NMR includes Topspin 1.3, Topspin 2.0 and XWIN-NMR Version 3.5 all from Bruker Biospin (Rheinstetten, Germany), Sparky 3 from Goddard and Kneller at the University of California (San Francisco, USA) and CARA 1.8.4 [144]. Reference spectra and typical chemical shifts of amino acids were obtained from the Biological Magnetic Resonance Bank (BMRB). The MS spectra were processed with Data Explorer Software from Applied Biosystems (Foster City, USA) or Flex Analysis v2.2 from Bruker Daltonics (Bremen, Germany). Topology models were generated using TMPres2D [68].

2. 2 Methods

2. 2. 1 Cloning procedures

For this study, YdgF was cloned into a pT7-7 vector with myc-his tag, see figure 10 for pT7-7 vector map. YdgF was amplified from genomic *E. coli* DNA kindly provided by Dr. F. Bernhard using a forward primer (cag gag aag gca tat gta tat tta ttg g) and a reverse primer (gtg aac cga att caa ctg cgc). The amplified fragments and Hsmr pT7-7 vector were digested with NdeI and EcoRI. The YdgF fragments were dephosphorylated and ligated into the vector using T4 DNA ligase.

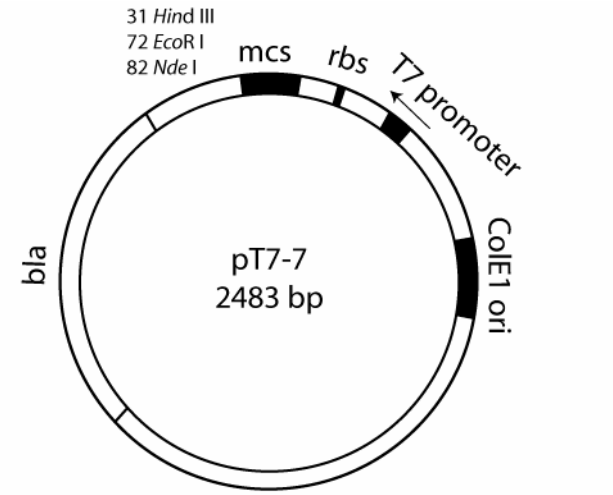

Figure 10. pT7-7 vector as originally designed. Most SMR proteins were expressed from this vector *in vitro* and *in vivo* with a myc-his tag, using NdeI and EcoRI as restriction enzymes. multiple cloning site (mcs), ribosomal binding site (rbs), beta lactamase (bla), origin (ori)

2. 2. 2 Protein production

2. 2. 2. 1 *In vitro* expression of SMR proteins

Bacterial cell-free extracts also called S30 extract were prepared from the *E. coli* strain A19 in a procedure modified after Zubay [145]. The cells were washed in buffer (10 mM Tris-acetate, pH 8.2, 14 mM $Mg(OAc)_2$), with 6 mM 2-mercaptoethanol and 0.6 mM KCl. The lysis buffer was the washing buffer supplemented with 1 mM dithiothreitol and 0.1 mM phenylmethanesulfonylfluoride.

The extract was dialyzed in washing buffer supplemented with 0.5 mM dithiothreitol and 0.6 mM KOAc. Endogenous mRNA was removed from the ribosomes by incubation of the extract with 400 mM NaCl at 42 °C for 45 min. Aliquots of the cell-free extract were frozen in liquid nitrogen and stored at -80 °C. The cell-free expression was performed in the continuous exchange mode using a membrane with a cutoff of 25 kDa for GFP and 15 kDa for all other proteins, to separate the reaction mixture (RM) containing ribosomes and all enzymes, from the feeding mixture (FM) providing the low molecular mass precursors. The ratio of RM/FM was 1:17 (v/v). This expression mode yields membrane proteins as precipitates. Reactions in the analytical scale of 70 µL were performed in microdialysers, and larger dispodialysers were used for preparative scale reactions with RM volumes of 500 µl to 1 mL. The reactions were incubated at 30 °C in a suitable shaker for 20 h.

The protocol for the cell-free reaction mixtures is given in table 8. Amino acid concentrations were adjusted with regard to the amino acid composition of the overproduced proteins. The least abundant amino acids (present at less than 3 % in the protein) were added at 1.25 mM, medium abundant (between 3 % and 8 %) at 1.8 mM and highly abundant (more than 8 %) at 2.5 mM final concentration. Amino acid specific labeling was achieved by replacing the corresponding amino acids by their isotopically labeled derivatives. For the soluble expression, mode detergents need to be added to the RM and FM at concentrations above their cmc.

component	final concentration in RM	final concentration in FM
S30-extract	35 %	-
Tris-acetate, pH 8.2	3.5 mM	3.5 mM
plasmid DNA	15 µg/mL	-
RNAsin	0.3 U/µL	-
T7 RNA polymerase	3 U/µL	-
E. coli tRNA 500	500 µg/mL	-
pyruvate kinase	40 µg/mL	-
acetyl phosphate	20 mM	20 mM
phosphoenol pyruvate	20 mM	20 mM
ATP	1.2 mM	1.2 mM
CTP	0.8 mM	0.8 mM
GTP	0.8 mM	0.8 mM
UTP	0.8 mM	0.8 mM
1.4-dithiothreitol	2 mM	2 mM
folinic acid	0.2 mM	0.2 mM
complete protease inhibitor	1 tablet per 10 mL	1 tablet per 10 mL
4-(2-hydroxyethyl)-1-piperazineethanesulfonic acid (HEPES)-KOH pH 8.0	100 mM	100 mM
ethylenediaminetetraacetic acid (EDTA)	2.8 mM	2.8 mM
magnesium acetate	13 mM	13 mM
Potassium acetate	290 mM	290 mM
polyethylenglycol 8000	2 %	2 %
sodium azide	0.05 %	0.05 %

Table 8. Protocol for cell-free protein expression. Amino acids were adjusted according to the composition of the expressed protein.

2. 2. 2. 2 *In vivo* shake flask expression of Hsmr and EmrE

Overexpression and purification of SMR proteins were adapted from protocols described [41, 146]. *E.coli* cells were grown at 30 °C (TA15) or 37 °C (all other cells) in Luria Bertani (LB) media. See table 9 for *E. coli* strains and plasmids used. 750 mL LB or other medium, see table 9 for media compositions, containing 100 µg/mL ampicillin in a 2 L flask was inoculated with 15 mL of overnight culture.

Expression of SMR proteins was induced with 0.5 mM IPTG (all cells except TA15) or a temperature shift to 42 °C for 20 min (TA15 cells only), at a cell density of A_{600}=1. Two hours later the cells were harvested by centrifugation (3800 *g* for 10 min at 4 ºC), washed with (100 mM NaCl, 10 mM Tris, 1 mM EDTA, pH 8) and pelleted by centrifugation (3800 *g* for 10 min at 4 ºC).

strains and plasmids	relevant genotype	reference
XL1-Blue	*recA1 lac[F'Tn10 (Tet) lacI lacZM15]*	[147]
A19	*rna19 gdhA2 his95 relA1 spoT1 metB1*	[148]
CT19	BL21(DE3) + *aspC, ilvE, trpB, tyrB, avtA*	[149]
BL21(DE3)	F^- *ompT gal dcm lon* $hsdS_B(r_B^- m_B^-)$ *λ(DE3 [lacI lacUV5-T7 gene 1 ind1 sam7 nin5])*	[150]
T7 Express	BL21(DE3) + *fhuA2 lacZ::T7 gene1 [lon] ompT gal sulA11 R(mcr-73::miniTn10--*Tet^S*)2 [dcm] R(zgb-210::Tn10--*Tet^S*) endA1 Δ(mcrC-mrr)114::IS10*	[151]
TA15	*melBLid nhaA1 nhaB1 lacZY*	[152]
GFP	in pIVEX 2.1	Roche
Hsmr	*hsmr NdeI-EcoRI* in pT7-7 with myc-his tag	[28]
EmrE	*emrE NdeI-EcoRI* in pT7-7 myc-his tag	[27]
EmrE E25A	*emrE NdeI-HindIII* in pET21a(+) with his tag	[153]
EmrE CAMY	*emrE NdeI-EcoRI* in pT7-7 myc-his tag	[154]
TBsmr	*tBsmr NdeI-EcoRI* in pT7-7 myc-his tag	[155]
YdgF	*ydgF NdeI-EcoRI* in pT7-7 myc-his tag	this study

Table 9. Bacterial strains and plasmids used. pT7-7 vector map in figure 10 and pET21a+ vector map in figure 11.

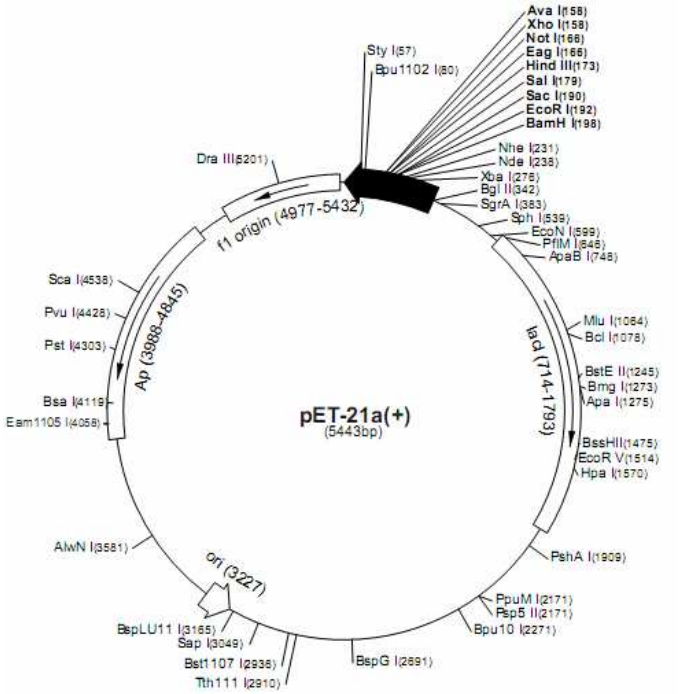

Figure 11. pET21a(+) vector map. EmrE E25A with his tag was cloned into this vector with *NdeI* and *HindIII* and expressed in the cell free expression system from this vector.

2. 2. 2. 3 Fermenter expression of Hsmr and EmrE

Expression of SMR proteins in a 10 L Biostat C fermenter was essentially as described for Erlenmeyer flask cultures. The aeration rate was 5 L/min and the broth was stirred at 300 rpm. The fermenter was inoculated with 100 mL preculture in minimal medium. Fermenter expressions were always induced by heat shock and either minimal or high cell density minimal medium, see table 10, was used.

name of medium	type of medium	Composition
LB	rich	25 g/L LB
2xyeast tryptophan (YT) [156]	rich	16 g/L tryptone, 5 g/L NaCl, 10 g/L yeast extract
minimal media [157]	synthetic	60 mM K_2HPO_4, 33 mM KH_2PO_4, 7.5 mM NH_4SO_4, 0.83 mM $MgSO_4$, 2.5 mM thiamine, 22 mM glucose or 11 mM ^{13}C glucose
minimal media (high cell density)	synthetic	60 mM K_2HPO_4, 33 mM KH_2PO_4, 12.5 mM NH_4SO_4, 0.83 mM $MgSO_4$, 2.5 mM thiamine, 222.4 mM glycerol
defined media [158]	synthetic	5.56 mM L-alanine, 1.9 mM L-arginine, 3.01 mM L-aspartic acid, 2.85 mM L-cysteine, 2.74 mM L-glutamine, 4.42 mM L-glutamic acid, 7.33 mM L-glycine, 6.44 mM L-histidine, 1.75 mM L-isoleucine, 1.75 mM L-leucine, 2.3 mM L-lysine, 1.68 mM L-methionine, 7.87 mM L-phenylalanine, 8.69 mM L-proline, 19.98 mM L-serine, 1.93 mM L-threonine, 0.94 mM L-tyrosine, 1.96 mM L-valine, 3.7 mM adenine, 2.29 mM guanosine, 1.59 mM thymine, 4.46 mM uracil, 1.8 mM cytosine, 18 mM sodium acetate, 12.7 mM succinic acid, 9.35 mM NH_4Cl, 21.25 mM NaOH, 60.27 mM K_2HPO_4, 0.01 mM $FeCl_3$, 4 mM $MgSO_4$, 110 mM D+glucose, 13.6 µM $CaCl_2$, 6.96 µM $ZnSO_4$, 11.8 µM $MnSO_4$, 0.24 mM L-tryptophan, 0.15 mM thiamine, 0.41 mM niacin, 4.1 µM D-biotin

Table 10. *E. coli* growth media.

2. 2. 3 Protein purification

Cells were resuspended in 5 mL lysis buffer/g wet cells (250 mM sucrose, 150 mM NaCl, 10 mM Tris-Cl pH 7.5, 2.5 mM $MgSO_4$, DNase I) and broken three times in a cell disrupter at 1.5 kbar. Cell debris was removed by centrifugation at 4550 *g* for 10 min. After centrifuging the supernatant at 223.000 *g* for 30 min, the membrane fraction was washed with (100 mM NaCl, 10 mM Tris, 1 mM EDTA, pH 8) for 45 min, centrifuged at 223.000 *g* for 30 min collected, frozen in liquid nitrogen and stored in fractions at -80 ºC until usage.

In vitro (soluble and precipitate) produced SMR proteins and *in vivo* produced membrane pellets were diluted into 25 mL solubilising buffer (2 M NaCl, 15 mM Na_xH_xPO4 pH 8.0, 10 mM imidazole, 1 % (w/v) DDM and complete protease inhibitor) for Hsmr or (100 mM NaCl, 50 mM Tris, pH 8.0, 1 mM DTT, 10 mM imidazole, 1 pill mini complete protease inhibitor and 1 % (w/v) DDM) for EmrE and incubated for 1 h at room temperature (RT). After removal of the unsolubilised components by centrifugation (184000 g, 50 min), the supernatant was mixed with Ni-NTA resin for 80 min at 4 ºC in a beaker. The resin was washed with wash buffer (2 M NaCl, 15 mM NaxHxPO4, pH 8.0, 30 mM imidazole, 0.1 % (w/v) DDM) for Hsmr or (100 mM NaCl, 50 mM Tris, pH 8.0, 1 mM DTT, 30 mM imidazole and 0.1 % (w/v) DDM) for EmrE until A_{280} was below 0.05.

The protein was eluted with the same buffer containing 300 mM imidazole and the approximate protein concentration was determined at A_{280} using the elution buffer as a blank.

2. 2. 4 Gel analysis

2. 2. 4. 1 SDS-polyacrylamide gel electrophoresis (PAGE)

Gels for SDS-PAGE were 10 % gels and run in a two buffer system [159]. The separation gel (25 % (v/v) 40 % acrylamide/bisacrylamide mixture, 43.6 % (v/v) gel buffer (3 M Tris pH 8.45, 0.3 % (w/v) SDS), 31.4 % (v/v) H_2O, 0.75 % (v/v) ammonium persulfate (APS) and 0.075 % (v/v) tetramethylethylendiamin (TEMED)) was cast first at RT and sealed from air with H_2O. After polymerization is completed, the stacking gel (10 % (v/v) 40 % acrylamide/bisacrylamide mixture, 20 % (v/v) gel buffer, 70 % (v/v) H_2O, 0.8 % (v/v) 10 % APS solution, 0.08 % (v/v) TEMED) is cast and a comb with 10 or 15 teeth is inserted. Samples were diluted 2 fold in loading dye (4 % (w/v) SDS, 12 % (w/v) glycerol, 50 mM Tris, 2 % (v/v) mercaptoethanol, 0.01 % (w/v) Serva blue G, pH 6.8) and applied to the gel just prior to the run. Gels are run with cathode buffer (0.1 M Tris, 0.1 M tricine, 0.1 % (w/v) SDS, pH 8.3) and anode buffer (0.2 M Tris, pH 8.9) at RT for 30 min at 25 V and the remaining time at 150 V.

2. 2. 4. 2 Blue native PAGE (BNPAGE)

BNPAGE utilized either home-made gradient gels with 4-18 % acrylamide concentration or 4-12 % NativePAGE™ Novex® System gels. The gradient gel recipe can be found in table 11. The 6x gel buffer contains 150 mM imidazole pH 7.0 and 54.6 % (w/v) amino caproic acid. Precooled gradient mixer and gradient gel pouring device are assembled in the cold room. The stacking gel is cast first, followed immediately by the gradient gel. A plug solution (33 % (v/v) 6x gel buffer, 67 % (v/v) glycerol) was used to push the gel solution completely into the casting chamber.

To achieve the best quality gels casting is performed as slow as possible in the cold room and the gels are left to polymerize overnight. Samples are applied in their own buffer with glycerol added to reach 10 % (v/v). The gels are run in the cold room with room temperature anode buffer (50 mM NaCl, 5 mM amino caproic acid, 1.25 mM EDTA, 50 mM imidazole pH 7.0) and cathode (50 mM tricine, 75 mM imidazole, 0.002 % (w/v) coomassie brilliant blue G250) buffer. Initially the gels are run at 50 V for 20 min, then for around 40 min at 250 V. As standards ferritin, catalase and bovine serum albumin (BSA) are used.

Protein solutions analyzed contained 1-30 µg Hsmr or standard proteins. Hsmr was generally dialyzed against 15 mM Tris, pH 8.0, 0 M NaCl before analysis. The gels are scanned directly after the run, fixed, stained, destained and scanned again. The recipes here are based on publications by Prof. Schägger [160, 161].

chemical	4 % gel mixture	18 % gel mixture
water	9.77 mL	0.35 mL
6x gel buffer	2.33 mL	2.0 mL
30 % acrylamide/bis-acrylamide mixture	1.86 mL	7.2 mL
80 % glycerol	-	2.4 mL
TEMED	7.5 µl	5.0 µl
10 % ammonium persulfate	75 µl	50 µl

Table 11. Pipetting scheme one set of small for gradient gels.

2. 2. 4. 3 Coomassie staining of PAGE

The staining method is particularly suitable for small membrane proteins [159]. Gels are fixed (50 % methanol, 10 % acetic acid) for 30 min, stained (10 % acetic acid, 0.025 % (w/v) coomassie brilliant blue G250) for 2 h and destained (10 % acetic acid) until a crystal clear background is achieved. All steps at RT with 100 mL of each solution and gentle agitation.

2. 2. 4. 4 Western blot

Protein samples were separated using the standard SDS-PAGE procedure and 12 % acrylamide/bisacrylamide gels. A prestained protein standard was used to allow assessment of the success of the blotting step. Sandwich of mats and wetted filter paper ensure tight contact between the gel and nitrocellulose membrane during the blotting step for 1 h at 4 °C at 350 mA in transfer buffer (0.3 % (w/v) Tris, 1.44 % (w/v) glycine). The membrane is blocked in 25 mL (0.242 % (w/v) Tris, 0.8 % (w/v) NaCl, 0.1 % (v/v) Tween 20, pH 7.6) with 1.25 g milk powder for 1 h at RT, washed three times at RT with 25 mL (0.242 % (w/v) Tris, 0.8 % (w/v) NaCl, 0.1 % (v/v) Tween 20, pH 7.6) and incubated with the primary antibody mouse anti-c-myc IgG clone 9E10 at 1:500 dilution in (0.242 % (w/v) Tris, 0.8 % (w/v) NaCl, 0.1 % (v/v) Tween 20, pH 7.6) for 1 h at RT. The membrane is washed three times at RT with 25 mL (0.242 % (w/v) Tris, 0.8 % (w/v) NaCl, 0.1 % (v/v) Tween 20, pH 7.6) and incubated 1 h at RT with the secondary antibody goat anti-mouse IgG horseradish peroxidase (HRP) conjugate at a 1:10000 dilution in (0.242 % (w/v) Tris, 0.8 % (w/v) NaCl, 0.1 % (v/v) Tween 20, pH 7.6).

The membrane was washed three times at RT with (0.242 % (w/v) Tris, 0.8 % (w/v) NaCl, 0.1 % (v/v) Tween 20, pH 7.6) and equal volumes of the HRP assay solutions (2.5 mM luminol, 0.4 mM p-cumaric acid, 100 mM Tris, pH 8.5) and (0.02 % (v/v) H_2O_2, 100 mM Tris, pH 8.5) were added for 1 min prior to luminescence detection using the Lumi-Imager F1™.

2. 2. 5 Protein concentration determination

2. 2. 5. 1 Protein concentration measurement by absorption spectroscopy

The concentration of purified proteins can be calculated from the absorption at 280 nm if the extinction coefficient (ε) is known. The Beer-Lambert Law is used for this calculation:

$$A = \varepsilon * l * c \qquad (10)$$

A= absorbance at 280 nm, ε= extinction coefficient, l= path length of the cuvette, c= concentration of the sample

protein	vector	tag	ε (M^{-1} cm^{-1})
Hsmr	pT7-7	myc-his	15930
EmrE	pT7-7	myc-his	31065
EmrE E25A	pET21a+	his	29575

Table 12. Extinction coefficients of SMR proteins for concentration measurements by UV absorption spectroscopy.

2. 2. 5. 2 Amido black assay

The amido black total protein concentration determination is insensitive to detergents and lipids and thus used for the measurement of total protein concentrations in membrane patches [162].

Protein samples containing 2 - 24 µg protein were diluted with water to 2 mL. 0.2 mL 10 % SDS was added and the sample vortexed. 0.3 mL Tris solution (1 M Tris, pH 7.5, 1 % SDS (w/v)) was added and the sample vortexed. 0.6mL 100 % trichloroacetic acid (TCA) are added and the sample vortexed. The samples are incubated for more than 3 min and the solutions spotted onto individual filter in a vacuum manifold. Vacuum is applied and each filtered washed with 6 % TCA. The filters are stained in 200 mL staining solution (45 % methanol, 10 % acetic acid) for 3 min under stirring. Rinse the filters with 200 mL water and wash three times with destaining solution (90 % methanol, 2 % acetic acid) under stirring for 1 min. The filters are washed once for 2 min in water. The filters were dried and the blue spots cut out. The blue spots are added to a plastic tube with 0.7 mL solubilising solution (25 mM NaOH, 0.05 mM EDTA in ethanol) and incubated for 20 min with repeated vortexing. The absorbance at 630 nm was measured and the protein concentration calculated from a standard curve.

2. 2. 6 Reconstitution protocols

2. 2. 6. 1 Reconstitution of Hmsr and EmrE

SMR proteins were reconstituted at various protein/lipid mol ratios during screens. For all reconstitution methods, 4 mg/mL lipid was used as stock solution. A protein/lipid mol ratio of 1:100 for solid state NMR, and a 1:450 mol ratio for fluorescence spectroscopy were best.

The optimal conditions used DDM mediated destabilization of *E. coli* total liposomes with a 1:2 lipid:detergent mol ratio and with biobeads mediated detergent removal. In detail, protein and lipid/detergent solutions were mixed and incubated for 1 h at RT, followed by detergent removal using pre-washed and sonicated SM-2 Biobeads. In total 3 times 30 mg biobeads/mg detergent were added and incubated for 1h at RT and once at 4 ºC overnight. Biobeads were removed and the liposomes pelleted by centrifugation. Detergent destabilization is achieved at R_{sat}, while liposome solubilisation is achieved at R_{sol}. Spectroscopically both points can be determined by light-scattering measurements at 540 nm. R_{sat} has the highest optical density and R_{sol} is reached at the lowest optical density following R_{sat}. Theoretically, R_{sat} and R_{sol} can be calculated using the following equation [163]:

$$D_{total} = D_{water} + R_{eff} * [lipid] \quad (11)$$

D_{water} = detergent cmc in the presence of lipids in mM, R_{eff} = effective detergent:lipid ratio in mixed lipid-detergent aggregates, [lipid] = concentration of lipids in mM

Reconstitution without liposome presoftening was performed as described but omitting the destabilization step. Reconstitution by gel filtration as described by Kiefer [164] was performed in the absence of imidazole. The bound protein was washed slowly with 20 column volumes (CV) of buffer with 4 mg/mL lipids. The thus reconstituted protein was then eluted in buffer containing 300 mM imidazole. Reconstitution by rapid dilution simply mixes the protein/detergent solution quickly with a sonicated lipid solution that reduces the detergent concentration below the critical micellar concentration (cmc) and thus forces the protein into liposomes [165]. Reconstitution using organic solvents (chloroform:methanol 1:1 ratio) first dried the protein preparation under a stream of nitrogen and then the protein was solubilised in buffer (2 M NaCl, 15 mM $Na_xH_xPO_4$, pH 8.0) by sonication [166].

2. 2. 6. 2 Preparation of EmrE E25A for NMR

EmrE E25A on a pET21a+ vector was produced as described above. Substrate incubation was performed for 30 min at RT with 3 µM etbr in the buffer (100 mM NaCl, 50 mM Tris, pH 8.0 and 1 mM dithiothreitol (DTT)). The etbr concentration was chosen to theoretically provide greater than 99 % occupancy at the binding site.

2. 2. 6. 3 Preparation of alanine-*d3* labelled Hsmr

Expression of Hsmr for the ^{2}H NMR study was conducted as described above but with the following exceptions. *In vivo* labelling with alanine-*d3* utilised the auxotrophic strain CT19. The cells were grown in unlabelled defined medium to a cell density of A_{600} = 1, pelleted at 25 °C for 5 min and resuspended in 1/4th volume defined medium containing alanine-*d3* [167]. After 10 min Hsmr expression was induced with 0.5 mM isopropyl β-D-1-thiogalactopyranoside (IPTG) and 10 min later bacterial DNA-dependent RNA polymerase was inhibited with 1 mg rifampicin per L medium [168]. Prior to NMR measurements Hsmr reconstituted in *E. coli* total lipids was washed twice with buffer made with D_2O depleted water. After the NMR measurements without substrates were completed the sample was removed from the rotor and incubated in 400 µL 2 M NaCl, 15 mM Na_xH_xPO4, pH 8.0 made with D_2O depleted water and 50 mM etbr for 30 min at RT. The sample was collected by centrifugation and returned to the MAS rotor for further NMR measurements.

2. 2. 6. 4 Freeze fracture analysis

Proteoliposomes in sample holders were frozen in ethane cooled to -180 ^{o}C by liquid nitrogen. Fracturing at –120 ^{o}C and replication at a shadowing angle of 45 ^{o} with platinum/carbon was performed with a BAF 060 freeze-fracturing unit. Freeze fracture analysis was performed by Dr. Winfried Haase at the Max Planck Institute of Biophysics.

2. 2. 7 Protein activity assay

2. 2. 7. 1 Radioactive assay TPP^+ binding assay

TPP^+ binding was assayed essentially as described in [27]. Briefly, Ni-NTA beads (20 µL/assay) were washed once in distilled water and twice in standard high salt buffer (2 M NaCl, 15 mM $Na_xH_xPO_4$, pH 8.5, 1 % DDM). The purified protein was added to the washed beads and the detergent concentration increased to 1 % DDM. The protein/bead mixture was mixed at 4 °C for 1 h. The unbound material was discarded, and the His-tagged protein bound to the beads was washed three times with 1 % DDM containing high salt buffer. Buffer containing 40 nM [^{3}H]TPP^+ was added, and the samples were incubated for 20 min at 4 °C. In each experiment, the values obtained in a control reaction with 40 µM unlabeled TPP^+ were subtracted. Separating the beads from the supernatant by pulse centrifugation stopped the binding reaction. The bead fraction was then incubated for 10 min at room temperature with 450 µl of 1 % DDM containing 300 mM imidazole in order to release the His-tagged protein from the beads. After spinning down the beads, the [^{3}H]TPP^+ associated radioactivity was measured by liquid scintillation. All binding reactions were performed in triplicate.

2. 2. 7. 2 Binding study using intrinsic tryptophan fluorescence

Fluorescence was recorded with a Jasco FP 6500 Fluorescence spectrometer. Excitation at 295 nm (bandwidth 2.5 nm) was used to selectively excite tryptophans and an emission wavelength at 330 nm (bandwidth 5 nm) was measured. All experiments were carried out in a 1x1 cm quartz cuvette in standard high salt buffer (2 M NaCl, 15 mM $Na_xH_xPO_4$, pH 8.5, 0.1 % DDM) at 25 °C. Hsmr at a final concentration of 4 µM was

used. TPP^+ or benzalkonium were added in sample buffer. The quenching of tryptophan fluorescence by substrate binding was analyzed using the binding equation as modified by Poget *et al*. [169].

$$y = P1/(2 * m) * (m + P2 + x)\text{^}2 - 4 * m * x)\text{^}0.5) + P3 * x \quad (12)$$

P1 = ΔF_{max} (difference between maximal fluorescence intensity of protein and protein + substrate), P2 = dissociation constant (K_d), P3 = fraction of non-specific TPP^+ binding, m = protein concentration

2. 2. 7. 3 Ethidium bromide transport assay

2. 2. 7. 3. 1 Bacteriorhodopsin

Bacteriorhodopsin (bR) in purple membrane patches was prepared from *Halobacterium salinarium* strain JW5, as described previously [127]. Purple membrane was used directly after density gradient purification with three additional washing steps to remove the sucrose [170].

2. 2. 7. 3. 2 Reconstitution of Hsmr

10 mg of *E. coli* total lipids were solubilised in 1 mL of 150 mM KCl, 1 M NaCl, 5 mM K-EDTA, pH 7.3 and 20 mg/mL DDM. Different NaCl concentrations were initially tested. To 0.752 mL of the resulting suspension 0.1 mg of Hsmr, in elution buffer, was added. Elution buffer was used to produce a final sample volume of 2.4 mL. Excess detergent was removed with 250 mg of degassed biobeads in an overnight incubation at 4 °C. The biobeads were then removed.

2. 2. 7. 3. 3 Reconstitution of EmrE

EmrE was reconstituted at a protein/lipid mol ratio of 1:450 for fluorescence spectroscopy in buffer (150 mM KCl, 5 mM K^+-EDTA pH 7.3), using the following method: 4 mg/mL *E. coli* total lipid extract was solubilised with 1:2 mol ratio DDM for 1 h at RT with sonication. Protein and lipid/detergent solutions were mixed at the required ratio and incubated for 1 h at RT, followed by detergent removal using pre-washed and sonicated SM-2 Biobeads. In total, 3 times 30 mg biobeads/mg detergent were added and incubated for 1 h at RT and once at 4 ºC overnight. Biobeads were removed and the liposomes pelleted by centrifugation.

2. 2. 7. 3. 4 Fusion of bR with Hsmr or EmrE containing liposomes

Bacteriorhodopsin (0.41 mg) was added to 1 mL of the Hsmr-proteoliposomes or EmrE-proteoliposomes. The mixture was freeze-thawed three times, which results in a 90 % inside-out orientation of bR in the vesicles [171]. If necessary, the sample was stored at –80 °C after the last freezing step. Proteoliposomes were centrifuged at 149,008 g, 30 min, 4 °C, and the resulting pellet was resuspended in 1 mL of 150 mM KCl, 1 M NaCl, 5 mM K-EDTA at pH 7.3 for Hsmr or 150 mM KCl, 5 mM K-EDTA at pH 7.3 for EmrE. The sample was sonicated in a water bath for 3 min to form unilamellar vesicles. The sample typically contained final concentrations of 1 µM Hsmr/EmrE, 15.4 µM bR, and 4.19 mM lipids.

2. 2. 7. 3. 5 Fluorescence measurements

All fluorescence measurements were carried out with a Jasco FP 6500 Fluorescence spectrometer. A 1x1 cm cuvette was kept at 25 °C by a thermostatic circulating water bath. Etbr measurements were carried out with excitation and emission wavelengths of 545 and 610 nm, respectively. Emission slits were kept constant at 10 nm; excitation

slits of 20 nm were used. In the cuvette, 220 µL of the bR/Hsmr proteoliposomes was diluted into 2 mL of 150 mM KCl, 1 M NaCl, 5 mM K-EDTA at pH 7.3, and 13.6 µM etbr. The sample was incubated in the dark for 5 min. Illumination at 545 nm excites etbr and enables bacteriorhodopsin to pump protons. The change in etbr fluorescence was measured over 200 s. Illumination was switched off and the system left to equilibrate for 5 min. ΔpH and Δψ are collapsed at a final concentration of 43.5 µM carbonyl cyanide 3-chlorophenylhydrazone (CCCP). 10 mM etbr stock solution and the various TPP^+ stock solutions were prepared in 150 mM KCl, 1 M NaCl, 5 mM K-EDTA at pH 7.3. The uncoupler CCCP was prepared as a 10 mM stock solution in water.

2. 2. 7. 3. 6 Data analysis

Maximal etbr fluorescence after 200 s (ΔF), at each TPP^+ concentration, was plotted with OriginPro 7.5 and this data representing etbr transport inhibition by TPP^+ was fitted using the dose response curve equation [172]:

$$y = A1 + (A2 - A1)/1 + 10\text{^}((\log 10(IC50) - x) * p) \quad (13)$$

A1 = minimal ΔΔF (ΔF without TPP^+ addition minus ΔF with least TPP^+ addition), A2 = maximal ΔΔF (ΔF without TPP^+ addition minus ΔF with most TPP^+ addition), IC_{50} = concentration at which 50 % inhibition is observed, p = Hill coefficient

The Hill coefficient p was set to 1 as it can be reasonably assumed that a functional Hsmr oligomer has a single binding site.

2. 2. 7. 4 TPP^+ transport assay

10 µL proteoliposomes prepared in 15 mM Tris, pH 7.0, 0 M KCl were diluted into 1 mL outside buffer (15 mM Tris, pH 9.5, 0.15 M KCl and valinomycin (0.5 µg/mL)) with initially a TPP^+ concentration of 3 µM. To obtain a calibration curve, several aliquots of TPP^+ are added, each increasing the final TPP^+ concentration by 3 µM. Tests at higher salt concentration used proteoliposomes in 15 mM Tris, pH 7.0, 0 M KCl, 2 M NaCl and outside buffer (15 mM Tris, pH 9.5, 0.15 M KCl, 2 M NaCl and valinomycin (0.5 µg/mL)). The TPP^+ uptake by proteoliposomes was determined with a specific electrode (MI-600) and a reference electrode (MI-402) from Microelectrodes Inc.. Potential measurements assay were recorded and analyzed with MetraHit and MetraWin10 from Gossen Metrawatt.

2. 2. 8 Centrifugation techniques

2. 2. 8. 1 Density gradient centrifugation

A discontinuous gradient from 0 to 40 % (w/v) sucrose was used to separate empty liposomes from proteoliposomes. 0.8 mL of each solution, starting with 40 %, was carefully layered into a 5mL centrifuge tube and left to equilibrate for 1 h. The 0.2 mL liposome or proteoliposome sample, at 4 mg/mL lipids, was carefully layered on top. Centrifugation at 101,843 g in a SW50.1 rotor and Beckman R class centrifuge was performed overnight at 4 °C.

2. 2. 8. 2 Analytical ultracentrifugation (AUC)

Analytical ultracentrifugation measurements were made in the Institut für Biophysik, Johann Wolfgang Goethe Universität in collaboration with Dr. Vitali Vogel, AK Prof. Mäntele. A Beckman XL-A Analytical Ultracentrifuge with an AN-50 TI rotor was used. The Hsmr molecular mass (M_p) and partial specific volume (υ_p) were estimated

from the amino acid composition to be 14526 kDa and 0.7533 mL/g respectively, using Sednterp software version 1.09 (http://www.jphilo.mailway.com/download.htm).
The partial specific volumes considered for the detergents were: $\bar{\upsilon}_p$ = 0.824 mL/g DDM [173] and $\bar{\upsilon}_p$ = 0.937 mL/g DPC [174]. For analytical ultracentrifugation analysis imidazole was removed and Hsmr exchanged into 2 M NaCl, 15 mM $Na_xH_xPO_4$, pH 8.0, (ρ = 1.08055 mg/mL, η = 1.2269x10^{-2}) with 0.1 % DDM or 0.1 % DPC using HiTrap desalting columns. Data analysis was performed using the program "Sedfit" version 94 [175] (http://www.analyticalultracentrifugation.com/sedphat/download.htm).

2. 2. 8. 2. 1 Sedimentation velocity experiments with Hsmr
Sedimentation velocity experiments were carried out at a rotor speed of 116444 g, at a sample concentration of 1.65 mg/mL for the DDM containing sample and 2 mg/mL for the DPC containing sample. 300 µL of the protein samples were loaded into 2-channel 1.2 cm path length centrepieces prior to velocity runs at 20 °C or 4 °C for DDM and DPC respectively. Absorbance scans were recorded every 5 min at 280 nm with 0.002 cm radial step-size. Sedimentation velocity profiles were analysed using size distribution analysis from the Sedfit programme providing a differential sedimentation coefficient distribution, c(s). This continuous c(s) distribution of the sedimentation coefficient analysis was performed with a grid size of 500, estimated frictional ratio, f/f_0, of 1.20 (corresponding to globular species) and sedimentation coefficients in the range of 0.5 – 20 S (in DDM) and 0.5 - 20 S (in DPC). S values reported are experimental and are $S_{(20°C,buffer)}$ or $S_{(4°C,buffer)}$ for DDM and DPC samples respectively. The continuous sedimentation coefficient analysis c(s) uses the following equation [176]:

$$f(c(s)) = \left\{ \sum_{i,j} \left[a(r_i, t_j) - \int c(s) L(s, D(s), r_i, t_j) ds \right]^2 \right\} = \min! \qquad (14)$$

c = concentration, a = concentration profile, r = radial, t = time, L = Lamm coefficient, D = diffusion coefficient

2. 2. 8. 2. 2 Sedimentation equilibrium experiments with Hsmr
Sedimentation equilibrium experiments were performed at a rotor speed of 8064 g and 18144 g, at a sample concentration of 0.56 mg/mL. 130 µL were loaded into a 2-channel centrepiece with 1.2 cm path length and the experiment was run at 20 °C. To obtain neutral buoyancy for the detergent DPC in the protein buffer, the salt content was reduced to 1 M NaCl and 25 % D2O are required (ρ = 1.04069 mg/mL, η = 1.1042x10^{-2}). Four samples with 0 %, 10 %, 15 % and 25 % D_2O were used for a global analysis of Hsmr molecular weight. Absorbance scans were recorded after 12 h, then every 2 h, at 280 nm with 0.03 cm radial step-size. Sedimentation equilibrium profiles were preliminarily analysed using the c(s) size distribution analysis from the Sedfit programme.

2. 2. 9. Chromatographic techniques
2. 2. 9. 1 Anionexchange chromatography
A 1 mL DEAE Sepharose fast flow IEX column was used with a flow rate of 4 mL/min. The column was washed with (0 M NaCl, 50 mM Tris, pH 8.0, 0.1 % DDM) for 20 CV and the sample applied in this buffer in 2 CV and washed for 10 CV. The protein was eluted with a gradient to (0.5 M NaCl, 50 mM Tris, pH 8.0, 0.1 % DDM) in 15 CV. The

entire purification was performed at 4 °C. Absorption at A_{280} and conductivity were measured.

2. 2. 9. 2 Desalting column or dialysis for buffer exchange

Efficient buffer exchange was achieved using 12 kDa cut-off dialysis membranes, stirred solutions of 1000 times the sample volume and three buffer changes within 24 h. Alternatively a 5 mL HiTrap Desalting column was washed with 25 mL target buffer, 1.5 mL sample was loaded and two 1 mL fractions were eluted in target buffer.

2. 2. 9. 3 Size exclusion chromatography

A home-made preparative gel filtration column with Superose 12 medium with adequate resolution (9369 plates/m, close to the theoretical 10000 plates/m) was used. The column was calibrated with acetone, blue dextran 2000, ferritin, aldolase, catalase, equine myoglobin, chicken ovalbumin, bovine γ globulin, bovine serum albumin (BSA) in 50 mM $Na_xH_xPO_4$, pH 7.0, 150 mM NaCl. The Stokes radii (R_s) of these proteins are known and the following equation is used obtain the partition coefficient K_D [177]:

$$K_D = \frac{(V_e - V_o)}{(V_t - V_o)} \qquad (15)$$

V_e= elution volume of the protein, V_o= void volume as determined by blue dextran, V_t= total volume as determined by acetone

The calibration standard curve plots R_s versus K_D or molecular weight (MW) versus K_D. The gel filtration column was equilibrated with sample buffer before 1.5 mL sample are applied. The sample buffer composition depends on the experiment and is indicated in the figure legend. Unless otherwise indicated size exclusion chromatography (SEC) was conducted at 4 °C and with a 1 mL/min flow rate. Absorption at A_{280} and conductivity were measured.

2. 2. 10 Mass spectrometry techniques

2. 2. 10. 1 Matrix assisted laser desorption (MALDI) MS and MS/MS

2. 2. 10. 1. 1 MALDI-TOF and MALDI TOF/TOF of tryptic digests

Samples were digested with trypsin in Tris or ammonium bicarbonate buffers at pH 8-9. A trypsin:protein ratio of 1:50 (w/w) was used and the reaction incubated at 37 °C for 12 h. The reaction was stopped by adding 10 % (v/v) formic acid. 1 µl sample and 1 µl alpha-cyano-4-hydroxy-cinnamic acid (3 mg/mL; 70 % (v/v) acetonitrile, 0.5 % (v/v) trifluoroacetic acid (TFA) were mixed and dried in the open air. Dried preparations were washed with 5 % (v/v) formic acid. All MS experiments were performed on an Ultraflex TOF/TOF from Bruker Daltonics in reflector mode. The low mass gate was set to 650 Da and the detection range to 700 – 5000 Da. Approximately 1200 shots were added for each MS spectrum. The resolution was approximately 15000 at m/z = 2000. All MS-spectra of tryptic digests were calibrated externally unless indicated otherwise. The external calibration ensures a mass accuracy of at least 50 ppm. The peptides of the referencing standard are listed in table 13A.

MS/MS experiments were performed using the LIFT methodology [178]. The mass accuracy of the precursor ion was 50 – 100 ppm, the mass accuracy of the fragment was 0.5 – 1.0 Da. The isolation width of the precursor ion selector was manually adjusted (0.5 % - 1 % of the mass of the precursor ion). The fragmentation was laser induced.

Depending on the intensity and the signal to noise ratio of the precursor ion 2000 – 20000 shots were added up.
Processing of MS spectra and MS/MS spectra used the program Flex Analysis v2.2 from Bruker Daltonics. For all spectra the settings in table 13B and table 13C were used. Further analysis utilised the programme Biotools v2.2 from Bruker Daltonics.

2. 2. 10. 1. 2 MALDI-TOF of proteins for total mass measurement

For MALDI sample preparation matrix (2,5-dihydroxy benzoic acid:2-hydroxy-5-methoxy benzoic acid = 10:1 (DHBs) and (40 mg/mL; solvent, 33 % acetonitrile/0.1 % TFA) was used. 1 µl sample solution was mixed with 1 µl matrix directly on the MALDI plate and dried in the open air. All MALDI measurements were conducted on a Voyager DE-Pro from Applied Biosystems in linear mode. The instrument settings of MALDI-TOF were selected in accordance with Bahr *et al*. [179]. A commercial calibration mixture from Applied Biosystems was used for internal and external calibrations, table 14. The MS spectra were processed with Data Explorer Software from Applied Biosystems including baseline correction, smoothing, calculation of mass lists and internal or external calibration.
All MS MALDI spectra were acquired and preliminary processed by Apotheker Björn Meyer in the group of Prof. Karas.

A

peptide	monoisotopic mass [M+H]
Des-Arg-bradykinin	904.4681
angiotensin I	1296.6853
Glu-fibrinopeptide B	1570.6774
ACTH_clip (1-17)	2093.0867
ACTH_clip (18-39)	2465.1989
ACTH_clip (7-38)	3657.9294

B

parameter	setting
peak detection algorithm	SNAP
signal to noise threshold	3
relative intensity threshold	0 %
maximal number of peaks	200
quality factor threshold	50
building block	averagine
smoothing algorithm (Savitzky Golay)	width = 0.2 m/z; 1 cycle
baseline substraction (median)	flatness = 0.8

C

parameter	setting
peak detection algorithm	SNAP
signal to noise threshold	3
relative intensity threshold	0 %
maximal number of peaks	500
quality factor threshold	0
building block	averagine
fragment peak width	0.75 m/z
smoothing algorithm (Savitzky Golay)	width = 0.2 m/z; 1 cycle
baseline substraction (median)	flatness = 0.8

Table 13. Data processing parameters. A) Peptides for external calibration of MS spectra (Applied Biosystems, SCIEX), B) parameters for the programme Flex Analysis v2.2 (Bruker Daltonics, Bremen) for processing of MS spectra, C) parameters for the programme Flex Analysis v2.2 (Bruker Daltonics, Bremen) for the processing of MS/MS spectra.

Protein	electric charge n	$(M+nH)^{n+}$ (average)
Insulin (bovine)	+1	5734.59
	+2	2867.80
thioredoxin (*E. coli*)	+1	11674.48
	+2	5837.74
apomyoglobin	+1	16952.56
	+2	8476.78

Table 14. Standards for MALDI-TOF mass spectrometry.

2. 2. 10. 2 Laser induced liquid bead ion desorption (LILBID)

LILBID is a novel mass spectrometry method first developed by the group of Professor Brutschy [180]. The analysis performed here was conducted as described previously for membrane protein complexes [181]. As for all MS techniques, the sample needs to have low salt and detergent concentrations.

Hsmr samples were eluted in the desired detergent from the Ni-NTA column and dialyzed with a molecular weight cut-off of 14 kDa for 24 h with salt and detergent free buffer to ensure suitability for LILBID measurements. Accordingly, the exact salt and detergent concentration of the LILBID samples is unknown. Micro droplets of the salt and detergent reduced Hsmr sample (diameter 50 µm) were produced at 10 Hz by a piezo-driven droplet generator and introduced into vacuum via differential pumping stages. The droplets are irradiated by synchronized high-power mid-infrared (mid-IR) laser pulses of typically 5 ns pulse length. The wavelength is tuned to the absorption maximum of water at around 3 µm corresponding to the excitation of its stretching vibrations. Above threshold intensity the radiation induces a rapid transition into the supercritical state which leads to the explosion of the droplets. The pre-formed ions in the liquid can escape into the gas phase, where they are mass analyzed in a TOF reflectron mass spectrometer. At low laser intensity LILBID desorbs ions out of the liquid very gently (ultra soft mode) enabling detection of the non-covalently assembled membrane protein complexes. Using the ultra soft mode, generally, ions carry an average of 10 % of the detergent molecules from their micelle. The semi-soft and harsh mode enable only the measurement covalently bound molecules in a detergent free state. For these experiments only the ultra soft mode was used. The signals from the detector are recorded by a transient recorder. For data acquisition and analysis user-written labview programs are used. The signal to noise ratio is improved by subtracting the unstructured background, caused by metastable loss of water and buffer molecules, from the original ion spectra. These difference spectra are smoothed by averaging the signal over a pre-set number of channels of the transient recorder, with the smoothing interval always lying within the time resolution of the TOF mass spectrometer. All LILBID measurements were carried out by Dipl.-Phys. Nina Morgner in the group of Prof. Brutschy.

2. 2. 11 Sample preparation for ^{1}H NOESY spectroscopy

25 mg DMPC and 3.13 mg TPP^{+} were dissolved separately in a 2 mL chloroform:methanol (1:1 (v/v)) mixture. The two solutions were mixed and the solvent was removed under a stream of nitrogen. The lipid:TPP^{+} film was redissolved in 2 mL of cyclohexane, frozen in liquid nitrogen, and lyophilized under vacuum overnight. Unilamellar vesicles were prepared by hydrating the lyophilised sample with 20 µL D_2O. The samples were homogenized by sonication.

2. 2. 12 NMR techniques

2. 2. 12. 1 Solution state and high resolution (HR) MAS NMR

Solution state NMR spectra were collected at 14.1 T or 21.1 T with Avance Spectrometer from Bruker Biospin and TXI HCN probeheads. The spectra were processed with Topspin 2.0 and Sparky 3. An average resonance list was obtained from the BMRB and used in Sparky for tentative assignment resonances to amino acid types. Spectra were collected in collaboration with Dipl.-Biochem. Max Stadler and Dr. Karla Werner from the group of Prof. Schwalbe. A schematic diagram of the heteronuclear single quantum coherence (HSQC) [182] type spectrum used is given in figure 12.

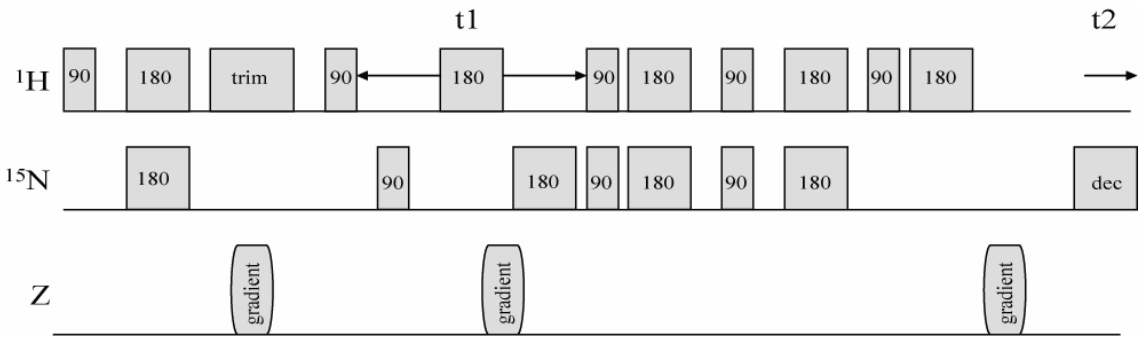

Figure 12. Schematic diagram of a HSQC pulse sequence. The pulse sequence shown is Bruker-implemented on Avance Spectrometer as hspcetf3gpsi.av. Phase sensitive detection in the indirect dimension, coherence pathway selection and water suppression are achieved using gradients [183]. For water suppression additionally a trim pulse is used. Sensitivity enhancement is afforded by an additional INEPT transfer so that both orthogonal in-phase proton magnetization components are detected [184, 185].

HR MAS NMR spectra were collected at 9.39 T with an Avance Spectrometer from Bruker Biospin and XWINNMR 3.5 as acquisition software or 9.39 T with an Avance II Spectrometer from Bruker Biospin and Topspin 1.3 as acquisition software. Experimental settings are specific to each experiment and indicated in the figure legends. All experiments were measured using 4 mm MAS DVT probeheads. 4 mm Bruker style zirconium rotors were sealed by HR MAS inserts and KEL-F bottom inserts were used. Spectra were processed with Topspin 2.0. CARA 1.8.4 [144] was used for peak assignment and integration. The NOESY pulse sequence is depicted in figure 13.

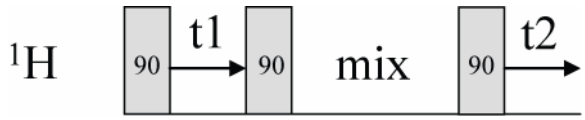

Figure 13. Schematic diagram of NOESY experiment. The NOESY [186] is a solution state NMR experiment but can also be used for hydrated liquid crystalline membranes at high speed MAS.

2. 2. 12. 2 NOESY analysis

The full matrix analysis described previously [187] enables NOESY cross relaxation rates to be determined from experimentally measured peak volumes (diagonal and cross peak). A minimum of two spectra (one spectrum at zero mixing time and a spectrum with a longer mixing time) are required for the analysis. The peak volume matrix A(0) at zero mixing time was approximated by a measurement at 10 ms mixing time.
The experimentally measured peak volumes are determined by the cross relaxation rates of the diagonal peaks as described by the following matrix equation:

$$A(t_m) = \exp(-Rt_m)A(0) \qquad (16)$$

$A(t_m)$ = peak volume matrix of experimental data at mixing time (t_m), $R(t_m)$ = relaxation rate matrix at mixing time tm, A(0) = experimentally determined peak volume matrix at mixing time zero (here approximated by a 10 ms mixing time)

To calculate the relaxation rate matrix from this the following equation is used:

$$R = -\frac{X(\ln D)X^{-1}}{t_m} \qquad (17)$$

R = relaxation rate matrix, X = matrix of eigenvectors, D = diagonal matrix of eigenvalues, t_m = mixing time

The relaxation rate matrix thus gives the calculated cross relaxation rate for each nucleus pair. This cross relaxation rate depends on the distance between the two nuclei and the time the two nuclei spend in each others vicinity. Thus the cross relaxation rate is a location probability for these two nuclei. Here the location probability of a substrate nucleus near all lipid nuclei is plotted.

2. 2. 12. 3 Solid state NMR

Solid state NMR spectra were collected at 9.39 T with an Avance Spectrometer from Bruker Biospin and XWINNMR 3.5 as acquisition software or 9.39 T with an Avance II Spectrometer from Bruker Biospin and Topspin 1.3 as acquisition software or 14.1 T with an Avance Spectrometer from Bruker Biospin and XWINNMR 3.5 as acquisition software. Experimental settings are specific to each experiment and indicated in the figure legends. All experiments were measured using 4 mm MAS DVT probeheads. 4 mm Bruker style zirconium rotors were sealed by HR MAS inserts and if space permitted KEL-F bottom inserts were used. Spectra were processed and line shapes fitted with Topspin 2.0. Professional display and tentative resonance assignment using a BMRB average resonance list was performed in Sparky 3. Figures 14 – 16 show schematic representations of the solid state NMR pulse sequences used in this thesis.

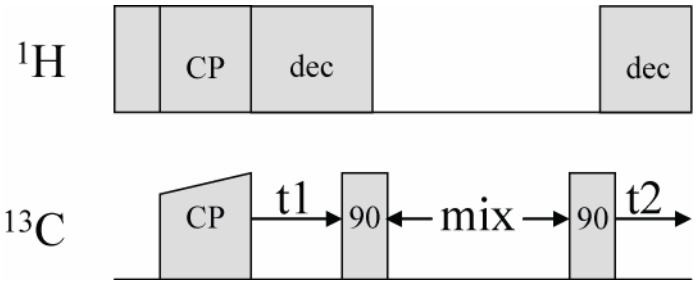

Figure 14. Schematic diagram of proton driven spin diffusion (PDSD) experiment [188]. Signal enhancement is achieved using variable amplitude CP. During the mixing step magnetization is shared between carbons using the strong dipolar couplings to protons and proton spin diffusion.

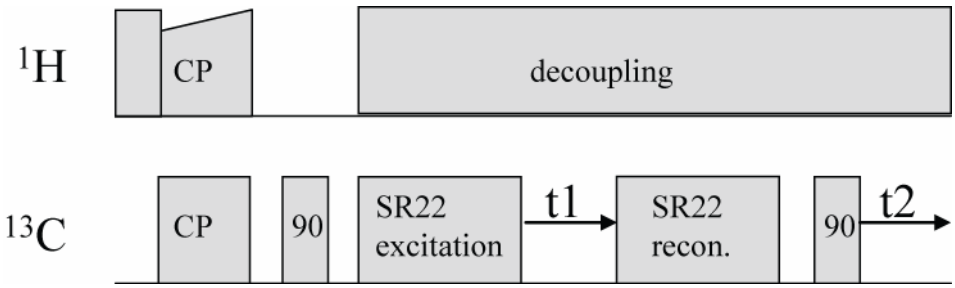

Figure 15. Schematic diagram of DQSQ experiment. The DQSQ experiment used is similar to the previously described INADEQUATE experiment for large spectral widths [189] but uses the R type sequence SR22 [190] for excitation and reconversion of double quantum magnetization.

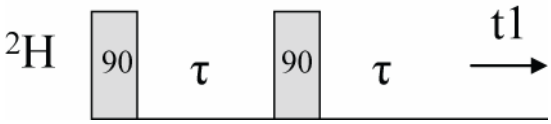

Figure 16. Schematic diagram of the quadruple echo experiment. The quadruple echo is used to enable static experiments with direct detection of fast relaxing quadruple nuclei with large spectral width [191].

Chapter 3 – Cell free expression

3. 1 Introduction

Here, an *E. coli* based home-made cell free expression system that combines *in vitro* transcription and *in vitro* translation is used under semi-continuous exchange conditions [49]. Figure 17 depicts a schematic representation of this cell free expression system. The expression of several SMR proteins was attempted. Only SMR proteins of the SMP and PSMR subgroups were chosen, as the aim of this work is the investigation of a multidrug transporter. [25] Initially, SMR proteins EmrE, TBsmr, Hsmr, YdgF and mutants of EmrE were screened for successful expression in the cell free protein synthesis system.

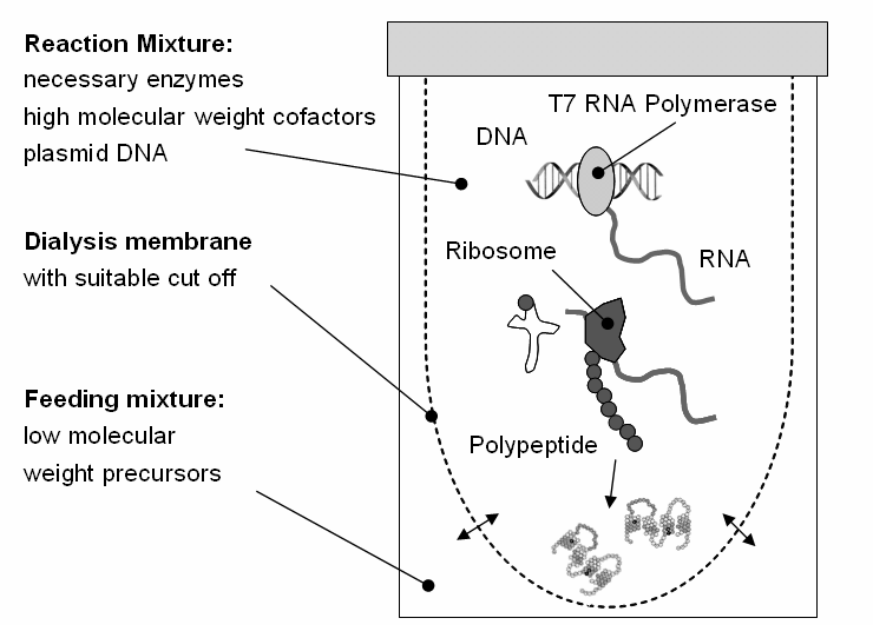

Figure 17. Schematic representation of the semi-continuous *E. coli* based cell free expression system with coupled transcripton and translation.

EmrE is the archetypal SMR protein and best studied member of the SMP subfamily. TBsmr was chosen based on its occurrence in the human pathogen *Mycobacterium tuberculosis,* the causative agent of tuberculosis. [155]. As a multidrug transporter TBsmr is likely involved in the soaring drug resistance of tuberculosis [192]. Hsmr was the first SMR protein described in the archaea domain of life and offers the chance of investigating a multidrug transporter in the presence of high salt concentrations. The unusual amino acid sequence of Hsmr, comprised roughly of 40 % alanine and valines, highlights the amino acid residues conserved in SMP proteins, and opens up unique isotope labeling opportunities [28]. The *E. coli* PSMR proteins YdgE/F were chosen for investigation as a representative heterooligomeric SMR protein pair [193]. The available expression modes and purification steps that were used are shown in a schematic overview in figure 18.

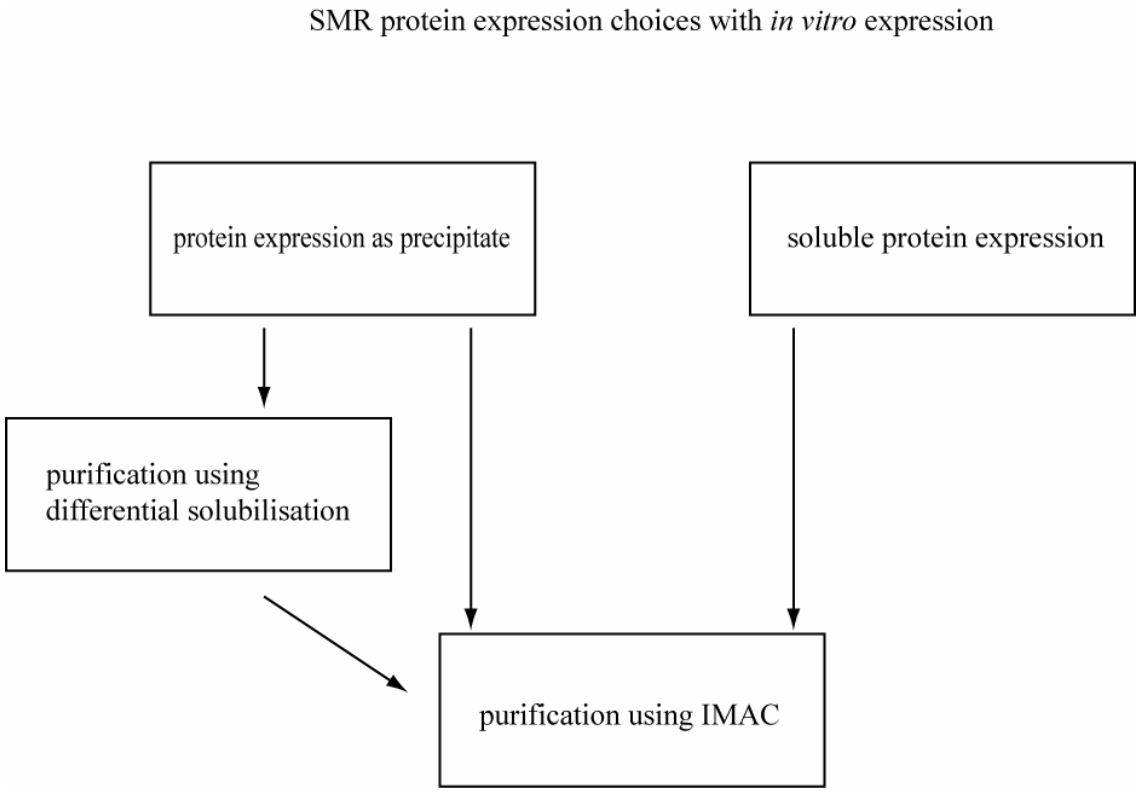

Figure 18. Choices for *in vitro* SMR protein expression. The flow diagram gives an overview of the choices regarding expression mode and protein purification when using cell free expression for the production of SMR proteins. immobilized metal affinity chromatography (IMAC)

3. 2 Expression of SMR proteins in an *E. coli* based cell free expression system

All SMR proteins tested could be successfully expressed as a precipitate in the home-made cell free expression system. Western blots of proteins obtained during initial expression attempts can be seen in figure 19. The hydrophobic SMR proteins precipitate in the hydrophilic environment of the cell free expression directly after translation. The precipitate contains mainly the expressed hydrophilic SMR protein and therefore provides a first crude purification from the multitude of proteins present in the cell free extract. The precipitate was collected by centrifugation and subjected to SDS-PAGE after solubilisation by SDS.

Particularly noteworthy is the successful expression of Hsmr using the home-made cell free expression system, as Schuldiner *et al.* were unable to produce Hsmr in an identical construct using the commercially available cell free expression system RTS 100 *E. coli* HY by Roche Diagnostics [36]. Immediately obvious is the occurrence of oligomeric species on denaturing SDS-PAGE. This remarkable resistance to oligomer dissociation was previously observed and the smearing between oligomerisation states indicates dynamic exchange between oligomerisation states [28, 36, 41, 146, 194]. This feature of SMR proteins is particularly visible using sensitive western blot analysis. The observed multimers on SDS-PAGE further foster discussions regarding the native oligomeric state of SMR proteins.

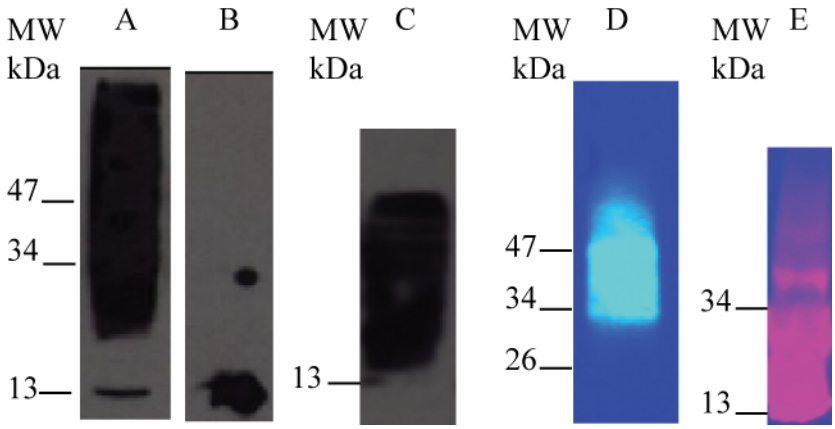

Figure 19. Screening SMR protein production by cell free expression in precipitation mode. This compound figure shows the successful precipitate expression of A) Hsmr, B) EmrE on one western blot, C) TBsmr, D) YdgF and E) EmrE CAMY each on separate western blots. The precipitate was solubilised using SDS and subjected to SDS-PAGE. SMR proteins were visualized using an anti-myc antibody which detects the C-terminal myc tag. SMR proteins run on SDS PAGE as monomers and multimers. Smearing between oligomerisation states indicates dynamic exchange between them [28, 36, 41, 146, 194].

3. 3 Choice of targets and improving purity

After initial screening, the proteins EmrE and Hsmr were chosen for further investigation, with first attempts concentrating only on Hsmr. Higher Hsmr purity than achievable by collecting the pelleted precipitate was desired and a further purification step was added. Some soluble proteins co-precipitate with the hydrophobic heterologous protein and it was tested whether pellet washes with detergents can selectively remove these soluble, contaminating proteins. The ideal detergent would extract all soluble proteins of the cell free extract, but would not solubilise or harm Hsmr. Table 15 summarizes the solubility of Hsmr in various wash buffers as detected by SDS-PAGE and western blot analysis. The buffers were maintained at pH 7 or 8 as at this pH Hsmr is functional and crossing of its isoelectric point is avoided [28]. The detergents chosen are grouped according to their ionic properties. Non-detergent substances were also used and are listed together. All detergent concentrations were chosen to be above the cmc.

It can be concluded that pellet washes with minimal Hsmr loss are possible using the nonionic detergent Tween (2 % Tween 80), the zwitterionic detergent 3-[(3-Cholamidopropyl)dimethylammonio]propanesulfonic acid (CHAPS) (3 % CHAPS) or the nondetergent buffers containing DHPC (5 % or 10 % DHPC), tetrafluoroethylene (TFE), 3:1 chloroform/methanol or 0.5 M urea. However, improvements in Hsmr purity were small and a different purification strategy was sought.

type of substance	name of substance and concentration	solubility (-, +,++,+++)
ionic		
	2 % SDS	+
	4 % SDS	++
zwitterionic		
	5 % DPC	+++
	3 % CHAPS	-
nonionic		
	0.5 % DDM	++
	2 % DDM	++
	2 % Triton X 100	++
	2 % Triton X 114	+
	2 % Tween 20	++
	2 % Tween 80	-
	4 % OG	+
	10 % OG	++
nondetergent		
	TFE	-
	5 % DHPC	-
	10 % DHPC	-
	NSDB-195	-
	NSDB-201	++
	NSDB-256	++
	5 % LPPG	++
	5 % LMPG	+
	10 % LMPG	++
	3:1 chloroform/methanol	-
	0.5 M urea	-
	1 M urea	+
	2 M urea	+
	3 M urea	+

Table 15. Purification of SMR proteins using differential solubilisation of the precipitation pellet. Pellets of precipitated Hsmr were washed twice in 0.2 M sodium phosphate wash buffer, pH 7. Detergent solutions were prepared in 50mM potassium phosphate buffer pH 8.0, 2 mM DTT. The pre-washed Hsmr pellets were solubilised for 30 min at 30 ºC with detergents and non-detergent substances. Urea, TFE and chloroform/methanol extractions were kept at RT. 10 µL of the wash solution were subjected to SDS-PAGE and western blot analysis. The amount of Hsmr solubilised was detected with an anti-myc tag antibody.

3. 4 Immobilized metal affinity purification

The used vectors include a hexahistag which is added to the C-terminal end of the SMR proteins. Hexahistags bind tightly to IMAC columns charged with nickel. A one step purification scheme for the target protein using affinity chromatography was devised.

Here, batch binding to the Ni-NTA beads was combined with wash and elution steps in plastic chromatography columns. Elution of the selectively immobilized target protein can be achieved using pH drop, competition with imidazole or ammonium hydroxide. Elution by lowering the pH to 4.6 should elute selectively monomers and dimers [195], whereas ammonium hydroxide elution [196] would be beneficial for subsequent biochemical assays. The most efficient method for elution of Hsmr in DDM micelles was evaluated and the western blot can be seen in figure 20. Elution from the nickel affinity column was most efficient using imidazole. The other methods were therefore no longer pursued.

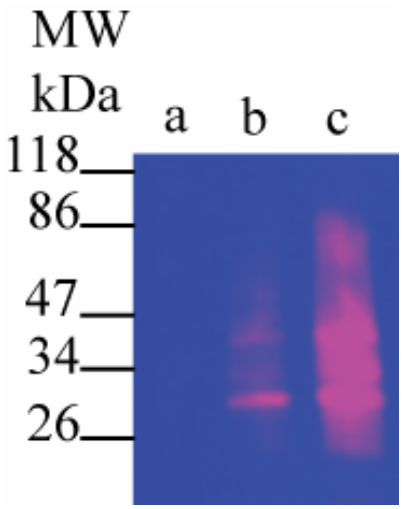

Figure 20. Affinity purification of solubilised Hsmr and evaluation of optimal elution method. Hsmr was eluted using three different methods. a) 0.4 M ammonium hydroxide, b) low pH 4.6 sodium acetate, c) 250 mM imidazole.

3. 5 Soluble expression

The expression of membrane proteins as precipitate requires efficient refolding protocols and the verification that native activity is regained. Therefore, soluble expression modes were sought for selected SMR proteins. Detergents and lipids provide a hydrophobic micellar environment for the nascent protein chain, which can prevent protein precipitation and enable correct protein folding. Initially, Hsmr *in vitro* expression, in the presence of various detergents above their cmc, was screened. The detergents chosen were successful in solubilizing Hsmr, as assessed during the differential solubilisation experiments, and are frequently successfully used detergents for membrane protein investigations. After cell free expression, a sample from the expression mixture was analysed by SDS-PAGE and western blot analysis. Hsmr was expressed in the presence of DDM and DPC as can be seen in figure 21a.

Expression in the presence of the zwitterionic detergent DPC was most efficient. A correlation between increasing cmc and increasing detergent interference with the transcription/translation machinery has been noted [197]. Accordingly, it is not surprising that DPC was the most successful detergent for the soluble expression of Hsmr. Next, the general suitability of DPC for the soluble SMR protein expression was assessed. Additionally, the effect of soluble versus precipitate expression on the oligomeric state of SMR proteins was investigated. The results can be seen on the Western blot figure 21b. Finally, the possibility of expressing Hsmr in the presence of liposomes was investigated using DOPC in the cell free reaction mixture, at concentrations far above the estimated lipid cmc. Expression in the presence of lipids is possible as seen in figure 21c.

A

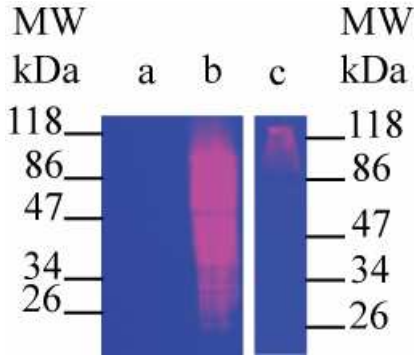

B

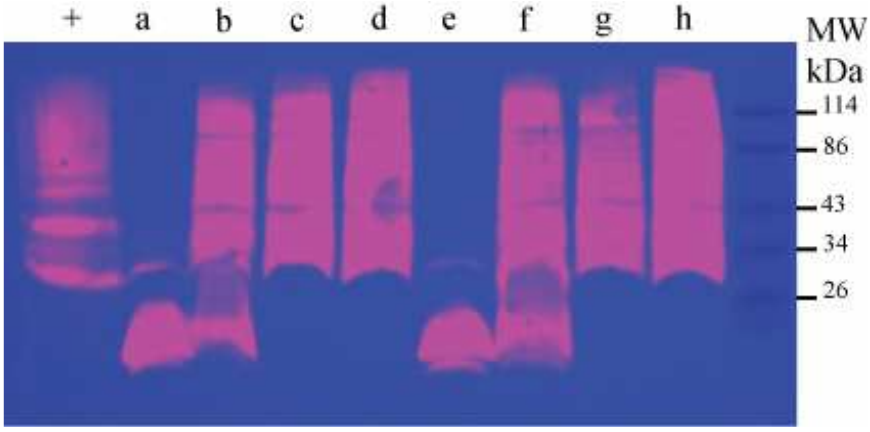

C

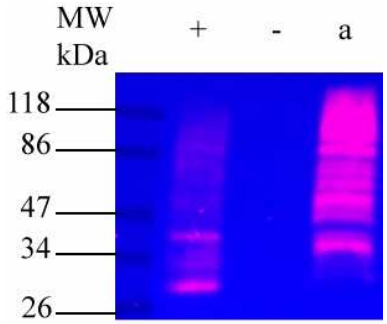

Figure 21. Soluble expression of SMR proteins in cell free expression systems. A) Screen of Hsmr expression using different detergents to provide a hydrophobic micellar environment for the nascent protein chain. Expression in a) 36.75 mM OG, b) 0.26 mM DDM and c) 2.25 mM DPC. B) Comparison of yields and oligomerisation state for EmrE a, e), TBsmr b, f), Hsmr c, g) and YdgF d, h) expressed as precipitate a-d) and soluble e-h) in 2.25mM DPC. +) as positive control 0.8 µg Hsmr expressed *in vivo* was used. C) Soluble expression in the presence of a) 8.5mM DOPC, +) Hsmr *in vivo* expressed as positive control and -) cell free extract as negative control are shown.

3. 6 Conclusion

In conclusion, the SMR proteins Hsmr, EmrE, TBsmr and YdgF can be obtained by cell free expression, as precipitates, and in the presence of detergents or lipids in a soluble form. Protein expression as precipitate can be combined with differential pellet solubilisation or IMAC. Expression in a soluble form is best achieved with the zwitterionic detergent DPC proved to be superior and protein purification utilises IMAC. The highest protein purity can be achieved using IMAC in combination with imidazole as the eluant.

Chapter 4 - Large scale *in vivo* Hsmr preparation and optimization of detergent and reconstitution conditions

4. 1 Introduction

Despite the abundance of membrane proteins, around 30 % of proteins in most proteomes [198], membrane proteins are less well studied than soluble proteins and grossly underrepresented in structural databases such as the Protein Data Bank [199]. The reluctance to study membrane proteins arises from their frequently low expression in native sources and heterologous expression systems [200]. Additionally, the preparation of membrane proteins is cumbersome due to the necessity to imitate a native-like hydrophobic environment in order to obtain functional and natively folded membrane proteins. Bearing this in mind, a particular effort regarding membrane protein expression, purification and optimization of handling procedures is required. Sought-after parameters are protein solubility, monodispersity, stability and functionality. Here conditions for *in vivo* expression of Hsmr and EmrE are sought as an alternative to the costly cell free expression and as a means of obtaining uniformly isotope labeled protein. Furthermore, protein purification and reconstitution conditions are optimized which are transferable to *in vitro* produced proteins.

4. 2 Overview of the optimization of Hsmr expression, purification and handling

In this chapter, optimizations regarding Hsmr preparation for solution-state methods and solid-state NMR are shown. Figure 22 summarizes the individual stages in the process of protein expression and purification.

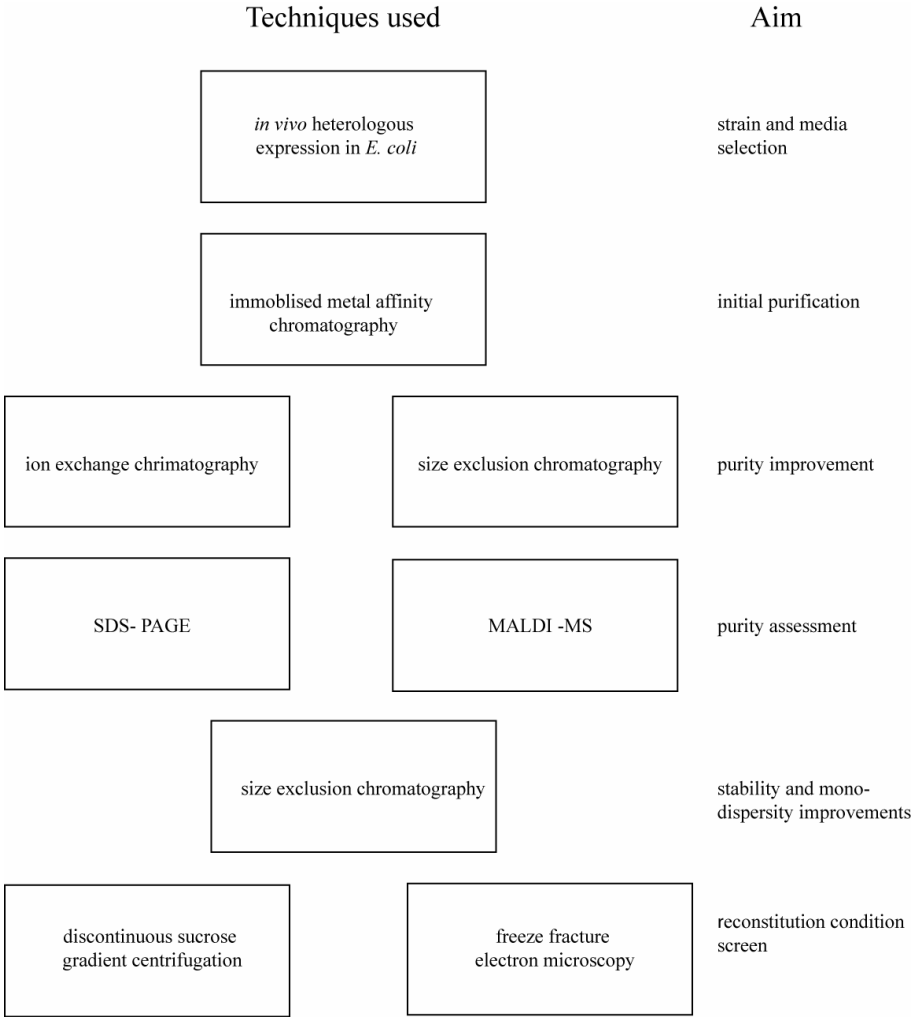

Figure 22. Overview of Hsmr sample preparation optimization performed.

4. 3 *In vivo* Hsmr protein expression optimization

Here, *in vivo* expression of Hsmr in *E. coli* cells was optimized regarding yield and possible isotope labeling schemes. In all cases the pT7-7 Hsmr myc-his tag construct described in the material and methods section was used. Transcription of Hsmr mRNA required the presence of T7 polymerase. In table 16, the utilized *E. coli* strains and their metabolic requirements are listed.

Figure 23 shows the yields that were obtained using different *E. coli* strains and media.

strain	genotype	auxotrophic	literature
CT19	BL21(DE3) + *aspC, ilvE, trpB, tyrB, avtA*	Leu, Val, Ile, Tyr, Trp, Phe, Asp, Ala	[149]
BL21(DE3)	F^- *ompT gal dcm lon* $hsdS_B(r_B^- m_B^-)$ *λ(DE3 [lacI lacUV5-T7 gene 1 ind1 sam7 nin5])*	no	[150]
T7 Express	BL21(D3) + *fhuA2 lacZ::T7 gene1 [lon] ompT gal sulA11 R(mcr-73::miniTn10--* Tet^S*)2 [dcm] R(zgb-210::Tn10--* Tet^S*) endA1 Δ(mcrC-mrr)114::IS10*	no	[151]
TA15	*melBLid nhaA1 nhaB1 lacZY*	no	[152]

Table 16. *E. coli* strains evaluated for use with Hsmr. Genotype and auxotrophy are listed to enable assessment of the usefulness of each strain with regards to isotope labeling experiments.

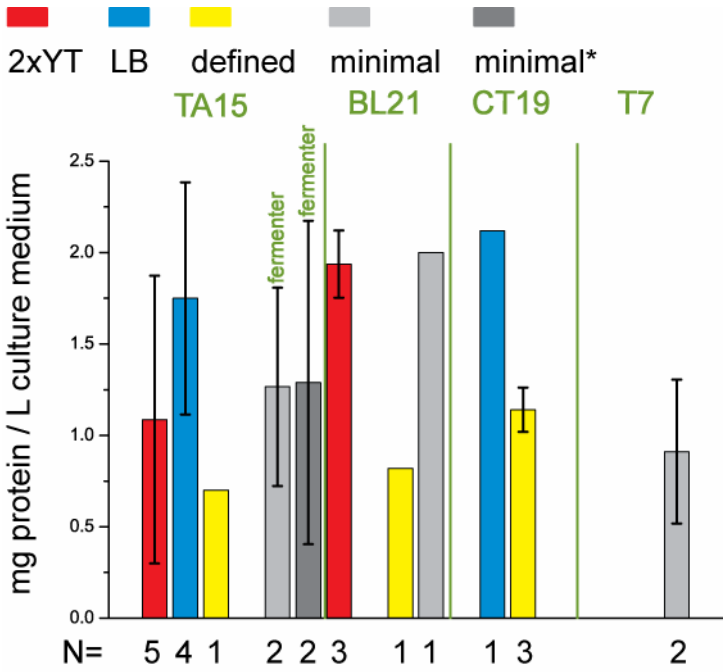

Figure 23. Hsmr expression yield in mg protein / L culture medium. The effect of different *E. coli* strains and media on the production of Hsmr can be seen. The standard deviation, if applicable, is indicated as a bar. Below the diagram the number of replicate experiments (N=) is indicated.

Initially, for all Hsmr protein expressions, TA15 cells were used. The differences in protein yields per L of medium are striking. TA15 cells encode T7 polymerase on a separate vector pG1-2 under the control of a heat shock promoter. Poor control over heat shock parameters such as heating, cooling, temperature maintenance and mixing in shake flask cultures are the likely causes of the poor yield reproducibility. Expression in a fermenter offers a potential solution to low yields by easing up scaling and providing potentially higher reproducibility. To improve reproducibility and potentially also the yields, the use of CT19, BL21(DE3) and T7 Express cells was evaluated. These strains support chemical induction of T7 polymerase production with IPTG. T7 Express cells offer the advantage of resistance against T1 phages whereas the auxotrophic strain CT19 enables amino acid specific isotope labeling (see table 16). Overall, the Hsmr yield was not only more reproducible but also higher when IPTG was used for induction. However, since IPTG mediated induction is very costly, Hsmr is expressed in TA15 cells when using a fermenter. In flask cultures, IPTG induction was preferentially carried out with T7 Express cells or, for amino acid specific labeling experiments, CT19 cells.

The highest yields were obtained with rich media (LB and 2xYT) and much lower yields with synthetic media (defined and minimal). In general, faster growth and higher heterologous protein expression are expected for rich media and the synthetic 19 amino acid containing defined medium. In fact, proteorhodopsin expression yields are known to be much higher with such a synthetic defined medium than in a rich medium [201]. The reasons for low yields with the synthetic defined medium remain unknown. In conclusion, depending on the strain, expression mode (fermenter versus flask) and isotope labeling scheme used different media were employed. See table 17 for an overview of combinations used.

media	labeling possibilities	suitable for auxotrophs
2xYT	no	yes
LB	no	yes
minimal media	uniform or pattern	No
minimal media (high cell density)	uniform or pattern	No
defined media	amino acid selective	Yes

Table 17. Overview of media for *E.coli* based SMR protein expression. The media compositions are detailed in the material and methods section.

Expression levels of proteins under the control of a T7 promoter can be boosted by using the antibiotic rifampicin to inhibit native *E. coli* polymerases [202]. This is inhibition of native transcription channels all metabolic energy, precursors and ribosomes to the production of the heterologous protein. Here, the effect of a rifampicin mediated yield increase was investigated for TA15 cells only and could not be reproduced. Nevertheless, the combination of the spin down methodology [203] and rifampicin was used for isotope labeling experiments. Briefly, the spin down methodology enables pulse labeling by the use of unlabelled media for the growth phase and switching to labeled media at high cell density for the heterologous protein expression phase. Rifampicin ensures the efficient use of labeled compounds for the heterologous product, and reduces required nutrient amounts by suppressing the native metabolism. These techniques reduce the necessary amount of labeled media and the nutrient content of the media, leading to significant cost savings.

To assess the success of the described expression yield optimization, the Hsmr overexpression, as % of total membrane protein, was measured. Unfortunately, a meager 1.6 % of the total membrane protein content consisted of Hsmr. Membrane protein overexpression of around 30 % have been described for various transporters [126, 134, 139, 204, 205]. However, several of these transporters are over expressed in their native host. Further, Hsmr has a highly biased amino acid composition and published values for other SMR proteins also suggest very low overexpression [42, 194].

4. 4 Optimization of Hsmr protein purification

Protein purification is achieved as detailed in the material and methods section. Briefly, the plasma membrane is collected, Hsmr solubilised by detergent and bound to a nickel affinity chromatography column via its hexahistag. Solubilisation of Hsmr is generally achieved using 1 % DDM, as previously described for all SMR proteins. However, the buffer contains 2 M NaCl as Hsmr is a halophilic protein from the extreme halophile *H. salinarium.* This high salt concentration was chosen based on the general observation that halophilic proteins denature below 1 M salt, and more specifically that Hsmr can bind the substrate TPP^+ with maximal affinity at a minimum of 2 M NaCl [28, 206]. *In vitro* and *in vivo* produced Hsmr can be successfully purified under these conditions. Hsmr is eluted in 0.1 % DDM, a concentration roughly five times above the DDM cmc. However, multiple bands on SDS-PAGE and western blots, for examples see figure 21B, suggest either residual protein contaminants or SDS resistant inconsistent oligomerisation behavior. Additionally, time dependent aggregation is visible as a pellet after slow centrifugation. Therefore, optimization of Hsmr purification conditions with regard to protein purity and stability were sought.

4. 4. 1 Ion exchange chromatography (IEX)

Particularly before the advent of IMAC, IEX was widely used for protein purification and SEC as final purification step [207]. Unfortunately, ion exchange chromatography is a poor choice for halophilic proteins since it requires the absence of salt in the beginning of the purification process and low salt concentrations during the majority of the process. However, it has been reported that many halophilic proteins, including membrane proteins, can maintain their native fold in the absence of salt and only activity and stability are compromised [79, 80]. Due to the acidic pI of Hsmr, an anion exchange column was used for Hsmr purification. In the absence of salt, the highly negatively charged Hsmr should bind tightly to the chosen anion exchanger together with all negatively charged contaminants. Following sample loading the column is washed with no salt buffer. Elution utilizes for differential elution a salt gradient. A typical chromatogram is seen in figure 24.

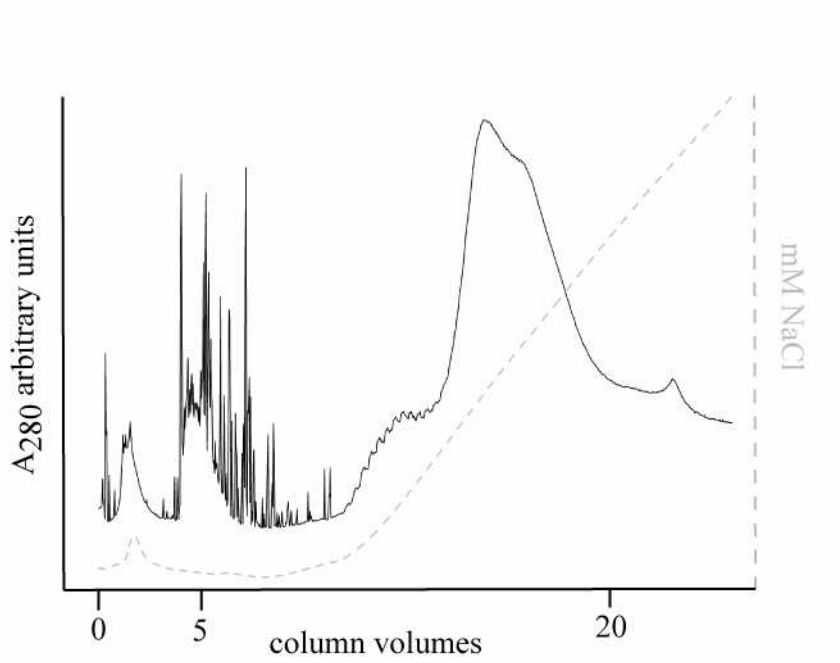

Figure 24. Anion exchange chromatography of Hsmr after IMAC. An anion exchange column was used to investigate the possibility of improving Hsmr purity after IMAC. Column loading was completed after less than 2 CV and washes with no salt buffer continued up to 10 CV, as can be seen from the red conductivity trace. Protein elution was initiated with a gradient to 0.5 M NaCl over 15 CV. During column loading, an increase in absorption at 280 nm indicates that imidazole traces and potentially also net positively charged proteins are washed through. During the wash process, nonspecifically bound, net positively charged proteins are eluted. The gradient elutes the vast majority of protein in one broad peak with two shoulders.

Not all material loaded binds to the anion exchange chromatography column. 6 % of the material contributing to the A_{280} absorption elute during binding and wash steps. This material includes imidazole and possibly contaminating proteins. However, since less than 6 % of contamination can be removed using IEX, the protein aggregation and inactivation risks associated with low salt concentrations are not warranted.
It can be concluded that traces of other proteins are present in Hsmr samples after IMAC. However, only a small amount (< 6 %) can be removed using ion exchange chromatography and thus does not warrant the risk of protein aggregation and deactivation due to low salt concentrations.

4. 4. 2 Size exclusion chromatography

SEC was evaluated as possible further purification method. SEC of Hsmr was performed in the presence of 2 M NaCl. The separation is based on the hydrodynamic radius of a molecule, the so called Stokes radius [208]. For globular proteins the separation is also approximately by molecular weight. A typical separation profile of Hsmr is shown in figure 25 A.

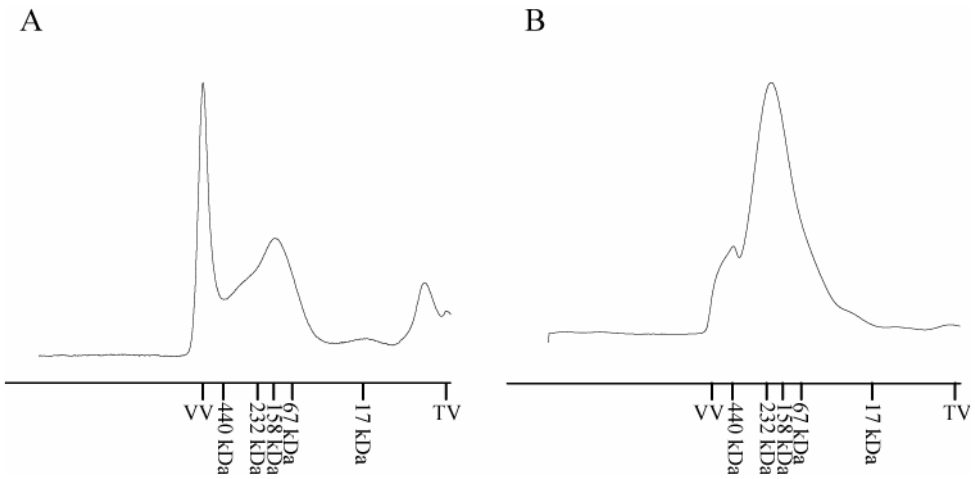

Figure 25. Gel filtration of Hsmr to improve sample homogeneity, assess molecular weight of Hsmr + micelle and test the effect of a low salt buffer. A) Hsmr in 0.1 % DDM and standard buffer (2 M NaCl, 15 mM $Na_xH_xPO_4$, pH 8.0, 300 mM imidazole) B) Hmsr in 0.1 % DDM and low salt buffer (10 mM NaCl, 15 mM $Na_xH_xPO_4$, pH 8.0). For the gel filtration run, standard buffer without imidazole and low salt buffer were used respectively. The gel filtration column was packed with Superose 12 medium. The calibration results are indicated below each trace. The void volume (VV) was determined using blue dextran 2000 and the total volume (TV) was measured using acetone. Peaks close to the total volume arise from imidazole and detergent molecules.

SEC of membrane proteins enables a rough molecular weight estimation of the protein-micelle complex, provided the column was calibrated with suitable standards [208]. The column used here was calibrated as described by Cohen *et al.* [177].

detergent	elution volume in mL	R_s in Å	MW of PDC in Da
DDM	39.30	4.57	136279.8
low salt DDM	39.36	4.56	134913.3

Table 18. Summary of the SEC data obtained for Hsmr. The corresponding gel filtration traces can be seen in figure 25. Stoke's radii and molecular weights were calculated using a calibration curve.

In figure 25A, the SEC chromatogram of Hsmr under high salt conditions reveals a peak in the VV which must arise from large aggregates (> 440 kDa), a peak centered roughly at 136 kDa and a small peak close to the total volume which arises from DDM molecules and imidazole. Since a single broad peak is observed in the useful volume range, SEC does not separate Hsmr and possible contaminating proteins. The peak at 136 kDa arises from the complex of Hsmr + DDM micelle. Expected molecular weights of this complex are listed in table 19. A molecular weight of 136 kDa suggests either that Hsmr can form multimers larger than tetramers, or that Hsmr + DDM micelles contain more than 50 kDa DDM, or does not obey the assumption of the behavior of an ideal globular protein. This highlights the shortcomings of SEC to estimate membrane protein molecular weights, and highlights the problem of Hsmr aggregation observed in standard high salt buffer with 0.1 % DDM.

oligomeric state	calculated Hsmr molecular weight (kDa)	estimated DDM micelle size (kDa)	estimated total molecular weight of Hsmr/micelle complex (kDa)
monomer	14.526	50	65
dimer	29.052	50	79
trimer	43.578	50	94
tetramer	58.104	50	108

Table 19. Hypothetical molecular weights of Hsmr + micelle complexes for various Hsmr oligomeric states. Hsmr molecular weight as calculated from the sequence using ProtParm [209] and DDM micelle size was calculated from its tabulated aggregation number [210].

Since some halophilic proteins such as bacteriorhodopsin from *Halobacterium salinarium* are known to survive low salt conditions unharmed [211], this was assessed for Hsmr in figure 25B. The ability to work in low salt buffers would be highly beneficial for most biochemical and NMR investigations. Hsmr again eluted as a single broad peak indicating that low salt concentrations (10 mM NaCl) did not affect the oligomerisation behavior of Hsmr. However, the precise molecular weight and oligomerisation state could not be determined.

Hsmr in standard high salt buffer has a lower Hsmr + micelle molecular weight and a better separation of aggregates from soluble protein than Hsmr in low salt buffer. Hsmr in low salt buffer has a more favorable ratio between aggregate peak and soluble protein peak. However, this is likely due to the continuum of Hsmr aggregation. The estimated molecular weight of Hsmr at low salt concentrations is around 135 kDa. Neither buffer system offers satisfactory protein stability. Oligomerisation of Hsmr is not surprising as previously judged as stabilization feature in halophiles [78]. SDS resistant oligomers and even unspecific aggregation in the presence of SDS has previously been reported for several proteins [212-216] and more specifically has been reported for TBsmr [146] and Hsmr [28]. A problem highlighted by these investigations is the time dependent instability of Hsmr which is aggravated by freeze-thawing.

4. 5 SDS-PAGE and MALDI-MS of Hsmr to assess protein purity

Generally, SDS-PAGE in combination with Coomassie staining is used to assess the purity of a protein preparation. For SMR proteins, the occurrence of multiple bands due to SDS resistant oligomerisation and exchange between these has been reported [28, 146]. Accordingly, the SDS-PAGE seen in figure 26, which exhibits several bands at multimer molecular weights but not at the monomer molecular weight, does not give a conclusive answer regarding purity. However, the band pattern was reproducible between preparations and identical to the pattern seen for *in vitro* transcribed Hsmr. Furthermore, western blots of Hsmr produced *in vitro* showed an identical pattern and smearing between states, see figure 21, endorsing the idea that the pattern is due to native Hsmr.

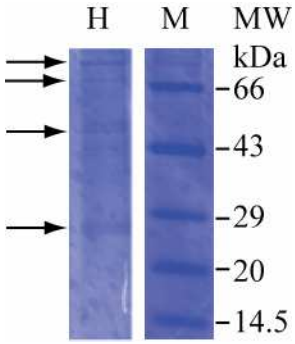

Figure 26. Hsmr *in vivo* produced, purified by IMAC in the presence of DDM and separated by SDS-PAGE. The gel exhibits distinct bands for Hsmr at a concentration of ~ 0.7 mg/mL at dimer, trimer, tetramer and undefined higher molecular weight, as indicated by arrows.

To further investigate the purity of the *in vivo* produced Hsmr, MALDI-TOF MS was employed. The sample was dialyzed to remove as much NaCl as possible and the total mass was determined, see figure 27.

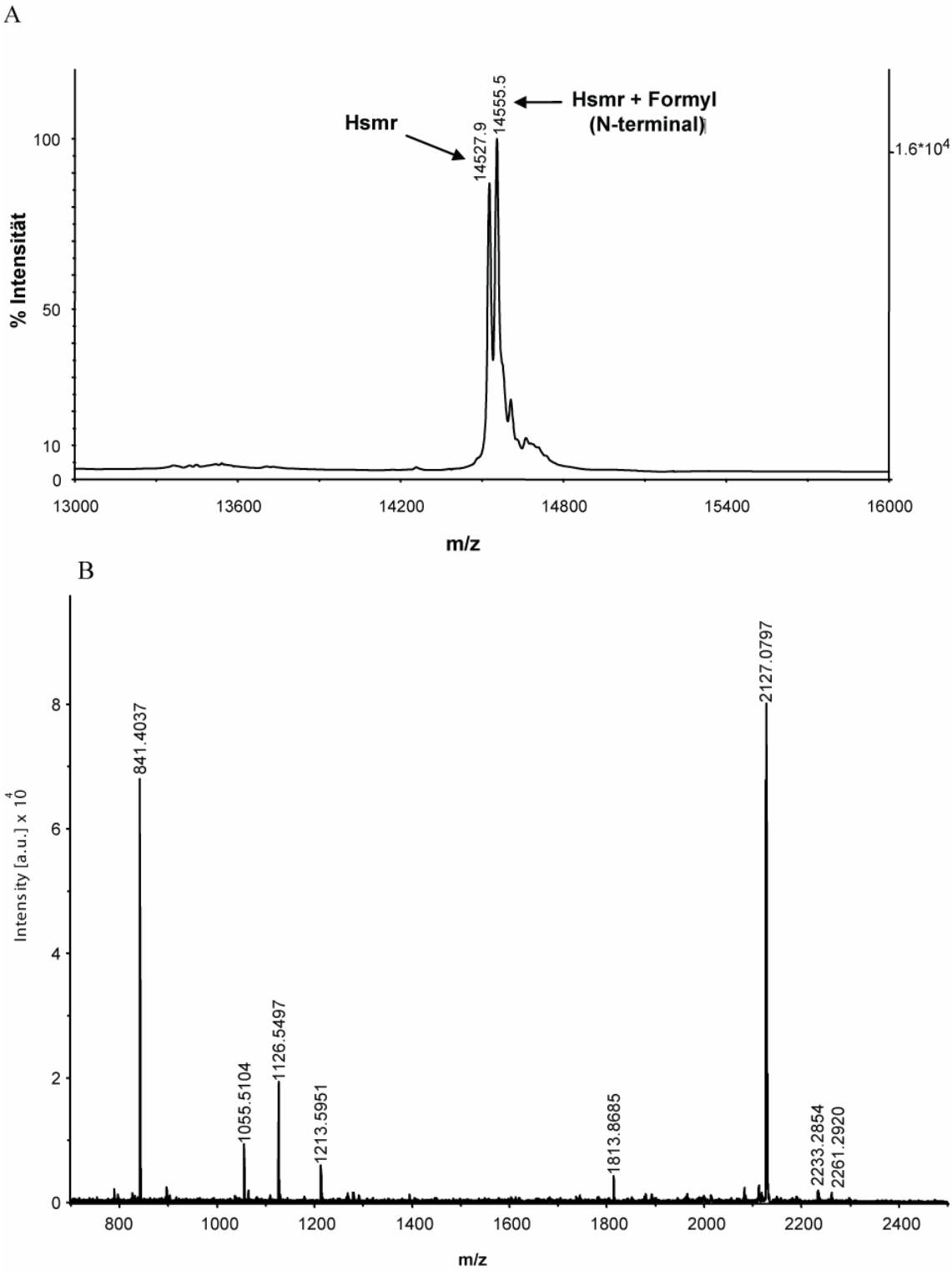

Figure 27. MALDI-TOF MS of *in vivo* produced Hsmr. The sample contained ~ 0.7 mg/mL Hsmr and was dialysed in 10 mM NaCl, 15 mM $Na_xH_xPO_4$, pH 8.0, 0.1 % DDM to reduce the salt concentration. A) The spectrum shows a pure protein preparation with a two major peaks around the expected molecular weight of 14526 Da and at the molecular weight of Hsmr+formylation. The spectrum was not calibrated. B) Tryptic digest of Hsmr at ~ 0.2 mg/mL dialysed into 25 mM ammonium bicarbonate, pH 8.0, < 0.1 % DDM, measured with internal calibration. Eight fragments could be detected and assigned to Hsmr, see table 21.

The protein preparations examined by SDS-PAGE in figure 26 and MALDI-TOF MS in figures 27 are identical. SDS-PAGE clearly exhibits several high molecular weight bands, including one around 29 kDa. A protein of 29 kDa was not detected by MALDI-TOF MS, nor multiplies charged peaks for hypothetical proteins of higher molecular weight. Generally, MALDI-TOF MS is thought to be a technique that should be able to detect even small amounts of soluble protein contaminants. From this, it can be concluded that *in vivo* produced Hsmr can be successfully purified with a single step IMAC purification protocol.

MALDI-TOF MS and tryptic digestion followed by MALDI-TOF MS of a different Hsmr sample verified the initial conclusion that Hsmr produced *in vivo* is pure and also confirmed that Hsmr is present in its formylated and unformylated form. The second MS investigation of Hsmr also used internal calibration and verified the predicted molecular weight of 14526 Da, see table 20.

	M+H (m/z)
measurement 1	14526.20
measurement 2	14528.17
measurement 3	14525.55
average	14526.64
Std	1.36
calculated	14526.5

Table 20. Hsmr total mass investigated by MALDI-TOF MS. Hsmr at ~ 0.2 mg/mL dialysed into 25 mM ammonium bicarbonate, pH 8.0, < 0.1 % DDM, measured with internal calibration.

Tryptic digestion and MALDI-TOF MS identified a total of 8 different peptides, the specific cleavages and 5 unspecific cleavages arising from sample instability in low salt buffers, see table 21 and figure 27B .

M+H (m/z)	**sequence**
841.4037	HHHHHH
1055.5104	VDHHHHHH
1126.5497	AVDHHHHHH
1213.5951	NSAVDHHHHHH
1813.5951	EEDLNSAVDHHHHHH
2127.0797	LISEEDLNSAVDHHHHHH
2233.2869	MHPYAYLAAAIAAEVAGTTALK
2261.2889	Formyl-MHPYAYLAAAIAAEVAGTTALK

Table 21. Hsmr tryptic digest investigated by MALDI-TOF MS. Highlighted are detected unspecific breakages (grey) and the observed specific tryptic fragments (black). Only two trypsin sites are situated outside the predicted TMS and only these hydrophilic fragments are detected.

In conclusion, IMAC provides pure *in vivo* produced Hsmr. The additional bands observed by SDS-PAGE and western blotting of Hsmr arise from different SDS resistant Hsmr oligomers and exchange between these oligomers. In a next step time stability of Hsmr needs to be improved and this is attempted below.

4. 6 Optimization of Hsmr time stability in detergent

Long-term stability of protein in detergent solution is a requirement for most biochemical methods. In particular, this is true for solution state NMR studies which require protein stability and monodispersity for several weeks at elevated temperatures. The major determinant of membrane protein stability in solution is the choice of detergent. Here, a selection of the detergents used in chapter 1 was assessed. The choice was narrowed to DDM, DPC, LPPG, OG and SDS. Nonionic detergents OG and DDM with 5 % glycerol, zwitterionic detergent DPC, ionic detergent SDS and single chain lipid LPPG were selected for investigation. All of these detergents have been used successfully for the extraction and reconstitution of several membrane proteins, as well as their analysis by NMR and x-ray crystallography [112, 217]. The additive glycerol has been shown to enhance membrane protein solubility in numerous cases [218]. Additionally, DPC, LPPG and SDS proved to be suitable as detergents for Smr, the *Staphylococcus aureus* SMR protein, in solution state NMR experiments [112]. Additionally, the use of glycerol as additive was examined. Glycerol is suggested to have salting out effects and therefore reduce the NaCl requirement of halophiles [78] and in general glycerol is thought to promote membrane protein stability [218, 219].

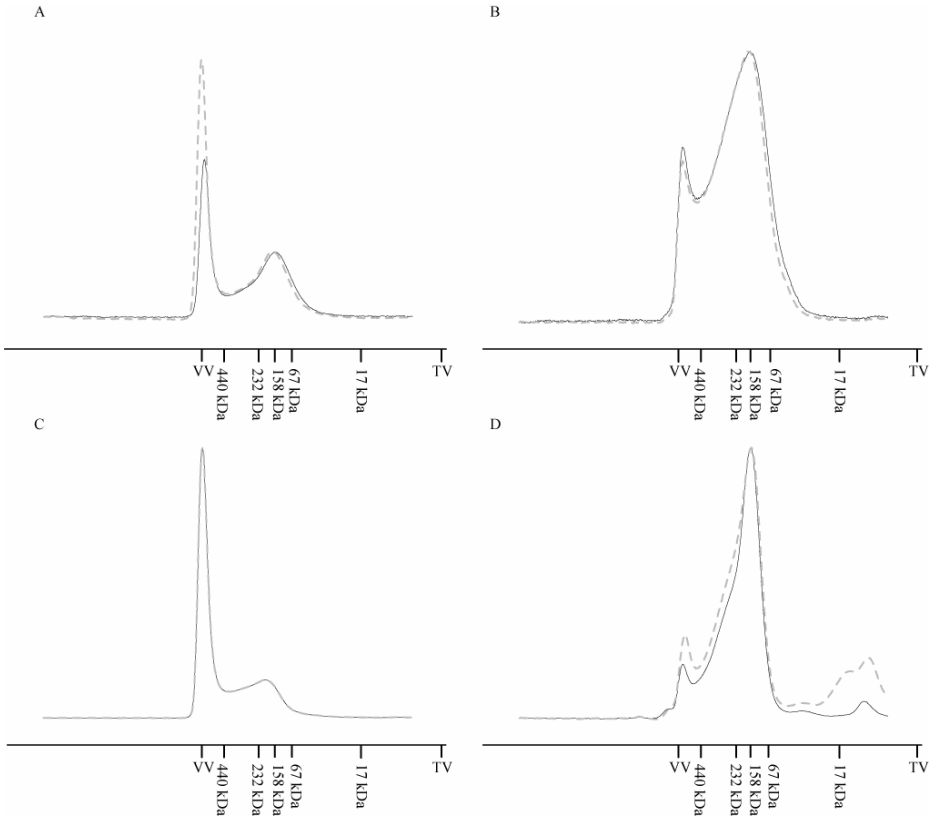

Figure 28. Gel filtration of Hsmr to assess protein stability in various buffers. After detergent exchange on the IMAC column, Hsmr was eluted in standard buffer (2 M NaCl, 15 mM $Na_xH_xPO_4$, pH 8.0, 300 mM imidazole) in the new detergent. For SDS samples, the SDS buffer (300 mM NaCl, 15 mM Tris, pH 8.0, 300 mM imidazole) was used. A) 0.1 % DDM + 5 % glycerol, B) 0.1% DPC, C) 0.1% LPPG, D) 0.41 % SDS. Samples were stored at 4 °C and run on the gel filtration at 4 °C at day 2 (black trace) and day 10 (red trace). SDS incubations and gel filtration runs were conducted at RT. For gel filtration runs standard buffer (2 M NaCl, 15 mM $Na_xH_xPO_4$, pH 8.0) was used. For SDS experiments, an alternative buffer was used (300 mM NaCl, 15 mM Tris, pH 8.0). The gel filtration column was home-made and packed with Superose 12 medium. The calibration results are indicated below each trace. The VV was determined using blue dextran 2000 and the TV was measured using acetone.

detergent	elution volume in mL	R_s in Å	MW of PDC in Da
DDM + glycerol	37.02	5.1	199870.2
LPPG	38.18	4.83	164486.8
OG	-	-	-
DPC	39.49	4.53	131999.4
SDS	39.50	4.53	131777.9

Table 22. Summary of the SEC data obtained for Hsmr. The corresponding gel filtration traces can be seen in figure 28. Stoke's radii and molecular weights were calculated using a calibration curve.

Hsmr was purified using; 1 % DDM as solubilising detergent, standard high salt buffer, and purified on an IMAC column using standard wash buffer with 0.1 % DDM and 30 mM imidazole. The detergent was exchanged on the IMAC column in the absence of imidazole to avoid protein elution. Hsmr, in the presence of OG, was eluted as visible aggregates and not investigated further. In all other cases, Hsmr was evaluated regarding aggregation by SEC after 2 and 10 days. Protein samples were stored at 4 °C and in the case of SDS containing buffers at RT. Figure 28 shows the two time traces for each detergent. The largest difference in quantity of aggregation was observed for Hsmr stored in the presence of 0.1 % DDM with 5 % glycerol. Therefore, no improvement over the previously tested condition of 0.1 % DDM, see figure 25, could be achieved. Despite being a suitable detergent for the solubilisation of SMR proteins from the plasma membrane, DDM is not suitable for Hsmr storage. Changes between day 2 and day 10 are small for LPPG, DPC and SDS. In fact, the two time point traces for Hsmr in LPPG overlap perfectly. The different expected micelle sizes (50 kDa for DDM, 19 kDa for DPC, 18 kDa for SDS, unknown for LPPG [210, 220, 221]) may give rise to the differences in calculated molecular weights, see table 22, ranging from 132 to 200 kDa. The detergents with the smallest micelle size give, as expected, the lowest molecular weight estimates. However, if the assumed micelle molecular weights are correct, the calculated PDC molecular weight cannot be explained by this alone. In other words, the PDC of DDM and SDS have a molecular weight difference of around 68 kDa. This cannot arise solely from the expected molecular weight difference of the micelles of only 32 kDa.
Additionally, there are substantial differences with regard to the extent of protein aggregation. The least aggregation is detected in buffers containing SDS, followed by DPC. Both detergents seem to be suitable for maintaining Hsmr stably in solution. SDS is known as a highly denaturing and α-helix inducing detergent and is generally used to unfold proteins, although SDS-PAGE of Hsmr showed that SDS is not able to unfold Hsmr or even break oligomerisation. SDS is an unconventional detergent for maintaining proteins in their native conformation. However, SDS has been used in a few cases for protein structure investigations by NMR and x-ray crystallography [222].

In conclusion, DDM, DPC and SDS are evaluated further with regards to their suitability for reconstitution and used for techniques that require Hsmr in the solution state.

4. 7 Reconstitution of Hsmr

4. 7. 1 Introduction to reconstitution optimization

Transport proteins like SMR proteins can only be fully functional in a vectorial environment. To assess the native structure and transport capability of SMR proteins, these need to be investigated when incorporated in a membrane. To obtain a highly controlled environment, *in vivo* expressed Hsmr is removed from the plasma membrane. Both *in vivo* and *in vitro* produced protein can then be reconstituted into an artificial membrane, which gives complete control over the lipid composition, vesicle size, proteins present and buffering of each compartment. Reconstitution of membrane proteins is commonly achieved by one of three methods: mechanical means such as freeze-thawing and sonication, dissolving protein and lipid in organic solvent with subsequent removal of the solvent, or detergent mediated procedures.
A literature review regarding the most commonly used and promising methods narrowed the choice to methods using solvents or detergents. However, transport proteins are mostly reconstituted using detergent based methods.
Of importance for the reconstitution process are protein stability and activity as well as uniform protein incorporation and orientation. Stability and activity of membrane proteins are mainly governed by the detergent choice and a homogeneous incorporation and preferential orientation in proteoliposomes. Directional protein insertion can be achieved by direct incorporation of the protein into preformed liposomes. Thus, transporters are preferentially reconstituted using preformed liposomes, rather than solubilised lipids. Successful reconstitution can be monitored using discontinuous density gradient centrifugation to separate empty liposomes and proteoliposomes with different protein:lipid ratios [223]. Further characterization of proteoliposomes can be achieved by freeze fracture electron microscopy. This method allows the protein distribution to be assessed as well as monitoring of proteoliposome homogeneity and protein aggregation.

Solvent-based reconstitution has been used successfully for example for diacylglycerol kinase and β–D-galactoside transport protein, using evaporation and dialysis as solvent removal methods [224]. However, the methodology has fallen out of favor as only few proteins are solvent resistant and show native fold and activity after this procedure.
With detergent-based reconstitution, protein incorporation into liposomes is initiated by decreasing the detergent concentration. This can be achieved using dialysis, gel chromatography, dilution or hydrophobic absorption. The method of choice depends mainly on detergent properties such as CMC and hydrophobicity but also on the desired speed of reconstitution and completeness of detergent removal. The most rapid detergent removal is achieved using gel filtration. However, detergents with a low CMC can only be removed efficiently by hydrophobic adsorption, which is also the best method for almost complete detergent removal. The speed of reconstitution can be effectively controlled using dialysis and hydrophobic adsorption. An excellent review on biobead based reconstitution was written by Rigaud *et al*. [225].

Besides choosing an appropriate methodology for Hsmr reconstitution, the choice of lipids and detergents is of prime importance. The choice of detergents was already narrowed down during the experiments investigating Hsmr solubility and monodispersity (Chapter 3 and 4.6). On one hand the selection of lipids was guided by trying to create as native an environment for Hsmr as possible but, on the other hand to keep the lipid composition as simple as possible. The native lipid composition of *H. salinarium* and *E. coli* are listed in table 23. The membrane lipid composition of archeae, like *H. salinarium*, is very different from prokaryotic and eukaryotic

membranes. Archeal lipids are built from isoprenoid units and linked to the glycerol backbone with an ether linkage. Nevertheless, previous studies on Hsmr have shown that it exhibits residual functionality when heterologously expressed in *E. coli* and therefore the *E. coli* lipid composition can serve as a guide for the selection of suitable liposome lipids [28].

Escherichia coli lipid composition [226]			
head group	%	chain length and unsaturation	%
PE	80.4	12:0	4.0
PG	14.9	14:0	3.5
CL	1.3	16:0	26.5
PS	not specified	16:1	34.1
LE	3.4	Δ17	not specified
		18:1	31.9

Halobacterium salinarium lipid composition [88, 226, 227]			
head group	%	chain length	%
non-polar	7	C20	not specified
PG	12	C40	not specified
PGP-Me	not specified		
PGS	not specified		
TGD-1	not specified		
S-TGD-1	not specified		
PA	not specified		

Table 23. Lipid composition of *E. coli* and *H. salinarium*. (PE , phosphatidylglycerol (PG), cardiolipin (CL), phosphatidylserine (PS), lysophosphatidylethanolamine (LE), phosphatidylglycerolmethylphosphate (PGP-Me), phosphatidylglycerosulfate (PGS), galactose1,6-mannose1,2-glucose1,1-sn-2,3-diphytanylglycerol (TGD-1), 3-HSO-galactose1,6-mannose1,2-glucose1,1-sn-2,3-diphytanylglycerol (S-TGD-1), PA (phosphatidic acid))

4. 7. 2 Hsmr reconstitution screen

Initially, a total *E. coli* lipid mixture was tested, as this most closely mimics the conditions found in the heterologous expression host. These first attempts utilized DDM to solubilise total *E. coli* lipids, and biobeads to catalyze the fast and efficient detergent removal. These reconstitutions at moderate protein to lipid mol ratios of 1:800 and 1:100 were successful as judged by discontinuous density gradient centrifugation and freeze fracture electron microscopy, shown in figure 29.

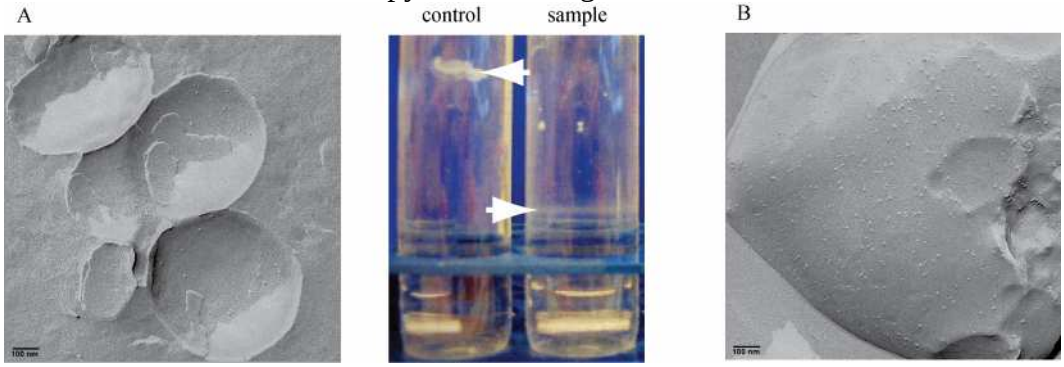

Figure 29. Hsmr in DDM reconstituted into *E. coli* total lipids. Initial Hsmr reconstitution utilized Hsmr solubilised in DDM and *E. coli* total lipid liposomes saturated with DDM as judged by A_{590} measurements. As successful examples, protein:lipid mol:mol reconstitution ratios 1:800 A) and 1:100 B) are shown.

After these initial successes, the aim was not only to find a simpler, more reproducible lipid combination, but also to increase the protein:lipid mol ratio further. Reducing the lipid content of samples is important for solid-state NMR experiments as the sample volume is limited by the rotor. Only at protein:lipid mol ratios of 1:100 or higher are sufficient numbers of spins available for detection of a suitable NMR signal. To fulfill this dual pretence a large variety of lipids was tested, alone and in combination with other lipids. Lipid properties, such as chain length, were matched in lipid mixtures and only bilayer forming lipids were tested singly. An overview is given in table 24. Figure 29 shows examples of selected positive results from sucrose density gradient centrifugation. Only samples that indicated successful incorporation at this step were evaluated further by freeze fracture electron microscopy. Unfortunately, many false positives due to protein aggregation were obtained, see figure 30. The success scoring in table 24 is based on the results of sucrose density gradient centrifugation and freeze fracture electron microscopy.

detergent	lipid	protein:lipid mol ratio	reconstitution method	success	method
DDM	*E.coli* lipids	1:800	rapid dilution	-	
DDM	*E.coli* lipids	1:800	biobeads	++	
DDM	*E.coli* lipids	1:250	biobeads	-	A
DDM	DOPC	1:200	biobeads	+-	
DDM	*E. coli* lipids	1:200	biobeads	++	
DDM	DMPC	1:100	biobeads	-	
DDM	DMPC	1:100	biobeads	-	
DDM	POPE/POPG/Cardiolipin (75/20/5)	1:100	biobeads	-	
DDM	POPC/POPG 5/1	1:100	biobeads	-	
DDM	POPE/POPG 3/1	1:100	biobeads	-	
DDM	*E. coli* lipids	1:100	biobeads	+++	
DDM	DMPC	1:75	biobeads	-	
DDM	*E. coli* lipids	1:75	biobeads	+-	
DDM	PML	1:75	biobeads	-	
DDM	POPC/POPG (5/1)	1:50	biobeads	-	
DDM	DMPC	1:50	biobeads	-	
DDM	DOPC	1:50	rapid dilution	-	B
DDM	DOPC	1:28	dialysis	-	C
DPC	DOPC	1:500	dialysis	-	
DPC	DOPC	1:500	dialysis	-	
DPC	*E.coli* lipids	1:250	dialysis	-	A
DPC	*E.coli* lipids	1:100	biobeads	-	
DPC	POPC/POPG (5/1)	1:50	biobeads	-	
DPC	DOPC	1:42	dialysis	-	C
OG	*E.coli* lipids	1:250	biobeads	-	A
OG	Archaeal lipid (16:0)	1:100	biobeads	-	
OG	DOPC	1:50	dialysis	-	C
SDS	DMPC	1:75	biobeads	-	
SDS	DOPC	1:75	biobeads	-	
SDS	PML	1:75	biobeads	-	
SDS	Archaeal lipids	1:75	biobeads	-	
SDS	POPC/PG (5/1)	1:75	biobeads	-	
SDS	*E.coli* lipids	1:75	biobeads	-	
Triton X-100	DMPC	1:75	biobeads	+-	
Triton X-100	*E.coli* lipids	1:75	biobeads	+-	
Triton X-100	PML	1:75	biobeads	-	
Organic solvent	*E.coli* lipids	1:800	-	-	D

Table 24. Overview of attempted reconstitution conditions. Tested conditions are grouped according to the utilized detergent, with increasing detergent/lipid ratio. The success is rated from +++ for uniform incorporation at a density expected for the utilized ratio without protein aggregation to – for failure to incorporate significant amounts of protein and protein aggregation. If more than one band was observed during density gradient centrifugation, only the lowest was investigated further by freeze fracture electron microscopy. Conditions marked with A) used liposome solutions without detergent pre-softening. Conditions marked with B) were tested using the rapid dilution methodology [165]. Conditions marked with C) were tested on an IMAC column [164], attempting the reconstitution of immobilized protein. Conditions marked with D) utilized an organic solvent based reconstitution method [228]. (1,2-Dimyristoyl-*sn*-phosphatidylcholine (DMPC), 1,2-Dioleoyl-*sn*-phosphatidylcholine (DOPC), purple membrane lipids (PML), 1-palmitoyl-2-Oleoyl-*sn*-phosphatidylethanolamine (POPE), 1-palmitoyl-2-Oleoyl-*sn*-phosphatidylglycerol (POPG)).

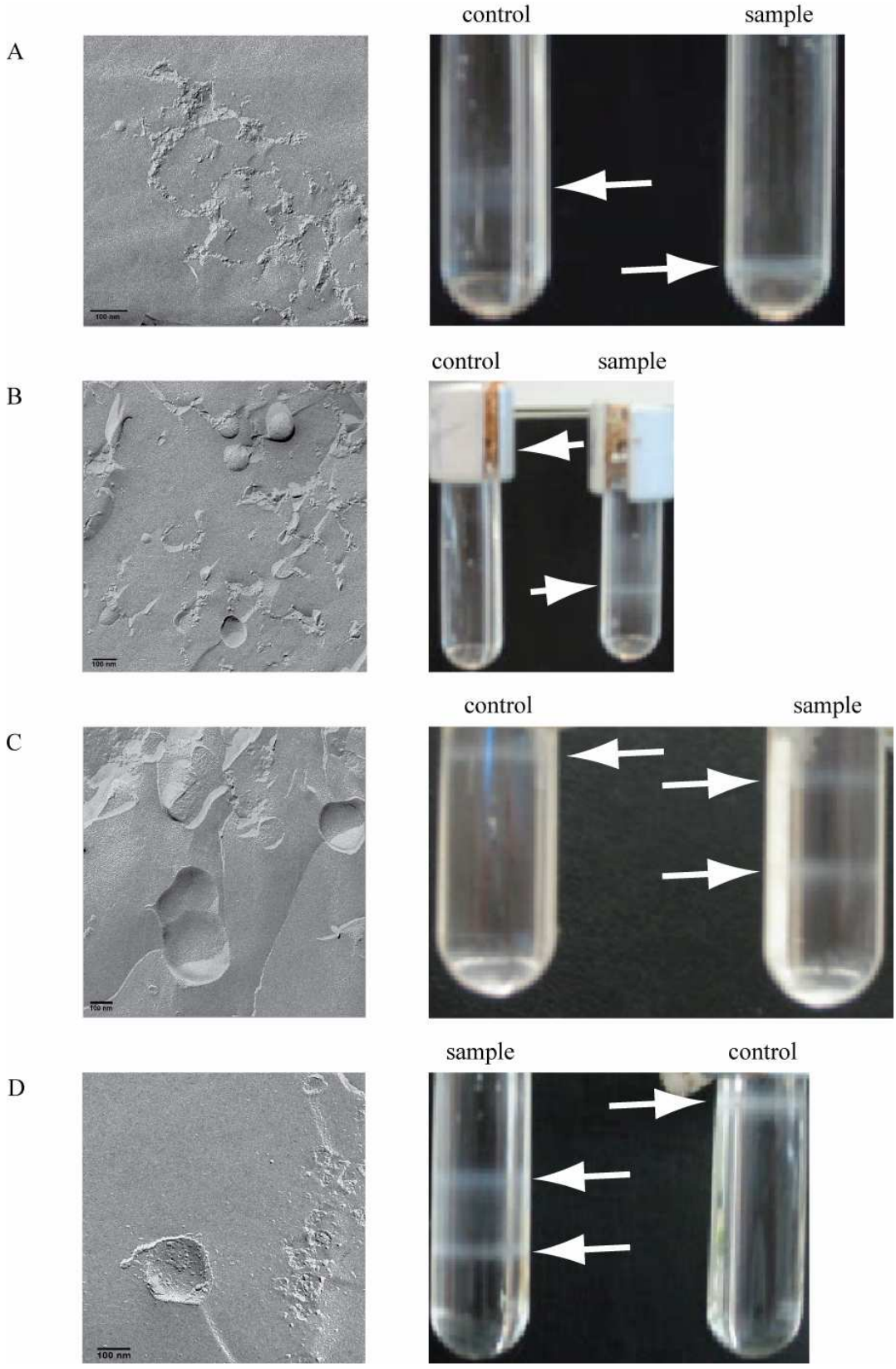

Figure 30. Examples of reconstitution trials – two step selection using density gradients and freeze fracture imaging to detect successful reconstitutions. A) Hsmr in 0.41 % SDS reconstituted into PML using SDS (1:75 mol:mol ratio) , B) Hsmr in SDS reconstituted into POPC/PG using SDS (1:75 mol:mol ratio), C) Hsmr in 0.1 % DDM reconstituted into PML using DDM (1:75 mol:mol ratio), D) Hsmr in 0.1 % DDM reconstituted into DMPC using DDM (1:75 mol:mol ratio). Standard buffer was used for all reconstitution trials with the exception of SDS containing samples.

The result after this extensive screen was sobering as the starting conditions were best. The lowest protein:lipid mol ratio achievable was 1:100 and DDM with *E. coli* total lipids proved to be the best detergent/lipid combination. Additionally, hopes to obtain directional insertion of Hsmr could not be realized. Directed incorporation requires the use of saturated liposomes instead of solubilised lipids [229]. Saturated lipids, defined as R_{sat}, were obtained initially by experimental determination [143], later by utilizing the theory developed by Lichtenberg *et al*. [230]. However, the dilute Hsmr protein solutions that were eluted from the IMAC column contributed sufficient detergent molecules to push protein-detergent-lipid mixtures from the R_{sat} value over the R_{sol} threshold, leading to solubilised lipids.

In conclusion, Hsmr can be reconstituted successfully into *E. coli* total lipid liposomes. The protein:lipid mol ratio attainable, 1:100, was sufficient for solid state NMR experiments on Hsmr.

4. 8 Conclusion

Hsmr can be purified to a high degree using IMAC as a single step. Detergents suitable for maintaining Hsmr long-term stability are DPC and SDS. DDM is suitable for short-term storage and reconstitution. Successful incorporation of Hsmr into liposomes could be achieved at a 1:100 protein:lipid mol ratio using DDM, *E. coli* total lipids and hydrophobic absorption based detergent removal. Hsmr can be successfully prepared both for solution-state methods and for solid-state NMR.

Chapter 5 - Hsmr oligomerisation state

5.1 Introduction

5. 1. 1 Introduction to oligomerisation

Protein characterisation naturally involves the assessment of a proteins oligomeric state and functional stoichiometry. Particularly important is the knowledge of the strength of the oligomerisation as it may have a regulatory role. Furthermore, determination of the interaction surface as either isologous or heterologous can limit the type of oligomerisation, as these are possible even within homooligomers. Interestingly, it has emerged in recent years that only around $1/5^{th}$ of all proteins are monomeric and that dimers are the most common quaternary structure. Additionally, it was observed that 79 % of all oligomers are homooligomers and these are almost exclusively symmetric [231]. Notable exceptions to this are membrane proteins, which are embedded in an asymmetric membrane environment and therefore limited with respect to possible symmetry axes. Local asymmetry, associated often with half-of-site reactivity, is commonly found as well as a reciprocating mechanism. An interesting example of local asymmetry and proposed half-of-site reactivity is haemolysin B [232].

AcrAB [18] and the F_1F_0 ATP synthase [233, 234] are prominent examples for the reciprocating mechanism. However, the reasons for the prevalence of oligomeric proteins are still under investigation. Currently it is thought that the key benefits of oligomerisation are: faster and less error prone folding of smaller proteins, better error control of the final protein, possibility for regulation at the level of protein assembly, greater stability and capability for a variety of functions [231, 235].

5. 1. 2 Introduction to Hsmr oligomerisation

Despite extensive investigations of the SMP protein [25] EmrE, its oligomerisation state could not be determined unequivocally, although most evidence suggests that EmrE is a functional dimer [27, 35, 40]. The oligomeric state of full length Hsmr has not been evaluated. Instead, Rath *et al.* used synthetic peptides of TMS 1 to 4 to assess the oligomerisation behaviour of Hsmr. They concluded that Hsmr can form either dimers or tetramers using two distinct interaction surfaces [70]. SDS-PAGE and SEC in this study suggest that Hsmr in detergent micelles is in a dynamic equilibrium between dimeric, trimeric, tetrameric and higher oligomeric states, but neither method is ideally suited for the investigation of oligomeric species. During SDS-PAGE, ideally all non-covalent interactions are broken and polypeptides migrate solely based on their molecular weight. However, several cases of SDS resistant multimers have been reported [236]. SEC separates molecular complexes based on their Stokes radius, which enables an estimate of the molecular weight only if the protein-detergent complex is approximately globular [177]. Additionally, the protein oligomeric state can only be derived if the amount of bound detergent is known [173]. To investigate the intriguing and elusive oligomeric state of solubilised full length Hsmr, three methods were employed: Native PAGE and AUC are typically used to obtain information regarding protein oligomeric states and the K_ds of these protein-protein interactions. In addition the new MS technique LILBID was used here.

5. 2 Analytical ultracentrifugation

One of the classical biochemistry techniques, the use of analytical ultracentrifugation to elucidate the mass, shape and stoichiometry of proteins, dates back to the 1930s [237]. More recently, methods have been developed that enable also the investigation of membrane proteins [174, 238]. The key benefits of analytical ultracentrifugation are the possibility for real time observation of sedimentation, and that both hydrodynamic and

thermodynamic data can be collected using either sedimentation velocity or sedimentation equilibrium experiments respectively. Sedimentation velocity experiments provide combined molecular mass and shape information, yielding the sedimentation coefficient S. During the experiment a strong centrifugal field is applied and a sedimentation boundary is formed which moves with time to the cell bottom. Absorption scans determine the rate of boundary movement and broadening. The thus determined experimental S values need to be reported as $S_{(temperature,buffer)}$ and for comparison between experiments adjusted to $S_{(20°C,water)}$ [239]. In contrast sedimentation equilibrium data supplies solely molecular weight information and is performed at low centrifugal fields. This enables the investigated molecules to reach an equilibrium position where sedimentation and diffusion are balanced. The equilibrium concentration distribution is analysed to obtain the apparent molecular weight MW_{app} [239]. For the investigation of even weak protein-protein interactions of membrane proteins, analytical ultracentrifugation is proving very successful, examples include the multidrug transporter EmrE [35] and BmrA [173] as well as the receptor ErbB [240].

5. 2. 1 Sedimentation velocity analysis of Hsmr

Here, sedimentation velocity was used to aim at the identification of the number of discrete Hsmr species and the Hsmr oligomeric state. The sedimentation velocity experiments can answer this question by measuring the sedimentation coefficients which are related to the molecular mass. However, if molecular weight information is sought, the frictional ratio of all species needs to be identical [176]. For Hsmr it is not known if this is true, and therefore only the experimental sedimentation coefficients $S_{(temperature,\ buffer)}$ and the number of discrete species are calculated. Sedimentation velocity experiments can be analysed using several methods, including a plot of ln radius of boundary midpoint against time, diffusion corrected analysis (G(s)), time derivative method (DCDT), fitting of the Lamm equation, equation 14 [239]. Here the model dependent continuous sedimentation coefficient analysis, c(s) analysis, which attempts to fit the experimental data to numeric solutions of the Lamm equation, was used. This analytical approach was chosen as it makes use of the whole sedimentation boundary and takes into account the effect of diffusion. It therefore provides a high-resolution determination of the sample homogeneity. Furthermore, even if the theoretical assumption of ideal sedimenting, non-interacting or slow interacting molecules (on the time-scale of the experiment) is not met; a valuable and valid average sedimentation coefficient can still be obtained.

5. 2. 1. 1 Sedimentation velocity analysis of Hsmr in DDM

As can be seen from figure 31A and more pronounced from the residuals analysis in figure 31B, the c(s) analysis in the computer program Sedfit9.4 does not provide a satisfactory fit of the data. Possible reasons for this dissatisfactory result are the use of estimates for the frictional ratio and different frictional ratios for different oligomeric species. Buffer density, viscosity and Hsmr partial specific volume can be computed using the computer program Sednterp. The frictional ratio of the PDC and the partial specific volume of the PDC can only be estimated. Here a typical frictional ratio for globular proteins (f/f_o = 1.2) and the calculated Hsmr partial specific volume (υ_p = 0.7533 mL/g) were used as estimates for the PDC. Nevertheless, in figure 31C the obtained sedimentation coefficient profile is depicted. The results should therefore be merely taken as a rough estimate of the sedimentation coefficient. A broad peak centred around 3.075 S, trailing to 16 S can be observed. The spike at 20 S is an analysis artefact. The sedimentation coefficient profile suggests that the sample is very inhomogeneous with a very broad size distribution around 15 S. The trace to higher

sedimentation coefficients probably arises from Hsmr aggregation in DDM, as already observed in chapter 4. From protein stability experiments, figure 25 and figure 28, it is known that DDM is not suitable for Hsmr long-term storage and aggregation occurs almost immediately. Below traces in figure 31A, the first 10-15 scans show a ladder-like or two-steps profile which indicates a fast sedimenting species is present. It sediments quickly to the cell bottom, therefore a drop in the plateau after ~15 scans is detected. However, DPC at 4 °C is known to provide a more stable protein preparation with little aggregation. In order to further investigate the native oligomerisation behaviour of Hsmr sedimentation velocity, experiments in DPC at 4 °C were also conducted.

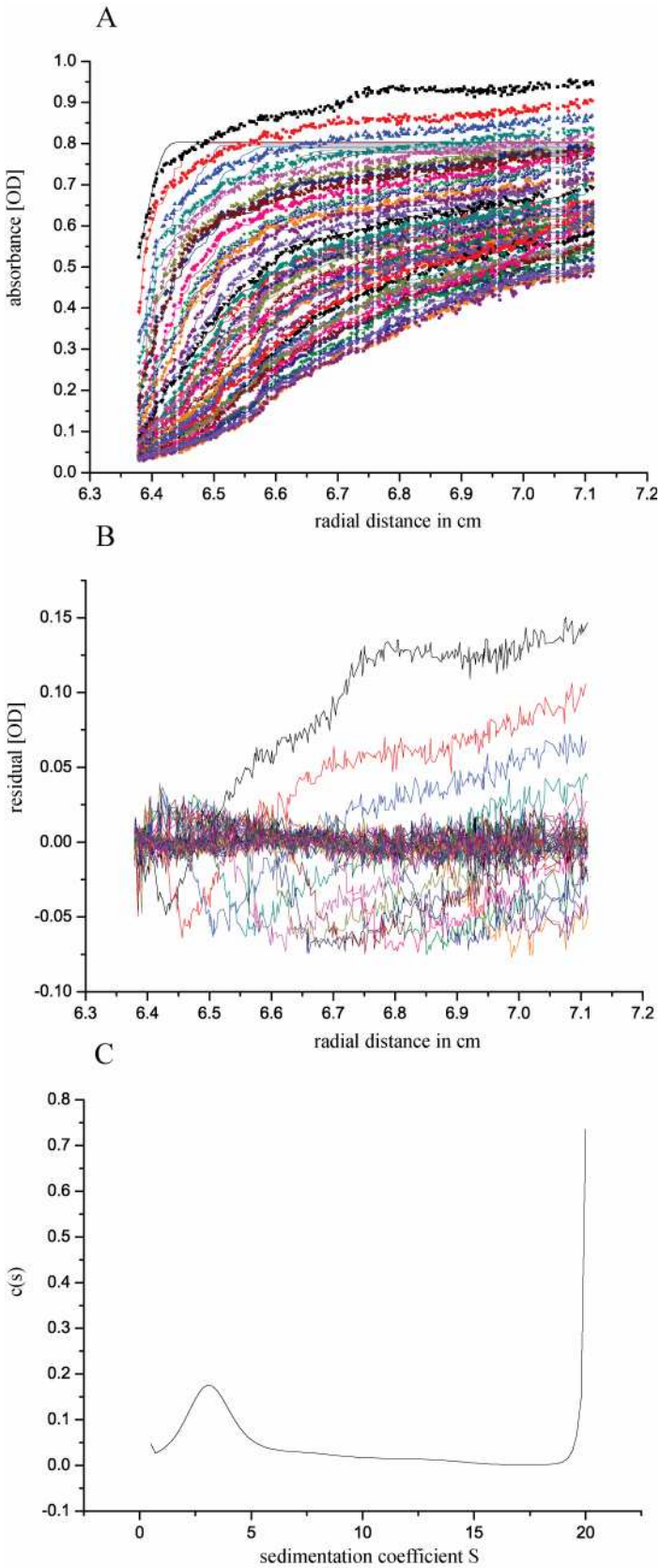

Figure 31. Sedimentation velocity of Hsmr in standard buffer and in the presence of 0.1 % DDM. A) Superimposed are experimental sedimentation profiles as individual data points and the fitted curves as lines from the c(s) analysis in Sedfit of Hsmr at 1.65 mg/mL in the presence of 0.1 % DDM. The last profile corresponds to 3 h 45 min sedimentation at 116444 g at 20 °C. B) Superimposed residuals between the experimental and fitted curves from A). C) c(s) analysis reveals one peak centred at 3.075 S with a large continuous trail to approximately 16 S. The spike at 20 S is a data analysis artefact.

5. 2. 1. 2 Sedimentation velocity analysis of Hsmr in DPC

As can be seen from figure 32A and more pronounced from the residuals analysis in figure 32B the c(s) analysis in the computer program Sedfit9.4 of Hsmr in DPC provides an acceptable fit of the data. The obtained sedimentation coefficient profile displayed in figure 32C, is shows a single peak centred at 1.5 S. A single peak centred at 1.5 S can be observed. The spike at 0.5 S is an analysis artefact. Here the absence of a two step profile indicates the absence of high molecular weight aggregates. The smaller S value for Hsmr in DPC indicates a lower oligomerisation state in DPC. Overall, the obtained sedimentation coefficient profile of Hsmr in DPC suggests that the sample is homogeneous and a single type of PDC with a small sedimentation coefficient is present.

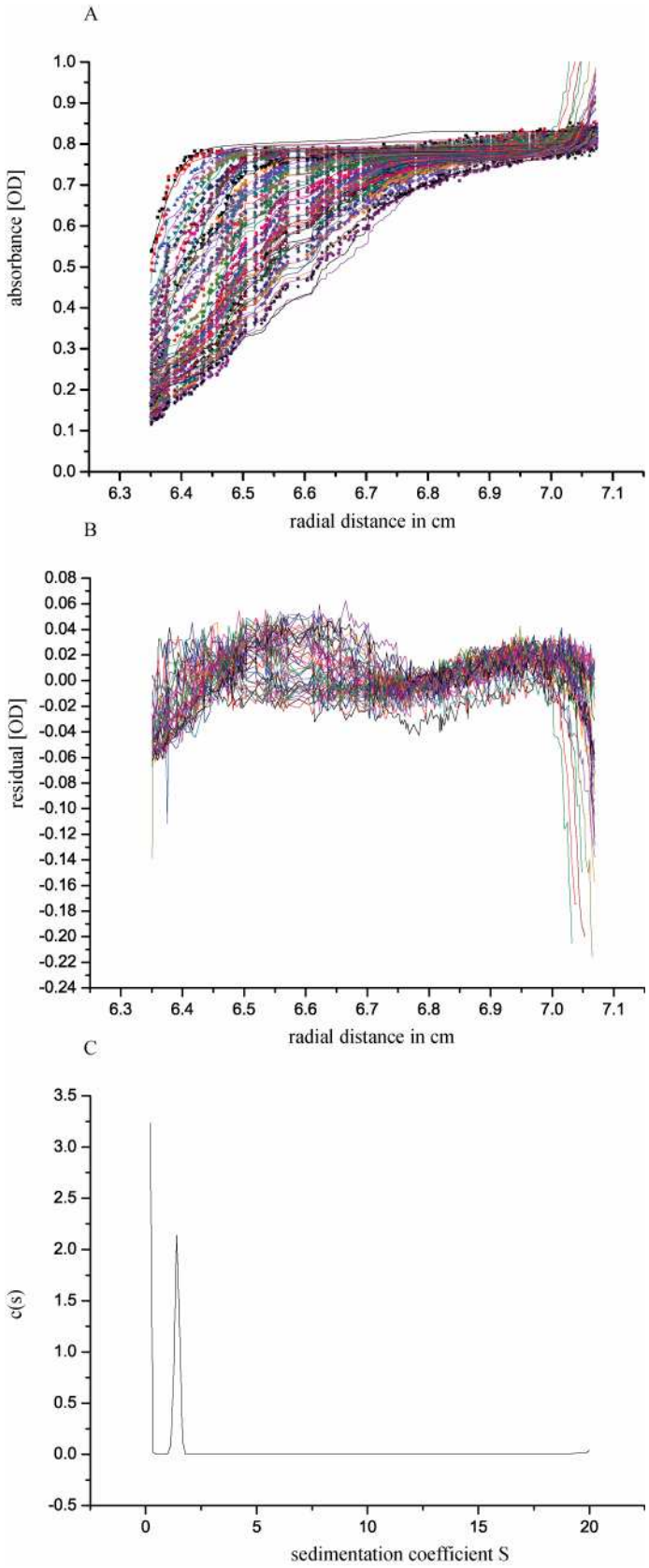

Figure 32. Sedimentation velocity of Hsmr in standard buffer and in the presence of 0.1 % DPC. A) Superimposed are experimental sedimentation profiles as individual data points and the fitted curves as lines from the c(s) analysis in Sedfit of Hsmr at 2.0 mg/mL in the presence of 0.1 % DPC. The last profile corresponds to 8 h 15 min sedimentation at 116444 g at 4 °C. B) Superimposed differences between the experimental and fitted curves from A). C) c(s) analysis reveals one peak centred at 1.5 S. The spike at 0.5 S is a data analysis artefact.

5. 2. 2 Sedimentation equilibrium analysis of Hsmr

In order to further investigate the native oligomerisation state of Hsmr and obtain the Hsmr molecular weight, sedimentation equilibrium analysis was performed. Sedimentation equilibrium analysis enables the measurement of the PDC molecular weight [239]. The contributions of the detergent micelle to the measured molecular weight can be removed using several approaches, namely, measurement of density increment, calculation of density increment by summation and density matching [241]. Currently, the most common approach, density matching, is also used here. Briefly, density matching requires the solvent to have the same density as the detergent. This renders the detergent neutrally buoyant and removes its contribution to the sedimentation behaviour of the PDC. However, the high salt content of the standard Hsmr buffer means that the buffer density (ρ=1.08055 g/mL) is already higher than the density of the detergent DPC ($1/ \upsilon_p$ = 1/0.937 mL/g = 1.067 g/mL) and thus cannot be density matched by adding D_2O. Therefore, a buffer with a lower salt concentration needs to be used for sedimentation equilibrium experiments. The standard buffer with just 1 M NaCl has a density of ρ=1.04069 g/mL, which enables DPC to have neutral buoyancy at a concentration of 25 % D_2O (ρ=1.067 g/mL).

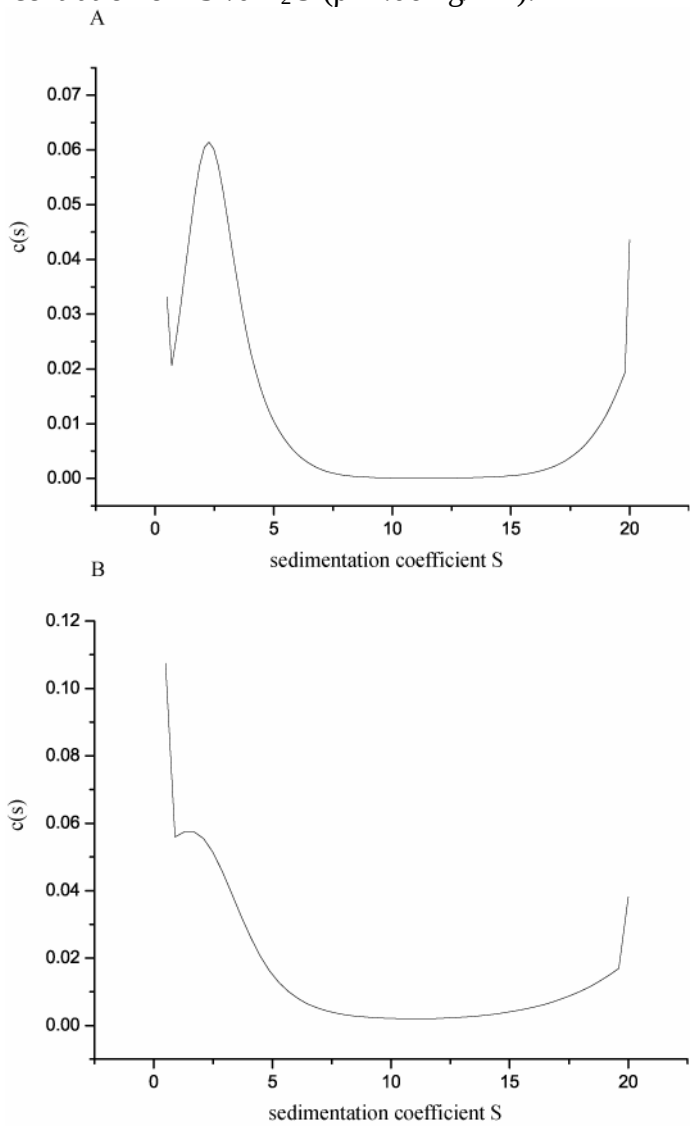

Figure 33. Initial analysis of Hsmr sedimentation equilibrium data using c(s) analysis. A single Hsmr sample in 1 M NaCl, 15 mM $Na_xH_xPO_4$, pH 8.0 was diluted to a final concentration

of 0.56 mg/mL with H_2O and/or D_2O. A) Hsmr in the presence of 15 % D_2O, B) Hsmr in the presence of 25 % D_2O was centrifuged at 18144 g.

To judge the data quality, sedimentation equilibrium data is first analysed by c(s) analysis. A single Hsmr preparation was diluted to obtain 1 M NaCl, 15 mM $Na_xH_xPO_4$, pH 8.0 with different H_2O and/or D_2O mixtures. A total of 4 samples with different D_2O concentrations were analysed at two rotor speeds (8046 g, 18144 g) to attain 2 different equilibrium positions per sample. Unfortunately, already the c(s) analysis revealed apparently inconsistent sample homogeneity, see figure 33. A possible reason for the different apparent number of sedimenting species and differences in sample homogeneity lies in the effects of D_2O and salt on halophilic proteins. In fact, it has been described that D_2O has salting out effects like NaCl, and that both compounds can have additive effects [78]. All other experimental conditions can be excluded as a source for inconsistencies since they are identical. It is therefore likely that sedimentation equilibrium experiments using the density matching approach are not feasible with Hsmr.

5. 2. 3 Analytical ultracentrifugation summary

Sedimentation velocity experiments revealed that Hsmr in DDM is unstable even at high salt concentrations and for short periods of time. Hsmr in DDM is found in a defined but broad range of sedimentation coefficients, arising from a continuum of oligomerisation or aggregation states. In contrast, Hsmr is stable in DPC at high salt concentrations and a single highly populated species of Hsmr is detected. Under these conditions Hsmr is predominantly homogeneous. The sedimentation equilibrium experiments performed in DPC at 1 M NaCl with different D_2O concentrations. D_2O and NaCl have additive effects for halophilic proteins and thus data generated at different D_2O concentrations could not be compared. Therefore the Hsmr molecular weight and thus the oligomerisation state of Hsmr in DPC could not be determined.

5. 3 BNPAGE

BNPAGE is the native PAGE technique suitable for most membrane proteins. Unlike SDS-PAGE during native PAGE the investigated proteins are denatured neither during sample preparation nor during electrophoresis. To investigate membrane proteins in their native state in solution detergent micelles need to be present. The blue dye coomassie acts here as detergent, adds a molecular weight dependent charge shift, and reduces the risks of protein aggregation by providing a uniform charge. Unfortunately, BNPAGE also requires low salt concentrations to avoid protein stacking and sample heating [161]. Finally, to obtain a very accurate membrane protein molecular weight, the standard curve generated with soluble proteins needs to be modified according to the formula described by Veenhoff *et al.* [242]. In the past, BNPAGE has been used successfully for the determination of very weak protein-protein interactions mainly of mitochondrial membrane proteins.

Here, various BNPAGE recipes [161] [160], NativePAGE™, Novex® System from Invitrogen, various low salt concentrations and different detergents were tested. Figure 34 depicts a typical BNPAGE of Hsmr and soluble proteins as molecular weight standards.

Figure 34. BNPAGE of Hsmr. The soluble proteins A) BSA, B) ferritin and C) catalase were used as molecular weight marker. Hsmr was investigated in 15 mM Tris pH 8.0, > 0 M NaCl and D) 0.1 % DPC or E) 0.1 % DDM. This gradient gel was not successful in separating Hsmr.

Despite avid testing, no conditions could be found for successfully electrophoresis of Hsmr. It has been reported previously that not all proteins can be investigated successfully by BNPAGE, even if the electrophoresis conditions are close to the native protein environment. Likely reasons for the failure of Hsmr electrophoresis by BNPAGE are: Hsmr aggregation due to extremely low salt concentration for a halophillic protein and potentially poor binding of the anionic dye and detergent coomassie to the highly acidic Hsmr. It was concluded that BNPAGE cannot be used to study the stoichiometry of solution-state Hsmr.

5. 4 LILBID

Laser induced liquid bead ion desorption is a novel MS technique which is capable of analysing ionic non-covalent macromolecular complexes. Briefly, solution droplets are injected into a vacuum chamber, irradiated at the frequency of water stretching vibrations, and the ionic molecules which are released by the bursting droplets then analysed by MS. The technique has been established using a variety of biomolecules including DNA, soluble proteins and membrane proteins [181, 243]. With respect to this study, the relevant LILBID validation used F_1F_0-ATP synthase c-rings. It could be shown that, using ultra soft ionization conditions, intact c-rings comprised of 11 to 15 protomers can be observed with LILBID, though SDS-PAGE analysis denatured these oligomers [181]. For Hsmr, SDS resistant oligomers are well documented, with dimers being the smallest oligomers observed. It could therefore be expected that LILBID enables the observation of the native Hsmr oligomerisation state. Figure 35 shows LILBID spectra of Hsmr in three different detergents. Along the x – axis, molecules are separated according to their mass/charge ratio, and their abundance recorded along the y – axis.

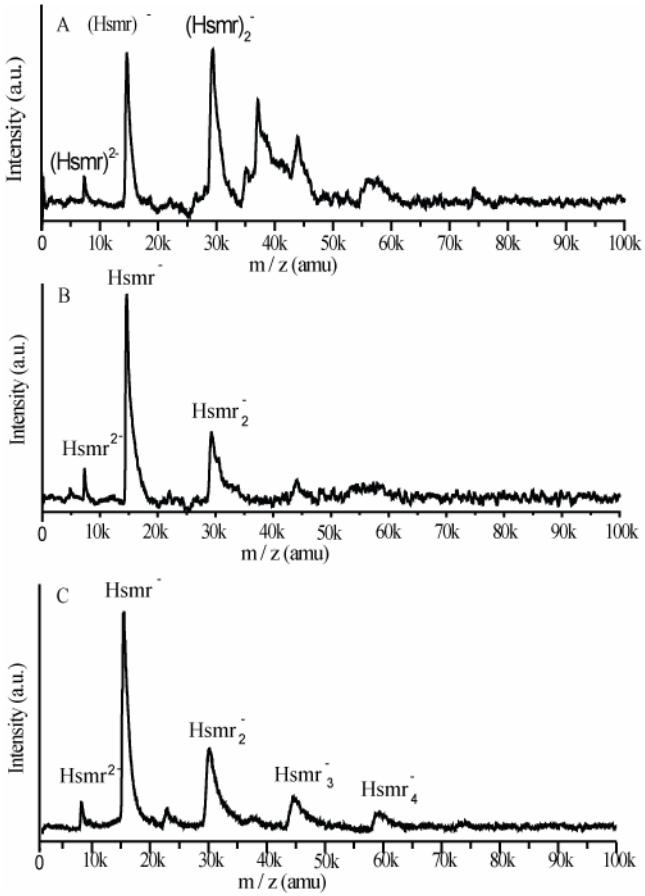

Figure 35. LILBID measurement of Hsmr in different detergents. Hsmr was measured in the ultra soft ionisation mode after being dialysed into 15 mM Tris, pH 8.0 without detergent. The detergent concentrations given are therefore the upper limit. A) $5.6x10^{-5}$ M Hsmr in < 0.1 % DDM, B) $5.51x10^{-5}$ M Hsmr in < 0.1 % DPC and C) $5.6x10^{-5}$ M Hsmr in < 0.41 % SDS.

It can be clearly seen that Hsmr in all detergents is present as monomer, dimer, trimer and tetramer. The fact that Hsmr at nearly 0 M NaCl could be detected by LILBID as discrete multimers suggests that Hsmr is not yet aggregated and probably correctly folded. The observation of the halophilic Hsmr at 0 M NaCl supports the hypothesis that halophillic proteins retain a nearly native fold at low salt concentrations but experience a time-dependent decrease in stability [80]. In the following, the effect of detergents on Hsmr oligomerisation is described. Indeed, the oligomerisation equilibrium is at a different position for each detergent, indicating that detergents effect Hsmr oligomerisation. In DDM, the detergent of choice for Hsmr functional investigations and reconstitution, Hsmr is mainly present as oligomer, see figure 35A. The dimeric Hsmr state is most populated. The origin of the peak at 38 kDa is unknown and not detected for the same Hsmr sample in different detergents. Not surprisingly, harsh detergents like DPC and SDS dissociate Hsmr more efficiently than the milder DDM. In the zwitterionic DPC and anionic SDS, monomeric Hsmr is clearly the most abundant state, figure 35B and figure 35C. Pentameric Hsmr cannot be detected in the presence of DPC and may only be anticipated in the presence of SDS. However in several ways the result is surprising: Hsmr was expected to be a stable dimer and/or tetramer in solution [36, 70], resistant to SDS mediated oligomer dissociation as witnessed by SDS-PAGE and the Hsmr homo-oligomerisation was expected to be self-limiting [70, 244].
In light of these LILBID results, the presence of multimers on SDS gels is not surprising, but the absence of monomers is. The fundamental difference in experimental parameters between LILBID and SDS PAGE was the salt concentration. LILBID

required low salt concentrations, while SDS PAGE could be performed with Hsmr in the presence of 2 M NaCl. Ionic concentrations are well known to effect oligomerisation behaviour in non-halophilic proteins [244] and for halophilic proteins oligomerisation is a suggested stabilizing mechanism [78]. The discrepancy between Hsmr oligomerisation behaviour as assessed by SDS-PAGE and LILBID cannot be elucidated conclusively. The discrepancy may arise from the ability of different methods to discriminate between molecular interactions, or may be due to the different salt concentrations. However, the lack of self-limiting oligomerisation as detected by SDS-PAGE and LILBID suggests that Hsmr in its native environment is present at low concentrations, thus avoiding its uncontrollable oligomerisation behaviour *in vivo.*

To follow this up, the effect of the Hsmr concentration on its oligomerisation state was investigated. This is necessary since it is known that not only the dissociation constant (K_d) determines a protein's oligomerisation state but that protein concentration can in some cases also influence the oligomeric state of a protein [244]. In figure 36, the degree of Hsmr oligomerisation at two different concentrations can be seen.

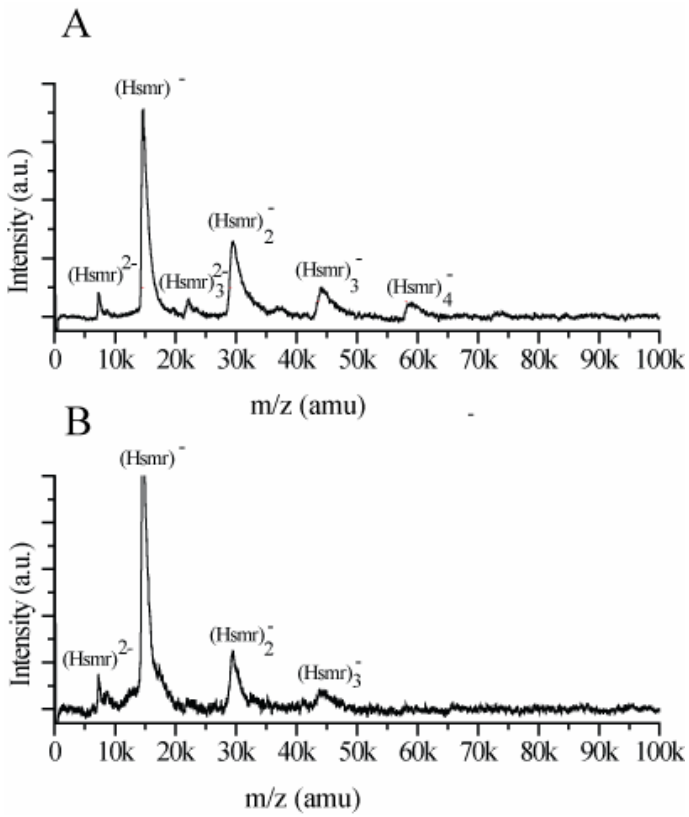

Figure 36. LILBID of Hsmr in SDS at different concentrations. Hsmr in < 0.41 % SDS at A) $5.6x10^{-5}$ M and B) $7x10^{-6}$ M. A concentration decrease of one order of magnitude leads to the disappearance of tetrameric Hsmr species and a reduced content of trimeric Hsmr.

Here Hsmr at $7x10^{-5}$ M = 1.0 mg/mL is investigated and present mainly as a monomer, but dimer, trimer and tetramer are also detected. After decreasing the concentration by only one order of magnitude, Hsmr tetramer can no longer be detected.
From this it is clear that Hsmr oligomerisation is concentration dependant and reversible. Such dynamic, reversible oligomerisation behaviour has been observed for many proteins and often has regulatory functions [245] [246] [247]. It can be

hypothesised that Hsmr activity in its native host is also regulated via oligomerisation but oligomerisation in the membrane was not investigated here.

Inferences from EmrE to the whole class of SMR proteins have to be treated cautiously. In particular, comparisons of Hsmr and TBsmr with EmrE are precarious, as *H. salinarium* and *M. tuberculosis* live under vastly different physiological conditions than *E. coli*. In fact, regarding the protein oligomerisation state, discrepancies within one protein family have been reported for organisms in different environmental conditions [244]. It is therefore likely that this is also the case here.

Unfortunately, the obtained data is not able to answer the question of the Hsmr oligomerisation state *in vivo*, as this would require assessment directly in the native *Halobacterium salinarium* plasma membrane. However, functional investigations suggest that SMR proteins are only functional as oligomers, which indicates that Hsmr is an obligate multimer. It can also be concluded that Hsmr is a transient oligomer in detergent solutions. In such a system, Hsmr oligomerisation behaviour is dynamic, reversible and can be manipulated by the choice of detergent and probably salt concentration.

5. 5 Conclusions regarding the Hsmr oligomerisation

The result that Hsmr is in dynamic equilibrium between a multitude of different oligomerisation states is supported by LILBID and analytical ultracentrifugation of Hsmr in the presence of DDM. Discrepancies between LILBID and analytical ultracentrifugation were found for Hsmr in DPC at high salt concentrations may derive from differences of the experimental conditions, and method inherent differences in resolution and sensitivity. The resolution and sensitivity of analytical ultracentrifugation is much lower than for LILBID and the samples investigated are more concentrated than those investigated by LILBID. Due to the low resolution of the analytical ultracentrifugation methods, the differentiation and quantitation of different oligomerisation states was not possible. Here, it is proposed that Hsmr, like EmrE (chapter 9), is in a concentration dependent equilibrium between monomer and oligomer. The transient oligomerisation of Hsmr in detergent solutions can be manipulated by the choice of detergent and probably salt concentration. Functional investigations suggest that SMR proteins are only functional as oligomers, which indicates that Hsmr is an obligate multimer.

Hsmr oligomerisation is not self-limiting. From this, it can be inferred that the oligomerisation surface is heterologous. Unfortunately, the obtained data is not able to answer the question of the Hsmr oligomerisation state *in vivo* as this would require assessment directly in the native *Halobacterium salinarium* plasma membrane.

Chapter 6 - Hsmr activity assays

6. 1 Introduction

Activity assays have always played a dominant role in elucidating structure-function relationships. The knowledge of a protein's functional mechanism lies at the heart to understanding proteins and the functions of living cells/organisms. Activity assays enable assessment of the success of purification methods and are necessary to verify that structural information of proteins is gained from natively folded proteins. In the case of membrane transport proteins, two types of activity assays can be distinguished. The first type of activity assay measures the ability of the detergent solubilised protein to bind its native substrates with a K_d similar to that observed *in vivo*. The second type of activity assay measures vectorial transport of substrates from one compartment to another, thus requiring the protein to be reconstituted in a membrane.

6. 2. Binding assays

Binding assays enable the substrate binding event to be studied separately from the rest of the catalytic cycle. This allows qualitative data regarding the substrate range and quantitative data such as substrate dissociation constants and protein:substrate stoichiometry to be obtained [248]. Binding studies can be performed with crude protein preparations or purified protein. For initial investigations, often crude preparations are used. But to obtain meaningful and reproducible data regarding one protein, a purified preparation is required. The most sensitive binding assays use photochemical reactions or radioactivity to generate a signal [249].

6. 2. 1 Radioactive TPP^+ binding assay

For EmrE a radioactive TPP^+ binding assay is widely used [27]. The basic idea of this assay is to selectively measure the specific binding of $[^3H]TPP^+$ to a known quantity of pure detergent solubilised protein immobilised on Ni-NTA beads. See Material and Methods section 2. 2. 7. 1 for a detailed description of the assay procedure.

Pure EmrE, solubilised in a DDM containing buffer at alkaline pH, exhibits strong and specific TPP^+ binding. EmrE K_ds of 10 nM – 25 μM have been reported [27] [37]. For Hsmr, TPP^+ binding assays were performed previously only on crude membrane preparations. The reported salt concentration dependent K_d of 40 - 200 nM is therefore merely an extrapolation [28]. Here, radioactive TPP^+ binding to pure Hsmr is investigated for the first time. A representative experiment is shown in figure 37.

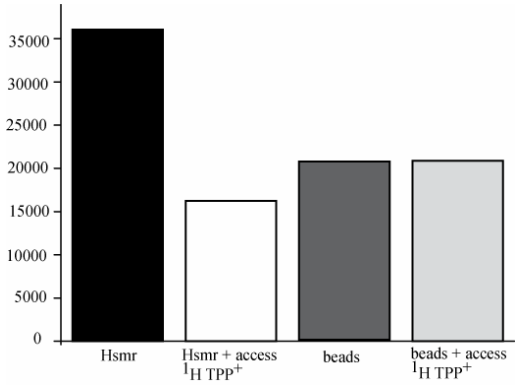

Figure 37. Purified Hsmr specifically binds TPP^+. Purified Hsmr (2 μg) in 2 M NaCl, 15 mM Tris, pH 8.5 and 1 % DDM was bound to Ni-NTA beads and then incubated with 25 nM radioactive $[^3H]TPP^+$. Identical binding reactions were performed with beads that had not been bound with Hsmr. Each TPP^+ reaction was performed in the presence and the absence of 25 μM non-radioactive $[^1H]$ TPP^+.

In this study, 1 µg purified Hsmr was shown to bind 0.25 pmol TPP^+ once non-specific binding is accounted for using the control measurements. This value can only be compared to ~ 10 µg total membrane protein containing Hsmr binding 0.5 pmol TPP^+ [28] and 1 µg purified EmrE binding 0.75 pmol TPP^+ [27]. This suggests that the produced and purified Hsmr is functional. However, the assay was only possible in the presence of 1 % DDM and at pH 8.5. Lower detergent concentrations and pH values published [28] proved to be printing errors [250]. Detergent concentrations far above the cmc are known to induce protein aggregation and should generally be avoided [222]. The necessity to provide such large excess of DDM highlights the already discussed instability of Hsmr in DDM, see Chapter 4.6. Therefore, alternatives to a radioactive binding assay were sought.

6. 2. 2 Binding study using intrinsic tryptophan fluorescence

A fluorescence assay based on tryptophan quenching to measure the affinity of SMR proteins for TPP^+ has been published previously with EmrE [251]. The technique relies on the fact that tryptophans are intrinsic fluorophores. The precise emission wavelength of fluorescence and fluorescence intensity of tryptophans is highly sensitive to the local environment. In particular changes in hydrophobicity and cation/π interactions are able to influence the fluorescence properties of tryptophan. Recently, it was shown for EmrE that changes in fluorescence intensity at 338 nm report mainly the occupancy of the binding site [252]. Further it could be seen that the binding pocket remains hydrophobic under all conditions as no Stoke shift is observed [252]. Cation/ π interactions between the conserved residue Trp63 and positively charged substrates such as TPP^+ have been proposed and implicated in substrate binding and transport [253]. Indeed, quenching of tryptophan fluorescence by TPP^+ by 22 % was observed for EmrE [251]. This further supports the evidence that Trp63 is directly involved in substrate binding and/or transport and does not merely fulfil a structural role.

Here, Hsmr substrate interactions, TPP^+ and benzalkonium, were investigated using tryptophan quenching to obtain the substrate K_d. Data were fit using a binding function, see equation 12 for details, that takes into account the approximately equimolar concentrations of protein and substrate as well as non-specific binding. This binding function has been previously used to fit Smr tryptophan quenching by TPP^+ [169].

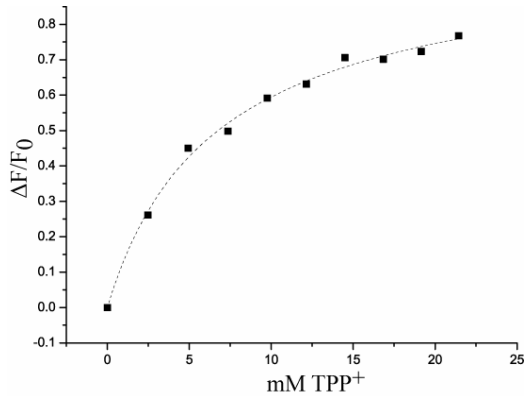

Figure 38. Hsmr tryptophan fluorescence changes upon TPP^+ binding. Binding of TPP^+ in the mM range to 4 µM Hsmr in 1 % DDM and standard high salt buffer leads to quenching of tryptophan fluorescence at 330 nm, but does not shift the fluorescence maximum. The relative fluorescence intensity change ($\Delta F/F_0$) upon addition of TPP^+ is plotted, and the solid lines represent the best fit of the binding function to the data [169]. K_d = 6.2 mM, fraction of non-specific binding = 0.0, ΔF_{max} = 0.945, R^2 = 0.995. ΔF = difference in fluorescence intensity between Hsmr without and with added substrate, F_0 = fluorescence intensity of Hsmr in the absence of substrate

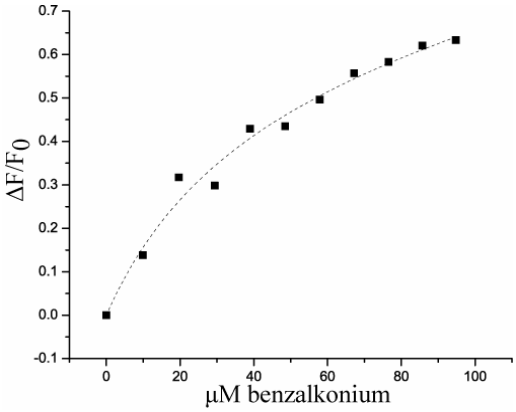

Figure 39. Hsmr tryptophan fluorescence changes upon benzalkonium binding. Binding of benzalkonium in the μM range to 4 μM Hsmr in 0.1 % DDM and standard high salt buffer leads to quenching of tryptophan fluorescence at 330 nm, but does not shift the fluorescence maximum. The relative fluorescence intensity change ($\Delta F/F_0$) upon addition of TPP^+ is plotted, and the solid lines represent the best fit of the binding function to the data [169]. K_d = 39.7 μM, fractional non-specific binding = 0.0, ΔF_{max} = 0.70, R^2 = 0.983. ΔF = difference in fluorescence intensity between Hsmr without and with added substrate, F_0 = fluorescence intensity of Hsmr in the absence of substrate

Fluorescence of the single tryptophan in Hsmr (Trp63) is quenched with TPP^+ by as much as 94.5 % (ΔFmax = 0.945), see figure 38, and with benzalkonium by as much as 70 % (ΔF_{max} = 0.70), see figure 39. Quenching of the Hsmr tryptophan fluorescence upon TPP^+ and benzalkonium addition is specific, as can be seen from the low fraction of non-specific binding, see figure 38 and figure 39. This suggests that the conserved, essential and only tryptophan residue Trp63 of Hsmr interacts directly with the substrates TPP^+ and benzalkonium.

The K_d observed here using tryptophan quenching with TPP^+ (K_d = 6.2 mM) is two orders of magnitudes higher than the K_d of Hsmr:TPP^+, anticipated by Professor Schuldiner's laboratory (K_d = 20 - 400 nM) [28] or the measured EmrE:TPP^+ K_d (K_d = 20 nM) [27]. During radioactive Hsmr assays, TPP^+ binding was only observed in the presence of 1 % DDM and high salt concentrations. These investigations suggested that Hsmr, at high salt and detergent concentrations, behaves similarly to EmrE. For soluble EmrE, TPP^+ binding could, among a dozen tested detergents, only be detected in the presence of DDM [27]. Therefore, buffer conditions identical to the radioactive assay were used here for the tryptophan quenching assay with TPP^+. However, high detergent concentrations may be detrimental to protein structure and generally time dependent Hsmr aggregation has been observed in the presence of DDM.

More successful were attempts to quench Trp63 fluorescence with benzalkonium. The K_d lies at the high end of expected substrate K_d's (K_d = 39.7 μM) and was measured in the presence of high salt buffer with only 0.1 % DDM. However, it is worth noting that reproducibility was also hampered by visible protein aggregation.

Although substrate induced specific tryptophan quenching of Trp63 could be observed for Hsmr with this assay, the poor reproducibility arising from Hsmr instability in DDM led to the renouncement of this assay.

6. 3 Transport assays

6. 3. 1 Ethidium bromide assay

Already the second SMR protein publication utilised an ethidium bromide based transport assay to judge protein activity [194]. Here, Smr reconstituted into liposomes was added to a solution with ethidium bromide, for which buffers were chosen to test all combinations of ΔpH and Δψ gradients. The observed ethidium bromide fluorescence intensity increases in the presence of the protein Smr and with ΔpH and Δψ was used as proof of vectorial ethidium transport [194].

A more elegant set-up to generate both ΔpH and Δψ uses the proton pump Bacteriorhodopsin [171]. Figure 40 is a schematic diagram of the assay set-up developed in our laboratory and used for this study [254].

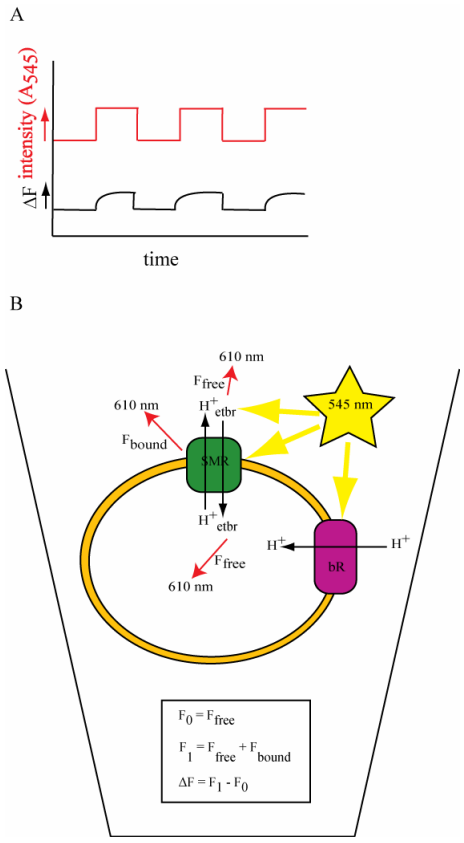

Figure 40. Schematic diagram of assay set-up to monitor transport of ethidium bromide by SMR proteins. A) SMR proteins and bR are co-reconstituted into liposomes and ethidium bromide is added to the buffer. Irradiation at 545 nm excites ethidium bromide and activates bR. During the illumination, bR pumps protons across the membrane, and the fluorescent molecule ethidium bromide emits light at 610 nm. The change of fluorescence intensity, ΔF, with time is measured. After an equilibration period in the dark the experiment can be repeated. B) During the assay, the ethidium bromide concentration is constant and the experiment starts with an equilibrium distribution of ethidium bromide. The fluorescence intensity of ethidium bromide is dependent on the polarity of its environment. F_{free} is the ethidium bromide fluorescence intensity in the assay buffer and is the background fluorescence F_0. During active transport, some ethidium bromide is bound to the SMR protein and an intermediate with increased fluorescence intensity F_{bound} is formed. The overall fluorescence intensity during active transport is therefore F_1. The differences in fluorescence intensity $\Delta F = F_1 - F_0$ are measured in this assay. ΔF arises from changes in F_1 during the assay which depends on changes in the populations of F_{bound} and F_{free}. As ΔpH and Δψ build up, the amount of ethidium bromide which is present in the high fluorescence state F_1 increases. A plateau ΔF_{max} is reached when the maximal ΔpH + Δψ gradient is established and the maximal supported ethidium bromide transport is observed [254].

This assay set-up is ideally suited to investigate the activity of Hsmr as both Hsmr and bR are halophilic proteins. Co-reconstitutions were attempted at different salt concentrations into *E. coli* total lipid liposomes. However, *E. coli* lipid membranes are known to be susceptible to proton leakage at high salt concentrations. The highest salt concentration which supported a ΔpH gradient which enables transport activity to be detected was 1 M NaCl. More robust results were obtained with 300 mM NaCl. It can be expected that at only 300 mM NaCl Hsmr does not exhibit its full activity but here a balance between ideal conditions for the protein and liposome leakage needs to be struck. Under these low salt concentrations (300 mM NaCl), a measurable and reproducible ethidium transport by Hsmr could be observed, see figure 41. The black solid curve is a representative trace for active ethidium bromide transport by Hsmr. The grey dashed trace was collected in the presence of the uncoupler CCCP which abolishes ΔpH and Δψ and no fluorescence increase is observed during the course of the experiment.

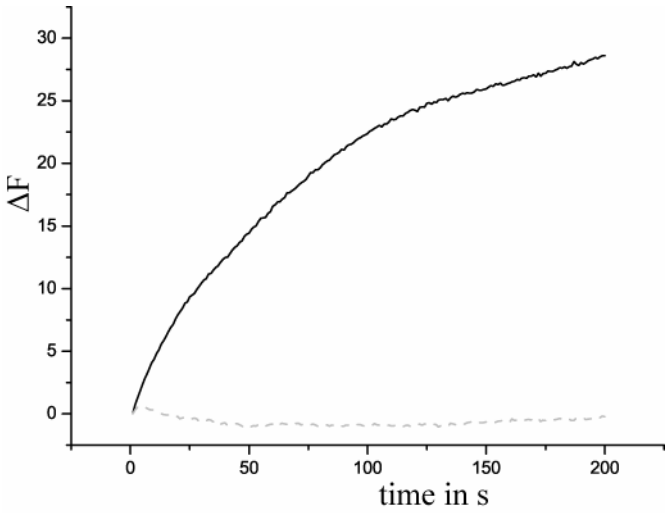

Figure 41. Ethidium bromide transport assay with Hsmr at 300 mM NaCl. The black solid trace is a typical profile of the fluorescence intensity increase observed with Hsmr mediated ethidium bromide transport. The grey dashed trace is a typical profile of the constant fluorescence intensity observed when Hsmr mediated ethidium bromide transport is impeded, here by the uncoupler CCCP mediated collapse of ΔpH and Δψ.

Substrate binding assays suggested that TPP^+ is an Hsmr substrate, see figure 37 and figure 38. To investigate this further, the ethidium bromide transport assay was conducted in the presence of varying amounts of TPP^+. Competition between the substrates for Hsmr leads to a reduction of the ethidium bromide fluorescence. A dose-response curve, see Materials and Methods equation 13, could be fitted to the data, see figure 42, and an IC_{50} of approximately 4 µM was determined.

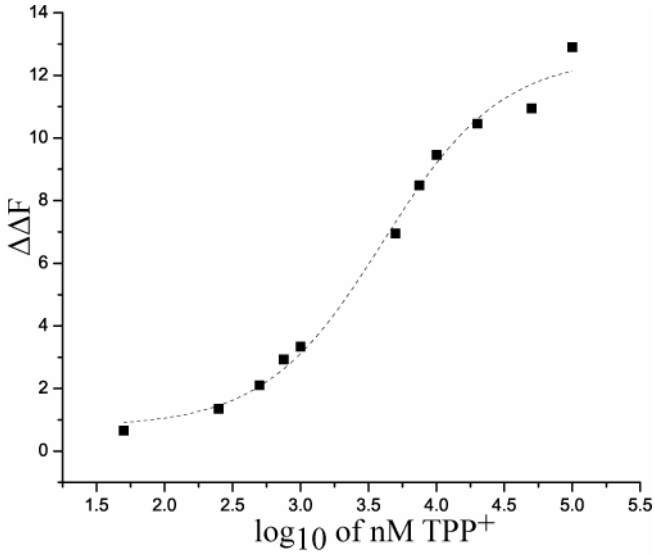

Figure 42. The dose-response plot for TPP^+, an inhibitor of ethidium bromide transport by Hsmr. 1 µM Hsmr co-reconstituted with bR in the presence of 13.6 µM ethidium bromide. Competition experiments with TPP^+ (IC_{50} = 4 µM) are shown here.

The IC_{50} value is the inhibitor concentration at which the substrate transport is reduced by 50 % [255], and is substrate concentration dependent. A K_i is the substrate concentration independent K_d of an inhibitor and therefore suitable for comparison between experiments conducted by different laboratories [255]. Assuming that: the reaction obeys Michaelis-Menten kinetics, binding is reversible and the inhibition competitive, the reaction mechanism is known and the substrate K_m is available; the IC_{50} can be converted into a K_i [255].
Under certain conditions, the IC_{50} and K_i can even be identical. These include the simple case of one substrate reaction obeying simple Michaelis-Menten kinetics with a reversible inhibitor at concentrations above the substrate K_m.

Unsuccessful attempts were made to use the coupled Hsmr/bR assay to determine the rate of ethidium bromide transport. Measurements of transport rate would further characterise Hsmr by enabling the assessment of the type of kinetics found and providing K_m and V_{max} values. If simple Michaelis-Menten kinetics apply, experiments in the presence of inhibitors can lead to the determination of the mode of inhibition. Unfortunately, none of this was possible here as the initial rate of ethidium bromide transport, measured as initial increase in ethidium bromide fluorescence, depends on two proteins. Firstly the initial transport rate is governed by the transporter Hsmr but secondly it depends on the concomitant build-up of $\Delta pH + \Delta\psi$ by bR.
For Hsmr, the type of inhibition of ethidium bromide transport by TPP^+ is yet undetermined, furthermore, the type of kinetic has not been determined previously and the K_m is unknown. However, it can be reasonably anticipated that TPP^+ is a competitive inhibitor with respect to etbr. Attempts to determine the Michaelis Menten constant K_m from the rate of ethidium bromide transport failed. The ethidium bromide transport rate is determined by three inseparable components namely, $\Delta pH + \Delta\psi$ generation by bR and ethidium bromide transport by Hsmr. Their undecipherable intermingling makes the determination of K_m with this assay impossible. It is therefore impossible convert the IC_{50} to a K_i. However, a K_i of 4 µM for TPP^+ binding to Hsmr would be in the expected range. TPP^+ K_i's reported for TBsmr are 4.3 µM when competing against methylviologen and 10 µM when competing against ethidium bromide [146, 254].

In conclusion, Hsmr can transport ethidium bromide actively in the presence of a bR generated ΔpH + Δψ gradient. TPP^+ can efficiently inhibit this transport at low concentrations with an IC_{50} of 4 µM. Further characterisations of transport kinetics and types of inhibition are hampered by the coupling of ΔpH + Δψ generation and ethidium bromide fluorescence.

6. 3. 2 TPP^+ transport assay measured with a TPP^+ electrode

The first transport assay on purified SMR proteins utilised a TPP^+ electrode to measure the rate of $MTPP^+$ transport [194]. This is an advancement of the common use of TPP^+ sensitive electrodes to measure TPP^+ concentrations as indicator of membrane integrity [256-258]. The TPP^+ transport assay as used by Grinius and Goldberg is schematically depicted in figure x. A ΔpH and Δψ dependent transport of $MTTP^+$ was observed for Smr. Weak transport activity was also observed in the presence of just ΔpH. Both ΔpH and Δψ were formed by using different buffers as assay buffer and proteoliposome reconstitution buffer. More precisely, the assay buffer has a pH of 9.5 and contained 150 mM KCl, while the proteoliposomes were filled with buffer at pH 7.0 and 0 mM KCl. A strong ΔpH and Δψ gradient is thus set up which can be dissipated either specifically by substrate/proton antiport or unspecifically by uncouplers and proton and ion leakage.

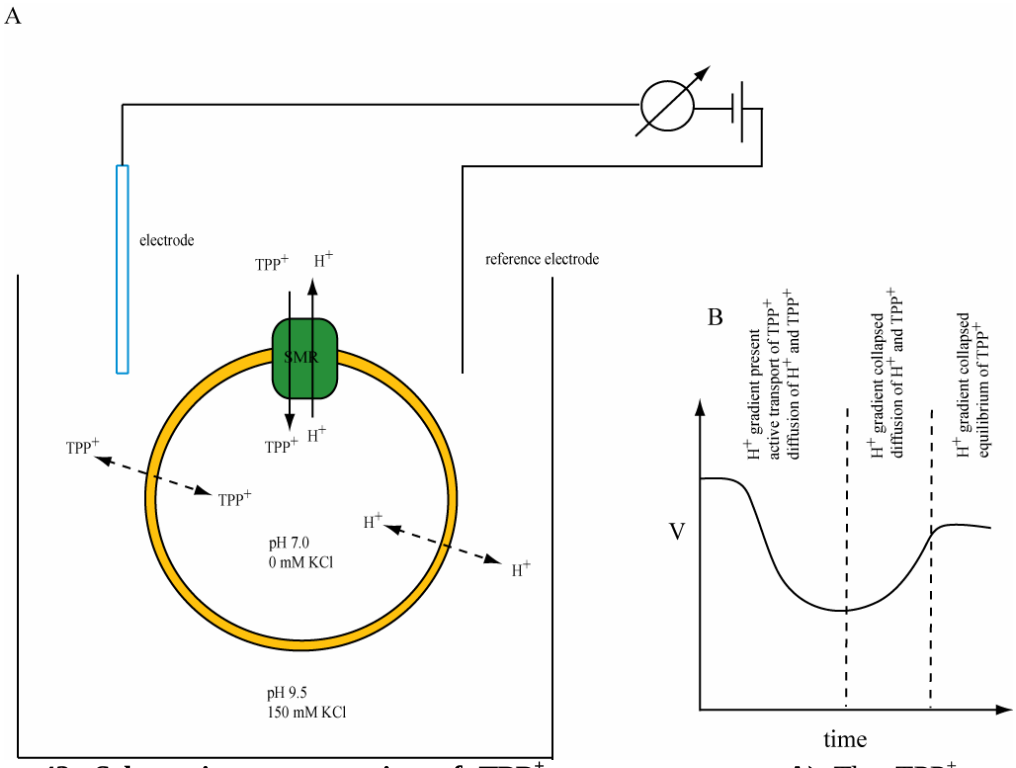

Figure 43. Schematic representation of TPP^+ transport assay. A) The TPP^+ sensitive electrode and reference electrode enable the measurement of potential changes, V, due to TPP^+ concentration changes. The read-out values are in the range of mV. B) The expected voltage profile of active TPP^+ transport is shown.

A similar experimental set-up was envisaged for Hsmr. The TPP^+ assay should be ideally conducted at high salt concentrations to observe maximal Hsmr transport efficiency. Alternatively, Hsmr could be investigated at more convenient low salt concentrations and accordingly less than maximal transport activity should be observed. Both approaches were used here.

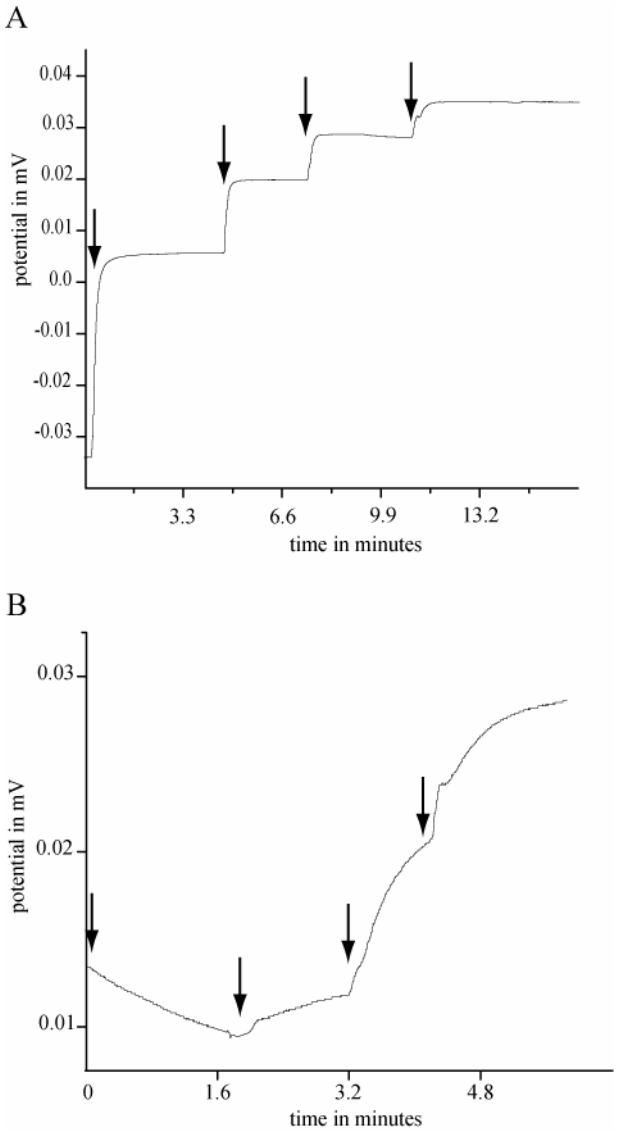

Figure 44. TPP^+ electrode measurements. A) Typical TPP^+ titration curve in standard buffer. At each arrow, TPP^+ at a final concentration of 3 µM is added and a sharp potential increase measured. B) Titration curve in the presence of standard buffer + 2 M NaCl and including 3 µM TPP^+. Additions of 2.15 µM TPP^+ final concentration at the arrows only show a slow and weak potential increase. Without calibration the mV values are arbitrary units and can only be used for comparison within one experiment.

In figure 44 a calibration curve of (A) Hsmr in the presence of standard low salt concentration buffer is compared with a calibration curve (B) in the presence of 2 M NaCl. The addition of TPP^+ to low salt buffer causes a sharp and large rise in potential. In the presence of high salt concentrations, the potential reading of the TPP^+ selective electrode is neither as fast responding as observed for low salt concentrations nor changes as strongly as for low salt concentrations. The TPP^+ sensitive electrode is actually a Ca^{2+} selective electrode and the TPP^+/Ca^{2+} selectivity ratio is 100 [259]. A selectivity ratio for TPP^+/Na^+ was not measured here but the supplier guarantees a selectivity ratio of 10000 for Ca^{2+}/Na^+ [260]. The presence of 2 M NaCl thus can be anticipated to interfere with the electrodes ability to measure small differences in TPP^+ concentrations. Indeed, this hypothesis was supported by the experiment seen in figure 44B and means that TPP^+ transport cannot be measured with the TPP^+ selective electrode in the presence of high salt concentrations.

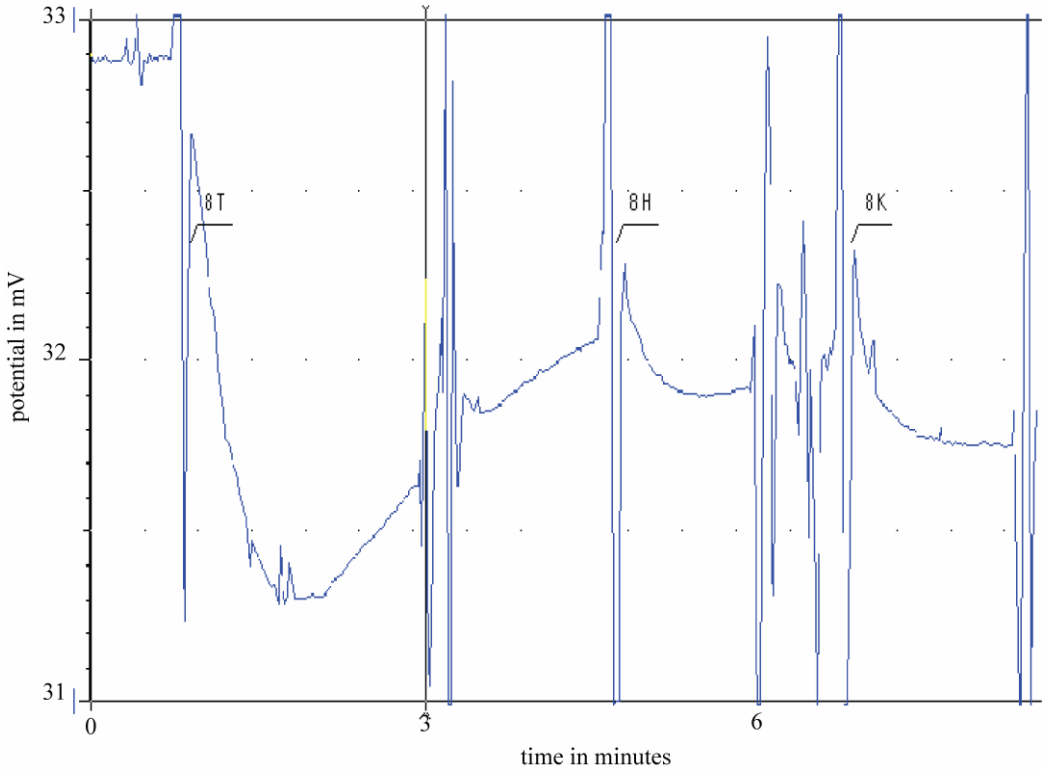

Figure 45. TPP^+ transport by TBsmr and Hsmr. A TPP^+ assay with standard buffer investigated sequentially the transport activity of TBsmr, Hsmr and empty liposomes. TBsmr was used as a positive control. TBsmr addition at the first indicator gives rise to a fast drop and large potential drop and slow potential rise. Addition of Hsmr at the second indicator causes a less pronounced and slower potential drop which is not recovered. At indicator three protein-free liposomes, used as negative control, are added and a slow potential drop is detected which is not recovered. Potential changes are measured in mV but are not calibrated and thus not comparable between experiments and should be treated as arbitrary units.

In figure 45, a typical low salt TPP^+ transport assay is depicted. The first addition are, as positive control, proteoliposomes with TBsmr and give rise to the expected TPP^+ transport curve. The expected transport curve shows an initial drop in potential due to dilution and transport of TPP^+ into the liposome, momentarily depleting the TPP^+ concentration in the outside buffer. This is followed by an increase in potential as the TPP^+ concentration returns almost to its steady-state value. This is possible as the TPP^+ concentration equalises between inside and outside the liposome. TPP^+ is a lipophilic substance and can traverse the membrane. This process is no longer counteracted by the active transport of TPP^+ by SMR proteins, as the proton gradient is depleted by active transport and proton leakage. From the TBsmr/TPP^+ transport measurement and its expected, typical curve it can be concluded that the TPP^+ electrode measurement set-up used here is functional.
The second addition contains proteoliposomes with Hsmr. The potential drop observed is smaller and the expected slow potential increase arising from equilibration of TPP^+ by diffusion is not observed. This suggests that the drop in TPP^+ generated potential arises from dilution effects only. Endorsement of this hypothesis arises from the third addition encompassing protein-free liposomes as the negative control. As expected liposomes afford only a dilution dependent drop of potential but no potential restoration is observed.
During these experiments Hsmr was treated identically to TBsmr. The inactivity of Hsmr is likely to arise from non-native salt conditions which lead to Hsmr inactivation.

Unfortunately, it must be concluded that the TPP^+ sensitive electrode cannot be used to measure Hsmr mediated TPP^+ transport due to experimental limitations and protein specific requirements.

6. 4 Conclusion

Several Hsmr activity assays were evaluated and improved here. From the radioactive TPP^+ binding assay and the tryptophan fluorescence quenching assay it can be concluded that Hsmr in soluble form is unstable but retains residual but varying binding activity in the presence of high salt concentrations and DDM. The transport assays, using a TPP^+ electrode and ethidium bromide fluorescence, showed that Hsmr reconstituted in *E. coli* total lipid liposomes exhibits transport activity at low salt concentrations. An electrophysiological transport assay using solid supported membranes was abandoned as not feasible due to the hydrophobic nature of the substrates leading to interactions with the tubings. The most useful assay for Hsmr activity is thus the ethidium bromide transport assay because it directly measures transport function, can be conducted at low salt concentrations and is very reproducible. The ethidium bromide fluorescence transport assay is the assay of choice for future activity measurements on Hsmr or other SMR proteins.

Chapter 7 - Solution state NMR on Hsmr

7. 1 Introduction

Several attempts have been made at elucidating the structure of SMR proteins by solution state NMR. Initially, EmrE was investigated in a chloroform/methanol/water mixture. Only approximately 60 % of the expected residues were observed, and only the secondary structure could be determined [261]. Later attempts to use overlapping peptides of EmrE solubilised by SDS to obtain a full-length structure [62], an approach pioneered for Bacteriorhodopsin [262], failed due to the insolubility of one fragment.
More successful were investigations of Smr. Solubilised in LPPG, the complete Smr backbone and 97 % of all Cβ nuclei were assigned [263]. Measurements of Smr in bicelles resulted in an almost complete backbone residue assignment [169], but neither experiment has resulted in a Smr structure.
During Hsmr purification inevitably detergents were used and several investigations of Hsmr in membrane mimicks, namely detergents, were performed. It was thus of interest if Hsmr retains a folded state in any of these detergents. Ultimately, of course a solution state structure of Hsmr would be desirable to enable the investigation of the structural features of halophilicity.

7. 2 Results and Discussion

Structure determination by solution state NMR is a process involving many sequential steps, starting with the initial screen of detergent, buffer and temperature conditions. For membrane proteins detergents are the key component. A successful detergent must yield a suitable spectral quality and support protein functionality. The best possible compromise between these two criteria is sought. Several groups have screened an extensive number of detergents, with vastly different properties regarding ionic state and chain length, for their ability to yield high quality NMR spectra of membrane proteins. Sets of proteins investigated were alpha helical membrane proteins [264], *Thermotoga maritime* membrane proteins [265] and a range of proteins with different numbers of transmembrane helices [112]. The outcome suggests that the optimal detergent for solution state NMR of a protein needs to be determined empirically. The suitability of conditions is generally assessed by 1D ^{1}H and 2D ^{1}H-^{15}N HSQC experiments. For Hsmr, this screen was simplified by the use of information from long term protein stability tests in chapter 4. This information obtained from SEC narrows in this case the detergent choices that need to be evaluated by NMR to DPC and SDS.

7. 2. 1 Hsmr in DPC

The aromatic and amide regions of a 1D ^{1}H spectrum of Hsmr in DPC is shown in figure 46. These regions are used for quality assessment [265].

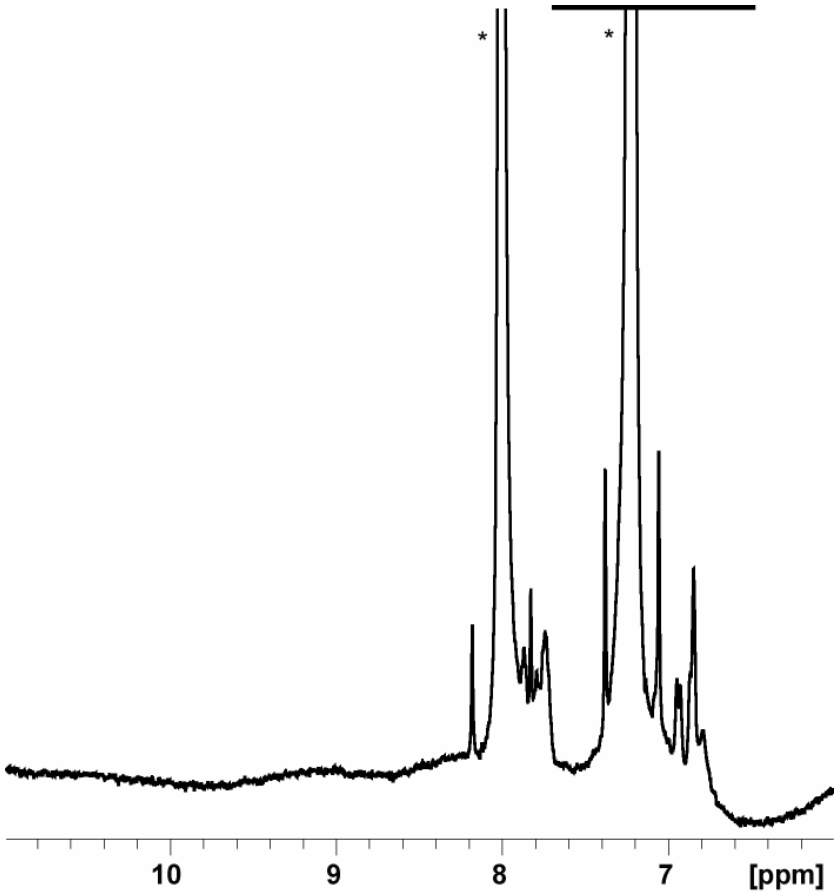

Figure 46. 1D ^{1}H spectrum of Hsmr in DPC with $K_xH_xPO_4$ buffer. Uniformly ^{15}N labelled Hsmr at 840 µM in 300 mM NaCl, 300 mM imidazole, 15 mM $K_xH_xPO_4$, pH 7.0, 0.1 % DPC, 10 % D_2O, 1 mM 3-(trimethylsilyl)propionic acid (TMSP) was measured at 298 K at 600 MHz. The spectrum was processed with 2 Hz exponential linebroadening. The black bar above the spectrum indicates the aromatic region. The asterisks highlight the ^{1}H resonances of imidazole, values were obtained from the BMRB entry bmse000096.

Many sharp peaks were observed in the ^{1}H spectrum in the range of 6.5 to 8.5 ppm. The line-width of these protein peaks is similar to each other. The resolution in the aromatic region, highlighted by a bar in figure 46, is moderate compared to published spectra of other proteins [265]. Most disappointingly, no peaks were detected downfield from 8.5 ppm. In particular, the lack of peaks in the high ppm range is worrying as they are indicative of a folded protein [265]. Here, the large peaks marked with asterisks arise from the presence of imidazole. In subsequent preparations, imidazole was removed by dialysis leading to improved spectra but prolonged sample preparation time.
For an initial assessment of the spectral quality attainable by a given protein often also 2D ^{1}H-^{15}N HSQCs are used [112, 264-266]. The % of expected resonances that can be observed can thus be assessed. HSQC experiments are chosen because they require only a simple, inexpensive uniform ^{15}N labelling scheme and these routine experiments are fast. Accordingly, to obtain more conclusive evidence regarding the suitability of this Hsmr preparation for NMR, a 2D ^{1}H-^{15}N HSQC was collected.

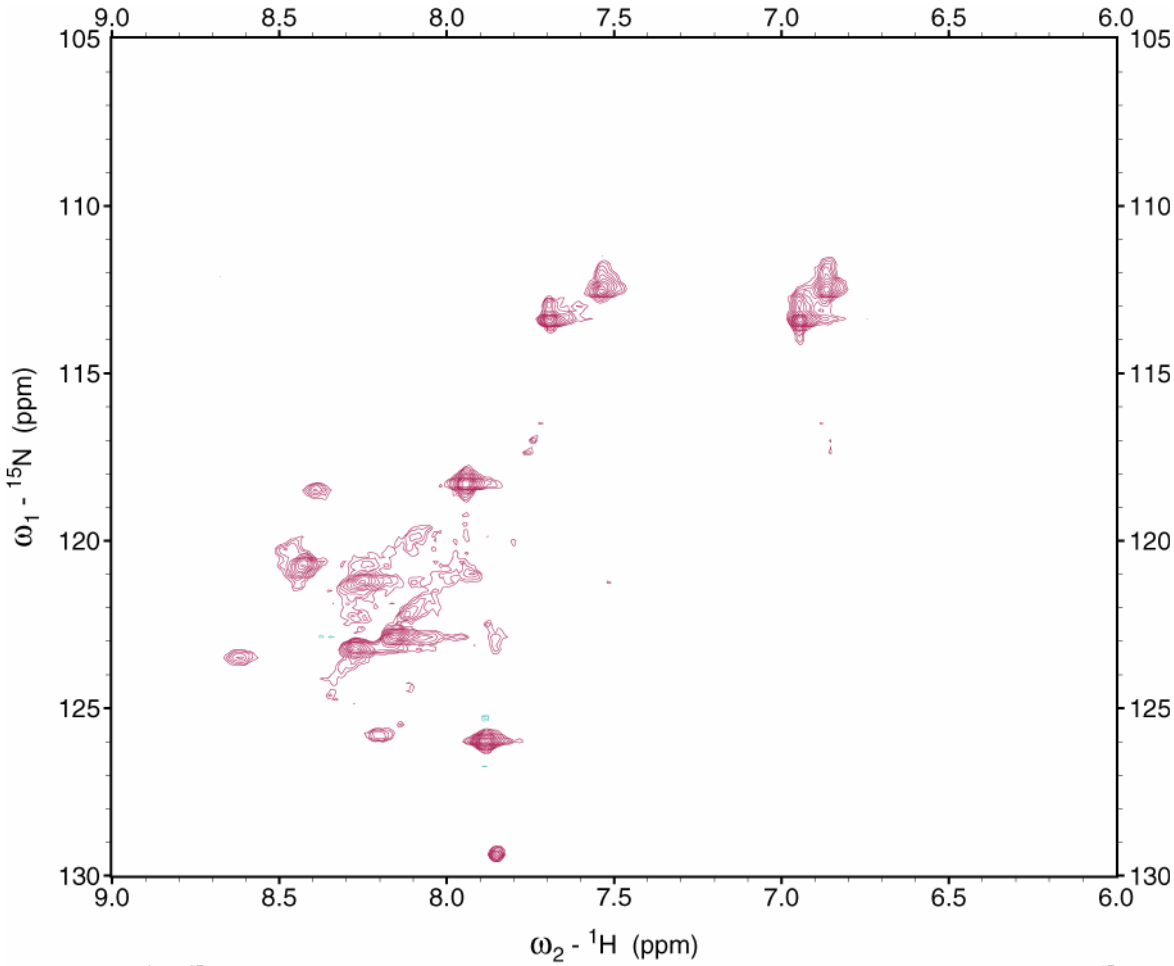

Figure 47. ^{1}H-^{15}N HSQC spectrum of Hsmr in DPC with $K_xH_xPO_4$ buffer. Uniformly ^{15}N labelled Hsmr at 840 µM in 300 mM NaCl, 300 mM imidazole, 15 mM $K_xH_xPO_4$, pH 7.0 , 0.1 % DPC, 10 % D_2O, 1 mM TMSP was measured at 298 K at 600 MHz ^{1}H frequency and 61 MHz ^{15}N frequency with a HSQC. The spectrum was acquired with 2048 points in the direct dimension and 512 points in the indirect dimension. A total of 44 transients were collected per slice. The spectrum was processed with quadratic sine modulation in both dimensions. Positive contour levels are displayed in maroon while negative contour levels are shown in turquoise. The spectrum was cropped to include all observed resonances.

Hsmr with myc-his tag has 139 amino acids and thus 139 backbone ^{1}H-^{15}N peaks are expected. The imidazole peaks should be located outside the spectral range (163.851 ppm and 290.715 ppm ^{15}N dimension, bmst000093) and should not disturb the 2D spectrum. Clearly, far less than 139 peaks are visible. The lack of peaks suggests that the PDC, which is in the case of membrane proteins the relevant unit, has a slow rotational correlation time. The resulting fast T_2 relaxation leads to excessive broadening of the signals and possibly even their disappearance. The observed peaks are of erratic size, probably arising from several unresolved peaks. The spread of chemical shifts observed is very limited, with only one peak in the 1H dimension at >8.5 ppm. Although solely alpha helical proteins generally suffer from poor chemical shift dispersion, a folded protein should exhibit a few resonances downfield of 8.5 ppm in the ^{1}H dimension. The 11 glycine residues and one tryptophan residues of Hsmr-myc-his are located exclusively in the Hsmr amino acid sequence, see figure 48.

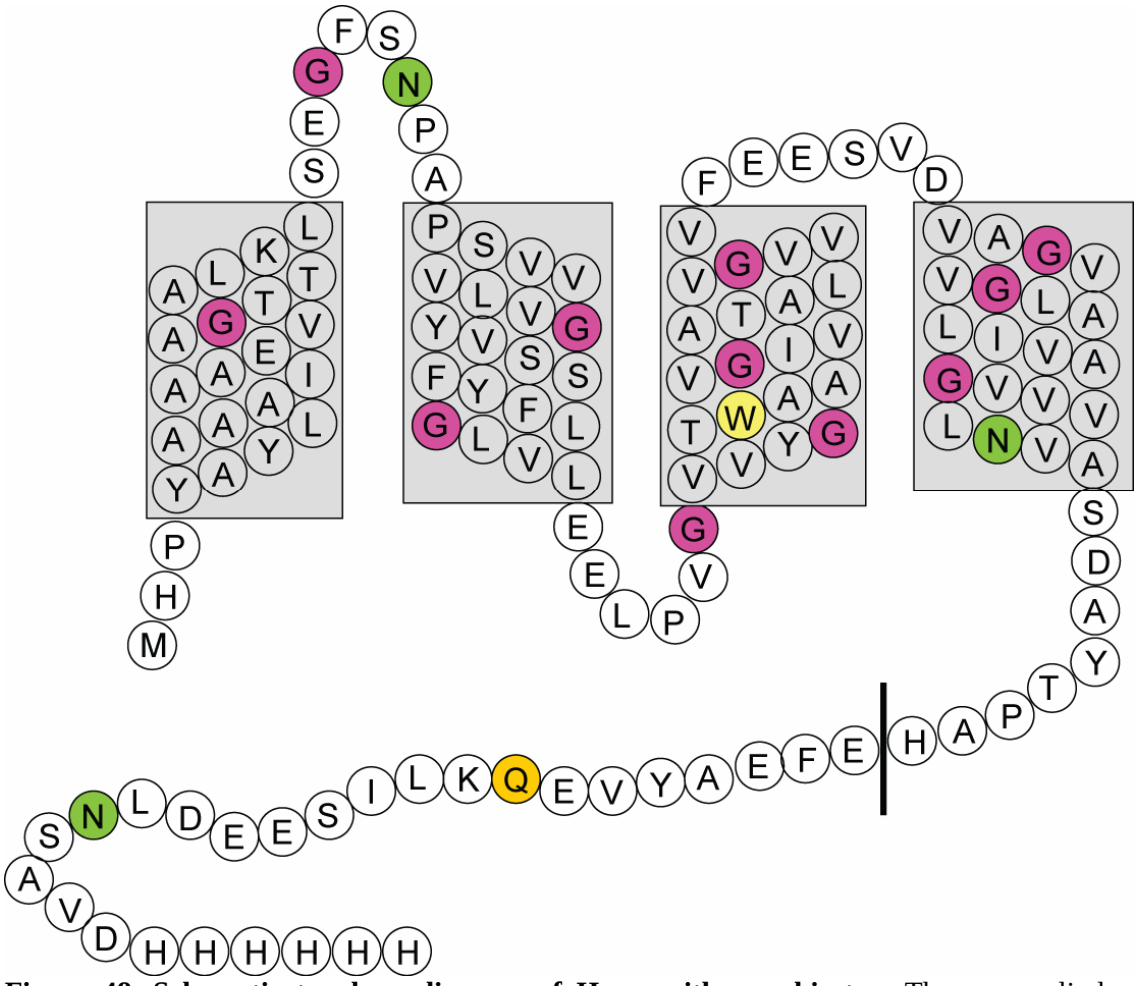

Figure 48. Schematic topology diagram of Hsmr with myc-his tag. The grey cylinders indicate the predicted TM helices and the black bar indicates the end of the protein sequence and start of the myc-his tag. Prediction of TM regions used HMMTOP [267]. The protein sequence is shown using the one letter code. Glycine residues in pink, tryptophan in yellow, asparagines in green and glutamine in orange.

The observed peaks therefore likely stem from the tag as the characteristic glycine (minimal observed chemical shift 88.30 ppm/3.01 ppm, maximal observed chemical shift 135.80 ppm/12.22 ppm and average chemical shift 109.72 ppm/8.34 ppm for $^{15}N/^{1}H$ nuclei respectively [268]) and tryptophan side-chain (minimal observed chemical shift 101.75 ppm/4.49 ppm, maximal observed chemical shift 134.89 ppm/11.67 ppm, average observed chemical shift 121.76 ppm/8.29 ppm for $^{15}N/^{1}H$ respectively [268]) peaks are absent. The tag is known to protrude from the PDC micelle as purification using IMAC is possible. The tag is thus expected to have motions in addition to the PDC motions leading to shorter rotational correlation times. This assessment is supported by the fact that the sidechains of asparagines and glutamine (Asn: 112.82 ppm 15N, 7.14 ppm and 7.34 ppm ^{1}H; Gln: 111.85 ^{15}N, 7.02 ppm and 7.22 ppm ^{1}H [268]), which are also expected to have motions in addition to the PDC motions, can be observed.
It can thus be concluded that Hsmr in DPC has a too long rotational correlation time and T_2 relaxation broadens the lines. This makes Hsmr in DPC unsuitable for NMR experiments.

7. 2. 2 Hsmr in SDS

Hsmr in SDS is extremely stable (see chapter 4) and could thus be subjected to a temperature scan. Two 1D ^{1}H spectra are shown in figure 49, exemplifying the resolution gain associated with even modest temperature increases.

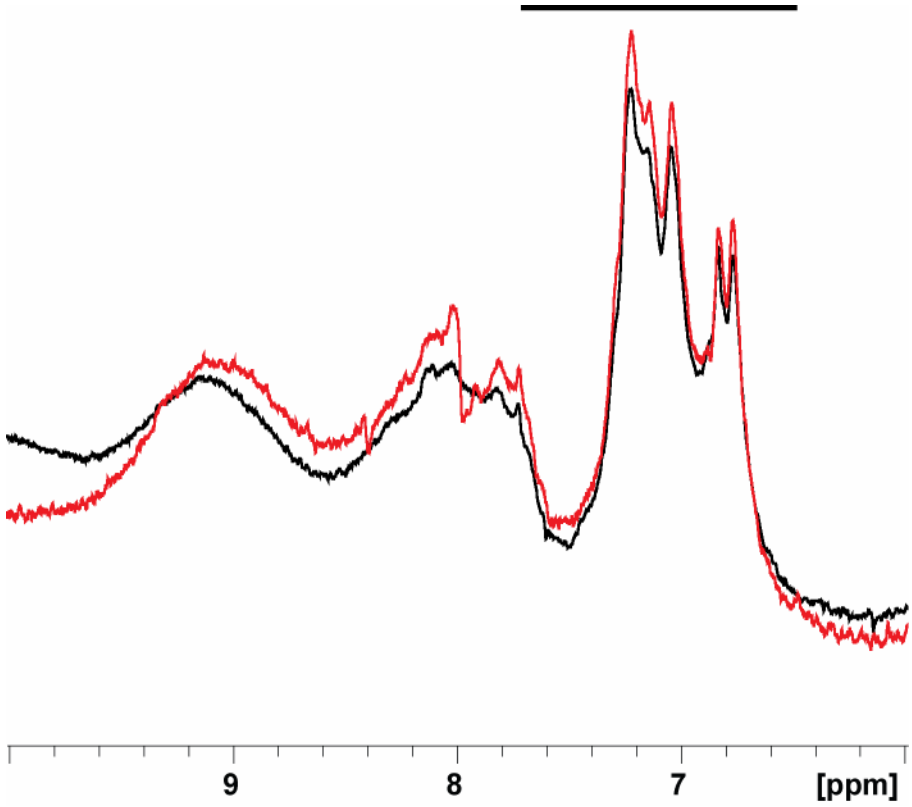

Figure 49. 1D ^{1}H spectra of Hsmr in Tris buffer with SDS at two different temperatures. Uniformly ^{15}N labelled Hsmr at 480 µM in 300 mM NaCl, 15 mM Tris, pH 8.0, 0.41 % SDS, 10 % D_2O, 1 mM TMSP was measured at 900 MHz. The spectra were processed with 2 Hz exponential line-broadening. The lowest temperature with maximal resolution was determined by comparison of 1D ^{1}H spectra. The spectrum in black was acquired at 303 K, while the spectrum in red was acquired at 310 K. The black bar above the spectra indicates the aromatic region.

The measurement at 310 K has a better resolution both in the aromatic region and around 8 ppm. 310 K was chosen as the temperature for further measurements. Hsmr in the presence of Tris and SDS exhibited again low spectral resolution in the aromatic region, see figure 49. A broad peak is detected downfield of 8.5 ppm in the ^{1}H dimension, an improvement compared to the 1D spectrum of Hsmr in DPC. For a more thorough assessment again a 2D ^{1}H-^{15}N HSQC was carried out.

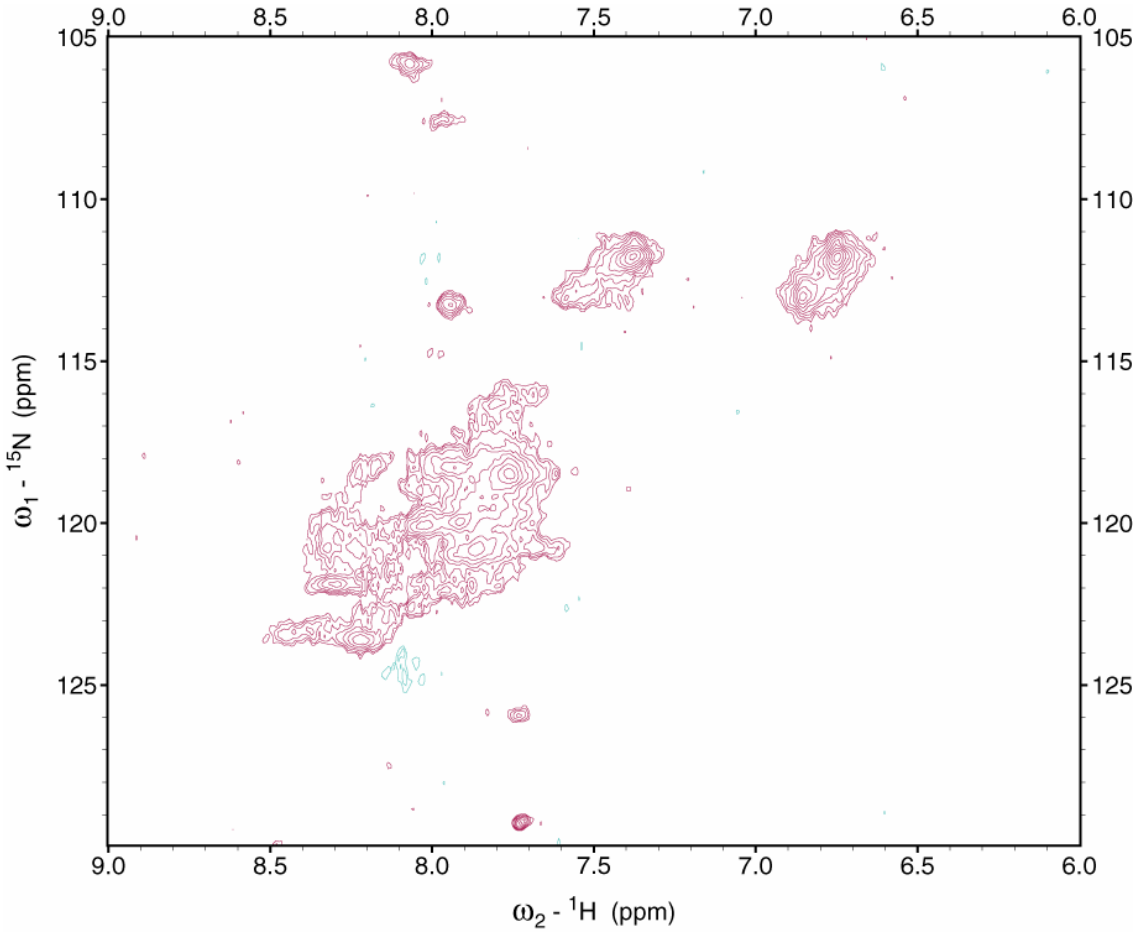

Figure 50. ^{1}H-^{15}N HSQC spectrum of Hsmr in SDS with Tris buffer. Uniformly ^{15}N labelled Hsmr at 480 µM in 300 mM NaCl, 15 mM Tris, pH 8.0 , 0.41 % SDS, 10 % D_2O, 1 mM TMSP was measured at 310 K at 900 MHz ^{1}H frequency and 91 MHz ^{15}N frequency with a HSQC. The spectrum was acquired with 2048 points in the direct dimension and 96 points in the indirect dimension. A total of 128 transients were collected per slice. The spectrum was processed with quadratic sine modulation in both dimensions. Positive contour levels are displayed in maroon while negative contour levels are shown in turquoise. The spectrum was cropped to include all observed resonances.

The ^{1}H-^{15}N HSQC of Hsmr in Tris buffer with SDS, figure 50, again shows low spectral resolution, inhomogeneous peak shape and line-width, too few peaks and a lack of peaks beyond 8.5 ppm in the ^{1}H dimension. However, the spectrum is an improvement over Hsmr in DPC in several aspects. Characteristic glycine peaks (109.75 ppm ^{15}N, 8.34 ppm ^{1}H [268]) can be detected although the intensity and number of resonances are not representative of 11 amino acids. Overall, this spectrum suggests that most peaks detected arise still from the myc-his tag, but some magnetization arises from Hsmr itself. The likeliest cause of the low % of expected peaks detected is again the PDC size.

Further improvements of sample conditions were made with respect to detergent concentration and pH. A detergent concentration of 1.5 % SDS theoretically ensures that every PDC contains only the minimal protein complex, likely a dimer. From the NMR spectroscopy point of view this is an improvement, but detergent concentrations high above the cmc can lead to protein aggregation and were thus avoided initially. To rule out the possibility that the relatively high but physiological pH of previous measurements (pH 8.0) causes a loss of many Hsmr resonances, HEPES at pH 6.8 was chosen here. A 2D ^{1}H-^{15}N HSQC was obtained of this optimised sample, see figure 51.

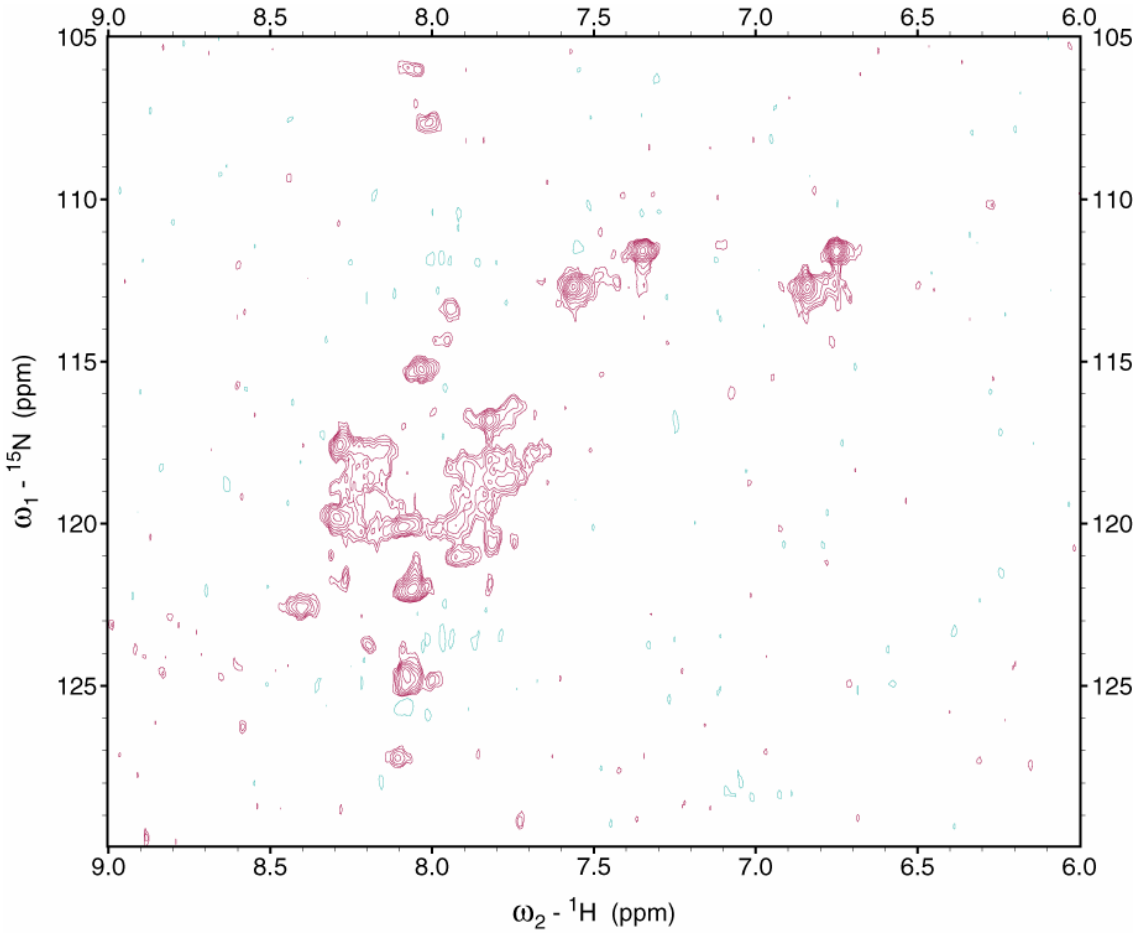

Figure 51. ^{1}H-^{15}N HSQC spectrum of Hsmr in SDS with HEPES buffer. Uniformly ^{15}N labelled Hsmr at 480 µM in 300 mM NaCl, 15 mM HEPES, pH 6.8 , 1.5 % SDS, 10 % D_2O, 1 mM TMSP was measured at 310 K at 900 MHz ^{1}H frequency and 91 MHz ^{15}N frequency with a HSQC. The spectrum was acquired with 2048 points in the direct dimension and 72 points in the indirect dimension. A total of 40 transients were collected per slice. The spectrum was processed with quadratic sine modulation in both dimensions. Positive contour levels are displayed in magenta while negative contour levels are shown in green. The spectrum was cropped to include all observed resonances.

Overall, Hsmr in HEPES and 1.5 % SDS gives rise to a spectrum similar to Hsmr in Tris and 0.41 % SDS. Again a few glycine resonances and no tryptophan resonances were found. This suggests that again the majority of peaks obtained arise from the tag. Lowering the pH does not enhance the number of visible ^{1}H-^{15}N resonances and thus excludes the high pH of previous experiments as the cause of the small number of observed resonances. Hsmr in HEPES and 1.5 % SDS exhibits resonances of more uniform size and increased resolution when compared to figure 50. This suggests that the increase of the SDS concentration indeed leads to a smaller PDC. However, the improvements in spectral quality are not sufficient. Hsmr in SDS micelles is therefore not amenable to structural characterisation by solution state NMR due to the low quality spectra obtained at two different pH values and SDS concentrations. The most likely causes of the poor spectral quality are the large PDC size and possibly unfolded Hsmr.

7. 3 Conclusion

The detergent DDM was shown in chapter 6 to support the substrate binding activity of Hsmr but the lack of long-term stability in this detergent, see chapter 4, rules out NMR investigations in this detergent. Other promising detergents were pre-selected for Hsmr long-term stability in chapter 4. The successful detergents DPC and SDS showed a large

PDC with Hsmr of approximately 132 kDa. A complex of this size is outside the realms of solution state NMR. However, investigations with Smr in LPPG suggested that SMR proteins can be highly mobile in detergent micelles and can tumble independently of the micelle, thus dramatically reducing the effective molecular weight [112]. The lack of sufficient numbers of resonances and spectral resolution as seen here suggests however that Hsmr is not tumbling inside the detergent micelle and the total PDC is too large for solution state NMR. The limited number of long-term structure supporting detergents further advocates a fast transition from heterologous membranes into artificial membranes. The structural investigation of Hsmr by solution state NMR was abandoned due to the lack of detergents which could support long-term protein stability in solution and give rise to NMR spectra with a quantitative number of peaks and high resolution.

Chapter 8 - Solid state NMR

8. 1 Introduction

Solid state NMR offers a wide range of possibilities for the investigation of membrane proteins and their interactions with lipids and ligands. During the work carried out for this thesis, three different solid state NMR approaches were chosen to study multidrug transporter of the SMR family. First, the membrane interaction of TPP^+, a ubiquitous multidrug transporter substrate, has been studied by ^1H MAS NMR. Next, the perspective to investigate structure and dynamics of uniformly ^{13}C labelled Hsmr using ^{13}C-^{13}C correlation spectroscopy has been evaluated. Finally, the global dynamics of Hsmr within lipid bilayers has been probed by static ^2H NMR.

8. 2 ^{1}H MAS NMR Studies on Substrate-Lipid Interactions

8. 2. 1 Membrane localisation of Hsmr substrates

One of the open questions related to multidrug efflux pumps is how they recognize and translocate many different, structurally diverse drugs. Although structurally distinct from each other, most of them are lipophilic which raises the question whether the membrane could act as a selectivity filter sorting these drugs with respect to their membrane localisation. This would enable them to enter the protein via the membrane. The access route of lipophilic substrates into multidrug transporters has been investigated thoroughly in particular for p-glycoprotein, an ABC transporter [269, 270]. For ABC transporters, three substrate uptake and efflux mechanism models have been discussed: the classical pump, hydrophobic vacuum cleaner [20] and flippase model [21].

So far, for secondary transporters, the classical pump mechanism is assumed. Direct evidence for the hydrophobic vacuum cleaner model was only obtained for LmrP [271] and the flippase mechanism has not been observable at all, for secondary multidrug transporters. Indirect evidence for substrate entry from the lipid bilayer was seen in the x-ray crystallography structure of AcrB [18]. The difficulties associated with investigating membrane proteins and the need to compare drugs with respect to their membrane activity has led to approaches which allow determining the substrate localisation. The localisation of the lipophilic substrates of multidrug transporter has been widely discussed and investigated previously [272].

8. 2. 2 NOESY spectroscopy of small molecules in lipid membranes

Nuclear overhauser spectroscopy was first developed as 1D technique for solution state NMR, later the potential as a 2D technique was realised in 1980 [186]. The NOE is a dipolar magnetization transfer between nuclei. This cross-relaxation shows a strong distance dependence (r^{-6})[109]. First NOESY spectra of hydrated lipid membranes using solid state MAS NMR were recorded at the end of the 1980s [273, 274] but the full potential of this technique was only realised by Gawrisch and co-workers [275]. The thorough testing of different quantitative data analysis methods and the ability to rule out extensive intramolecular spin diffusion as source of lipid cross peaks paved the way for the general applications of this technique [187]. The membrane location of many diverse small molecules [275-277] has thus been investigated using NOESY MAS NMR. The molecules were located in four membrane regions, namely; head group, glycerol backbone, upper acyl chain and end of the acyl chains. Here, the location of the Hsmr and EmrE substrates ethidium bromide and TPP^+ in hydrated unilamellar DMPC vesicles is investigated.

8. 2. 3 ^{1}H NOESY MAS spectroscopy of ethidium bromide

Observation of measurable lipid substrate cross peaks using this technique ideally requires a mol ratio in the range of 1:4.5 [272]. The high concentration of substrate molecules in the lipid membrane may force a certain membrane localisation [276] or lead to substrate aggregation. For ethidium bromide, no experimental conditions (buffer, pH, temperature) and concentration range could be found that yielded strong diagonal peaks and measurable cross peaks. This probably is caused by ethidium bromide stacking [278]. The self-association into dimers has been observed below 8 mM, but higher aggregates are found above this threshold [278]. For NOESY MAS, fast anisotropic molecular tumbling is required which is significantly reduced in case of molecular multimers within the membrane. All conditions feasible for NOESY spectroscopy used here exceed these concentrations. Therefore, the membrane location of ethidium bromide in DMPC membranes could not be determined by NOESY spectroscopy.

8. 2. 4 NOESY spectroscopy of TPP^{+}

For mixtures of TPP^{+}/DMPC membranes, NOESY spectra of high quality could be obtained. A total of 12 spectra with mixing times ranging from 10 ms to 1 s were acquired. A representative NOESY spectrum can be seen in figure 52. The spectrum was acquired with a mixing time of 400 ms.

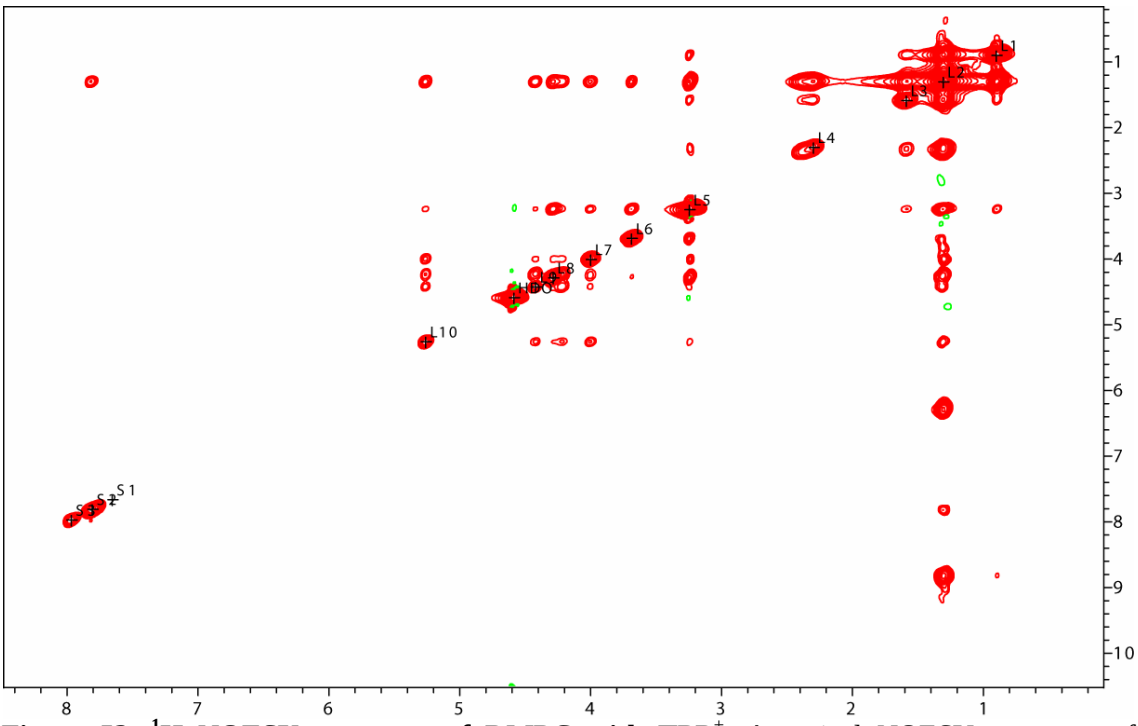

Figure 52. ^{1}H NOESY spectrum of DMPC with TPP^{+}. A typical NOESY spectrum of unilamellar [279] DMPC vesicles in the Lα phase [280] with TPP^{+} at a 1:4.5 TPP^{+}:lipid mol ratio.. The diagonal peaks were named L1-L10 for lipids, HDO for water and S1-S3 for the substrate TPP^{+} from top right to bottom left. The NOESY experiment was conducted at 310 K with MAS at 8000 Hz and a mixing time of 400 ms. The spectrum was acquired using States-TPPI and ^{1}H was measured at 400.13 MHz. The spectrum was acquired with 4096 points in the direct dimension and 256 points in the indirect dimension. A total of 8 transients were collected per slice. The spectrum was processed with squared sine modulation in both dimensions. Positive contour levels are displayed in red while negative contour levels are shown in green.

The diagonal peaks in the NOESY spectrum were arbitrarily labelled from the top right corner with L1-L10 for lipid peaks, S1-S3 for substrate peaks and HDO for the water

peak. The spectrum is very well resolved and lipid-lipid cross peaks are abundant. To see the lipid-substrate cross peaks of much lower intensity, figure 53 shows only the lipid-substrate region of the spectrum in figure 52.

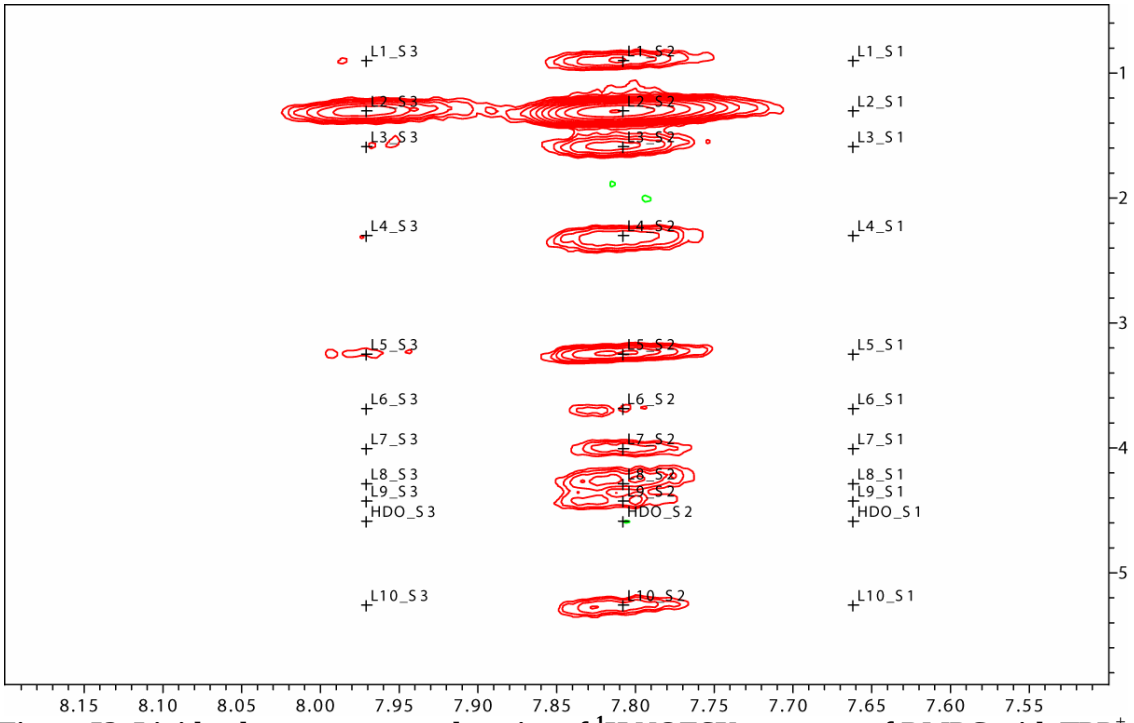

Figure 53. Lipid-substrate cross-peak region of ^{1}H NOESY spectrum of DMPC with TPP^{+}. The lipid-substrate cross-peak region of, figure 52, a TPP^{+}:DMPC (1:4.5 mol ratio) NOESY spectrum with 400 ms mixing time is enlarged here. Locations of possible cross-peaks are automatically labelled using the diagonal peak assignment shown in figure 54. The NOESY experiment was conducted at 310 K with MAS at 8000 Hz and a mixing time of 400 ms. The spectrum was acquired using States-TPPI and ^{1}H was measured at 400.13 MHz. The spectrum was acquired with 4096 points in the direct dimension and 256 points in the indirect dimension. A total of 8 transients were collected per slice. The spectrum was processed with quadratic sine modulation in both dimensions. Positive contour levels are displayed in red while negative contour levels are shown in green.

It can be clearly seen that of the three substrate nuclei S1, S2 and S3 only S2 has measurable cross peaks with all lipid nuclei and S3 has barely measurable cross peaks with two lipid nuclei (L2 and L5). The assignment of the arbitrary lipid nuclei names to the DMPC molecule was obtained from literature values [187] and is depicted in figure 54. Similarily, the assignment of the substrate nuclei was derived from a previous investigation of TPP^{+} in egg phosphocholine membranes [276]. Also see figure 54 for the assignment.

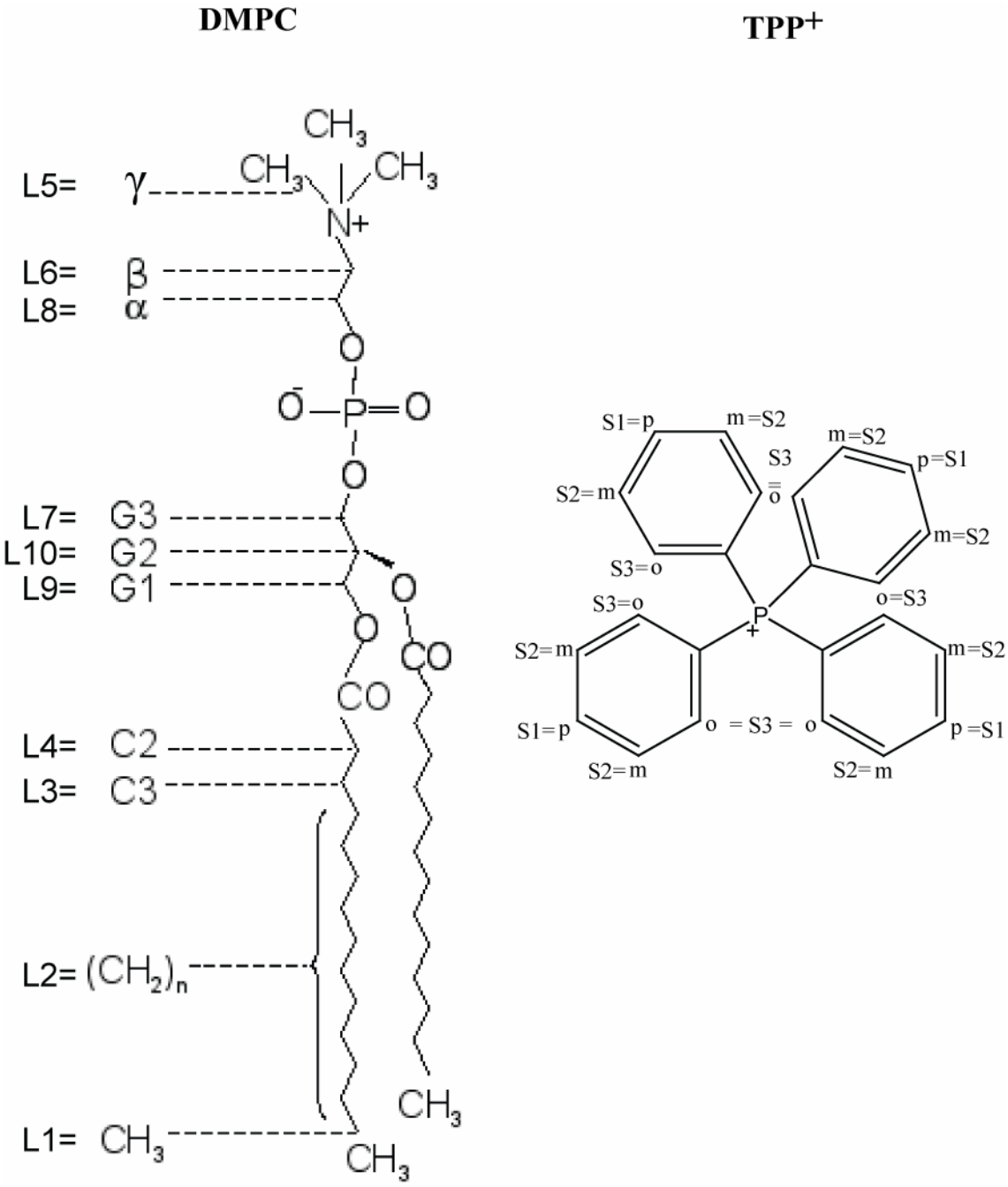

Figure 54. Schematic drawing of DMPC and TPP$^+$ labelled with chemical name and spectrum nomenclature at each position. The ^{1}H peaks for DMPC and TPP$^+$ are labelled arbitrarily in the spectrum: CH_3 = L1, CH_2 = L2, C3 = L3, C2 =L4, G1 = L9, G2 = L10, G3 = L7, α = L8, β =L6 and γ = L5 for DMPC and S3 = *ortho*, S2 = *meta*, S1 = *para* for TPP$^+$.

In the enlarged lipid-substrate cross-peaks region it can clearly be seen that only for the S2 nuclei (*meta* position on the benzene ring) measurable cross-peak with all lipids can be detected. For the substrate nucleus S1 (*para* position on the benzene ring), no cross peaks with lipids could be detected. Finally, for S3 (*ortho* position on the benzene ring), barely measurable cross peaks could be detected with lipid nuclei L2 (acyl chain CH_2 groups) and L5 (phosphocholine head group CH_3 groups, γ). In the following analysis, only the S2 nucleus is utilised because cross peak volumes at the signal to noise ratio result in erratic results.

All lipid-lipid and S2-lipid cross peak volumes were analysed using the full matrix approach [187] which calculates the cross relaxation rates between all peaks simultaneously (see material and methods for details). Lipid molecules in the L_α phase, as used here, undergo axial rotations, lateral diffusion, vertical motion and trans-gauche isomerisations on the µs to ps time scale [275]. Similarly, small molecules like TPP^+ can be expected to undergo motions in the lipid membrane. The cross peak volumes used here are used to calculate cross relaxation rates to determine location probabilities, and represent a time averaged and lipid molecule averaged localisation.
Figure 55 shows the NOESY cross peak volume build up curves from 12 different mixing times measured for TPP^+ in DMPC vesicles.

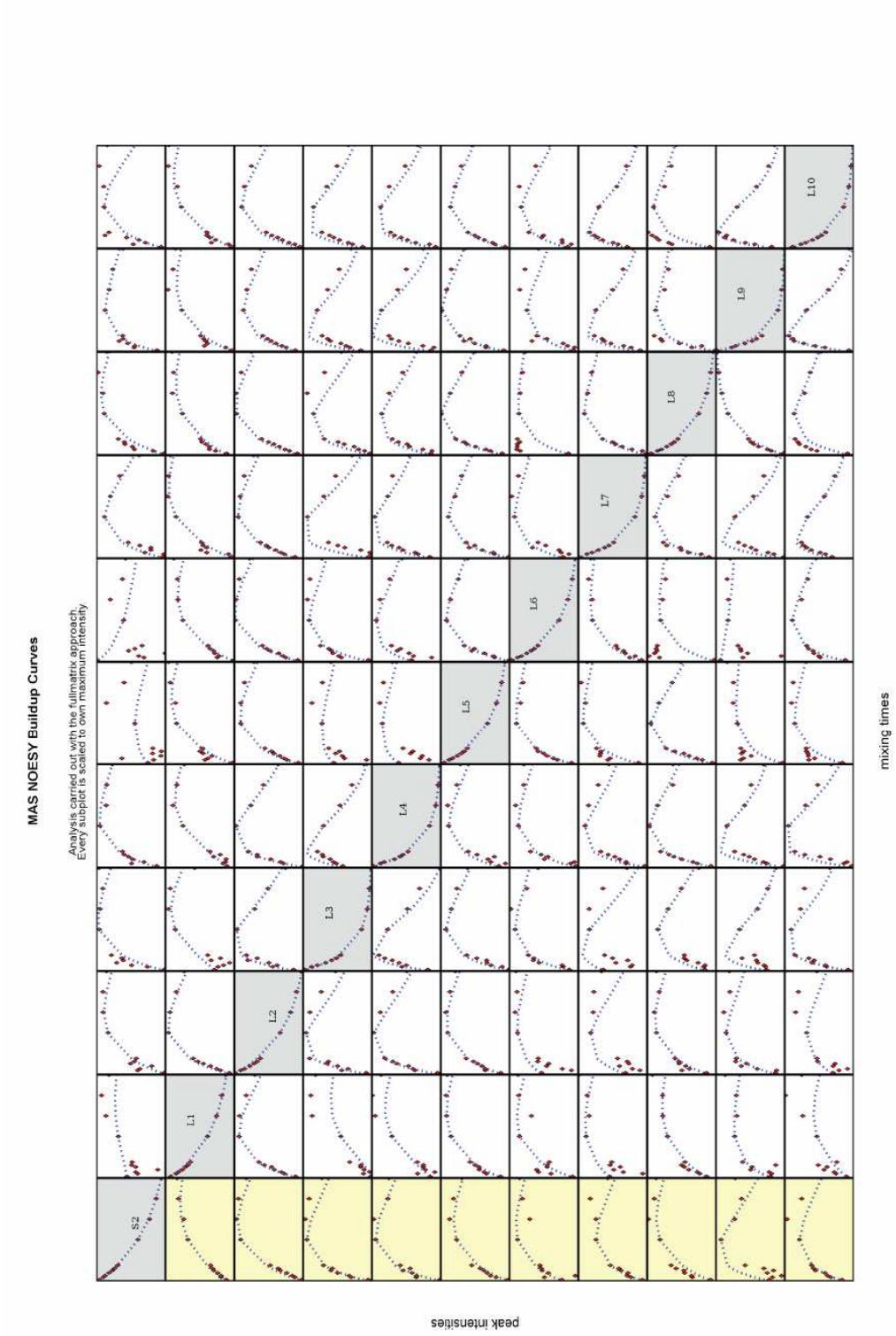

Figure 55. Overview of diagonal and cross-peak volumes at all measured mixing times, fitted using the full matrix approach. Horizontal axes of individual graphs represent the mixing time from 0 to 1 s. The vertical axes represent the diagonal and cross-peak volumes scaled individually from 0 to 1 for each graph. The filled red circles show measured peak volumes while the dotted blue line represents the best fit to the data points using the full matrix analysis. Graphs of diagonal peaks are have a grey background, while lipid-substrate cross-peak graphs have a yellow background.

The boxes show individual cross peak or diagonal peak volumes as a function of mixing time and the best fitting cross relaxation rate as determined by the full matrix analysis is also shown. Boxes with grey background belong to diagonal peaks. With yellow background are the boxes showing lipid-S2 cross peak volumes. The cross relaxation rate indicates the relative location probability of a nucleus. The distribution of the *meta* protons of TPP^+ in a DMPC membrane are shown as distribution probabilities in figure 56.

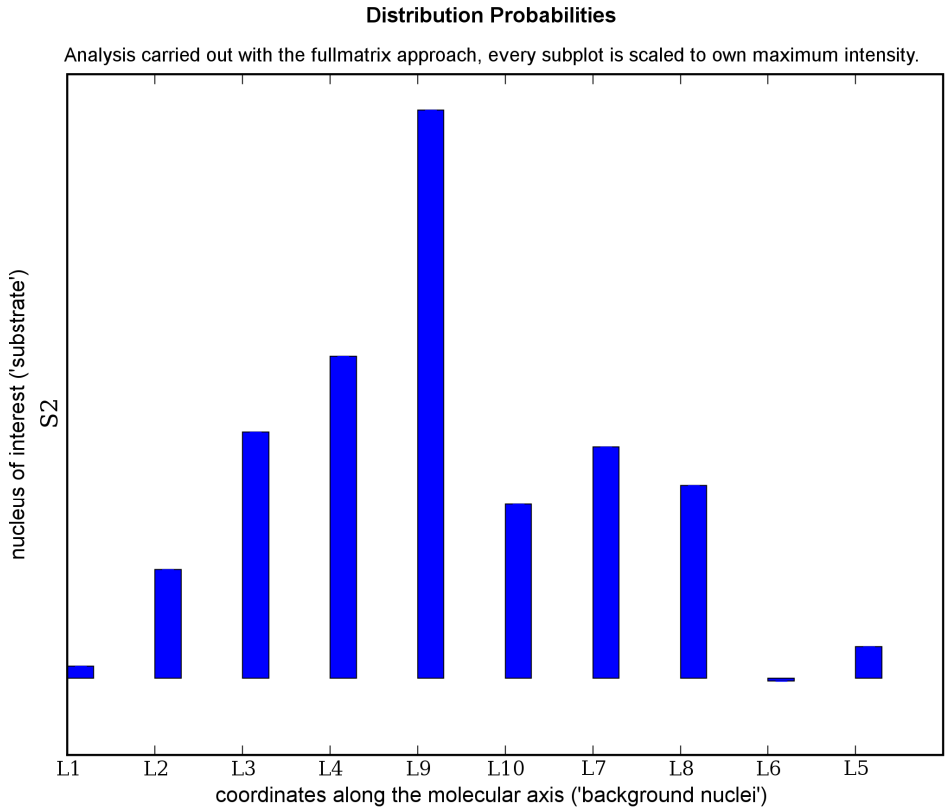

Figure 56. Bar plot indicating the location probability of the TPP^+ nucleus S2 (*meta* position) along the DMPC chain. The lipid nuclei are arranged in the order found in the lipid, left most the CH_3 group of the acyl chain and right most the choline head group γ protons. L1 = CH_3, L2 = CH_2, L3 = C3, L4 = C2, L9 = G1, L10 = G2, L7 = G3, L8 = α, L6 = β and L5 = γ. The highest location probability is found in the glycerol backbone.

The smooth distribution profile suggests that the majority of TPP^+ *meta* protons resides at the top of the acyl chain (L3, L4) and in the glycerol backbone (L9, L10, L7). A more hydrophobic localisation of TPP^+ in the membrane was expected due to its high predicted octanol-water partition coefficient $\log P_{ow} = 5.11$ [281].

8. 2. 5 Conclusions

Here, the location probability of TPP^+ in unilamellar DMPC vesicles in the L_α (liquid crystalline) phase was determined using MAS-NOESY spectroscopy and the full matrix analysis of cross-peak volumes. Taking the benzene ring *meta* substituent protons as indicators suggests that TPP^+ is located mainly at the top of the acyl chain and in the glycerol backbone of DMPC. This is in accordance with previously analysed multidrug transporter substrates [272]. Independent studies on TPP^+ and tetraphenyl boron (TPB^+) in egg phosphatidylcholine suggested a concentration dependent localisation of TPP^+. At high TPP^+ concentrations, the main location of TPP^+ was near the choline head group, while at low TPP^+ concentrations the preferred localisation was in the acyl chain

[276]. A possible concentration dependent relocalisation of TPP^+ in DMPC membranes was not investigated here.
The efficient removal of lipophilic TPP^+ from a bacterial cell would be aided by access to the multidrug transporter binding sites from the glycerol backbone region of the lipid membrane. The flippase and hydrophobic vacuum cleaner models of multidrug transporter would thus seem evolutionary more favourable for lipophilic substrates than the classical pump mechanism.

8. 3 ^{13}C MAS NMR on U-^{13}C Hsmr

While drug-lipid interaction studies by ^{1}H MAS NMR allow an important insight, more direct experiments using labelled transporter proteins are needed to elucidate the structural basis of multidrug efflux. In the following, the potential of solid state NMR on U-^{13}C labelled Hsmr in lipid bilayers has been evaluated.

8. 3. 1 Introduction to ^{13}C MAS NMR on membrane proteins

In contrast to solution state NMR, there is not yet an established suite of experiments for the membrane protein structure determination by solid state NMR. The few structural investigations of membrane proteins that have been attempted by solid state NMR have relied heavily on 2D symmetric homonuclear correlation experiments such as PDSD, RFDR and DARR, although recently the use of a few heteronuclear experiments has been shown on model proteins such as ubiquitin [119], thioredoxin [282], GB1 [283] and phospholamban [122].
2D homonuclear experiments allow the measurement of ^{13}C-^{13}C through space correlations and thereby theoretically enable the assignment of all carbon resonances of one amino acid residue as well as long distance restraints in one experiment. These experiment types all rely on dipolar coupling to transfer the magnetization in a distance dependent manner between nuclei. The heavy reliance on homonuclear ^{13}C spectra in solid state NMR arises from difficulties associated with the measurement of ^{1}H signals, and low efficient magnetization transfers between ^{13}C and ^{15}N nuclei.
Briefly, the acquisition of ^{1}H spectra in the solid state is hampered by the extremely large and strong homonuclear ^{1}H dipolar coupling network which severely limits the spectral resolution at the available MAS speeds (routinely up to 15 kHz) and decoupling power (approximately 100 kHz). Heteronuclear experiments, such as ^{13}C - ^{15}N correlations, however, are challenged by the low magnetic susceptibility of both nuclei and the long magnetization transfer times causing excessive signal loss by relaxation. Today the most promising experiments, at least for the initial investigation, to judge the feasibility of structure determination by solid state NMR are therefore ^{13}C-^{13}C correlation experiments. Several studies have already investigated the effectiveness for various ^{13}C-^{13}C dipolar recoupling experiments [284]. Here, the solid state NMR suitability of Hsmr regarding residue specific assignment was investigated using homonuclear ^{13}C-^{13}C correlation spectra and two different isotope labelling schemes.

8. 3. 2 ^{13}C MAS NMR on Hsmr

The initial solid state NMR assessment of Hsmr used an *in vivo* uniformly ^{13}C labelled protein which was reconstituted at 1:100 protein:lipid mol ratio in *E. coli* total lipids. As shown in chapter 4, these conditions afford the most uniform and dense protein incorporation as judged by sucrose density gradient centrifugation and freeze fracture analysis. Also, these conditions were shown in chapter 6 to yield active protein as judged using an bR coupled ethidium bromide transport assay [254]. Latter experiments used a uniformly ^{13}C labelled Hsmr, selectively unlabelled at the abundant alanine and valine residues [285]. In theory, for complete residue specific resonance assignment, a

single uniformly labelled protein sample is required. However, if spectral crowding due to poor signal dispersion, large number of resonances, large abundance of a specific residue type and line-broadening are present, it may be necessary to resort to the use of several partially labelled samples. Many such approaches have been documented for solid state NMR investigations. These include specific unlabelling [285], pattern labelling [286, 287], amino acid specific labelling [158] and amino acid group labelling [288] . For investigations of the suitability of Hsmr for structural studies, specific unlabelling of the highly abundant amino acids alanine and valine, together comprising nearly 40 % of all Hsmr amino acids, were chosen. This approach can be expected to have a large effect on spectral quality while being inexpensive.

The first 2D experiment used was a PDSD spectrum, a homonuclear ^{13}C-^{13}C correlation experiment (see materials and methods). The sample was measured in the frozen state, to enable cross polarisation from protons to be used for signal enhancement and to ensure long-term protein stability.
A spinning speed of 10000 Hz was chosen to remove most of the ^{13}C chemical shift anisotropy, and ensure long-term stable sample spinning. The ^{1}H-^{13}C dipolar couplings was decoupled during the ^{13}C evolution periods to remove line-broadening effects. Mixing took place without decoupling, i.e. in the presence of ^{1}H-^{13}C dipole couplings. The resulting ^{13}C linebroadening and spectral overlap enabled ^{13}C-^{13}C spin diffusion. Measurements were carried out for several mixing times. Here, a short mixing period (20 ms) is chosen to spatially limit spin diffusion. It has been previously shown that at such short mixing times magnetization is transferred only between one bond neighbours, thus providing strictly intraresidue cross peaks [123]. This is confirmed here (see figure 57 for an overlay of two different mixing times). The effect on spectral crowding of uniformly ^{13}C labelled Hsmr or uniformly ^{13}C labelled and selectively unlabelled alanine and valine Hsmr are shown for the CαCβ region in figure 58A) and 58B) respectively.

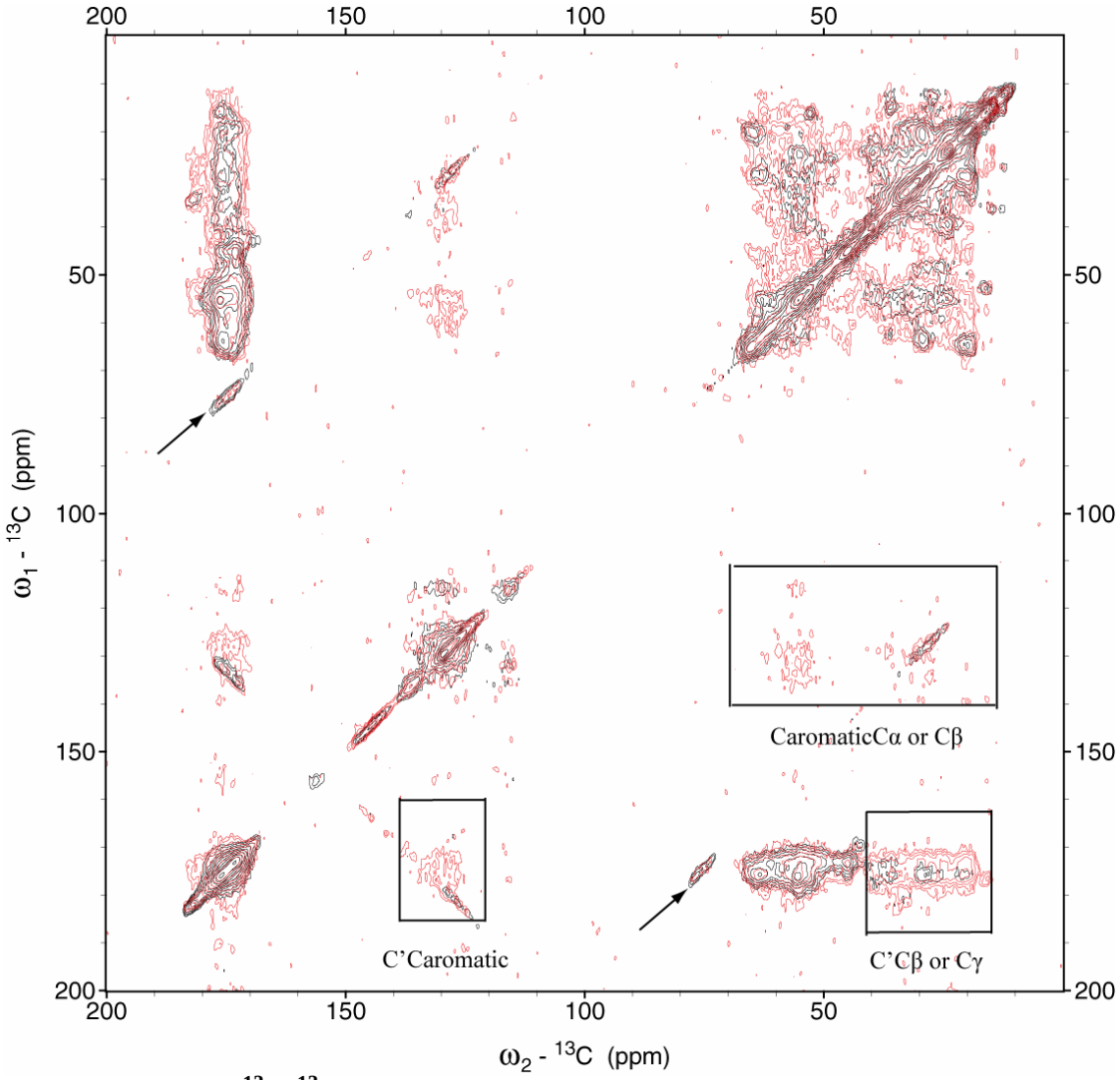

Figure 57. 2D ^{13}C-^{13}C PDSD experiments on selectively unlabelled Hsmr reconstituted into *E. coli* total lipids. A PDSD spectrum with a mixing time of 20 ms is shown in black while the PDSD experiment with a spin diffusion step of 200 ms is shown in red. The sample was uniformly ^{13}C labelled, with the exception of and Ala and Val. Hsmr was reconstituted into *E. coli* total lipids at a protein:lipid mol ratio of 1:100. Spinning side bands occurring are indicated by arrows. Two or more bond correlations are indicated by boxes.
The PDSD experiment on Hsmr was measured at 235 K and a spinning rate of 10000 Hz. The spectra were acquired using TPPI and ^{1}H was measured at 400.13 MHz and ^{13}C was measured at 100.62 MHz. The spectrum was acquired with 2098 points in the direct dimension and 256 points in the indirect dimension. A total of 128 transients were collected per slice. The spectrum was processed with exponential line broadening of 50 Hz in the direct dimension and quadratic sine modulation in the indirect dimension.

At first glance the PDSD spectra in figure 57 reveal an intense diagonal, which arises from the short magnetization transfer time of 20 ms (black spectrum) and natural abundance ^{13}C signals from the lipids (both spectra). Although ^{13}C has a natural abundance of only 0.1 %, the lipids are present at a 100 fold mol excess compared to the protein. The intense diagonal may in general limit the ability to detect low intensity cross peaks due to limitations of the dynamic range during acquisition. In particular, the intense diagonal may limit the detection of cross peaks close to the diagonal.
Also immediately evident are the two strong lines running parallel to the diagonal. In figure 57, the spinning sideband are indicated by arrows. If the spinning speed cannot be chosen such that the chemical shift anisotropy is completely removed, it is chosen in

such a way as to avoid interference between cross peaks and the spinning sidebands of the diagonal, as is seen here.
The overlay of spectra acquired with respective 20 ms and 200 ms mixing times allows the progress of spin diffusion to be assessed. Indeed, the black spectrum (20 ms) shows mainly one bond correlations, namely CαC', CβCα, CβCγ and CaromaticCaromatic cross peaks. The red spectrum (200 ms) shows more cross peaks, now also including two or more bond correlations namely C'Caromatic, CaromaticC α, CaromaticCβ, C'Cβ and C'Cγ, highlighted in the spectrum by boxes. A decrease of the diagonal intensity is clearly visible and arises from the longer pulse sequence and concomitantly increased relaxation.

For resonance assignment, individual peaks must be discernible for 'assignment walks' between residues to be carried out. The CαCβCγ region of uniformly and selectively unlabelled Hsmr are enlarged in figure 58 to enable resonance assignment and the effect of selective alanine and valine unlabelling to be detected.

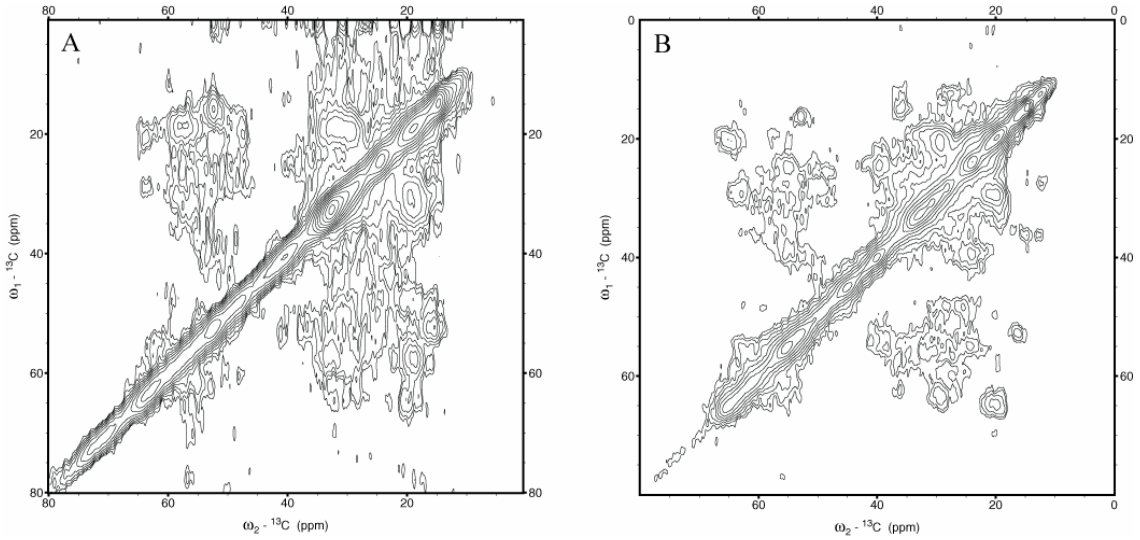

Figure 58. PDSD Cαβ region of uniformly ^{13}C labelled Hsmr and selectively unlabelled Hsmr. A) uniformly ^{13}C labelled Hsmr and B) uniformly ^{13}C labelled Hsmr selectively unlabelled with alanine and valine. The PDSDs were acquired with 20 ms mixing time. The PDSD experiment on uniformly labelled Hsmr was measured at 190 K at a 9500 Hz MAS spin rate. The spectrum was acquired with 1398 points in the direct dimension and 128 points in the indirect dimension. The PDSD experiment on selectively unlabelled Hsmr was measured at 235 K and 10000 Hz MAS rate. The spectrum was acquired with 2098 points in the direct dimension and 256 points in the indirect dimension. Both spectra were measured with ^{1}H at 400.13 MHz and ^{13}C at 100.62 MHz using TPPI and a total of 128 transients per slice. The spectra were processed with exponential line broadening of 50 Hz in the direct dimension and a squared sine modulation in the indirect dimension. Only positive contour levels are shown.

As can be clearly seen in figure 58A) and 58B), a few narrow resonances, a few broad resonances and large areas of unresolved magnetization are observable. The number of discrete resonances is increased in the spectrum of selectively unlabelled Hsmr, and the area covered by unresolved magnetization is reduced. These changes occur in a region of typical alanine and valine chemical shifts and this resolution increase is thus attributed to the isotope dilution by specific unlabelling. However, it must be noted that in neither sample the resolution was sufficient to observe the expected 139 Cα (fully labelled sample) or 91 Cα (selectively unlabelled sample) diagonal peaks or 128 CαCβ

(fully labelled sample) or 80 CαCβ (selectively unlabelled sample) cross peaks. Additionally, it must be noted that the individual peaks observed could not be assigned to spin groups and amino acids types. An INADEQUATE type experiment could alleviate problems with assigning spin groups and amino acid types. Figure 59 shows a theoretical DQSQ spectrum for three amino acids.

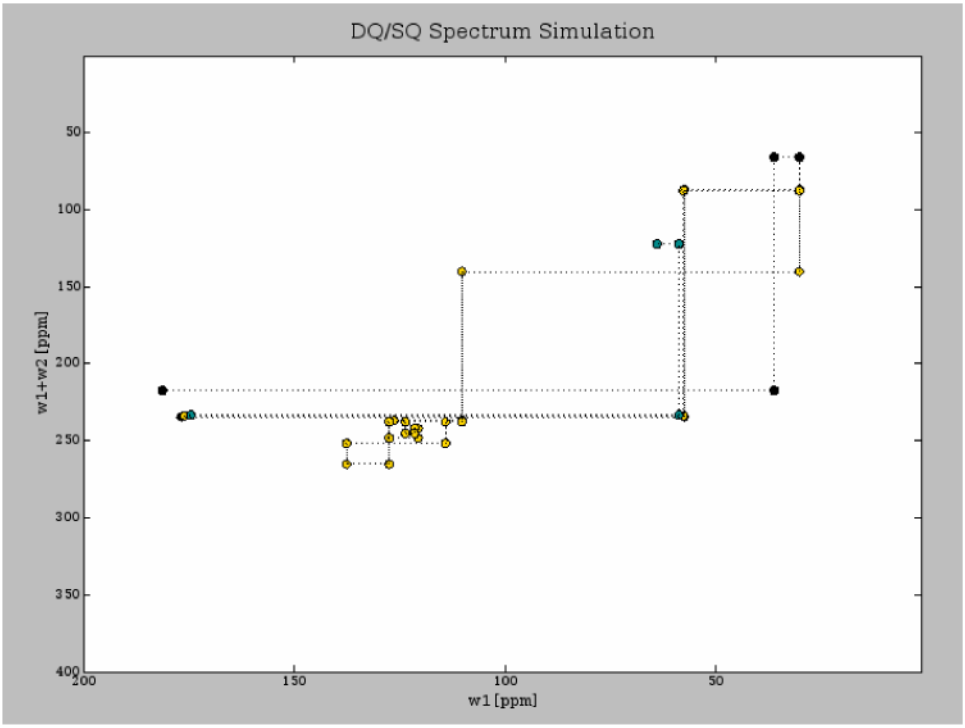

Figure 59. Theoretical spectrum of three amino acids in a 2D DQSQ spectrum. The DQSQ correlation pattern of glutamate (black), tryptophan (yellow) and serine (green) is shown here. The pattern is diagnostic of the amino acid type but crowding is also observed, particularly in the C' and Cα region. The average chemical shifts for the amino acids, as reported in the BMRB, were used here.

Figure 60 shows an INADEQUATE type DQSQ experiment of Hsmr. Although more individual resonances can be resolved, not a single spin group could be completely assigned. Here, again it is observable that Hsmr samples have a large line-width and poor chemical shift spread, making Hsmr a poor candidate for structural characterisation by solid state NMR. Recently published ^{13}C-^{13}C PDSD spectra of EmrE in 2D DMPC crystals by solid state NMR also report problems with unresolved resonances [136].

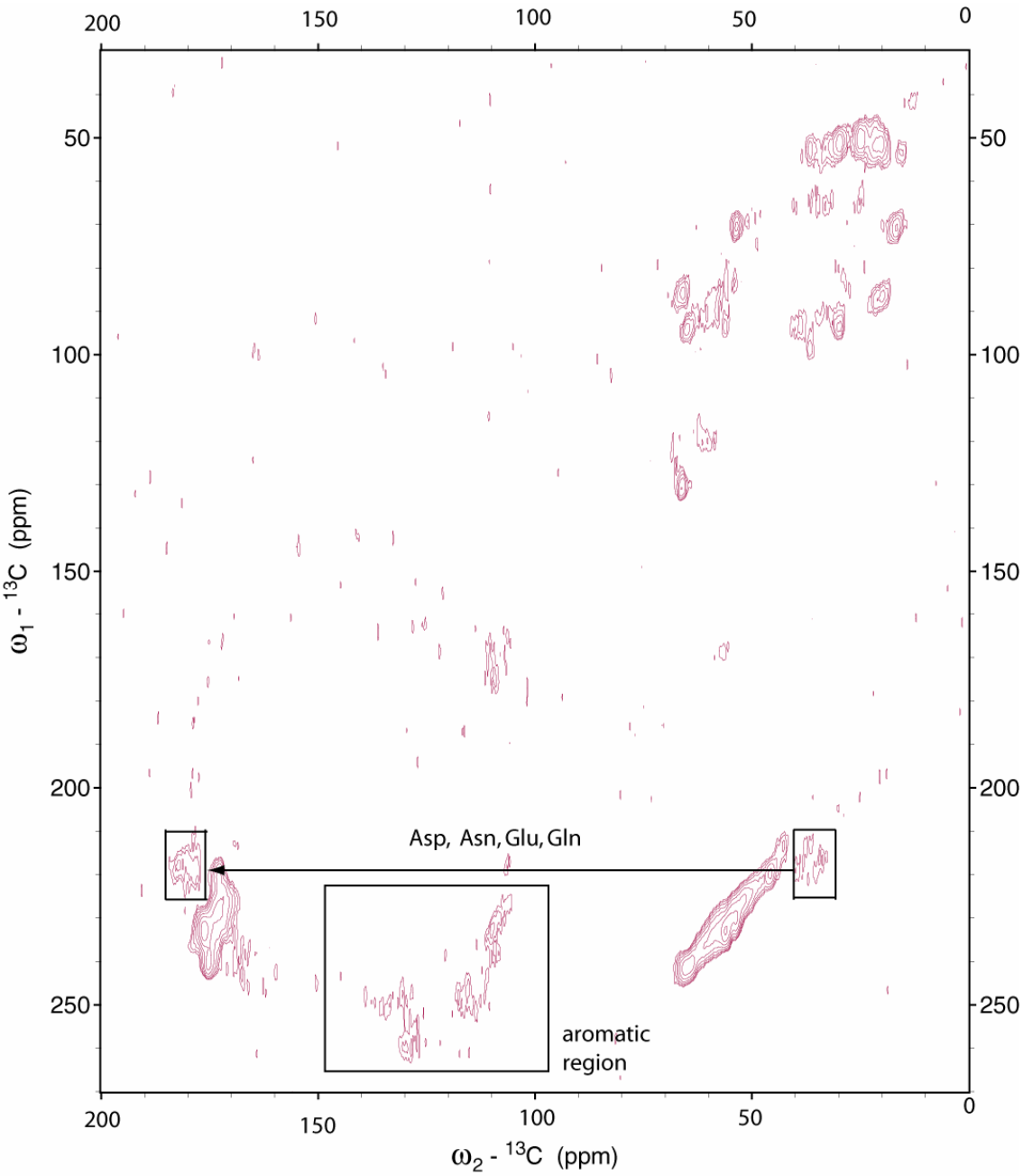

Figure 60. 2D ^{13}C-^{13}C DQSQ experiment on selectively unlabelled Hsmr reconstituted into *E. coli* total lipids. Part of an assignment walk was possible for the acidic amino acids and their uncharged derivatives (Asp, Glu, Asn and Gln) due to their characteristic Cγ and Cδ shifts respectively. The aromatic region is highlighted with a box. An arrow indicates the 1 bond correlations likely arising from Asp, Asn (CβCδ) and Glu, Gln (CγCδ). The DQSQ experiment on Hsmr was measured at 220 K and 10000 Hz MAS rate. Double quantum (DQ) coherence was generated using a SR22 sequence. The sample was uniformly ^{13}C labelled and Ala, Val ^{12}C unlabelled. Hsmr reconstituted into *E. coli* total lipids at a protein:lipid mol ratio of 1:100. The spectra were acquired in phase sensitive mode (States-TPPI) and 1H was measured at 600.12 MHz and ^{13}C was measured at 150.91 MHz. The spectrum was acquired with 1796 points in the direct dimension and 240 points in the indirect dimension. A total of 512 transients were collected per slice. The spectrum was processed with exponential line broadening of 50 Hz in the direct dimension and a squared sine modulation in the indirect dimension. Only positive contour levels are shown.

8. 3. 3 Conclusion

Hsmr was investigated using two different ^{13}C labelling schemes and using several ^{13}C - ^{13}C correlation experiments. The resulting PDSD and DQSQ spectra show poor resolution due to broad line width, a limited chemical shift spread and high amino acid type redundancy. A limited chemical shift spread is typical for alpha helical membrane proteins, but the large line-width indicates structural heterogeneity of the sample. Sucrose gradient centrifugation and freeze fracture electron microscopy indicate a macroscopically homogenous sample. Theoretically, Hsmr could be in exchange between distinct conformational states such as binding or release conformations leading to sample heterogeneity. However, Hsmr in the absence of substrate and a pH gradient can be expected to have its conformational space limited to the binding position. More likely, freeze trapping of thermal motions on the ms range are the cause of microscopic sample heterogeneity [132, 289]. This is commonly observed with solid state NMR of biological materials and the protein is considered natively folded for unaligned and non-crystalline proteins with linewidth between 1 and 4 ppm [124, 290].
In order to obtain a more global view, static ^{2}H NMR has been used to probe Hsmr mobility within the lipid bilayer.

8. 4 ^{2}H NMR on Ala-d3-Hsmr

8. 4. 1 Molecular dynamics from static ^{2}H solid state NMR

Solid state NMR is well suited to studies of molecular motion as a large range of motional regimes can be investigated through the analysis of their effects onto anisotropic spin interactions. Relaxation studies as well as lineshape analysis of chemical shift anisotropy (CSA), dipolar and quadrupole couplings allow a wide frequency range to be charaterised.
Mostly, however, the study of protein dynamics by solid state NMR has historically relied on ^{2}H quadrupole NMR. Spin lattice relaxtion times are sensitive to motions in the order of the inverse Larmor frequency (10^{-6} s) while the typical quadrupolar Pake pattern response to motions of the inverse of the quadrupolar coupling constant (167 kHz für static C-D; 10^{-3} s). Processes accessible by ^{2}H NMR cover a range of 10^{-10} to 10^{-4} s. In case of membrane proteins, this can involve sidechain flexibility, helix wobbling, internal fluctuations and rotational diffusion. Seminal work on protein dynamics using ^{2}H NMR was conducted collagen [291, 292], bacteriorhodopsin [293] [294] and pancreatic phospholipase A2 [295] in the 1980s. ^{2}H is a spin 1 quadrupolar nucleus and can be incorporated into biomolecules as a replacement for ^{1}H. Deuterium offers the advantage of low natural abundance (0.01 % [296]), numerous possible incorporation sites and simple incorporation during sample preparation. [297]. The quadrupole-coupling constant dominates the deuterium powder pattern and a Pake pattern is observed. The expected unscaled linewidth of the Pake pattern lies in the hundreds of kHz (167kHz quadrupole coupling for C-D). Large spectral width thus required for these experiments means specifically tailored NMR experimental conditions and pulse sequences, generally a standard quadrupole echo experiment (see materials and methods), need to be used.[298]. In contrast to the large quadrupole-coupling constant linewidth the chemical shift dispersion of ^{2}H is small and identical to ^{1}H [299]. Accordingly, the site specific resolution of samples labelled at multiple positions is poor. Therefore, static experiments are preferred over ^{2}H MAS.

8. 4. 2 Dynamics of Hsmr reconstituted in E. coli lipids by ^{2}H NMR

Investigations into the 3D structure of Hsmr by solid state NMR have indicated the presence of motions occurring in the proteins structure.

Here, the global motional regime of Hsmr incorporated into *E. coli* total lipid liposomes is directly investigated using static ^{2}H NMR. During static experiments the full anisotropy of all NMR interactions is observed. Deviations of the observed lineshape from the theoretical powder pattern can thus be directly, without simulations, attributed to protein dynamics. Hsmr global protein dynamics were investigated using deuterated alanine, chosen due to its abundance (19 alanine residues) and distribution in three of the four proposed Hsmr transmembrane helices, (see figure 61). Due to the poor chemical shift dispersion of deuterons and the fact that the spectrum is dominated by the quadrupole-coupling constant, only global alanine dynamics can be investigated. Alanine-d3 is ideally suited for the investigation of backbone mobility as it offers increased sensitivity due to three reporting deuterons and the fast rotation around the Cαβ bond ensures that at ambient temperatures the quadrupole-coupling constant is reduced to 51.7 kHz [292]. Deviations from this quadrupole-coupling constant report directly on protein backbone mobility and the methyl group environment. See figure 62 for the alanine-d3 chemical structure.

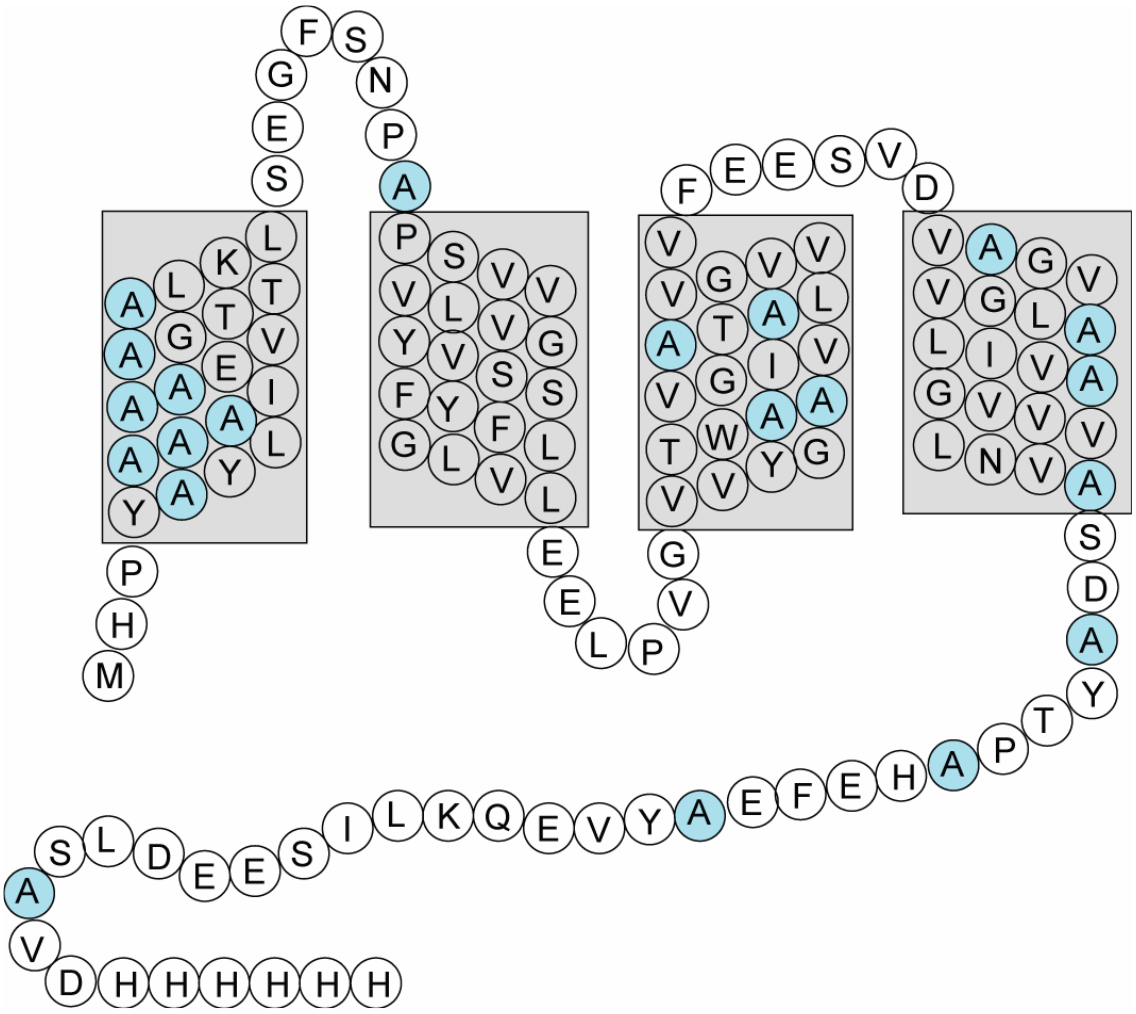

Figure 61. Topology diagram of Hsmr with myc-his tag and highlighted alanine residues. Alanines are highlighted in blue and the proposed transmembrane regions are depicted as grey boxes [267]. Two alanine residues are located in the myc-his tag and one alanine in the C-terminus.

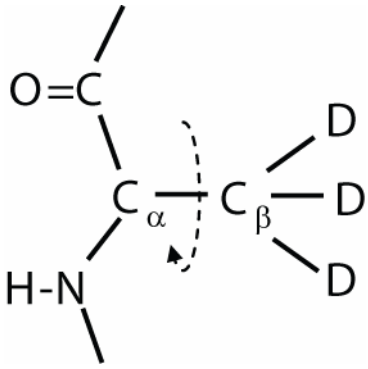

Figure 62. Chemical structure of alanine-d3.

Here, Hsmr mobility in the exchange mode, i.e. with substrate but without pmf, was assessed at 283 K and 230 K reconstituted into total *E. coli* lipids in the absence and presence of 100 fold excess of the substrate ethidium bromide. The native Hsmr environment is the plasma membrane of H. *salinarium*, and is most closely mimicked by *E. coli* lipids. These two temperatures were chosen to measure Hsmr mobility in gel/L_β phase membranes (283 K) and largely immobilised by freezing (230 K) [300]. At 283 K, *E. coli* lipids are below the liquid-crystalline phase transition temperature (20-25 °C) [301], but the membrane still exhibits extensive motions [300] [302]. These low temperatures were beneficial for the longevity of the fragile protein Hsmr.
Samples measured at 230 K should have negligible backbone mobility and merely side chain bond rotations, around the CαCβ bond of alanine are observed. This low temperature was chosen as a control measurement to provide the lineshape of immobile protein. Among the known Hsmr substrates, ethidium bromide was selected for this investigation, as transport activity assays in this study (chapter 6) directly showed its active transport. The membrane integrity was preserved in the presence of excess ethidium bromide, see figure 63.

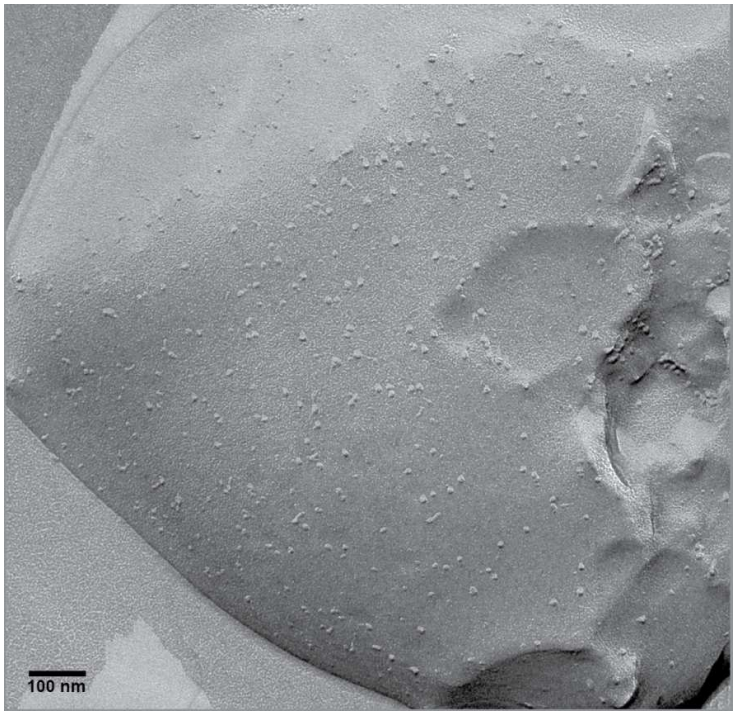

Figure 63. Freeze fracture analysis of Hsmr in *E. coli* total lipids with ethidium bromide. Hsmr reconstituted at 1:100 protein/lipid mol ratio in *E. coli* lipids and spiked with ethidium bromide, 100 fold mole excess during incubation, was subjected to freeze fracture analysis after several days of NMR measurements at 283 K and 230 K.

Hsmr NMR spectra without and with the substrate ethidium bromide, figure 64A)C) and 64B)D), are essentially identical at 230 K. It can be seen that the ^{2}H spectrum is dominated by the quadrupolar interactions. The observed lineshape arises from the superposition of the quadrupole-coupling constants of 19 alanine-d3 molecules incorporated into non-equivalent sites.

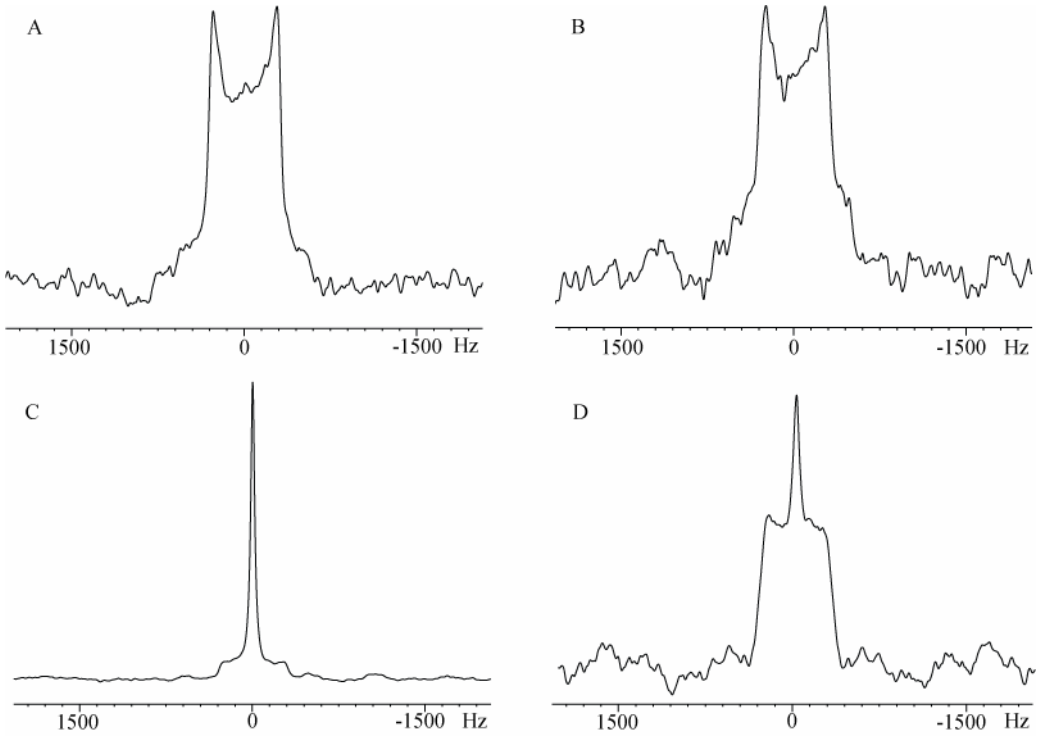

Figure 64. Static ^{2}H spectra of alanine-d3 labelled Hsmr. Hsmr reconstituted at 1:100 protein/lipid mol ratio in *E. coli* lipids was measured static with a quadrupole echo pulse sequence (see materials and methods) at 230 K A), B) and at 283 K C), D). Hsmr without substrate is shown in A) and C) while Hsmr after incubation with an excess of ethidium bromide is shown in B) and D). The same sample was used for all four measurements and incubation with etbr led to a reduction in sample quantity. The spectra were acquired using ^{2}H 92 MHz with 4892 points. A total of ~ 400,000 transients were collected per spectrum. The spectra were processed with exponential line broadening of 2500 Hz.

The apparent quadrupole coupling constant χ at 230 K can be calculated and is 49.0 kHz for Hsmr without substrate and 45.6 kHz for Hsmr in the presence of ethidium bromide. The quadrupole coupling constant is only apparent as it is a superposition of 19 individual quadrupole couplings. The apparent effective quadrupole coupling constants are very similar and compare favourably with the literature value of 49 kHz [303]. Hsmr without and with substrate at 230 K is thus largely immobile and methyl group rotation is impeded in the folded protein as judged by ^{2}H NMR lineshape analysis. Reducing methyl group rotation by temperature requires temperatures smaller than 120 K [297].

In contrast, Hsmr in *E. coli* total lipid membranes at 283 K is expected to be more mobile, to undergo increased thermal fluctuations and possibly conformational changes. Indeed, the ^{2}H NMR spectra of Hsmr without substrate (figure 64C)) and Hsmr with substrate (figure 64D)) are dramatically different from the frozen Hsmr spectra (figure 64A) and figure 64B)). At 283K, the observed static ^{2}H NMR spectra are composed of at least two components. At least one cumulative broad Pake pattern shaped contribution is superimposed on one cumulative narrow contribution. Calculation of the

apparent quadrupole-coupling constant for the broad component is hampered by the absence of the expected "horns". Taking the outmost shoulder as horn, the apparent quadrupolar-coupling constant is 48.5 kHz for Hsmr without substrate and 42.5 kHz for Hsmr with substrate. Both quadrupole-coupling constants are very similar to the apparent quadrupolar-coupling constant observed for frozen Hsmr. However, the absence of the "horns" provides evidence that the broad component is indeed a superposition of several distinct quadrupolar-coupling constants. If for Hsmr without substrate it is assumed that only two components contribute to the spectrum then it can be concluded that one component undergoes slow motions on the ^{2}H time scale (10^{-3} to 10^{-6} s) yielding a powder pattern-like component. By contrast the second component then can be concluded to undergo fast motions on the ^{2}H time scale (10^{-3} to 10^{-6} s) yielding a nearly isotropic lineshape. The narrow component can be expected to have contributions from residual natural abundance D_2O as observed previously [292]. The contribution should be very small, as D_2O depleted H_2O was used during the sample preparation, and even the natural abundance of D_2O is low with just 0.01 % [296]. A 90° pulse experiments with the spinning speed set equal to the sweep width to remove all anisotropic interactions [298], see figure 65, reveals two signals. The sharp D_2O peak has a small integral compared to the broad alanine peak and concomitantly produces only a minor contribution to the narrow component in figures 64. It can thus be derived that at 283 K the majority of alanine residues is largely immobile while several Hsmr alanine residues are remarkably mobile. These mobile alanine residues are likely tag and loop residues.

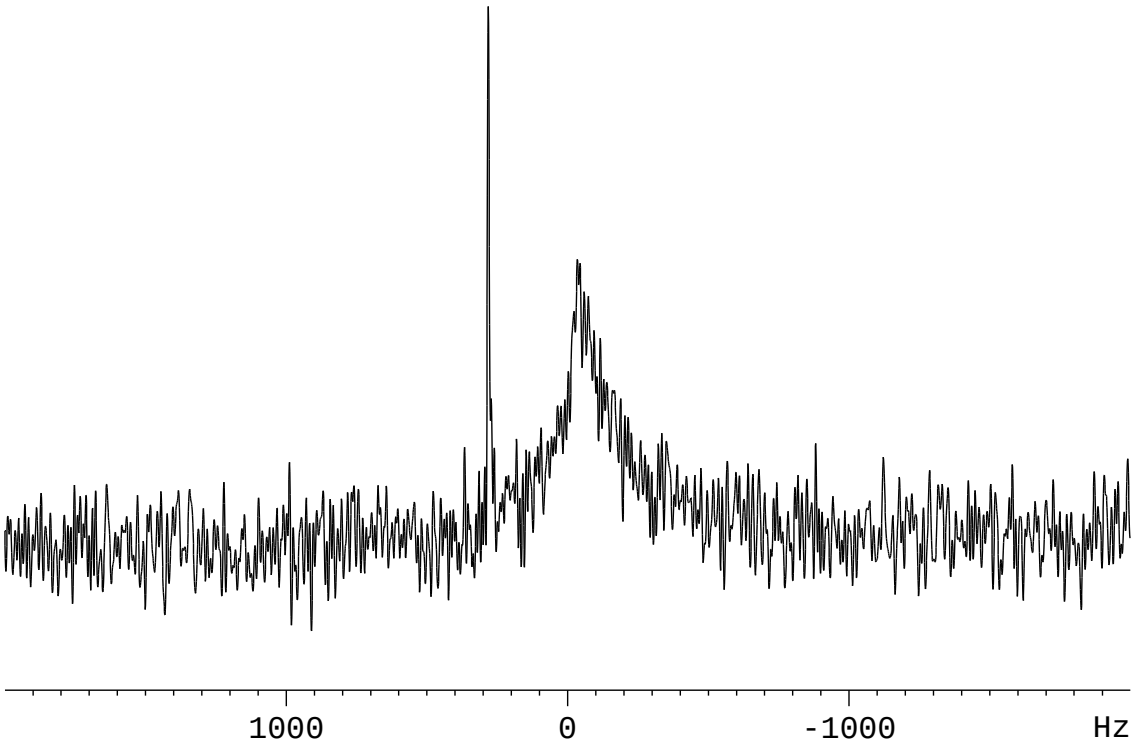

Figure 65. ^{2}H spectra of alanine-d3 labelled Hsmr at 8000 Hz MAS. Hsmr reconstituted at 1:100 protein/lipid mol ratio in *E. coli* lipids was measured at 283 K and 8000 Hz MAS. The spectrum was acquired using ^{2}H 92 MHz with 1596 points. A total of 100,000 transients were collected per spectrum. The spectra were processed with an exponential line broadening of 1 Hz. The narrow peak (left hand side) arises from D_2O, while the right broad peak is due to alanine-d3.

For Hsmr with substrate, figure 64D), a significant decrease in signal intensity of the narrow components to the total signal is observed. Correspondingly, the signal intensity of the powder pattern components increased with respect to the total signal. The addition of the substrate ethidium bromide to Hsmr in exchange mode could be the cause of reduced transmembrane mobility or accumulation of ethidium bromide in the membrane could affect the protein mobility.
The overall large mobility of Hsmr transmembrane segments embedded in an anisotropic lipid membrane is surprising. Unexpectedly, large protein mobility of transmembrane regions however has also been reported for other transport proteins including LmrA and LacY [304, 305]. No attempt was made to quantify these components, because transmembrane dynamics have previously been proven to exhibit a loss of signal intensity due to intermediate rate motions [306]. A direct correlation of integrals and spin numbers is thus not possible. Equally importantly, to obtain integrals of the fast and slow components the complex experimental spectrum needs to be deconvoluted. A total of 19 separate alanine contributions and D_2O give rise to the observed lineshape and fitting so many parameters with no additional information is not sensible.
Discussions about possible mechanisms enabling the broad substrate specificity of multidrug transporter include protein flexibility as a contributing factor [307, 308]. Most investigations into substrate recognition however have been performed on soluble transcription factors of multidrug transporters [9, 10, 12, 13]. The large dynamics observed here, of the transmembrane region of a protein embedded in a lipid membrane, support the notion that protein mobility plays a role in substrate recognition for Hsmr. This is further supported here by the limitation of protein conformational flexibility upon substrate binding. The complementary limited substrate mobility in the bound state was detected with the fluorescence based ethidium bromide transport assay [254].

8. 4. 3 Conclusion

Hsmr incorporated into an *E. coli* total lipid membrane showed differential global mobility, as judged by a global lineshape analysis of 19 alanine residues, as a function of temperature and presence of substrate. Hsmr in *E. coli* total lipid membrane frozen at 230 K yielded a single Pake pattern with a quadrupole splitting typical for proteins. At the higher temperature (280 K), Hsmr was present in a gel phase *E. coli* total lipid membrane and lineshape analysis revealed alanine residues in different motional regimes and as well as contributions from residual D_2O. Hsmr incorporated into a gel phase membrane showed several remarkably mobile alanine residues. Their mobility was reduced upon substrate addition supporting the notion that protein flexibility is one mechanism of multidrug transporter to enable recognition of highly diverse substrates.

Chapter 9 - Investigations of EmrE and its key residue for substrate transport E14 – in the membrane embedded dimer EmrE is asymmetric

9. 1 Introduction

Here, *E. coli* EmrE, a member of the SMR protein SMP subclass and its structural model, is investigated [25]. EmrE transports a diverse array of aromatic, positively charged substrates, including ethidium bromide, in exchange for protons [39]. Like all SMP proteins, EmrE has the highly conserved key residue E14 in its proposed first TM helix [27, 154]. It has been shown that E14 is an essential residue and directly involved in drug and proton binding [65] [64, 309]. It can reasonably be assumed, that the E14s of both protomers in a dimer form a shared binding pocket [19, 44, 47]. See figure 66 for a schematic representation of helices 1 forming an ethidium bromide binding pocket. Whether EmrE forms a symmetric or an asymmetric dimer should be reflected in the chemical shifts of residues such as E14, which are likely to be found at the dimerisation interface. This provided the motivation for the direct, non-invasive investigations of E14 in EmrE. Here, E14 in EmrE was ^{13}C labelled using a cell free expression system and investigated reconstituted in *E. coli* total lipids by solid state NMR.

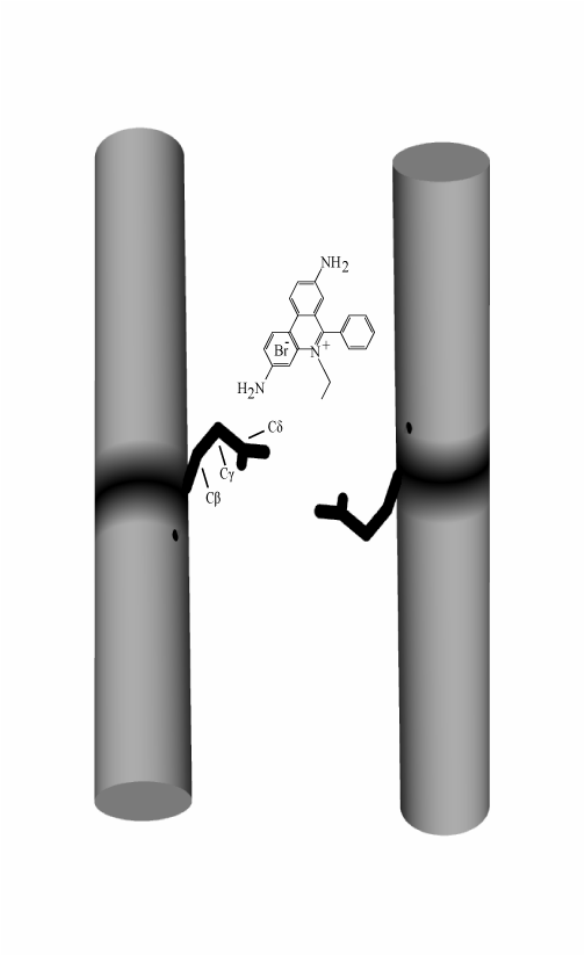

Figure 66. Schematic model of the TM helices 1 of dimeric EmrE with ethidium bromide. The sidechain of residue E14 is depicted as stick model and the nuclei are labelled according to the IUPAC convention. The inherent asymmetry of ethidium bromide suggests that its binding pocket should also be asymmetric.

9. 2 Results

9. 2. 1 Sample preparation

In order to investigate the electronic structure of E14 in EmrE, a selectively labelled sample was required. For this, *in vitro* transcription and translation has to be employed, as selective glutamate labelling *in vivo* is difficult due to isotope scrambling [310]. In addition, a single glutamate mutation is necessary to avoid spectral overlap, and to obtain unambiguous data. Cell free protein expression has been carried out both as precipitate followed by solubilisation in DDM and also directly in the presence of DDM. The resultant ^{13}C E14 EmrE E25A was reconstituted into native *E. coli* lipids. Sample purity, labelling efficiency, activity and sample homogeneity were carefully examined.

9. 2. 1. 1 Protein purity

Protein purity was analysed by MALDI-TOF mass spectrometry and SDS PAGE. A typical spectrum is shown in figure 67 and the measurements are summarised in table 25.

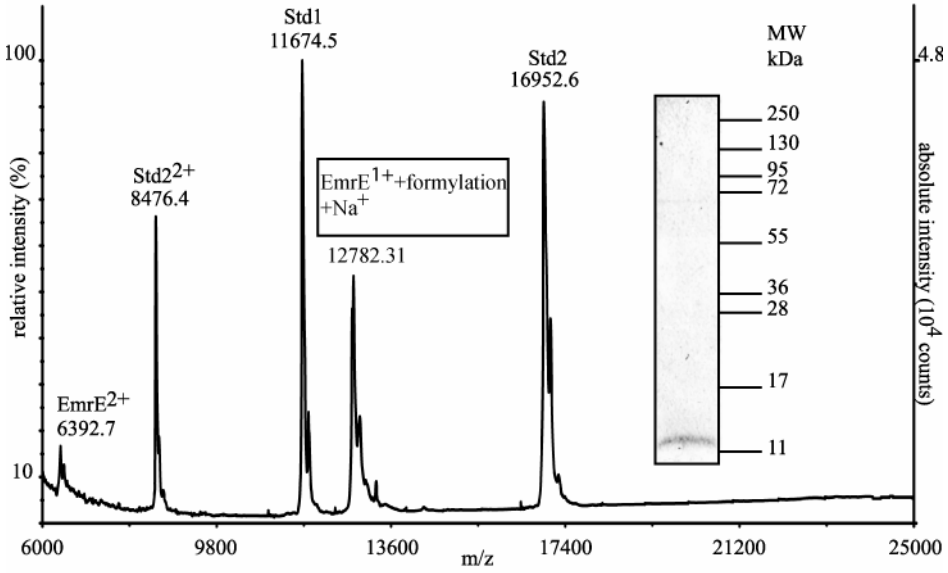

Figure 67. Representative MALDI-TOF mass spectrum of purified $^{13}C/^{15}N$ glutamate labelled EmrE E25A. Triplicate measurements give a mass of 12,785.34 ± 2.68 Da for EmrE E25A $^{13}C/^{15}N$ glutamate labelled, formylated and with attached sodium. The mass measured here agrees well with the expected mass for EmrE E25A $^{13}C/^{15}N$ glutamate labelled formylated and with attached sodium (12780.1 Da). Peaks of the reference compounds used for internal two-point calibration are labelled Std1 and Std2. No other signals were detected. These data show that EmrE E25A is pure and confirm conventional SDS PAGE analysis (see inset picture, above).

	theoretical M_r	theoretical M_r + formylation (28 Da) + Na^+ (23 Da)	m/z
measurement 1	12729.1	12780.1	12782.31
measurement 2	12729.1	12780.1	12787.42
measurement 3	12729.1	12780.1	12786.29
average (sdv)	12729.1	12780.1	12785.34 ± 2.68

Table 25. Average EmrE E25A masses from three independent MALDI-TOF experiments using internal calibration. Listed are measured values (m/z) corresponding to the singly charged $^{13}C,^{15}N$ glutamate labelled EmrE E25A formylated and with attached sodium ion. Additionally, the theoretical average masses (M_r) of $^{13}C,^{15}N$ glutamate labelled EmrE E25A and of $^{13}C,^{15}N$ glutamate labelled EmrE E25A formylated with attached sodium were calculated. The presence of formylation is verified by MS after tryptic digestion, see figure 69.

The peak at 12,785.34 ± 2.68 Da agrees well with the mass expected for $^{13}C/^{15}N$ glutamate labelled EmrE E25A formylated and with attached sodium (12780.1 Da). Formylation was confirmed by MS after tryptic digestion, see figure 69. The absence of other signals and the result of SDS PAGE show EmrE E25A is pure. Mass spectrometry, in addition to SDS PAGE, is a very sensitive tool to assess contamination with soluble proteins. Membrane proteins other than EmrE are not present in the cell free expression system.

9. 2. 1. 2 Scrambling and labelling efficiency

The absence of ^{13}C glutamate scrambling in the *in vitro* expression system was verified by performing a complete translation and transcription experiment without DNA template. A ^{13}C-NMR analysis of the whole reaction mixture did not show any signs of glutamate to glutamine conversion, see figure 68.

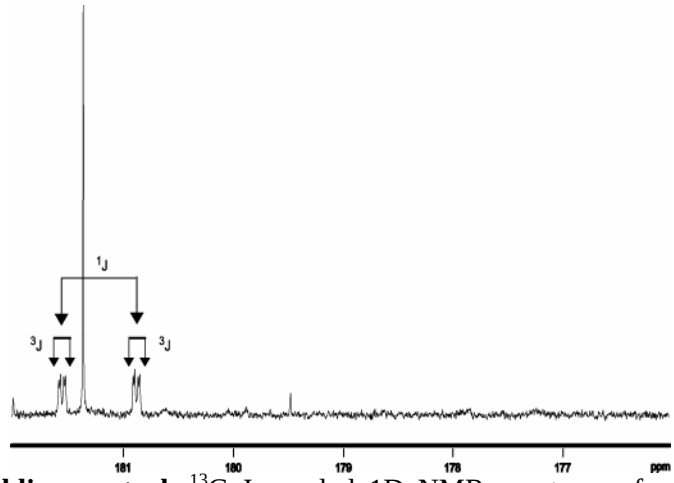

Figure 68. Scrambling control. ^{13}C J-coupled 1D NMR spectrum of cell free reaction. A complete cell free translation and transcription experiment was performed under standard conditions with uniformly labelled ^{13}C glutamate but omitting a DNA template [12]. Here, the carbonyl section of the reaction mixture is shown. Typical glutamate Cδ chemical shifts and the expected J-coupling pattern were observed [311]. By contrast, no Cδ chemical shifts and J-coupling pattern were detected for glutamine, a metabolic pathway neighbour [312]. The spectrum was collected at 300 MHz ^1H Larmor frequency with 8 k transients.

However, the labelling efficiency of glutamate depends on dilution effects. Dilution effects describe the conversion of unlabelled amino acids into the amino acid which was supplied in an isotope labelled form. This dilution effect could be assessed using MALDI-TOF spectrometry of tryptic EmrE E25A digests. In figure 69 spectra of tryptic digests of EmrE E25A before and after dialysis can be seen. Prolonged sample handling leads to the increased occurrence of a specific N-terminal degraded EmrE E25A fragment. Only the N-terminal tryptic digestion fragments are detected for EmrE E25A as the remaining fragments are extremely hydrophobic.

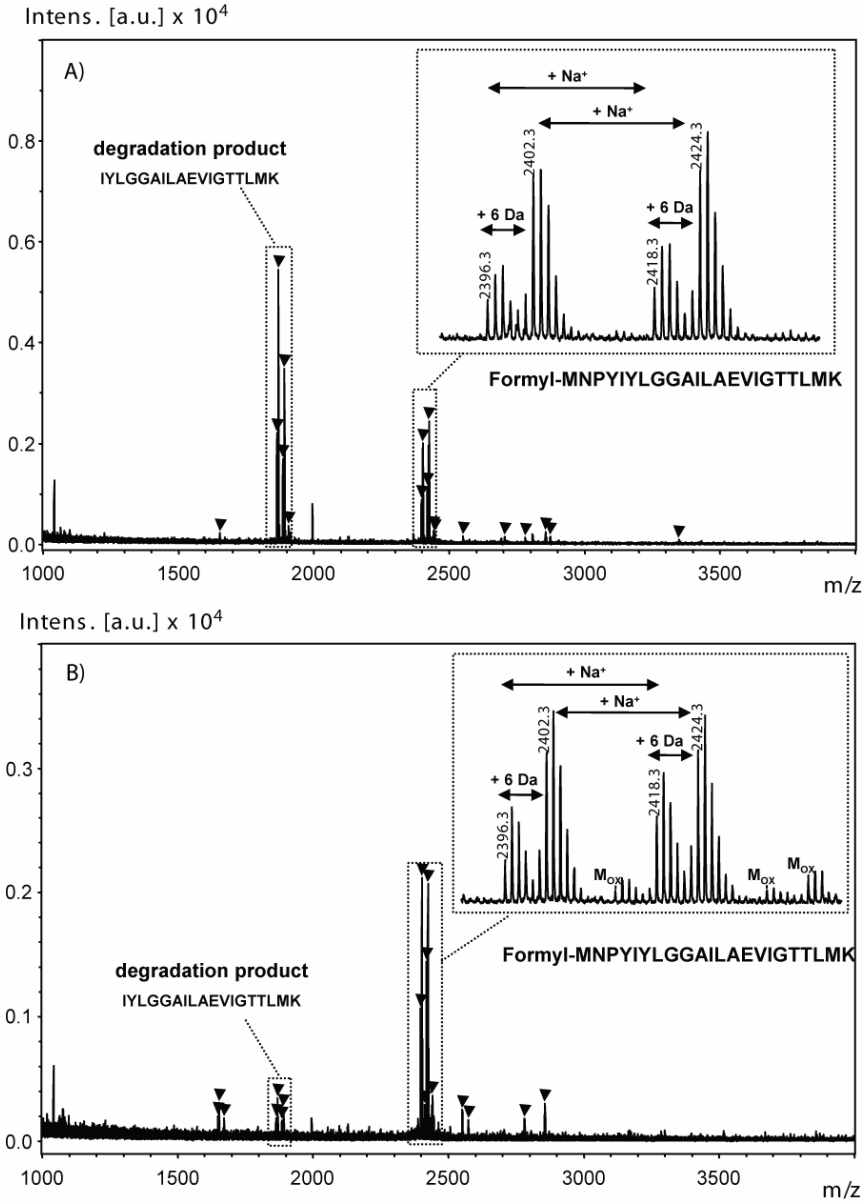

Figure 69. MALDI-TOF spectra of tryptic digests of $^{13}C/^{15}N$ labelled EmrE E25A. A) EmrE E25A dialysed (24 h at 4°C) prior to tryptic digestion; B) EmrE E25A not dialysed before tryptic digestion. Only the N-terminal tryptic digestion fragment is detected for EmrE E25A. During dialysis the abundance of a specific N-terminal degradation product increases. The insets show enlargements of the formylated peaks and enable quantitation of the labelled peaks (a difference of 6 Da is expected between $^{12}C/^{14}N$ glutamate and $^{13}C/^{15}N$ glutamate) as well as sodium attachments (addition of 23 Da) and methionine oxidations (M_{ox}) to be seen. Spectra are corrected by subtraction of buffer peaks and triangles indicate signals above the noise level. Peaks close to 1000 m/z are known matrix peaks and are ignored.

The inset shows that the EmrE E25A N-terminal fragment is mainly correctly $^{13}C/^{15}N$ labelled at E14, but fragments with a mass corresponding to $^{12}C/^{14}N$ E14 are also present. The labelling efficiency can be calculated and is 64 % ± 1 %. The expected technique inherent error is 20 %. The low labelling efficiency was unexpected. MS analysis of uniformly $^{13}C/^{15}N$ labelled amino acid glutamic acid confirmed the manufacturer's claim of 98 % labelling efficiency. The discrepancy of amino acid and protein labelling efficiency must arise from glutamic acid contamination of the cell free extract or dilution. However, if MALDI-TOF is used to assess protein labelling efficiencies such low values are typically encountered [313]. The low labelling efficiency of course is the main cause of low NMR signal intensity.

Formylation was confirmed by MS and MS/MS after tryptic digestion, see figure 69 and figure 70. The assignment of the tryptic fragments and the formylation by MS were verified by MS/MS mass spectrometry. Figure 70 shows the MS/MS spectrum obtained when the formylated N-terminal EmrE E25A fragment from tryptic digestion was selected as precursor ion. The major ions in this type of spectrum are the y and b ions. A nearly complete ion pattern of the N-terminal fragment was observed. All b ions clearly show the mass shift of 28 Da due to the formylation of the N-terminal methionine residue. If the spectrum is enlarged, see insets for the high molecular weight y ions, the peak doublets separated by 6 Da can be clearly seen. The doublets arise due to the selection of the formylated N-terminal fragment of EmrE E25A with both labelled and unlabelled glutamate as precursor ion. This confirms the presence of formylation, fragment assignment in figure 69 and calculated labelling efficiency.

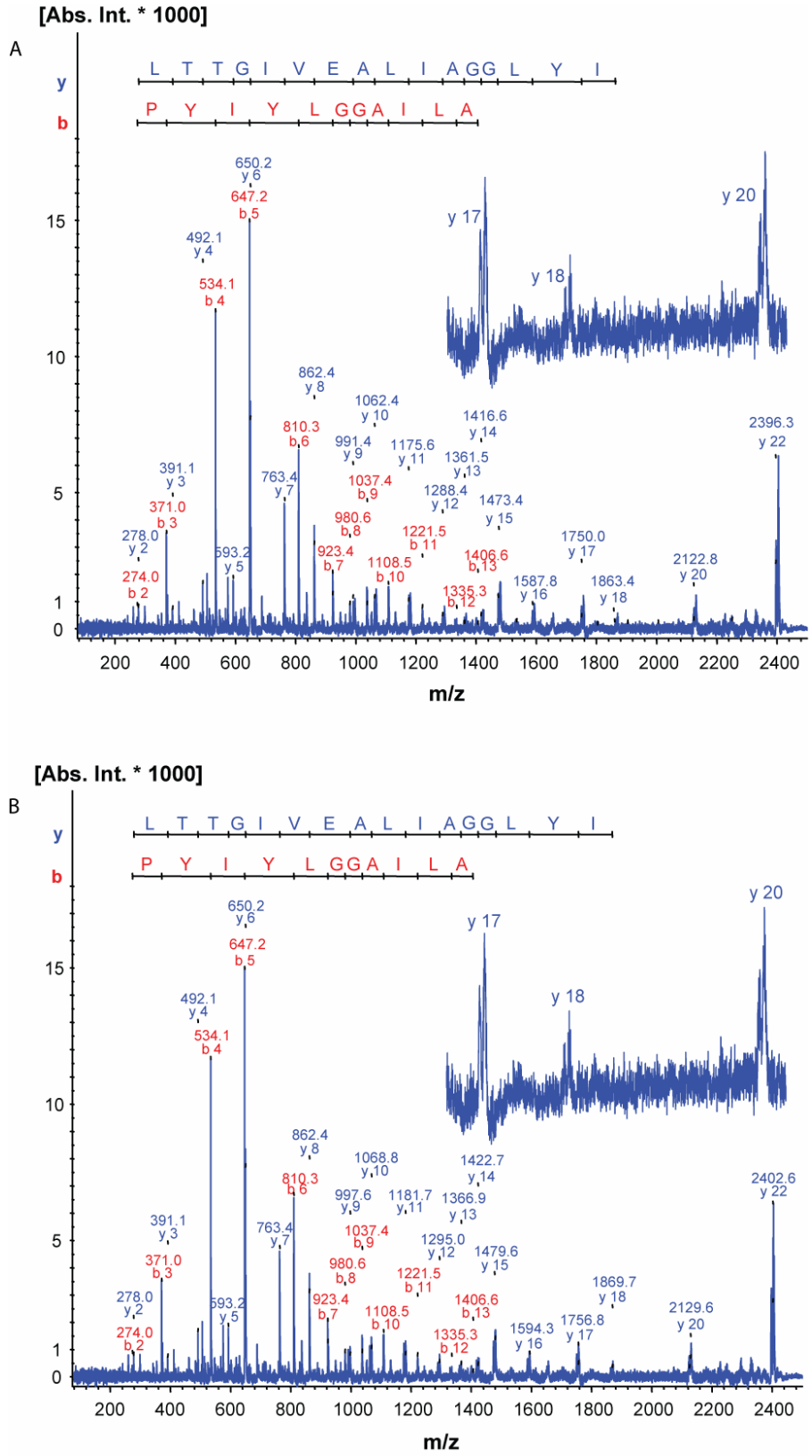

Figure 70. MS/MS of an EmrE E25A tryptic digest. Part A and B show the same spectrum but in A) the ions of the $^{12}C/^{14}N$ glutamate unlabelled N-terminal tryptic fragment are highlighted while in B) the ions of the $^{13}C/^{15}N$ glutamate labelled N-terminal tryptic fragment are highlighted. The precursor ions of $^{13}C/^{15}N$ glutamate labelled and $^{12}C/^{14}N$ glutamate unlabelled N-terminal EmrE E25A fragment are selected together and the pattern of double peaks is seen for all ions of the y and b series. The insets show an enlargement of the high mass y ions and the double peaks separated by 6 Da can be seen.

9. 2. 1. 3 Reconstitution and sample homogeneity

Purified protein solubilised in DDM was directly reconstituted into *E. coli* total lipids at a 1:100 mol ratio. *E. coli* lipids were selected to ensure a native membrane environment. Reconstitution was consistently successful, as monitored by freeze fracture microscopy. Even after many days of NMR experiments, samples were very homogeneous without any aggregates as shown in figure 71.

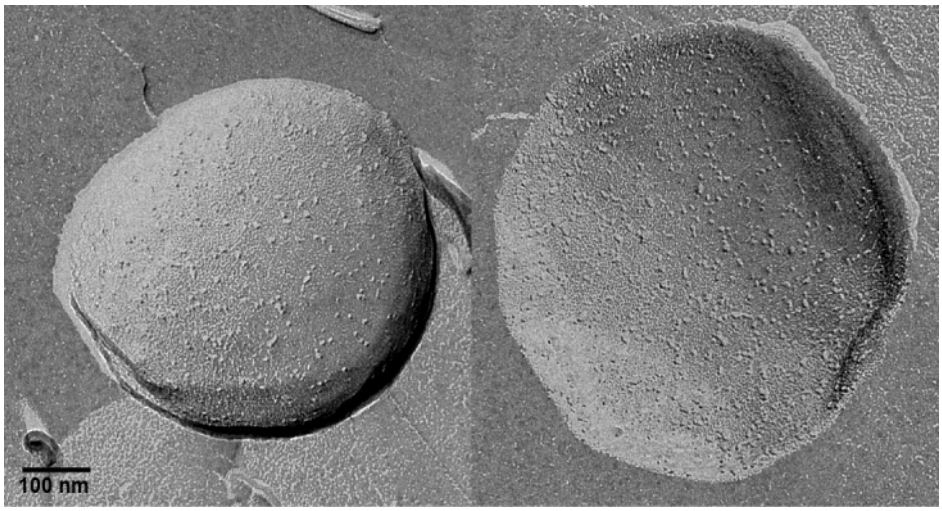

Figure 71. Representative freeze fracture electron micrograph of EmrE E25A in *E. coli* total lipids. After ten days of MAS NMR experiments, the sample (EmrE E25A incubated with etbr) was subjected to freeze fracture analysis. EmrE E25A, visible as particles in the fracture face, was incorporated evenly into similarly sized *E. coli* total lipid liposomes. The sample was very homogeneous and no protein aggregation was detected.

The interpretation of the NMR data relies on the knowledge of the observed EmrE E25A oligomeric species. For wild type EmrE the majority of studies indicate a dimeric organisation in solution and crystals [19, 35, 36, 40, 56]. Here the novel MS technique LILBID, already used to investigate Hsmr in chapter 5, was used to assess the oligomeric species of wild type EmrE under the conditions used in this study. As can be seen in figure 72 EmrE is present as dimer and monomer in solution. A decrease of EmrE concentration by one order of magnitude increases the monomeric population. This contrasts with older observations of the Schuldiner lab which suggest that heat treatment (80 °C for 10 min) is necessary to separate dimers [314]. However, it is supported by a more recent publication from the Schuldiner lab suggesting that EmrE in solution is mainly present as a dimer [56]. The observations made here suggest that the ratio of monomeric and dimeric EmrE species depend on the EmrE concentration in solution. This is in accordance with the results for Hsmr, see chapter 5, and has been previously described for other proteins [245] [246] [247]. Overall it can be concluded that the solution oligomeric state of EmrE in my hands is similar to previously reported solution oligomeric states for EmrE. This lends support to the extrapolation of membrane oligomeric state determinations in other studies to the system investigated here.

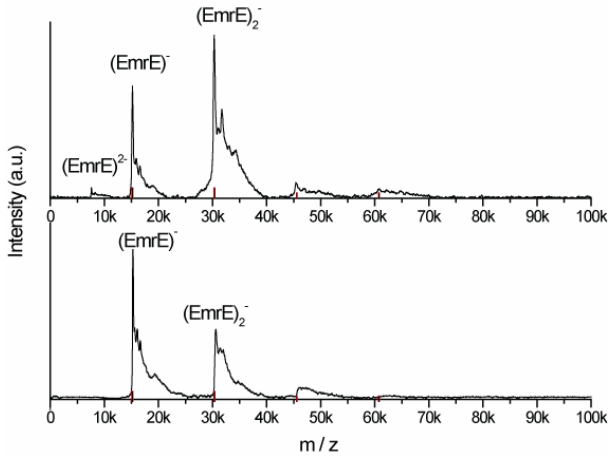

Figure 72. LILBID of EmrE in DDM at different concentrations. EmrE in < 0.1 % DDM, 10 mM Tris, pH 8.0, 2.5 mM DTT at A) $6.7x10^{-5}$ M and B) $6.7x10^{-6}$ M is measured under ultrasoft LILBID conditions. At both concentrations monomers and dimers are detected but in different ratios.

9. 2. 1. 4 Transport activity of EmrE E25A

The activity of cell free produced EmrE E25A and wild type EmrE prepared *in vivo* was verified with a previously described ethidium bromide transport assay [254]. The assay methodology is described in the Materials and Methods chapter 2 and the experiments are discussed in detail for Hsmr in chapter 6.

Briefly, in the course of the assay, bR driven H^+ pumping and etbr fluorescence is initiated by light excitation at 545 nm. EmrE then uses the generated pH gradient as energy source for an antiport of etbr. The transport can be detected by an increase of etbr total fluorescence intensity due to binding to a transport cycle intermediate [254]. The time traces in figure 73 show an increase of total fluorescence for EmrE produced *in vivo* and EmrE E25A produced cell free both as precipitate and in the presence of detergent. Traces are almost identical and transport activity ceases when adding CCCP which uncouples both ΔpH and Δψ [194], nigericin which uncouples ΔpH [39], or TPP^+ a competitive non-fluorescent substrate [27]. These data verified that active protein was produced using *in vitro* translation/transcription and that both expression modes, as precipitate or in the presence of detergent, are possible. As a consequence of these results, all NMR experiments described below were carried out on EmrE E25A expressed as precipitate due to the significantly higher yields.

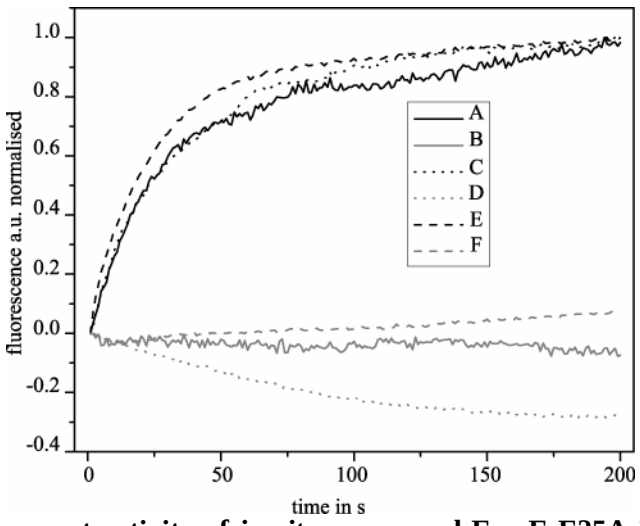

Figure 73. Etbr transport activity of *in vitro* expressed EmrE E25A in *E. coli* total lipid liposomes. EmrE E25A expressed as precipitate (A), EmrE E25A expressed soluble in the presence of detergents (C) and wild type EmrE expressed *in vivo* (E) all show transport activity in the presence of a pH gradient as judged by the increase in etbr fluorescence intensity (see text). Time traces B, D and F are negative controls generated by adding to samples A, C and E the uncoupler CCCP which collapses the proton motif force (B), the ionophore nigericin which collapses the pH gradient (D) or the competitive but non-fluorescent substrate TPP^+ (E). The experiments show that EmrE E25A produced *in vitro* as precipitate is active.

9. 2. 2 1D NMR

DQF ^{13}C MAS NMR spectra of ^{13}C glutamate labelled EmrE E25A in *E. coli* lipids are shown in figure 74a) and 74b). Filtering was necessary to remove the ^{13}C natural abundance contributions (1.1%), from lipids and unlabelled residues, which overlap with the resonances of E14. However DQF does not affect the signal of the naturally occurring 0.01 % spin pairs. Their spectral contribution has been probed with *E. coli* lipids, figure 74c), which show a clear signal in the DQF spectrum at the CH_2 position. This result is not surprising considering the large number of lipids per protein with 24-28 CH_2 groups per lipid.

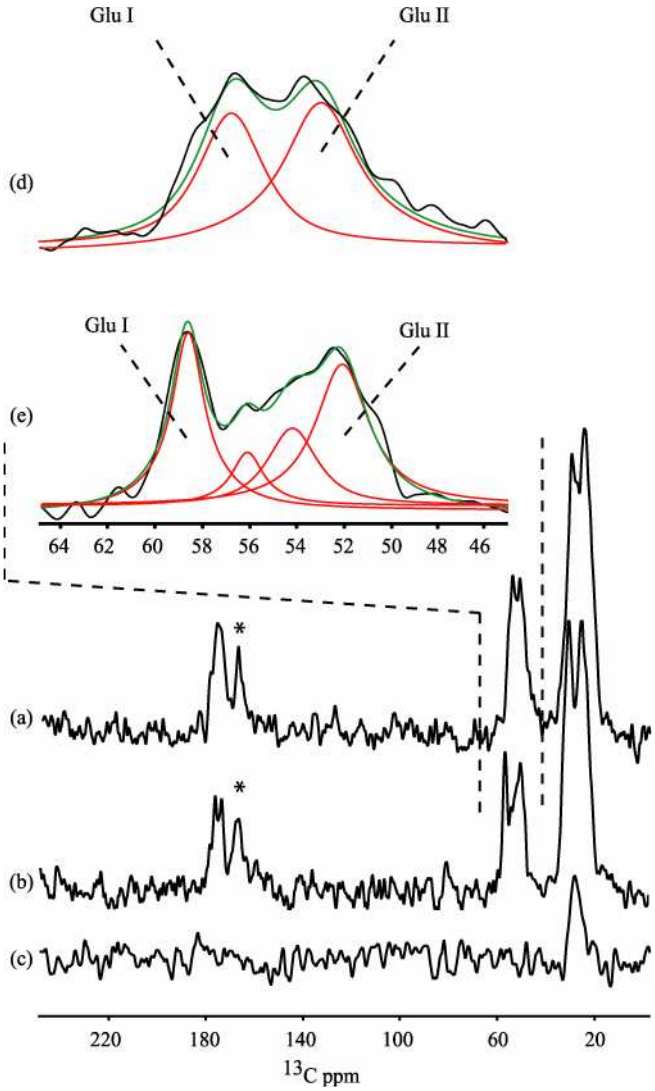

Figure 74. 1D ^{13}C MAS NMR spectra of EmrE E25A, in *E. coli* total lipids and Cα line shape fitting. (a) The single glutamate mutant EmrE E25A was selectively ^{13}C glutamate labelled and reconstituted into *E. coli* total lipid liposomes at a 1:100 protein:lipid mol ratio. ^{13}C double quantum filtering (25k acquisitions) was used and a symmetric peak doublet is observed for the Cα signal around 55 ppm. (b) After the addition of etbr the Cα peak doublet is retained but becomes asymmetric (70k acquisitions). (c) DQF efficiently removes the background signal of the 1.1% naturally occurring ^{13}C nuclei, but does not affect the signal of the naturally occurring 0.01% spin pairs. Their spectral contribution has been probed with *E. coli* lipids which show a clear signal in the DQF spectrum at the CH_2 position. (d) A line shape analysis of the Cα resonances of E14 in EmrE E25A shows two peaks. (e) Upon addition of etbr, Glu I and Glu II are shifted and additional populations are observed. Protein spectra (a, b, d, e) were acquired at 150.9 MHz and the lipid spectrum (c) at 100.62 MHz ^{13}C Larmor frequency. ^{13}C spectra at 150.90 MHz a) and b) and at 100.62 MHz c) were recorded on 600 MHz Bruker Avance and 400 MHz Bruker Avance spectrometers respectively using 4 mm MAS DVT probeheads. Sample measurements were performed at 200 K with a MAS spinning rate of 10,000 ±5 Hz. DQF spectra were collected with the $SR22^9_4$ pulse sequence [190]. Marked with an asterisk is a spectrometer artefact occurring at 168 ppm at 150.90 MHz. Exponential 150 Hz line broadening was used. For chemical shift anisotropy line shape fitting in Topspin 2.0 the Solids Lineshape Analysis tool was used with mixed Gaussian/Lorentzian line shapes.

The spectrum shown in figure 74a reveals a symmetric Cα doublet (labelled Glu I and Glu II) which becomes asymmetric upon addition of etbr (see figure 74b). A line shape analysis of the Cα resonances of E14 in EmrE E25A, figure 74d, shows that both peaks

are of similar integral intensity with a line width of 3 ppm (Glu I) and 4 ppm (Glu II). A further line shape analysis upon addition of etbr, figure 74e), shows that Glu I and Glu II are shifted, become more narrow (1.8 and 2.8 ppm) and additional populations are observed. Here, a minimum of four peaks is required for an adequate description of the whole line shape. The minor populations contribute 28 % to the total magnetization. The Cα splitting was stable during long measurements and reproducible, as verified with two independent sample preparations (see figure 75).

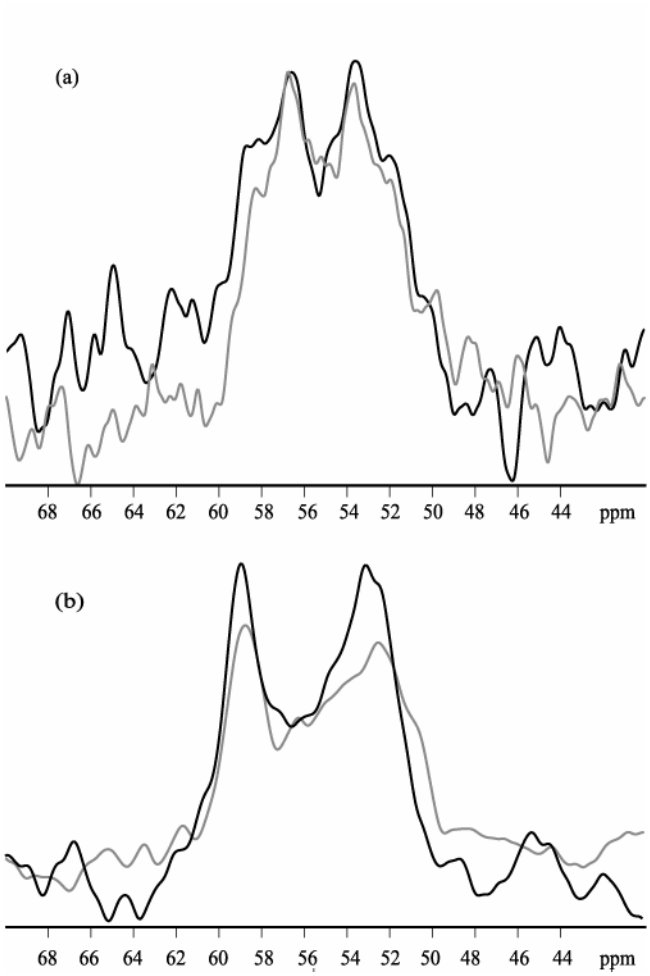

Figure 75. Reproducibility of the Cα splittings. Two independent preparations of EmrE E25A and time stability are assessed here. The reproducibility of the unusual peak multiplicity was verified using two independently produced EmrE E25A samples (46 k and 25 k scans) (a) and the time stability was assessed using EmrE E25A+etbr before and after 2D spectroscopy (70 k and 24 k scans) (b) preparations showed the same ^{13}C lineshape. Spectra were acquired at a ^{13}C frequency of 150.90 MHz on a Bruker Avance 600 spectrometer. Sample measurements were performed at 200 K with MAS spinning rate of 10,000 ±5 Hz. DQF spectra were also collected with the $SR22^{9}_{4}$ pulse sequence [190]. Exponential 150 Hz line broadening was used.

The spectral contributions of natural abundance spin pairs (0.01 %), which will not be suppressed by double quantum filtering, was assessed by acquiring a ^{13}C DQF spectrum of neat *E. coli* lipids (figure 74c). Despite the very low abundance of naturally occurring spin pairs, a CH_2 signal can clearly be seen. This observation is not surprising considering that 100 lipids with ~28 methylene groups contribute approximately 30 % of the magnetization to the EmrE E25A glutamate side chain signal.

9. 2. 3 2D DQSQ spectra

In order to unambiguously assign C', Cα, Cβ, Cγ and Cδ resonances, and to check whether all resonances are doubled, two dimensional ^{13}C DQSQ experiments were carried out. These correlation spectra contain chemical shift information for all nuclei in the direct dimension and depict bond connectivities in the indirect dimension [315]. 2D spectra without substrate (figure 76a) and with etbr (figure 76b) indicate at first inspection multiple peaks, with distinct chemical shifts, for each nucleus. INADEQUATE type assignment walks starting from both major Cα peaks shown in figure76a and figure 76b confirm peak doublets for all E14 carbons. An unambiguous assignment in this type of spectra is aided by the fact that the sum of two peak frequencies in the direct dimension is equal to their frequencies in the indirect dimension. As already indicated in figure 74, the set of resonances connected to the less shielded Cα is designated Glu I (blue lines in figure 76) and the other Glu II (red lines in figure 76). Chemical shifts for both Glu I and Glu II with and without etbr are summarised in table 26.

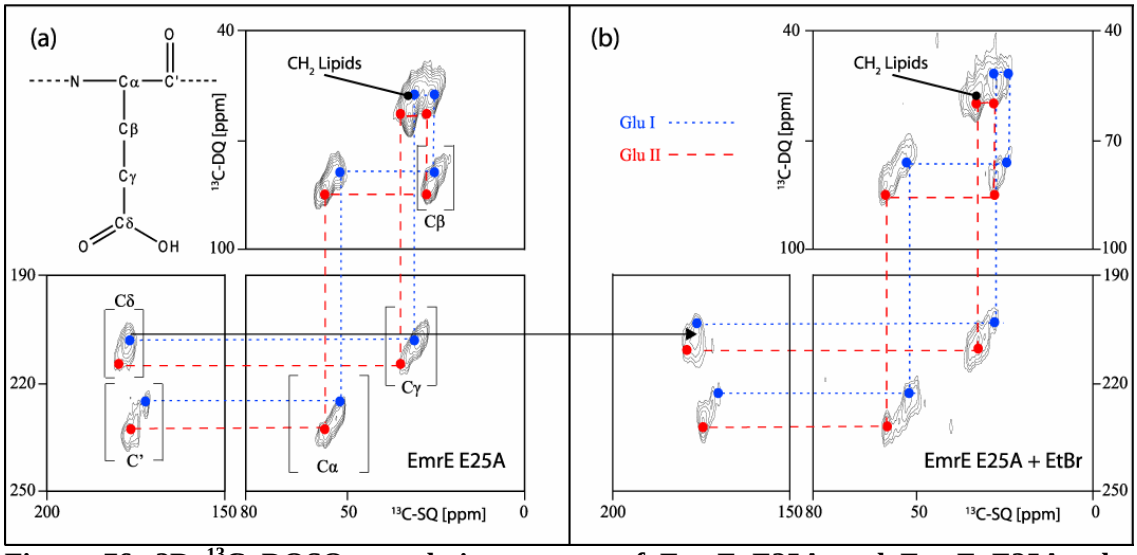

Figure 76. 2D ^{13}C DQSQ correlation spectra of EmrE E25A and EmrE E25A+etbr. Assignment of all C', Cα, Cβ, Cγ, Cδ resonances has been aided by the fact that strongly dipole coupled one-bond neighbours produce a signal in the indirect dimension at the sum of their individual chemical shifts. The spectrum shows at least two peaks for each resonance. Assignment walks for both E14 populations Glu I (blue) and Glu II (red) are indicated in both spectra. Residual ^{13}C natural abundance of lipid CH_2 groups (see figure 74c) is highlighted. A black arrow indicates the shift of Cδ Glu II upon substrate addition. Chemical shifts are given in table 26. (a) EmrE E25A has been measured with 4k scans per increment and (b) EmrE E25A+etbr was acquired with 5k scans per increment.

^{13}C spectra at 150.90 MHz were recorded on 600 MHz Bruker Avance spectrometers using 4 mm MAS DVT probeheads. The measurements were performed at 200 K with a MAS spinning rate of 10,000 ±5 Hz. The DQSQ correlation spectra were of the INADEQUATE type [316, 317] by using the $SR22^9_4$ pulse sequence previously described [318] and TPPI acquisition [319]. 400 µs DQ excitation and reconversion time was used. ^1H decoupling during the DQ excitation and reconversion was achieved using continuous wave irradiation at ~100 kHz and during t1 and t2 evolution composite decoupling with SPINAL 64 [320] at 83.3 kHz was used. Experiments were recorded with 45,000 Hz sweepwidth in the direct dimension and 90,000 Hz in the indirect dimension. Exponential 150 Hz line broadening was used in both dimensions.

The spectra were recorded with 128 or 96 increments in the indirect dimension and 2720 points in the direct dimension.

(a)	^{13}C chemical shifts of E14 of EmrE E25A (ppm)				
	C’	Cα	Cβ	Cγ	Cδ
Glu I	177.3	56.8	27.8	33.5	180.1
Glu II	172.4	53.1	25.4	30.9	177.2

(b)	^{13}C chemical shifts of E14 of EmrE E25A with etbr (ppm)				
	C’	Cα	Cβ	Cγ	Cδ
Glu I	174.6	58.7	27.3	32.6	178.9
Glu II	170.9	52.9	23.5	28.1	176.3

Table 26. ^{13}C chemical shifts of E14 in EmrE E25A with and without etbr. Chemical shift values for both observed E14 populations were derived from the 2D DQSQ spectra.

9. 2. 4 Line shape analysis

Multiple distinct molecular environments are suggested by the need for at least two distinct sets of chemical shifts to describe the ^{13}C spectra of E14. To obtain a more quantitative picture, a line shape analysis was carried out for the Cα peaks which showed the most pronounced splitting. The symmetric Cα doublet of EmrE E25A can be adequately described by two resonances of similar integral intensity with respective line widths of 3.0 (Glu I) and 4.0 ppm (Glu II) (figure 74d). The different chemical shifts of these two resonances are indicative of two inequivalent EmrE E25A populations. The line width indicates a limited amount of heterogeneity.

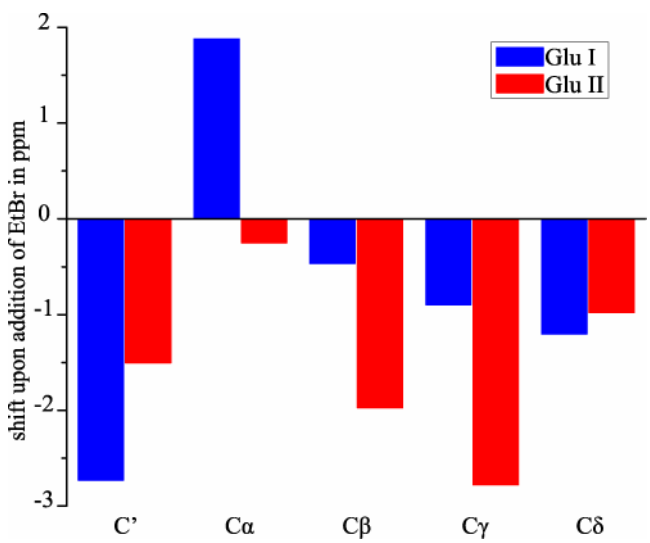

Figure 77. ^{13}C chemical shift shift analysis. Changes in EmrE E25A chemical shifts after substrate addition were investigated. The displacement of chemical shifts was calculated as follows: 13Cδ (Cδ EmrE E25A+etbr) – 13Cδ (Cδ EmrE E25A) = 13CΔδ (chemical shift displacement). Negative values indicate a decrease of chemical shift values after substrate addition, whereas positive values indicate an increase of chemical shift values after substrate addition. Both major E14 populations are displayed (Glu I in blue and Glu II in red).

In contrast, at least four peaks are required to describe the asymmetric Cα line shape which is observed in the presence of etbr (figure 74e). The two main peaks Glu I and Glu II are of equal integral intensity. The two additional peaks contribute 28 % magnetization to the spectrum. The addition of etbr therefore causes E14 to be present in more than two distinct molecular environments. The line width of both main peaks is

reduced to 1.8 (Glu I) and 2.8 ppm (Glu II) compared to EmrE E25A without substrate, suggesting a decrease in structural heterogeneity concomitant with an increase of populations.

9. 3 Discussion

9. 3. 1 General

In this study, the proposed active site structure of the functional homodimeric EmrE with and without the substrate etbr was investigated. For this investigation, the single glutamate mutant EmrE E25A was selectively isotope labelled at the remaining conserved E14. This enabled unambiguous chemical shift assignment and simplified data interpretation. The capability of *E. coli* based cell free transcription and translation systems to express wild type EmrE in a functional form with and without detergent was previously shown [36, 197]. Furthermore, it has been reported that amino acid selective isotope labelling without dilution or scrambling is possible [49].

Several control experiments verified that cell free expressed EmrE E25A is indeed functional and correctly labelled. Preparations as precipitate as well as in the presence of detergent produce functional protein. The precipitation method was preferred here as the protein yield was higher.

The protein was reconstituted into *E. coli* lipids under conditions that allow the protein to be functional in the exchange mode. This active protein conformation was trapped by freezing with liquid nitrogen. Non-invasive solid state NMR revealed significantly different chemical shifts between both E14s with and without addition of ethidium bromide. This indicates an asymmetric homodimer for EmrE with and without substrate bound.

In this study the key to understanding the chemical environment of glutamate lies in the chemical shifts.

9. 3. 2 Inequivalence of E14s in homodimeric EmrE is genuine

These data clearly show two distinct and similarly abundant populations of E14 (Glu I and Glu II). A number of controls were carried out to exclude the possibility that the observed E14 populations were caused by sample preparation problems such as impurities, incorrect ^{13}C labelling, aggregation or sample disintegration.

EmrE E25A preparations contain no protein contamination as judged by MALDI-TOF mass spectrometry and SDS PAGE (figure 67). No isotope scrambling took place as verified by analytical NMR analysis (figure 68) and as judged by the spectral pattern characteristic for glutamic acid (figure 76). Dilution of glutamate was observed (figure 69), leading to only 64 % NMR spectroscopically observable EmrE E25A molecules and concomitantly long NMR acquisition times. Aggregation could be excluded by freeze fracture microscopy which was performed after NMR measurements and detected no signs of protein aggregation (figure 71). Finally, sample deterioration, due to e.g. radiofrequency irradiation, can be excluded because the spectra of frozen samples did not change with time (figure 75a)). Results were reproducible as judged by additional, independent sample preparations (figure 75b)).

9. 3. 3 The E14s of different protomers in the homodimeric EmrE binding pocket are asymmetric

Possible reasons for the genuine inequivalence of E14 could be (a) freeze trapping of general conformational flexibility (b) freeze trapping of conformations which are in dynamic exchange (c) a protonation/deprotonation equilibrium or (d) a structurally asymmetric dimer.

(a) Freeze trapping of thermal motions causes increased line widths. At least two sets of chemical shifts are found for all glutamate nuclei with chemical shift differences between +1.9 ppm (Glu I Cα versus Glu I Cα+etbr) and -2.8 ppm (Glu II Cγ versus Glu II Cγ+etbr) (see Fig. 6). Peak doubling has been observed previously by solid state NMR and structural significance could be assigned in cases with large chemical shift changes (>1.5 ppm) whereas smaller differences were suggested to arise from motions in the ms range [132, 289]. H/D exchange infrared spectroscopy is commonly used to judge relative membrane protein mobility. The amides of EmrE reconstituted in both DMPC and *E. coli* total lipids (as in this study) showed only negligible exchange, while for example the lactose transporter LacY exchanges 95 % of all amide protons within 24 hours [305, 321]. This suggests that EmrE is remarkably immobile in the absence of substrate, similar to the K^+ channel Slik and bacteriorhodopsin [305]. Extensive work on the soluble multidrug-binding protein QacR suggests a rigid drug-binding pocket with distinct and overlapping mini-pockets for different drugs. It is anticipated that a similar mechanism for multidrug binding is employed by EmrE and other multidrug transporters [13]. This suggests restricted mobility of the empty EmrE E25A binding pocket. Similarly, theoretical considerations suggest that empty EmrE should be immobile and only the presence of etbr and H^+ should enable conformational changes [322]. Taking all of this into consideration, the broad line widths likely reflect structural heterogeneity caused by small, thermal fluctuations about an equilibrium structure. Thermal fluctuations could not account for peak multiplicities. Large line widths are commonly encountered in solid state NMR of biological materials and are considered native for unaligned and non-crystalline proteins between 1 and 4 ppm [124, 290].
(b) Theoretically EmrE E25A could be in exchange between distinct conformational states such as binding or release conformations. However, this is unlikely in the absence of substrate and energetic coupling to ΔpH or Δψ gradients to drive the protein conformational changes normally associated with substrate transport. EmrE E25A in the absence of substrate and a pH gradient can thus be expected to have its conformational space limited to the binding position and thus cannot itself lead to peak multiplicity. Furthermore, if EmrE E25A would be in dynamic exchange between binding and release conformation, H/D exchange rates similar to LacY would be expected. However, FTIR spectroscopy detects a slow H/D exchange rate for EmrE and suggests EmrE to be rigid when reconstituted in a lipid environment [323].
(c) Cδ, Cγ and Cβ shifts are sensitive to protonation state and long-range electrostatic interactions. All observed Cδ chemical shifts are found in the typical range for protonated and deprotonated glutamate Cδ [324]. A possible explanation for the observation of two distinct glutamate Cδ chemical shifts could be differences in the protonation states of E14 near its pKa. Both wild type EmrE and the single glutamate mutant E25C/D84C have a reported pKa of 7.5 [64] and accordingly in this study approximately 50 % of the glutamates are expected to be protonated at pH 8.0. However, the Cα and C' chemical shifts are only weakly affected by side chain protonation/deprotonation or long-range electrostatic interactions at the side chain nuclei Cδ, Cγ, Cβ [325] [326]. More specifically, using model peptides glutamate C' and Cα were shown to maximally shift 1 ppm while Cδ shifts up to 4 ppm upon side chain protonation/deprotonation [326]. Therefore, a protonation/deprotonation equilibrium can be excluded to explain the observed backbone peak multiplicity.
(d) Equally sized glutamate populations could be explained if EmrE would form an asymmetric dimer. In an asymmetric dimer both (φ/ψ) torsion angles and therefore the secondary structures are different leading to variations in the C' and Cα chemical shift values, as detected here. In addition, the side chain nuclei Cβ, Cγ and Cδ are less affected by the protein secondary structure but monitor hydrogen-bonding, χ angle,

protonation/deprotonation, long range electrostatic interactions and other effects on their electronic environment. Therefore, both distinct sets of E14 Cβ, Cγ and Cδ shifts indicate that the side chains within the homodimer are found in different chemical environments. They are inequivalent.
Based on this evidence it can be concluded that the peak splitting is genuine and caused by the asymmetry of functional EmrE E25A dimers in *E. coli* lipid liposomes at pH 8.0. This conclusion is also supported by the similar intensities of both Glu I and Glu II.

9. 3. 4 Interpretation of E14 line shape and chemical shifts

The symmetric line shape of EmrE E25A Cα could be fitted best by two peaks of similar integral intensity (figure 74). The line widths are most likely caused by residual structural heterogeneity trapped by sample freezing, as discussed above. The chemical shifts belonging to these two E14 populations show significant differences (table 26). The chemical shifts of both backbone carbons differ by 4.9 ppm for C' and 3.7 ppm for Cα. The chemical shifts of these backbone atoms are mainly influenced by the backbone secondary structure and neighbouring residues. In the EmrE homodimer, both E14s have the same preceding and proceeding amino acid, so the differences must be caused by slightly different backbone conformations.
Three liquid state NMR studies on SMR proteins (EmrE and Smr) have been reported before [61, 263, 327]. All studies used non-native membrane mimicking conditions such as chloroform/methanol for monomeric EmrE [61], LPPG micelles for dimeric Smr [263] or biPC bicelles for dimeric Smr [169]. Interestingly, no asymmetry was observed and the reported ^{13}C chemical shifts of E14 deviate from our measurements up to 8.4 ppm (figure x). This underlines the importance of a native lipid environment and supports arguments that the dimer only assumes an asymmetric conformation in its active state within the membrane [40, 289, 290, 328].

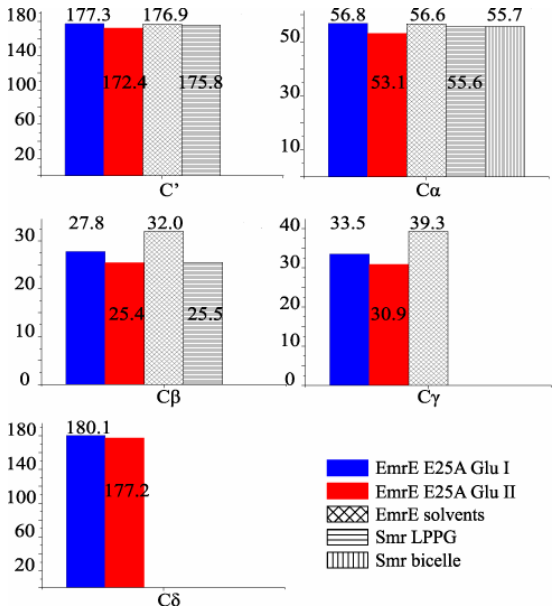

Figure 78. ^{13}C chemical shifts of EmrE E25A in liposomes compared to Smr and EmrE chemical shifts in solution. Chemical shifts of reconstituted EmrE E25A (this study) were compared to Smr and EmrE chemical shifts obtained by liquid-state NMR on solubilised samples. Solution state NMR ^{13}C chemical shifts of dimeric Smr in LPPG micelles (BMRB code: 6796), dimeric Smr in biPC bicelles [169] and monomeric EmrE in a solvent system (BMRB code: 4136) were adjusted to comply with our referencing compound tetramethylsilane. All available chemical shifts were used.

9. 3. 5 Interpretation of E14 line shape and chemical shifts upon substrate addition

Upon substrate addition, the Cα line shape becomes asymmetric and was reproduced best by fitting under the assumption of four peaks. The line widths of both main peaks Glu I and Glu II was considerably reduced, which is most likely caused by reduced thermal motions in the presence of the substrate etbr. After addition of the substrate etbr, the transporter should be in equilibrium exchange conformations. These conformations include an open state of EmrE E25A, an exchange intermediate and one release position. Therefore, additional peaks would be expected as seen in figure 74. Not all of these resonances are populated equally, possibly due to the different residence times for each state and an unsaturated binding pocket. However, the etbr concentration was chosen to theoretically provide greater than 99 % occupancy at the binding site.
It is not possible to unequivocally assign both E14 populations Glu I and Glu II found in EmrE E25A to both main populations found in the presence of substrate. Assuming that the more shielded Glu I population is the same in both situations, changes in chemical shifts can be discussed. Only with this assignment, realistic chemical shift changes are obtained.
The differences between E14 chemical shifts without and with etbr are summarized in figure 77. Changes of up to -2.8 ppm are observed. Upon substrate binding both glutamate Cδ chemical shifts change towards values indicative of protonation or long-range electrostatic interactions. The Cβ and Cγ chemical shifts concertedly shift upfield supporting the notion that the chemical environment of both E14s within the asymmetric homodimer changes. This suggests that both glutamates coordinate etbr giving rise to two different etbr/glutamate interactions and therefore different chemical shifts.

9. 3. 6 An asymmetric binding pocket of EmrE in the context of known EmrE data

Asymmetry has been reported for SMR proteins before. A subgroup of EmrE-like SMR proteins (YdgE/F[193, 329], yvdR/S, ykkC/D [193], EbrA/EbrB [54, 55, 330]) has been found to act as heterooligomers with a defined topology for each molecule. Such heterooligomers are obviously asymmetric at the glutamate residue and for EbrA/B it could be shown that the two glutamates are functionally inequivalent [55]. Additionally, EmrE can be manipulated to force it into a unique and defined topology. A dimer produced this way to yield one C_{in} and one C_{out} protomer showed functional inequivalence of the E14s [33].
Independently, EPR spectroscopy on EmrE in solution revealed a heterogeneous conformational state at E14, an asymmetric dimer was seen in the EM structure [44, 331] and an antiparallel dimer was observed by x-ray crystallography [19]. Figure 79 shows this x-ray crystallography model of EmrE with TPP^+.
It can be postulated that the monomers take up a unique fold as seen by liquid state NMR and CD spectroscopy but upon dimerisation each protomer assumes a different conformation. Such induced asymmetry has been previously described for HIV1 reverse transcriptase, hot dog thioesterase PaaI and for the trimeric multidrug transporter AcrB [18, 332, 333]. Further, a true dual topology, MCR-2 accessory protein, has been recently described in eukarotes [334]. The here observed asymmetry at the EmrE E25A binding pocket however is consistent with both the parallel and the antiparallel arrangement of protomers in a dimer. H^+ release studies [65], carbodiimide reactivity [335] and fluorescence spectroscopy [252] enable only the global accessibility of the two E14 residues in a dimer to be investigated. These techniques, unlike the solid state NMR experiments used here, do not afford site-specific resolution or directly monitor structural parameter.

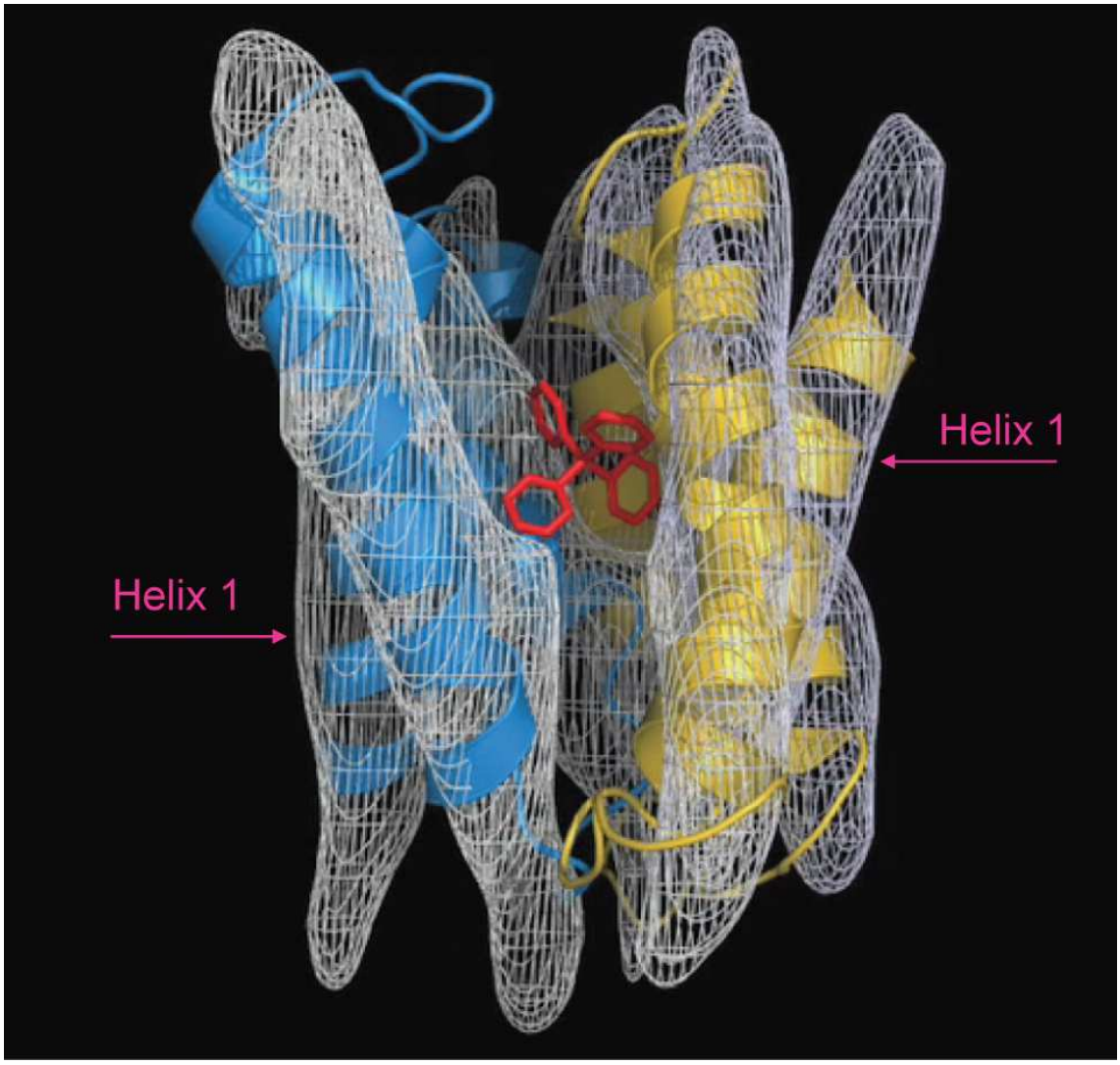

Figure 79. EmrE backbone structure by x-ray crystallography from 3D crystals modelled into the EM electron density of the EmrE 2D crystals. This EmrE model is asymmetric and displays dual topology of EmrE. The modelling work was provided as supplementary data by Chen *et al.* [19].

9. 4 Conclusion

These data show directly that both E14 in the EmrE dimer are in a structurally inequivalent environment and coordinate substrate binding. This structural asymmetry could be consistent with both an antiparallel and parallel dimer topology.

Here cell free expression was used for the first time to supply a membrane transport protein for the investigation by solid state NMR. The cell free expression methodology proved its applicability for solid state NMR.

Chapter 10 - References

1. White, S. *Membrane Proteins of known 3D structure*. [cited 30.07.2007]; Available from: http://blanco.biomol.uci.edu/Membrane_Proteins_xtal.html.
2. BiologyOnline. *Membrane Transport Protein*. [cited 19.12.2007]; Available from: http://www.biology-online.org/dictionary/Membrane_Transport_Protein.
3. Sobczak, I. and J.S. Lolkema, *Structural and mechanistic diversity of secondary transporters.* Curr Opin Microbiol, 2005. **8**(2): p. 161-7.
4. WorldHealthOrganization. *Antimicrobial resistance*. 2002 [cited 10.12.2007]; Available from: http://www.who.int/mediacentre/factsheets/fs194/en/.
5. Putman, M., H.W. van Veen, and W.N. Konings, *Molecular properties of bacterial multidrug transporters.* Microbiology and Molecular Biology Reviews, 2000. **64**(4): p. 672-693.
6. Poole, K., *Mechanisms of bacterial biocide and antibiotic resistance.* Journal of Applied Microbiology Symposium Supplement, 2002. **92**: p. 55S-64S.
7. Van Bambeke, F., E. Balzi, and P.M. Tulkens, *Antibiotic efflux pumps - Commentary.* Biochemical Pharmacology, 2000. **60**(4): p. 457-470.
8. Saier, M.H., Jr. and I.T. Paulsen, *Phylogeny of multidrug transporters.* Seminars in Cellular and Devlopmental Biology, 2001. **12**(3): p. 205-13.
9. Zheleznova, E.E., et al., *Structural basis of multidrug recognition by BmrR, a transcription activator of a multidrug transporter*. Cell, 1999. **96**(3): p. 353-62.
10. Zheleznova, E.E., et al., *Preliminary structural studies on the multi-ligand-binding domain of the transcription activator, BmrR, from Bacillus subtilis.* Protein Science, 1997. **6**(11): p. 2465-2468.
11. Zheleznova, E.E., et al., *A structure-based mechanism for drug binding by multidrug transporters.* Trends Biochem Sci, 2000. **25**(2): p. 39-43.
12. Schumacher, M.A., et al., *Structural basis for cooperative DNA binding by two dimers of the multidrug-binding protein QacR.* Embo Journal, 2002. **21**(9): p. 2301-2301.
13. Schumacher, M.A., M.C. Miller, and R.G. Brennan, *Structural mechanism of the simultaneous binding of two drugs to a multidrug-binding protein.* Embo Journal, 2004. **23**(15): p. 2923-2930.
14. Vazquez-Laslop, N., et al., *Recognition of multiple drugs by a single protein: a trivial solution of an old paradox.* Biochemical Society Transactions, 2000. **28**: p. 517-520.
15. Dawson, R.J.P. and K.P. Locher, *Structure of a bacterial multidrug ABC transporter.* Nature, 2006. **443**(7108): p. 180-185.
16. Ward, A., et al., *Flexibility in the ABC transporter MsbA: Alternating access with a twist.* Proceedings of the National Academy of Sciences of the United States of America, 2007. **104**(48): p. 19005-19010.
17. Murakami, S., et al., *Crystal structures of a multidrug transporter reveal a functionally rotating mechanism.* Nature, 2006. **443**(7108): p. 173-179.
18. Seeger, M.A., et al., *Structural asymmetry of AcrB trimer suggests a peristaltic pump mechanism.* Science, 2006. **313**(5791): p. 1295-1298.
19. Chen, Y.-J., et al., *X-ray structure of EmrE supports dual topology model.* Proceedings of the National Academy of Sciences of the United States of America, 2007. **104**(48): p. 18999-19004.
20. Raviv, Y., et al., *Photosensitized Labeling of a Functional Multidrug Transporter in Living Drug-Resistant Tumor-Cells.* Journal of Biological Chemistry, 1990. **265**(7): p. 3975-3980.

21. Higgins, C.F. and M.M. Gottesman, *Is the Multidrug Transporter a Flippase.* Trends in Biochemical Sciences, 1992. **17**(1): p. 18-21.
22. Saier, M.H.J. *Transport Classification Database*. [cited 30.07.07]; Available from: http://www.tcdb.org.
23. Alam, M.M., et al., *Analysis on distribution and genomic diversity of high-level antiseptic resistance genes qacA and qacB in human clinical isolates of Staphylococcus aureus.* Microbial Drug Resistance-Mechanisms Epidemiology and Disease, 2003. **9**(2): p. 109-121.
24. Noguchi, N., et al., *Antiseptic susceptibility and distribution of antiseptic-resistance genes in methicillin-resistant Staphylococcus aureus.* FEMS Microbiol Lett, 1999. **172**(2): p. 247-53.
25. Bay, D.C., K.L. Rommens, and R.J. Turner, *Small multidrug resistance proteins: A multidrug transporter family that continues to grow.* Biochimica et Biophysica Acta (BBA) - Biomembranes, 2007. **In Press, e-pub ahead of print**.
26. Schuldiner, S., et al., *Precious things come in little packages.* Journal of Molecular Microbiology and Biotechnology, 2001. **3**(2): p. 155-162.
27. Muth, T.R. and S. Schuldiner, *A membrane-embedded glutamate is required for ligand binding to the multidrug transporter EmrE.* Embo Journal, 2000. **19**(2): p. 234-240.
28. Ninio, S. and S. Schuldiner, *Characterization of an archaeal multidrug transporter with a unique amino acid composition.* Journal of Biological Chemistry, 2003. **278**(14): p. 12000-12005.
29. Chenna, R., et al., *Multiple sequence alignment with the Clustal series of programs.* Nucleic Acids Research, 2003. **31**(13): p. 3497-3500
30. Ninio, S., Y. Elbaz, and S. Schuldiner, *The membrane topology of EmrE - a small multidrug transporter from Escherichia coli.* Febs Letters, 2004. **562**(1-3): p. 193-196.
31. Paulsen, I.T., et al., *Molecular Characterization of the Staphylococcal Multidrug-Resistance Export Protein Qacc.* Journal of Bacteriology, 1995. **177**(10): p. 2827-2833.
32. Rapp, M., et al., *Identification and evolution of dual-topology membrane proteins.* Nature Structural & Molecular Biology, 2006. **13**(2): p. 112-116.
33. Rapp, M., et al., *Emulating membrane protein evolution by rational design.* Science, 2007. **315**(5816): p. 1282-1284.
34. Soskine, M., et al., *On parallel and antiparallel topology of a homodimeric multidrug transporter.* Journal of Biological Chemistry, 2006. **281**(47): p. 36205-36212.
35. Butler, P.J., et al., *The Escherichia coli multidrug transporter EmrE is a dimer in the detergent-solubilised state.* Journal of Molecular Biology, 2004. **340**(4): p. 797-808.
36. Elbaz, Y., et al., *In vitro synthesis of fully functional EmrE, a multidrug transporter, and study of its oligomeric state.* Proceedings of the National Academy of Sciences of the United States of America, 2004. **101**(6): p. 1519-24.
37. Sikora, C.W. and R.J. Turner, *Investigation of ligand binding to the multidrug resistance protein EmrE by isothermal titration calorimetry.* Biophysical Journal, 2005. **88**(1): p. 475-82.
38. Yerushalmi, H., M. Lebendiker, and S. Schuldiner, *Negative dominance studies demonstrate the oligomeric structure of EmrE, a multidrug antiporter from Escherichia coli.* Journal of Biological Chemistry, 1996. **271**(49): p. 31044-31048.

39. Rotem, D. and S. Schuldiner, *EmrE, a multidrug transporter from Escherichia coli, transports monovalent and divalent substrates with the same stoichiometry.* Journal of Biological Chemistry, 2004. **279**(47): p. 48787-93.
40. Ubarretxena-Belandia, I., et al., *Three-dimensional structure of the bacterial multidrug transporter EmrE shows it is an asymmetric homodimer.* Embo Journal, 2003. **22**(23): p. 6175-81.
41. Yerushalmi, H., M. Lebendiker, and S. Schuldiner, *Emre, an Escherichia-Coli 12-kDa Multidrug Transporter, Exchanges Toxic Cations and H+ and Is Soluble in Organic-Solvents.* Journal of Biological Chemistry, 1995. **270**(12): p. 6856-6863.
42. Ma, C. and G. Chang, *Structure of the multidrug resistance efflux transporter EmrE from Escherichia coli.* Proceedings of the National Academy of Sciences of the United States of America, 2004. **101**(9): p. 2852-2857.
43. Pornillos, O., et al., *X-ray structure of the EmrE multidrug transporter in complex with a substratei.* Science, 2005. **310**(5756): p. 1950-1953.
44. Koteiche, H.A., M.D. Reeves, and H.S. Mchaourab, *Structure of the substrate binding pocket of the multidrug transporter EmrE: Site-directed spin labeling of transmembrane segment 1.* Biochemistry, 2003. **42**(20): p. 6099-6105.
45. Tate, C.G., et al., *The projection structure of EmrE, a proton-linked multidrug transporter from Escherichia coli, at 7 A resolution.* Embo Journal, 2001. **20**(1-2): p. 77-81.
46. Tate, C.G., I. Ubarretxena-Belandia, and J.M. Baldwin, *Conformational changes in the multidrug transporter EmrE associated with substrate binding.* Journal of Molecular Biology, 2003. **332**(1): p. 229-42.
47. Soskine, M., S. Steiner-Mordoch, and S. Schuldiner, *Crosslinking of membrane-embedded cysteines reveals contact points in the EmrE oligomer.* Proceedings of the National Academy of Sciences of the United States of America, 2002. **99**(19): p. 12043-12048.
48. Jack, D.L., et al., *A broad-specificity multidrug efflux pump requiring a pair of homologous SMR-type proteins.* Journal of Bacteriology, 2000. **182**(8): p. 2311-2313.
49. Klammt, C., et al., *High level cell-free expression and specific labeling of integral membrane proteins.* European Journal of Biochemistry, 2004. **271**(3): p. 568-580.
50. Saier, M.H., Jr., *Protein secretion and membrane insertion systems in gram-negative bacteria.* Journal of Membrane Biology, 2006. **214**(2): p. 75-90.
51. White, S.H. and G. Von Heijne, *The machinery of membrane protein assembly.* Current Opinion in Structural Biology, 2004. **14**: p. 397-404.
52. Poolman, B., E.R. Geertsma, and D.J. Slotboom, *A missing link in membrane protein evolution.* Science, 2007. **315**(5816): p. 1229-1231.
53. Kikukawa, T., et al., *Anti-parallel membrane topology of two components of EbrAB, a multidrug transporter.* Biochemical and Biophysical Research Communications, 2007. **358**(4): p. 1071-1075.
54. Kikukawa, T., et al., *Two-component bacterial multidrug transporter, EbrAB: Mutations making each component solely functional.* Biochimica et Biophysica Acta - Biomembranes, 2006. **1758**(5): p. 673-679.
55. Zhang, Z.G., et al., *Functional characterization of the heterooligomeric EbrAB multidrug efflux transporter of Bacillus subtilis.* Biochemistry, 2007. **46**(17): p. 5218-5225.
56. Steiner-Mordoch, S., et al., *Parallel topology of genetically fused EmrE homodimers.* Embo Journal, 2008. **27**(1): p. 17-26.

57. Amadi, S., H.A. Koteiche, and H.S. Mchaourab. *Structure of the Escherichia coli multidrug transporter EmrE in liposomes*. in *Biophysical Society, 51st Annual Meeting*. 2007. Baltimore, Maryland: Biophysical Journal.
58. Fleishman, S.J., et al., *Quasi-symmetry in the cryo-EM structure of EmrE provides the key to modeling its transmembrane domain.* Journal of Molecular Biology, 2006. **364**(1): p. 54-67.
59. Daley, D.O., et al., *Global topology analysis of the Escherichia coli inner membrane proteome.* Science, 2005. **308**(5726): p. 1321-1323.
60. Nara, T., et al., *Anti-parallel Membrane Topology of a Homo-dimeric Multidrug Transporter, EmrE.* The Journal of Biochemistry (Tokyo), 2007. **142**(5): p. 621-625.
61. Schwaiger, M., et al., *NMR investigation of the multidrug transporter EmrE, an integral membrane protein.* European Biophysical Journal, 1998. **254**: p. 610-619.
62. Venkatraman, J., G.A.N. Gowda, and P. Balaram, *Structural analysis of synthetic peptide fragments from EmrE, a multidrug resistance protein, in a membrane-mimetic environment.* Biochemistry, 2002. **41**(21): p. 6631-6639.
63. Lehner, I., et al., *The key residue for substrate transport (E14) in the EMRE dimer is asymmetric.* J Biol Chem, 2007.
64. Yerushalmi, H. and S. Schuldiner, *An Essential Glutamyl Reidue in EmrE, a Multidrug Antiporter from Escherichia coli.* Journal of Biologicial Chemistry, 2000. **275**(8): p. 5264-5269.
65. Soskine, M., Y. Adam, and S. Schuldiner, *Direct evidence for substrate-induced proton release in detergent-solubilized EmrE, a multidrug transporter.* Journal of Biological Chemistry, 2004. **279**(11): p. 9951-5.
66. Yerushalmi, H., S.S. Mordoch, and S. Schuldiner, *A single carboxyl mutant of the multidrug transporter EmrE is fully functional.* Journal of Biological Chemistry, 2001. **276**(16): p. 12744-12748.
67. Yerushalmi, H. and S. Schuldiner, *A model for coupling of H+ and substrate fluxes based on "time-sharing" of a common binding site.* Biochemistry, 2000. **39**(48): p. 14711-14719.
68. Spyropoulos, I.C., et al., *TMRPres2D: high quality visual representation of transmembrane protein models.* Bioinformatics, 2004. **20**: p. 3258-3266.
69. Gasteiger, E., et al., *ExPASy: the proteomics server for in-depth protein knowledge and analysis.* Nucleic Acids Research, 2003. **31**(13): p. 3784-3788.
70. Rath, A., R.A. Melnyk, and C.M. Deber, *Evidence for assembly of small multidrug resistance proteins by a "two-faced" transmembrane helix.* Journal of Biological Chemistry, 2006. **281**(22): p. 15546-15553.
71. Danson, M.J. and D.W. Hough, *Structure, function and stability of enzymes from the Archaea.* Trends in Microbiology, 1998. **6**(8): p. 307-314.
72. Ng, W.V., et al., *Genome sequence of Halobacterium species NRC-1.* Proceedings of the National Academy of Sciences of the United States of America, 2000. **97**(22): p. 12176-12181.
73. Bruins, M.E., A.E.M. Janssen, and R.M. Boom, *Thermozymes and their applications - A review of recent literature and patents.* Applied Biochemistry and Biotechnology, 2001. **90**(2): p. 155-186.
74. Grant, W.D., *Life at low water activity.* Philosophical Transactions of the Royal Society of London Series B-Biological Sciences, 2004. **359**(1448): p. 1249-1266.
75. Lanyi, J.K., *Light Energy Conversion in Halobacterium halobium.* Microbiological Reviews, 1978. **42**(4): p. 682-706.

76. Lanyi, J.K., *Salt-Dependent Properties of Proteins from Extremely Halophilic Bacteria.* Bacteriological Reviews, 1974. **38**(3): p. 272-290.
77. Madern, D., C. Pfister, and G. Zaccai, *Mutation at a Single Acidic Amino-Acid Enhances the Halophilic Behavior of Malate-Dehydrogenase from Haloarcula-Marismortui in Physiological Salts.* European Journal of Biochemistry, 1995. **230**(3): p. 1088-1095.
78. Madern, D., C. Ebel, and G. Zaccai, *Halophilic adaptation of enzymes.* Extremophiles, 2000. **4**(2): p. 91-98.
79. Yang, L.F., et al., *A Na+/H+ antiporter gene of the moderately halophilic bacterium Halobacillus dabanensis D-8(T): cloning and molecular characterization.* Fems Microbiology Letters, 2006. **255**(1): p. 89-95.
80. Binbuga, B., A.F.B. Boroujerdi, and J.K. Young, *Structure in an extreme environment: NMR in high salt.* Protein Science, 2007.
81. Marg, B.L., et al., *A two-alpha-helix extra domain mediates the halophilic character of a plant-type ferredoxin from halophilic archaea.* Biochemistry, 2005. **44**(1): p. 29-39.
82. Oesterhelt, D., W. Stoeckenius, and P. Sidney Fleischer and Lester, *[69] Isolation of the cell membrane of Halobacterium halobium and its fractionation into red and purple membrane*, in *Methods in Enzymology*. 1974, Academic Press. p. 667-678.
83. Gmelin, W., et al., *The crystal structure of the L1 intermediate of halorhodopsin at 1.9 angstroms resolution.* Photochemistry and Photobiology, 2007. **83**(2): p. 369-77.
84. Kunji, E.R., et al., *Electron crystallographic analysis of two-dimensional crystals of sensory rhodopsin II: a 6.9 A projection structure.* Journal of Molecular Biology, 2001. **308**(2): p. 279-93.
85. Greene, R.V. and R.E. Macdonald, *Partial-Purification and Reconstitution of the Aspartate Transport-System from Halobacterium-Halobium.* Archives of Biochemistry and Biophysics, 1984. **229**(2): p. 576-584.
86. Smith, R.L., et al., *Functional similarity between archaeal and bacterial CorA magnesium transporters.* Journal of Bacteriology, 1998. **180**(10): p. 2788-2791.
87. Albers, S.V., et al., *Bioenergetics and solute uptake under extreme conditions.* Extremophiles, 2001. **5**(5): p. 285-294.
88. Kates, M., *Membrane-Lipids of Extreme Halophiles - Biosynthesis, Function and Evolutionary Significance.* Experientia, 1993. **49**(12): p. 1027-1036.
89. Yamauchi, K., et al., *Archaebacterial lipid models: highly salt-tolerant membranes from 1,2-diphytanylglycero-3-phosphocholine.* Biochimica et Biophysica Acta (BBA) - Biomembranes, 1992. **1110**(2): p. 171-177.
90. Nirenberg, M. and J.H. Matthaei, *Dependence of Cell-Free Protein Synthesis in E Coli Upon Naturally Occurring or Synthetic Polyribonucleotides.* Proceedings of the National Academy of Sciences of the United States of America, 1961. **47**(10): p. 1588-&.
91. Nakano, H. and T. Yamane, *Cell-free protein synthesis systems.* Biotechnology Advances, 1998. **16**(2): p. 367-384.
92. Ferreras, A.C., et al., *Efficient and faithful in vitro translation of natural and synthetic mRNA with human ribosomes.* International Journal of Molecular Medicine, 2004. **13**(4): p. 527-536.
93. Kung, H.F., et al., *DNA-directed in vitro synthesis of beta-galactosidase. Studies with purified factors.* Journal of Biological Chemistry, 1977. **252**(19): p. 6889-6894.

94. Shimizu, Y., et al., *Cell-free translation reconstituted with purified components.* Nature Biotechnology, 2001. **19**(8): p. 751-755.
95. Kim, D.M. and C.Y. Choi, *A semicontinuous prokaryotic coupled transcription/translation system using a dialysis membrane.* Biotechnology Progress, 1996. **12**(5): p. 645-649.
96. Spirin, A.S., et al., *A continuous cell-free translation system capable of producing polypeptides in high yield.* Science, 1988. **242**(4882): p. 1162-4.
97. Kigawa, T., et al., *Cell-free production and stable-isotope labeling of milligram quantities of proteins.* Febs Letters, 1999. **442**(1): p. 15-9.
98. Ishihara, G., et al., *Expression of G protein coupled receptors in a cell-free translational system using detergents and thioredoxin-fusion vectors.* Protein Expression and Purification, 2005. **41**(1): p. 27-37.
99. Berrier, C., et al., *Cell-free synthesis of a functional ion channel in the absence of a membrane and in the presence of detergent.* Biochemistry, 2004. **43**(39): p. 12585-91.
100. Sonar, S., et al., *Cell-Free Synthesis, Functional Refolding, and Spectroscopic Characterization of Bacteriorhodopsin, an Integral Membrane-Protein.* Biochemistry, 1993. **32**(50): p. 13777-13781.
101. Vinarov, D.A., C.L.L. Newman, and J.L. Markley, *Wheat germ cell-free platform for eukaryotic protein production.* Febs Journal, 2006. **273**(18): p. 4160-4169.
102. Klammt, C., et al., *Cell-free Expression of Integral Membrane Proteins for Structural Studies*, in *Cell-free Protein Synthesis - Methods and Protocols*, A.S. Spirin and J.R. Swartz, Editors. 2007, Wiley-VCH.
103. Ozawa, K., et al., *15N-Labelled proteins by cell-free protein synthesis. Strategies for high-throughput NMR studies of proteins and protein-ligand complexes.* FEBS Journal, 2006. **273**(18): p. 4154-4159.
104. Klammt, C., et al., *Cell-free expression as an emerging technique for the large scale production of integral membrane protein.* FEBS Journal, 2006. **273**(18): p. 4141-4153.
105. Jermutus, L., L.A. Ryabova, and A. Pluckthun, *Recent advances in producing and selecting functional proteins by using cell-free translation.* Current Opinion in Biotechnology, 1998. **9**(5): p. 534-48.
106. Klammt, C., et al., *Functional analysis of cell-free-produced human endothelin B receptor reveals transmembrane segment 1 as an essential area for ET-1 binding and homodimer formation.* Febs Journal, 2007. **274**(13): p. 3257-3269.
107. Klammt, C., et al., *Cell-free production of G protein-coupled receptors for functional and structural studies.* Journal of Structural Biology, 2007. **158**(3): p. 482-493.
108. Clore, G.M. and A.M. Gronenborn, *Structures of Larger Proteins in Solution - 3-Dimensional and 4-Dimensional Heteronuclear Nmr-Spectroscopy.* Science, 1991. **252**(5011): p. 1390-1399.
109. Rattle, H., *An NMR Primer for Life Scientists*. 1995: Partnership Press.
110. Chill, J.H., et al., *NMR study of the tetrameric KcsA potassium channel in detergent micelles.* Protein Science, 2006. **15**(4): p. 684-698.
111. Pervushin, K., et al., *Attenuated T-2 relaxation by mutual cancellation of dipole-dipole coupling and chemical shift anisotropy indicates an avenue to NMR structures of very large biological macromolecules in solution.* Proceedings of the National Academy of Sciences of the United States of America, 1997. **94**(23): p. 12366-12371.

112. Krueger-Koplin, R.D., et al., *An evaluation of detergents for NMR structural studies of membrane proteins.* Journal of Biomolecular Nmr, 2004. **28**(1): p. 43-57.
113. Liang, B. and L.K. Tamm, *Structure of outer membrane protein G by solution NMR spectroscopy.* Proceedings of the National Academy of Sciences of the United States of America, 2007. **104**(41): p. 16140-5.
114. Laws, D.D., H.M. Bitter, and A. Jerschow, *Solid-state NMR spectroscopic methods in chemistry.* Angewandte Chemie (English Edition), 2002. **41**(17): p. 3096-129.
115. Ketchem, R.R., et al., *Macromolecular structural elucidation with solid-state NMR-derived orientational constraints.* J Biomol NMR, 1996. **8**(1): p. 1-14.
116. Jaroniec, C.P., et al., *High-resolution molecular structure of a peptide in an amyloid fibril determined by magic angle spinning NMR spectroscopy.* Proceedings of the National Academy of Sciences of the United States of America, 2004. **101**(3): p. 711-716.
117. Rienstra, C.M., et al., *De novo determination of peptide struchture with solid-state magic-angle spinning NMR spectroscopy.* Proceedings of the National Academy of Sciences of the United States of America, 2002. **99**(16): p. 10260-10265.
118. Castellani, F., et al., *Structure of a protein determined by solid-state magic-angle-spinning NMR spectroscopy.* Nature, 2002. **420**(6911): p. 98-102.
119. Seidel, K., et al., *High-Resolution Solid-State NMR Studies on Uniformly [(13)C,(15)N]-Labeled Ubiquitin.* Chemistry and Biochemistry, 2005. **6**(9): p. 1638-1647.
120. Hiller, M., et al., *Solid-state magic-angle spinning NMR of outer-membrane protein G from Escherichia coli.* Chemistry and Biochemistry, 2005. **6**(9): p. 1679-84.
121. Lorch, M., et al., *How to Prepare Membrane Proteins for Solid-State NMR: A Case Study on the alpha-Helical Integral Membrane Protein Diacylglycerol Kinase from E. coli.* Chemistry and Biochemistry, 2005. **6**(9): p. 1693-1700.
122. Andronesi, O.C., et al., *Determination of membrane protein structure and dynamics by magic-angle-spinning solid-state NMR spectroscopy.* Journal of the American Chemical Society, 2005. **127**(37): p. 12965-74.
123. van Gammeren, A.J., et al., *Residual backbone and side-chain C-13 and N-15 resonance assignments of the intrinsic transmembrane light-harvesting 2 protein complex by solid-state Magic Angle Spinning NMR spectroscopy.* Journal of Biomolecular Nmr, 2005. **31**(4): p. 279-293.
124. Kobayashi, M., et al., *Signal assignment and secondary structure analysis of a uniformly [C-13, N-15]-labeled membrane protein, H+-ATP synthase subunit c, by magic-angle spinning solid-state NMR.* Journal of Biomolecular Nmr, 2006. **36**(4): p. 279-293.
125. Frericks, H.L., et al., *Magic-angle spinning solid-state NMR of a 144 kDa membrane protein complex: E-coli cytochrome bo(3) oxidase.* Journal of Biomolecular Nmr, 2006. **36**(1): p. 55-71.
126. Patching, S.G., et al., *Low 13C-background for NMR-based studies of ligand binding using 13C-depleted glucose as carbon source for microbial growth: 13C-labeled glucose and 13C-forskolin binding to the galactose-H+ symport protein GalP in Escherichia coli.* Journal of the American Chemical Society, 2004. **126**(1): p. 86-7.
127. Mason, A.J., G.J. Turner, and C. Glaubitz, *Conformational heterogeneity of transmembrane residues after the Schiff base reprotonation of*

bacteriorhodopsin: 15N CPMAS NMR of D85N/T170C membranes. Febs Journal, 2005. **272**(9): p. 2152-64.

128. Yamaguchi, S., et al., *Secondary structure and backbone dynamics of Escherichia coli diacylglycerol kinase, as revealed by site-directed solid-state 13C NMR.* Biochim Biophys Acta, 2004. **1698**(1): p. 97-105.
129. Watts, A., *Solid-State NMR in Drug Design and Discovery for Membrane-embedded targets.* Nature Reviews Drug Discovery, 2005. **4**: p. 555-568.
130. Luca, S., White, J.F., Sohal, A.K., Filippov, D.V., van Boom, J.H., Grisshammer, R., Baldus, M., *The conformation of neurotensin bound to its G protein-coupled receptor.* Proceedings of the National Academy of Sciences of the United States of America, 2003. **100**(19): p. 10706-10711.
131. Lopez, J., et al., *The Structure of the Neuropeptide Bradykinin Bound to the Human G-Protein Coupled Receptor Bradykinin B2 as Determined by Solid-State NMR Spectroscopy.* Angewandte Chemie (English Edition), 2008. **47**(9): p. 1668-1671.
132. Venkata, R., et al., *Solid state NMR Evidence for a protonation switch in the binding pocket of the H1 receptor upon binding of the agonist histamine.* Journal of the American Chemical Society, 2007.
133. Glaubitz, C., et al., *^{31}P-CP-MAS NMR studies on TPP+bound to the ion-coupled multidrug transport protein EmrE.* Febs Letters, 2000. **480**: p. 127-131.
134. Patching, S.G., et al., *Substrate affinities for membrane transport proteins determined by 13C cross-polarization magic-angle spinning nuclear magnetic resonance spectroscopy.* Journal of the American Chemical Society, 2004. **126**(10): p. 3072-80.
135. Patching, S.G., et al., *The nucleoside transport proteins, NupC and NupG, from Escherichia coli: specific structural motifs necessary for the binding of ligands.* Organic & Biomolecular Chemistry, 2005. **3**(3): p. 462-70.
136. Agarwal, V., et al., *MAS Solid-State NMR Studies on the Multidrug Transporter EmrE.* Biochemica et Biophysica Acta - Biomembranes, 2008. **1768**(12): p. 3036-3043.
137. Appleyard, A.N., et al., *Selective NMR observation of inhibitor and sugar binding to the galactose-H+ symport protein GalP, of Escherichia coli.* Biochimica Et Biophysica Acta-Biomembranes, 2000. **1509**(1-2): p. 55-64.
138. Spooner, P., et al., *Structural Information on a Membrane Transport Protein from Nuclear Magnetic Resonce Spectroscopy Using Sequence-Selctive Nitroxide Labeling.* Biochemistry, 1999. **38**: p. 9634-9639.
139. Spooner, P.J.R., et al., *Weak substrate binding to transport proteins studied by NMR.* Biophysical Journal, 1998. **75**(6): p. 2794-2800.
140. Spooner, P.J.R., A. Watts, and P.J.F. Henderson, *Magic-Angle Spinning Nmr-Studies on the Galactose-H+ Symport Protein of Escherichia-Coli.* Biophysical Journal, 1993. **64**(2): p. A51-A51.
141. Spooner, P.J.R., et al., *Nmr Observation of Substrate in the Binding-Site of an Active Sugar-H+ Symport Protein in Native Membranes.* Proceedings of the National Academy of Sciences of the United States of America, 1994. **91**(9): p. 3877-3881.
142. Spooner, P.J.R., A. Watts, and P.J.F. Henderson, *Functional-Characteristics of the Sugar-H+ Symport Proteins from Magic-Angle-Spinning Nmr.* Biophysical Journal, 1994. **66**(2): p. A38-A38.
143. Mason, A.J., et al., *Amino acid type selctive isotope labelling of the multidrug ABC transporter LmrA for solid-state NMR studies.* Febs Letters, 2004. **568**: p. 117-121.

144. Keller, R., *The Computer Aided Resonance Assignment Tutorial*. 1st ed. 2004: CANTINA Verlag.
145. Zubay, G., *In-Vitro Synthesis of Protein in Microbial Systems.* Annual Review of Genetics, 1973. **7**: p. 267-287.
146. Ninio, S., D. Rotem, and S. Schuldiner, *Functional analysis of novel multidrug transporters from human pathogens.* Journal of Biological Chemistry, 2001. **276**(51): p. 48250-48256.
147. Bullock, W.O., J.M. Fernandez, and J.M. Stuart, *XL1-Blue:a high efficiency plasmid transforming recA Escherichia coli strain with beta-galactosidase selection.* BioTechniques, 1987. **5**: p. 376-379.
148. E.coligeneticstockcenter. *E. coli genetic stock center*. 2007 [cited 03.12.2007]; Available from: http://cgsc.biology.yale.edu/.
149. Fiaux, J., et al., *Uniform and residue-specific N-15-labeling of proteins on a highly deuterated background.* Journal of Biomolecular Nmr, 2004. **29**(3): p. 289-297.
150. Studier, F.W., et al., *Use of T7 RNA polymerase to direct expression of cloned genes.* Methods Enzymology, 1990. **185**: p. 60-89.
151. NewEnglandBiolabs. *Competent Cells*. 2007 [cited 01.10.07]; Available from: http://www.neb.uk.com/productcatalogue/productinfo.aspx?id=/New%20England%20Biolabs/Competent%20Cells/Competent%20E%20coli/C2523@UK@GUEST@1@@XX@.
152. Goldberg, E.B., et al., *Characterization of a Na+/H+ Antiporter Gene of Escherichia-Coli.* Proceedings of the National Academy of Sciences of the United States of America, 1987. **84**(9): p. 2615-2619.
153. Manolikas, T., *Etablierung und Optimierung der Probenpräparation der integralenMembranproteine EmrE und DGK für Festkörper-NMR und ESR Studien*, in *University of Frankfurt am Main*. 2004, Johann Wolfgang Goethe Universität: Frankfurt am Main.
154. Gutman, N., S. Steiner-Mordoch, and S. Schuldiner, *An amino acid cluster around the essential Glu-14 is part of the substrate- and proton-binding domain of EmrE, a multidrug transporter from Escherichia coli.* Journal of Biological Chemistry, 2003. **278**(18): p. 16082-7.
155. De Rossi, E., et al., *mmr, a Mycobacterium tuberculosis gene conferring resistance to small cationic dyes and inhibitors.* Journal of Bacteriology, 1998. **180**(22): p. 6068-6071.
156. Sambrook, J. and T. Maniatis, *Molecular Cloning: A Laboratory Manual (Library Binding).* 1989.
157. Davies, B. and E. Mingioli, *Mutants of Escherichia coli requiring methionine or vitamin B12.* Journal of Bacteriology, 1950. **60**: p. 17-28.
158. Waugh, D.S., *Genetic tools for selective labeling of proteins with alpha-15N-amino acids.* Journal of Biomolecular Nmr, 1996. **8**(2): p. 184-92.
159. Schaegger, H., *Tricine-Sodium Dodecyl Sulfate-Polyacrylamide Gel Electrophoresis for the Separation of Proteins in the Range from 1 to 100 kDa.* Analytical Biochemistry, 1987. **166**: p. 368-379.
160. Schaegger, H. and G. Von Jagow, *Blue Native Electrophoresis for Isolation of Membrane Protein Complexes in enzymatically active form.* Analytical Biochemistry, 1991. **199**: p. 223-231.
161. Schagger, H., *Blue Native Electrophoresis*, in *Membrane Protein Purification and Crystallization*, C. Hunte, G. von Jagow, and H. Schaegger, Editors. 2003, Elsevier Science, USA.

162. Kaplan, R.S. and P.L. Pedersen, *Determination of Microgram Quantities of Protein in the Presence of Milligram Levels of Lipid with Amido Black B-10.* Analytical Biochemistry, 1985. **150**(1): p. 97-104.
163. Rigaud, J.L. and D. Levy, *Reconstitution of membrane proteins into liposomes.* Methods Enzymology, 2003. **372**: p. 65-86.
164. Kiefer, H., *In vitro folding of alpha-helical membrane proteins.* Biochimica Et Biophysica Acta-Biomembranes, 2003. **1610**(1): p. 57-62.
165. Mitsumoto, Y. and T. Mohri, *Reconstitution of the L-Leucine-H+ Cotransporter of the Plasma-Membrane from Chang Liver-Cells into Proteoliposomes.* Biochimica Et Biophysica Acta, 1991. **1061**(2): p. 171-174.
166. Yerushalmi, H., M. Lebendiker, and S. Schuldiner, *EmrE, an E. coli 12kDa Multidrug Transporter, exchanges toxic cations and H+ and is soluble in organic solvents.* Journal of Biological Chemistry, 1995. **270**(12): p. 6856-6863.
167. Marley, J., M. Lu, and C. Bracken, *A method for efficient isotopic labeling of recombinant proteins.* Journal of Biomolecular NMR, 2001. **20**(1): p. 71-5.
168. Lee, K.M., E.J. Androphy, and J.D. Baleja, *A novel method for selective isotope labeling of bacterially expressed proteins.* Journal of Biomolecular NMR, 1995. **5**(1): p. 93-6.
169. Poget, S.F., S.M. Cahill, and M.E. Girvin, *Isotropic bicelles stabilize the functional form of a small multidrug-resistance pump for NMR structural studies.* Journal of the American Chemical Society, 2007. **129**(9): p. 2432-+.
170. Oesterhelt, D. and W. Stoeckenius, *Isolation of the cell membrane of Halobacterium halobium and its fractionation into red and purple membrane.* Methods Enzymology, 1974. **31**(A): p. 667-678.
171. Perozo, E. and W.L. Hubbell, *Voltage Activation of Reconstituted Sodium-Channels - Use of Bacteriorhodopsin as a Light-Driven Current Source.* Biochemistry, 1993. **32**(39): p. 10471-10478.
172. Copeland, R.A., et al., *Estimating K-I Values for Tight-Binding Inhibitors from Dose-Response Plots.* Bioorganic & Medicinal Chemistry Letters, 1995. **5**(17): p. 1947-1952.
173. Ravaud, S., et al., *The ABC transporter BmrA from Bacillus subtilis is a functional dimer when in a detergent-solubilized state.* Biochemical Journal, 2006. **395**: p. 345-353.
174. Noy, D., J.R. Calhoun, and J.D. Lear, *Direct analysis of protein sedimentation equilibrium in detergent solutions without density matching.* Analytical Biochemistry, 2003. **320**(2): p. 185-192.
175. Schuck, P., *Size-distribution analysis of macromolecules by sedimentation velocity ultracentrifugation and Lamm equation modeling.* Biophysical Journal, 2000. **78**(3): p. 1606-1619.
176. Schuck, P. *Analytical Ultracentrifugation*. 2007 [cited 26.11.2007]; Available from: http://www.analyticalultracentrifugation.com/sedfit_help_cs.htm.
177. Cohen, E., et al., *Purification of Na+,K+-ATPase expressed in Pichia pastoris reveals an essential role of phospholipid-protein interactions.* Journal of Biological Chemistry, 2005. **280**(17): p. 16610-16618.
178. Suckau, D., et al., *A novel MALDI LIFT-TOF/TOF mass spectrometer for proteomics.* Analytical and Bioanalytical Chemistry, 2003. **376**(7): p. 952-965.
179. Bahr, U., et al., *Delayed extraction time-of-flight MALDI mass spectrometry of proteins above 25,000 Da.* Journal of Mass Spectrometry, 1997. **32**(10): p. 1111-1116.

180. Wattenberg, A., F. Sobott, and B. Brutschy, *Detection of intact hemoglobin from aqueous solution with laser desorption mass spectrometry.* Rapid Communications in Mass Spectrometry, 2000. **14**(10): p. 859-861.
181. Meier, T., et al., *A tridecameric c ring of the adenosine triphosphate (ATP) synthase from the thermoalkaliphilic Bacillus sp strain TA2.A1 facilitates ATP synthesis at low electrochemical proton potential.* Molecular Microbiology, 2007. **65**(5): p. 1181-1192.
182. Bodenhausen, G. and D.J. Ruben, *Natural Abundance N-15 Nmr by Enhanced Heteronuclear Spectroscopy.* Chemical Physics Letters, 1980. **69**(1): p. 185-189.
183. Kay, L.E., P. Keifer, and T. Saarinen, *Pure Absorption Gradient Enhanced Heteronuclear Single Quantum Correlation Spectroscopy with Improved Sensitivity.* Journal of the American Chemical Society, 1992. **114**(26): p. 10663-10665.
184. Schleucher, J., et al., *A general enhancement scheme in heteronuclear multidimensional NMR employing pulsed field gradients* Journal of Biomolecular Nmr, 1994. **4**.
185. Palmer, A.G., et al., *Sensitivity Improvement in Proton-Detected Two-Dimensional Heteronuclear Correlation NMR Spectroscopy* Journal of Magnetic Resonance, 1991. **93**: p. 151-170.
186. Kumar, A., R.R. Ernst, and K. Wuthrich, *A two-dimensional nuclear Overhauser enhancement (2D NOE) experiment for the elucidation of complete proton-proton cross-relaxation networks in biological macromolecules.* Biochemical and Biophysical Research Communications, 1980. **95**(1): p. 1-6.
187. Huster, D., K. Arnold, and K. Gawrisch, *Investigation of lipid organization in biological membranes by two-dimensional nuclear overhauser enhancement spectroscopy.* Journal of Physical Chemistry B, 1999. **103**(1): p. 243-251.
188. Szeverenyi, N.M., M.J. Sullivan, and G.E. Maciel, *Observation of Spin Exchange by Two-Dimensional Fourier-Transform C-13 Cross Polarization-Magic-Angle Spinning.* Journal of Magnetic Resonance, 1982. **47**(3): p. 462-475.
189. Hong, M., *Solid-state dipolar INADEQUATE NMR spectroscopy with a large double-quantum spectral width.* Journal of Magnetic Resonance, 1999. **136**(1): p. 86-91.
190. Carravetta, M., et al., *Symmetry principles for the design of radiofrequency pulse sequences in the nuclear magnetic rsonance of rotating solids.* Chemical Physics Letters, 2000. **321**: p. 205-215.
191. Davis, J.H., et al., *Quadrupolar Echo Deuteron Magnetic-Resonance Spectroscopy in Ordered Hydrocarbon Chains.* Chemical Physics Letters, 1976. **42**(2): p. 390-394.
192. Dorman, S.E. and R.E. Chaisson, *From magic bullets back to the Magic Mountain: the rise of extensively drug-resistant tuberculosis.* Nature Medicine, 2007. **13**(3): p. 295-298.
193. Jack, D.L., et al., *A Broad-Specificity Multidrug Efflux Pump Requiring a Pair of Homologous SMR-Typ Proteins.* Journal of Bacteriology, 2000. **182**(8): p. 2311-2313.
194. Grinius, L.L. and E.B. Goldberg, *Bacterial multidrug resistance is due to a single membrane protein which functions as a drug pump.* Journal of Biological Chemistry, 1994. **269**(47): p. 29998-30004.
195. Qiagen. *Ni-NTA Spin Handbook*. 2007 [cited 20.09.07]; Available from: http://www.1qiagen.com.

196. Bieber, A.L., K.A. Tubbs, and R.W. Nelson, *Metal ligand affinity pipettes and bioreactive alkaline phosphatase probes - Tools for characterization of phosphorylated proteins and peptides.* Molecular & Cellular Proteomics, 2004. **3**(3): p. 266-272.
197. Klammt, C., et al., *Evaluation of detergents for the soluble expression of alpha-helical and beta-barrel-type integral membrane proteins by a preparative scale individual cell-free expression system.* Febs Journal, 2005. **272**(23): p. 6024-6038.
198. Clough, J.L., et al., *Prokaryotic membrane transport proteins: amplified expression and purification,* in *Structural genomics on membrane proteins*, K. Lundstrom, Editor. 2006, CRC. p. 21-37.
199. Berman, H.M., K. Henrick, and H. Nakamura, *Announcing the worldwide Protein Data Bank.* Nature Structural Biology 2003. **10**(12): p. 980.
200. Grisshammer, R., *Understanding recombinant expression of membrane proteins.* Current Opinion in Biotechnology, 2006. **17**(4): p. 337-340.
201. Pfleger, N., *Expression yields of proteorhodopsin - personal communication*. 2007.
202. Studier, F.W. and B.A. Moffatt, *Use of Bacteriophage-T7 Rna-Polymerase to Direct Selective High-Level Expression of Cloned Genes.* Journal of Molecular Biology, 1986. **189**(1): p. 113-130.
203. Steen, R., et al., *T7-Rna Polymerase Directed Expression of the Escherichia-Coli Rrnb-Operon.* Embo Journal, 1986. **5**(5): p. 1099-1103.
204. Baldwin, S.A. and P.J. Henderson, *Homologies between sugar transporters from eukaryotes and prokaryotes.* Annual Review of Physiology, 1989. **51**: p. 459-71.
205. Hellmich, U.A., *LmrA overexpression in E.coli and L. lactis - personal communication*. 2007.
206. Lanyi, J.K., *Bacteriorhodopsin.* Annual Review of Physiology, 2004. **66**: p. 665-88.
207. Bioscience, A., *Ion Exchange Chromatography & Chromatofocussing - Principle and Methods*. 2007, Amersham Bioscience.
208. Cohen, E., et al., *Purification of Na,K-ATPase expressed in Pichia pastoris: Specific interactions with lipids.* Journal of General Physiology, 2005. **126**(1): p. 12a-12a.
209. Gasteiger E., et al., *Protein Identification and Analysis Tools on the ExPASy Server*, in *The Proteomics Protocols Handbook*, J.M. Walker, Editor. 2005, Humana Press. p. 571-607
210. Sigma-Aldrich. *Detergent selection table.* 2007 [cited 16.10.2007]; Available from: http://www.sigmaaldrich.com/img/assets/15402/Detergent_Selection_Table.pdf.
211. Oesterhelt, D. and W. Stoeckenius, *Rhodopsin-like protein from the purple membrane of Halobacterium halobium.* Nature: New Biology, 1971. **233**(39): p. 149-52.
212. Huang, K.S., et al., *Refolding of an Integral Membrane-Protein - Denaturation, Renaturation, and Reconstitution of Intact Bacteriorhodopsin and 2 Proteolytic Fragments.* Journal of Biological Chemistry, 1981. **256**(8): p. 3802-3809.
213. Sagne, C., et al., *SDS-resistant aggregation of membrane proteins: Application to the purification of the vesicular monoamine transporter.* Biochemical Journal, 1996. **316**: p. 825-831.
214. Cowling, R.T. and H.C. Birnboim, *Preliminary characterization of the protein encoded by human Testis-Enhanced Gene Transcript (TEGT).* Molecular Membrane Biology, 1998. **15**(4): p. 177-187.

215. Bullis, B.L., et al., *Properties of the Na+/H+ exchanger protein - Detergent-resistant aggregation and membrane microdistribution.* European Journal of Biochemistry, 2002. **269**(19): p. 4887-4895.
216. Manley, D.M., et al., *Secondary structure and oligomerization of the E-coli glycerol facilitator.* Biochemistry, 2000. **39**(40): p. 12303-12311.
217. Tamm, L.K. and B.Y. Liang, *NMR of membrane proteins in solution.* Progress in Nuclear Magnetic Resonance Spectroscopy, 2006. **48**(4): p. 201-210.
218. Wang, D.N., et al., *Practical aspects of overexpressing bacterial secondary membrane transporters for structural studies.* Biochimica et Biophysica Acta, 2003. **1610**(1): p. 23-36.
219. Auer, M., et al., *High-yield expression and functional analysis of Escherichia coli glycerol-3-phosphate transporter.* Biochemistry, 2001. **40**(22): p. 6628-35.
220. Anatrace. *Fos-Choline 12 Technical Information*. 2007 [cited 20.09.2007]; Available from: http://www.anatrace.com.
221. Quina, F.H., et al., *Growth of Sodium Dodecyl-Sulfate Micelles with Detergent Concentration.* Journal of Physical Chemistry, 1995. **99**(46): p. 17028-17031.
222. Prive, G.G., *Detergents for the stabilization and crystallization of membrane proteins.* Methods, 2007. **41**(4): p. 388-397.
223. Young, H.S., et al., *How to make tubular crystals by reconstitution of detergent-solubilized Ca2+-ATPase.* Biophysical Journal, 1997. **72**(6): p. 2545-2558.
224. Koenig, B. and H. Sandermann, *Beta-D-galactoside transport in Escherichia coli. Solubilization in organic solvent and reconstitution of binding.* European Journal Biochemistry, 1984. **145**(2): p. 397-402.
225. Rigaud, J.-L., et al., *Detergent removal by non-polar poystyrene beads.* European Biophysical Journal, 1998. **27**: p. 305-319.
226. Ingram, L.O., *Changes in Lipid-Composition of Escherichia-Coli Resulting from Growth with Organic-Solvents and with Food-Additives.* Applied and Environmental Microbiology, 1977. **33**(5): p. 1233-1236.
227. Brown, R.H. and J. Stevenson, *Variation in Composition of a Purified Membrane Fraction from Halobacterium-Salinarium with Phase of Growth.* Antonie Van Leeuwenhoek Journal of Microbiology and Serology, 1971. **37**(1): p. 89-&.
228. Yerushalmi, H., M. Lebendiker, and S. Schuldiner, *EmrE, an Escherichia coli 12-kDa Multidrug Transporter, Exchanges Toxic Cations and H+ and Is Soluble in Organic Solvents.* Journal of Biologicial Chemistry, 1995. **270**(12): p. 6856-6863.
229. Xiao, L., W.S. Xie, and F.Y. Yang, *A method for uni-directional reconstitution of human erythrocyte glucose transporter.* Biochemistry and Molecular Biology International, 1998. **44**(6): p. 1217-1223.
230. Lichtenberg, D., R.J. Robson, and E.A. Dennis, *Solubilization of Phospholipids by Detergents - Structural and Kinetic Aspects.* Biochimica Et Biophysica Acta, 1983. **737**(2): p. 285-304.
231. Goodsell, D.S. and A.J. Olson, *Structural symmetry and protein function.* Annual Review of Biophysics and Biomolecular Structure, 2000. **29**: p. 105-153.
232. Zaitseva, J., et al., *A structural analysis of asymmetry required for catalytic activity of an ABC-ATPase domain dimer.* Embo Journal, 2006. **25**(14): p. 3432-3443.
233. Abrahams, J.P., et al., *Structure at 2.8-Angstrom Resolution of F1-Atpase from Bovine Heart-Mitochondria.* Nature, 1994. **370**(6491): p. 621-628.

234. Noji, H., et al., *Direct observation of the rotation of F-1-ATPase.* Nature, 1997. **386**(6622): p. 299-302.
235. Mei, G., et al., *The importance of being dimeric.* Febs Journal, 2005. **272**(1): p. 16-27.
236. Manning, M. and W. Colon, *Structural basis of protein kinetic stability: Resistance to sodium dodecyl sulfate suggests a central role for rigidity and a bias toward beta-sheet structure.* Biochemistry, 2004. **43**(35): p. 11248-11254.
237. Gralen, N. and T. Svedberg, *The molecular weight of crotoxin.* Biochemical Journal, 1938. **32**(8): p. 1375-7.
238. Fleming, K.G., *Analysis of membrane proteins using analytical ultracentrifugation*, in *Analytical ultracentrifugation - Techniques and Methods*, D.J. Scott, S.E. Harding, and A.J. Rowe, Editors, RCS Publishing. p. 432-447.
239. Cole, J.L. and J.C. Hansen, *Analytical Ultracentrifugation as a contemporary biomolecular research* Journal of Biomolecular Techniques, 1999. **10**: p. 163-176.
240. Stanley, A.M. and K.G. Fleming, *The transmembrane domains of ErbB receptors do not dimerize strongly in micelles.* Journal of Molecular Biology, 2005. **347**(4): p. 759-772.
241. Butler, P.J. and C.G. Tate, *Correcting for the Buoyancy of Macromolecules: Density Increments and Apparent Partial Specific Volumes with Particular Reference to the Study of Membrane Proteins* in *Analytical Ultracentrifugation*, D.J. Scott, S.E. Harding, and A.J. Rowe, Editors. 2005, RSC Publishing: London. p. 133-448.
242. Veenhoff, L.M., et al., *Mechanistic aspects and structural organiszation of secondary sugar transporter*. 2001, Rijksuniversiteit Groningen: Groningen. p. 128.
243. Morgner, N., H.D. Barth, and B. Brutschy, *A new way to detect noncovalently bonded complexes of biomolecules from liquid micro-droplets by laser mass spectrometry.* Australian Journal of Chemistry, 2006. **59**(2): p. 109-114.
244. Nooren, I.M.A. and J.M. Thornton, *Structural characterisation and functional significance of transient protein-protein interactions.* Journal of Molecular Biology, 2003. **325**(5): p. 991-1018.
245. Qazi, O., et al., *The H-C fragment of tetanus toxin forms stable, concentration-dependent dimers via an intermolecular disulphide bond.* Journal of Molecular Biology, 2007. **365**(1): p. 123-134.
246. Carroll, N.M., et al., *Characterization of recombinant acetolactate synthase from Leuconostoc lactis NCW1*. Enzyme and Microbial Technology, 1999. **25**(1-2): p. 61-67.
247. Bessonneau, P., et al., *The SecYEG preprotein translocation channel is a conformationally dynamic and dimeric structure.* Embo Journal, 2002. **21**(5): p. 995-1003.
248. Lodish, H., et al., *Identification and Purification of Cell-Surface Receptors*, in *Molecular Cell Biology*. 2000, W. H. Freeman and Company: New York.
249. Lodish, H., et al., *Purifying, Detecting and Characterizing Proteins*, in *Molecular Cell Biology*. 2000, W. H. Freeman and Company: New York.
250. Schuldiner, S., *Hsmr radioactive TPP+ assay - personal communication*. 2004.
251. Elbaz, Y., et al., *Substrate-induced tryptophan fluorescence changes in EmrE, the smallest ion-coupled multidrug transporter.* Biochemistry, 2005. **44**(19): p. 7369-77.
252. Adam, Y., et al., *The fast release of sticky protons: Kintetics of substrate binding and proton release in a multidrug transporter*. Proceedings of the

National Academy of Sciences of the United States of America, 2007. **104**(46): p. 17989-17994.
253. Zacharias, N. and D.A. Dougherty, *Cation-pi interactions in ligand recognition and catalysis.* Trends in Pharmacological Sciences, 2002. **23**(6): p. 281-287.
254. Basting, D., et al., *Transport cycle intermediate in small multidrug resistance protein is revealed by substrate fluorescence. The FASEB Journal*, 2008. **22**(2): p. 365-373.
255. Cheng, Y. and W.H. Prusoff, *Relationship between Inhibition Constant (K1) and Concentration of Inhibitor Which Causes 50 Per Cent Inhibition (I50) of an Enzymatic-Reaction.* Biochemical Pharmacology, 1973. **22**(23): p. 3099-3108.
256. Katsu, T., H. Nakagawa, and K. Yasuda, *Interaction between polyamines and bacterial outer membranes as investigated with ion-selective electrodes.* Antimicrobial Agents and Chemotherapy, 2002. **46**(4): p. 1073-1079.
257. Wingrove, D.E., J.M. Amatruda, and T.E. Gunter, *Glucagon Effects on the Membrane-Potential and Calcium-Uptake Rate of Rat-Liver Mitochondria.* Journal of Biological Chemistry, 1984. **259**(15): p. 9390-9394.
258. Kamo, N., et al., *Membrane-Potential of Mitochondria Measured with an Electrode Sensitive to Tetraphenyl Phosphonium and Relationship between Proton Electrochemical Potential and Phosphorylation Potential in Steady-State.* Journal of Membrane Biology, 1979. **49**(2): p. 105-121.
259. Mootha, V.K., S. French, and R.S. Balaban, *Neutral carrier-based "Ca2+-selective" microelectrodes for the measurement of tetraphenylphosphonium.* Analytical Biochemistry, 1996. **236**(2): p. 327-330.
260. microelectrodes. *MI-600 Ca2+ sensitive electrode*. 2007 [cited 13.11.2007]; Product description]. Available from: http://www.microelectrodes.com.
261. Schwaiger, M., et al., *NMR investigation of the multidrug transporter EmrE, an integral membrane protein.* European Journal of Biochemistry, 1998. **254**(3): p. 610-619.
262. Katragadda, M., J.L. Alderfer, and P.L. Yeagle, *Assembly of a Polytopic Membrane Protein Structure from the Solution Structures of Overlapping Peptide Fragments of Bacteriorhodopsin.* Biophysical Journal, 2001. **81**: p. 1029-1036.
263. Poget, S.F., et al., *NMR assignment of the dimeric S-aureus small multidrug-resistance pump in LPPG micelles.* Journal of Biomolecular Nmr, 2006. **36**: p. 10-10.
264. Page, R.C., et al., *Comprehensive evaluation of solution nuclear magnetic resonance spectroscopy sample preparation for helical integral membrane proteins.* Journal of Structural and Functional Genomics, 2006. **7**(1): p. 51-64.
265. Columbus, L., et al., *Expression, purification, and characterization of Thermotoga maritima membrane proteins for structure determination.* Protein Science, 2006. **15**(5): p. 961-975.
266. Kigawa, T., Y. Muto, and S. Yokoyama, *Cell-Free Synthesis and Amino Acid-Selective Stable-Isotope Labeling of Proteins for Nmr Analysis.* Journal of Biomolecular Nmr, 1995. **6**(2): p. 129-134.
267. Tusnady, G.E. and I. Simon, *The HMMTOP transmembrane topology prediction server.* Bioinformatics, 2001. **17**(9): p. 849-850.
268. BiologicalMagneticResonanceDataBank. *Statistics Calculated for Selected Chemical Shifts from Atoms in the 20 Common Amino Acids*. 2007 [cited 30.11.2007]; Available from: http://www.bmrb.wisc.edu/ref_info/statsel.htm.
269. Altenberg, G.A., et al., *Unidirectional Fluxes of Rhodamine-123 in Multidrug-Resistant Cells - Evidence against Direct Drug Extrusion from the Plasma-*

Membrane. Proceedings of the National Academy of Sciences of the United States of America, 1994. **91**(11): p. 4654-4657.
270. Sharom, F.J., *Shedding light on drug transport: structure and function of the P-glycoprotein multidrug transporter (ABCB1).* Biochemical Cell Biology, 2006. **84**(6): p. 979-992.
271. Bolhuis, H., et al., *Energetics an Mechanism of Drug Transport Mediated by the Lactococcal Multidrug Transporter LmrP.* The Jounal of Biological Chemistry, 1996. **271**(39): p. 24123-24128.
272. Siarheyeva, A., J.J. Lopez, and C. Glaubitz, *Localization of multidrug transporter substrates within model membranes.* Biochemistry, 2006. **45**(19): p. 6203-11.
273. Forbes, J., et al., *Some New Developments in Solid-State Nuclear Magnetic-Resonance Spectroscopic Studies of Lipids and Biological-Membranes, Including the Effects of Cholesterol in Model and Natural Systems.* Journal of the Chemical Society-Faraday Transactions I, 1988. **84**: p. 3821-3849.
274. Forbes, J., C. Husted, and E. Oldfield, *High-Field, High-Resolution Proton Magic-Angle Sample-Spinning Nuclear Magnetic-Resonance Spectroscopic Studies of Gel and Liquid-Crystalline Lipid Bilayers and the Effects of Cholesterol.* Journal of the American Chemical Society, 1988. **110**(4): p. 1059-1065.
275. Holte, L.L. and K. Gawrisch, *Determining Ehtanol Distribution in Phospholipid Multilayers with MAS-NOESY Spectra.* Biochemistry, 1997. **36**: p. 4669-4674.
276. Ellena, J.F., et al., *Localization of hydrophobic ions in phospholipid bilayers using 1H nuclear Overhauser effect spectroscopy.* Biochemistry, 1987. **26**(14): p. 4584-92.
277. Yau, W.M., et al., *The preference of tryptophan for membrane interfaces.* Biochemistry, 1998. **37**(42): p. 14713-14718.
278. Malatesta, F., et al., *Potentiometric characterization of ethidium bromide and of its reactions with nucleic acids.* Analytical Biochemistry, 2004. **334**(1): p. 62-71.
279. Maulucci, G., et al., *Particle size distribution in DMPC vesicles solutions undergoing different sonication times.* Biophysical Journal, 2005. **88**(5): p. 3545-3550.
280. AvantiPolarLipids. *Phase Transition Temperatures for Glycerophospholipids*. 2007 [cited 16.12.2007]; Available from: http://www.avantilipids.com/PhaseTransitionTemperaturesGlycerophospholipids.html.
281. Molinspiration. *LogP predictor (miLogP2.2).* 2005 [cited 16.12.2007]; Available from: http://www.molinspiration.com/services/logp.html.
282. Marulanda, D., et al., *Resonance assignments and secondary structure analysis of E-coli thioredoxin by magic angle spinning solid-state NMR spectroscopy.* Journal of Physical Chemistry B, 2005. **109**(38): p. 18135-18145.
283. Franks, W.T., et al., *Four-dimensional heteronuclear correlation experiments for chemical shift assignment of solid proteins.* Journal of Biomolecular Nmr, 2007. **39**(2): p. 107-131.
284. Crocker, E., et al., *Dipolar assisted rotational resonance NMR of tryptophan and tyrosine in rhodopsin.* Journal of Biomolecular Nmr, 2004. **29**(1): p. 11-20.
285. Vuister, G.W., et al., *2d and 3d Nmr-Study of Phenylalanine Residues in Proteins by Reverse Isotopic Labeling.* Journal of the American Chemical Society, 1994. **116**(20): p. 9206-9210.

286. Castellani, F., et al., *Structure of a protein determined by solid-state magic-angle-spinning NMR spectroscopy.* Nature, 2002. **420**: p. 98-102.
287. Goldbourt, A., L.A. Day, and A.E. McDermott, *Assignment of congested NMR spectra: Carbonyl backbone enrichment via the Entner-Doudoroff pathway.* Journal of Magnetic Resonance, 2007. **189**(2): p. 157-165.
288. Hong, M. and K. Jakes, *Selective and extensive 13C labeling of a membrane protein for solid-state NMR investigations.* Journal of Biomolecular NMR, 1999. **14**(1): p. 71-4.
289. Böckmann, A., et al., *Solid state NMR sequential resonance assignments and conformational analysis of the 2x10.4 kDa dimeric grorm of the Bacillus subtilis protein Crh.* Journal of Biomolecular Nmr, 2003. **27**: p. 232-339.
290. Hong, M., et al., *Structure of an elastin-mimetic polypeptide by solid-state NMR chemical shift analysis.* Biopolymers, 2003. **70**: p. 158-168.
291. Jelinski, L.W., et al., *Deuterium Nuclear Magnetic-Resonance of Specifically Labeled Native Collagen - Investigation of Protein Molecular-Dynamics Using the Quadrupolar Echo Technique.* Biophysical Journal, 1980. **32**(1): p. 515-529.
292. Jelinski, L.W., C.E. Sullivan, and D.A. Torchia, *H-2 Nmr-Study of Molecular-Motion in Collagen Fibrils.* Nature, 1980. **284**(5756): p. 531-534.
293. Keniry, M.A., H.S. Gutowsky, and E. Oldfield, *Surface Dynamics of the Integral Membrane-Protein Bacteriorhodopsin.* Nature, 1984. **307**(5949): p. 383-386.
294. Herzfeld, J., et al., *Contrasting Molecular-Dynamics in Red and Purple Membrane-Fractions of the Halobacterium-Halobium.* Biophysical Journal, 1987. **52**(5): p. 855-858.
295. Allegrini, P.R., et al., *Side-chain dynamics of two aromatic amino acids in pancreatic phospholipase A2 as studied by deuterium nuclear magnetic resonance.* Biochemistry, 1985. **24**(13): p. 3268-73.
296. BrukerBiospin, *NMR properties of selected isotopes*, in *Bruker Almanac*. 2003, Bruker Biospin: Karlsruhe.
297. Beshah, K., E.T. Olejniczak, and R.G. Griffin, *Deuterium Nmr-Study of Methyl-Group Dynamics in L-Alanine.* Journal of Chemical Physics, 1987. **86**(9): p. 4730-4736.
298. Duer, M.J., *Introduction to Solid-state NMR Spectroscopy*: Blackwell Publishing.
299. Hoffman, R. *Hydrogen (Proton, Deuterium and Tritium) NMR.* 2007 [cited 15.12.2007]; Available from: http://chem.ch.huij.ac.il/nmr/techniques/1d/row1/h.html.
300. Gruner, S.M., et al., *Lipid Polymorphism - the Molecular-Basis of Nonbilayer Phases.* Annual Review of Biophysics and Biophysical Chemistry, 1985. **14**: p. 211-238.
301. Clausell, A., et al., *Influence of polymyxins on the structural dynamics of Escherichia coli lipid membranes.* Talanta, 2003. **60**(2-3): p. 225-234.
302. Siminovitch, D.J., *Solid state NMR studies of proteins: the view from static 2H NMR experiments.* Biochemical Cell Biology, 1998. **76**: p. 411-422.
303. Liu, W., et al., *Role of side-chain conformational entropy in transmembrane helix dimerization of glycophorin A.* Biophysical Journal, 2003. **84**(2): p. 162a-162a.
304. Siarheyeva, A., et al., *Probing the molecular dynamics of the ABC multidrug transporter LmrA by deuterium solid-state nuclear magnetic resonance.* Biochemistry, 2007. **46**(11): p. 3075-3083.

305. le Coutre, J., et al., *Fourier transform infrared spectroscopy reveals a rigid alpha-helical assembly for the tetrameric Streptomyces lividans K+ channel.* Proceedings of the National Academy of Sciences of the United States of America, 1998. **95**(11): p. 6114-6117.
306. Spiess, H.W. and H. Sillescu, *Solid Echoes in the Slow-Motion Region.* Journal of Magnetic Resonance, 1981. **42**(3): p. 381-389.
307. Neyfakh, A.A., *Mystery of multidrug transporters: the answer can be simple.* Molecular Microbiology, 2002. **44**(5): p. 1123-1130.
308. Lewinson, O., et al., *Promiscuity in multidrug recognition and transport: the bacterial MFS Mdr transporters.* Molecular Microbiology, 2006. **61**(2): p. 277-284.
309. Yerushalmi, H., S. Steiner-Mordoch, and S. Schuldiner, *A Single Carboxyl Mutant of the Multidrug Transporter EmrE Is Fully Functional.* Journal of Biologicial Chemistry, 2001. **276**(16): p. 12744-12748.
310. Sachs, R.K., K.M. Halverson, and B.A. Barry, *Specific isotopic labeling and photooxidation-linked structural changes in the manganese-stabilizing subunit of photosystem II.* Journal of Biological Chemistry, 2003. **278**(45): p. 44222-44229.
311. London, R.E. and T.E. Walker, *Asymmetric Nmr-Spectra of Weakly Coupled Nuclei - a Common Characteristic in the C-13 Nmr-Spectra of [U-C-13]-Labeled Molecules and in Natural Abundance Proton-Coupled C-13 Spectra.* Organic Magnetic Resonance, 1981. **15**(4): p. 333-338.
312. Keseler, I.M., et al., *EcoCyc: a comprehensive database resource for Escherichia coli.* Nucleic Acids Research, 2005. **33**: p. D334-D337.
313. Meyer, B., *mass spectrometry of proteins - personal communication*. 2007.
314. Rotem, D., N. Sal-man, and S. Schuldiner, *In Vitro Monomer Swapping in EmrE, a Multidrug Transporter from Escherichia coli, Reveals That the Oligomer Is the Functional Unit.* The Jounal of Biological Chemistry, 2001. **276**(51): p. 48243-48249.
315. Zhang, F.L., et al., *Double-quantum biased covariance spectroscopy: Application to the 2D INADEQUATE experiment.* Journal of Magnetic Resonance, 2005. **174**(2): p. 219-222.
316. Lesage, A., et al., *Determination of through-bond carbon-carbon connectivities in solid-state NMR using the INADEQUATE experiment.* Journal of the American Chemical Society, 1997. **119**(33): p. 7867-7868.
317. Lesage, A., M. Bardet, and L. Emsley, *Through-bond carbon-carbon connectivities in disordered solids by NMR.* Journal of the American Chemical Society, 1999. **121**(47): p. 10987-10993.
318. Carravetta, M., et al., *Estimation of carbon-carbon bond lengths and medium-range internuclear: Distances by solid-state nuclear magnetic resonance.* Journal of the American Chemical Society, 2001. **123**(43): p. 10628-10638.
319. Drobny, G., et al., Symposium of the Faraday Society, 1979. **13**: p. 49.
320. Fung, B.M., A.K. Khitrin, and K. Ermolaev, *An improved broadband decoupling sequence for liquid crystals and solids.* Journal of Magnetic Resonance, 2000. **142**(1): p. 97-101.
321. Arkin, I.T., et al., *Determining the secondary structure and orientation of EmrE, a multi-drug transporter, indicates a transmembrane four-helix bundle.* Biochemistry, 1996. **35**(22): p. 7233-7238.
322. Krupka, R.M., *Limits on the tightness of coupling in active transport.* Journal of Membrane Biology, 1999. **167**(1): p. 35-41.

323. Arkin, I.T., et al., *Determining the Secondary Structure and Orientation of EmrE, a Multi-Drug Transporter, Indicates a Transmenbrane Four-Helix Bundle.* Biochemistry, 1996. **35**: p. 7233-7238.
324. Betz, M., et al., *Long-range nature of the interactions between titratable groups in Bacillus agaradhaerens family 11 xylanase: pH titration of B-agaradhaerens xylanase.* Biochemistry, 2004. **43**(19): p. 5820-5831.
325. Neal, S., et al., *Rapid and accurate calculation of protein H-1, C-13 and N-15 chemical shifts.* Journal of Biomolecular Nmr, 2003. **26**(3): p. 215-240.
326. Richarz, R. and K. Wuethrich, *Carbon-13 NMR Chemical shifts of the common amino acid residues measured in aqueous solutions of the linear tetrapeptides H-gly-gly-X-L-Ala-OH.* Biopolymers, 1978. **17**: p. 2133-2141.
327. Poget, S.F., M.E. Girvin, and p.i.c.n.f.a.o. webpage, *NMR structural studies of a small multidrug-resistance pump in bicelles.* Biophysical Journal, 2007: p. 173a-173a.
328. Straus, S.K., T. Bremi, and R.R. Ernst, *Experiments and strategies for the assignment of fully C-13/N-15-labelled polypeptides by solid state NMR.* Journal of Biomolecular Nmr, 1998. **12**(1): p. 39-50.
329. Nishino, K. and A. Yamaguchi, *Analysis of a complete library of putative drug transporter genes in Escherichia coli.* Journal of Bacteriology, 2001. **183**(20): p. 5803-5812.
330. Masaoka, Y., et al., *A two-component multidrug efflux pump, EbrAB, in Bacillus subtilis.* Journal of Bacteriology, 2000. **182**(8): p. 2307-2310.
331. Tate, C.G., et al., *The projection structure of EmrE, a proton-linked multidrug transporter from Escherichia coli, at 7A resolution.* Embo Journal, 2001. **20**(1): p. 77-81.
332. Wang, J., et al., *Structural Basis of Asymmetry in the Human-Immunodeficiency-Virus Type-1 Reverse-Transcriptase Heterodimer.* Proceedings of the National Academy of Sciences of the United States of America, 1994. **91**(15): p. 7242-7246.
333. Kunishima, N., et al., *A novel induced-fit reaction mechanism of asymmetric hot dog thioesterase PaaI.* Journal of Molecular Biology, 2005. **352**(1): p. 212-228.
334. Sebag, J.A. and P.M. Hinkle, *Melanocortin-2 receptor accessory protein MRAP forms antiparallel homodimers.* Proceedings of the National Academy of Sciences of the United States of America, 2007. **104**(51): p. 20244-20249.
335. Weinglass, A.B., et al., *Exploring the role of a unique carboxyl residue in EmrE by mass spectrometry.* Journal of Biological Chemistry, 2005. **280**(9): p. 7487-92.